MATHEMATICAL MODELS FOR HEAT AND MASS TRANSFER IN NANOFLUID FLOWS

A THESIS SUBMITTED TO THE UNIVERSITY OF KWAZULU-NATAL
FOR THE DEGREE OF DOCTOR OF PHILOSOPHY
COLLEGE OF AGRICULTURE, ENGINEERING & SCIENCE

By
Sami MS Ahamed
School of Mathematics, Statistics & Computer Science
March 2018

Contents

Abstract

The behaviour and evolution of most physical phenomena is often best described using mathematical models in the form of systems of ordinary and partial differential equations. A typical example of such phenomena is the flow of a viscous impressible fluid which is described by the Navier-Stokes equations, first derived in the nineteenth century using physical approximations and the principles of mass and momentum conservation. The flow of fluids, and the growth of flow instabilities has been the subject of many investigations because fluids have wide uses in engineering and science, including as carriers of heat, solutes and aggregates. Conventional heat transfer fluids used in engineering applications include air, water and oil. However, each of these fluids has an inherently low thermal conductivity that severely limit heat exchange efficiency. Suspension of nanosized solid particles in traditional heat transfer fluids significantly increases the thermophysical properties of such fluids leading to better heat transfer performance.

In this study we present theoretical models to investigate the flow of unsteady nanofluids, heat and mass transport in porous media. Different flow configurations are assumed including an inclined cylinder, a moving surface, a stretching cone and the flow of a polymer nanocomposite modeled as an Oldroyd-B fluid. The nanoparticles assumed include copper, silver and titanium dioxide with water as the base fluid. Most recent boundary-layer nanofluid flow studies assume that the nanoparticle volume fraction can be actively controlled at a bounding solid surface, similar to temperature controls. However, in practice, such controls present significant challenges, and may, in practice, not be possible. In this study the nanoparticle flux at the boundary surface is assumed to be zero.

Unsteadiness in fluid flows leads to complex system of partial differential equations. These transport equations are often highly nonlinear and cannot be solved to find exact solutions that describe the evolution of the physical phenomena modeled. A large number of numerical or semi-numerical techniques exist in the literature for finding solutions of nonlinear systems of equations. Some of these methods may, however be subject to certain limitations including slow convergence rates and a small radius of convergence. In recent years, innovative linearization techniques used together with spectral methods have been suggested as suitable tools for solving systems of ordinary and partial differential equations. The techniques which include the spectral local linearization method, spectral relaxation method and the spectral quasiliearization method are used in this study to solve the transport equations, and to determine how the flow characteristics are impacted by changes in certain important physical and fluid parameters. The findings show that these methods give accurate solutions and that the speed of convergence of solutions is comparable with methods such as the Keller-box, Galerkin, and other finite difference or finite element methods.

The study gives new insights, and result on the influence of certain events, such as internal heat generation, velocity slip, nanoparticle thermophoresis and random motion on the flow structure, heat and mass transfer rates and the fluid properties in the case of a nanofluid.

Declaration 1: Plagiarism

The work described in this study was carried out under the supervision and direction of Professor P. Sibanda in the School of Mathematics, Statistics and Computer Science, College of Agriculture, Engineering and Science, University of KwaZulu-Natal, Pietermaritzburg Campus. I hereby declare that no portion of the work referred to in this thesis has been submitted in support of an application for another degree or qualification of this or any other university or institution of learning. The thesis is my original work except where due reference and credit is given.

Sign: ....

Sami MS Ahamed Date

Sign: ....

Prof. P. Sibanda Date

Declaration 2: Publications

In this section, I indicate my contribution to the following published papers.

1. **S. M. S. Ahamed**, S. Mondal, and P. Sibanda, Thermo-diffusion effects on unsteady mixed convection in a magneto-nanofluid flow along an inclined cylinder with a heat source, Ohmic and viscous dissipation, Journal of Computational and Theoretical Nanoscience, 13, 1670-1684, 2016.

   This article forms the main body of Chapter 2. The mathematical formulations that describe the flow model, the computational results and draft discussion was done by Sami MS Ahamed.

2. **S. M. S. Ahamed**, S. Mondal and P. Sibanda, Impulsive nanofluid flow along a vertical stretching cone, International Journal of Heat and Technology, 35(4), 1005 - 1014, 2017.

   This is part of Chapter 3. This article, is an extension of the work in Chapter 2 with changes in the flow geometry. In this paper, the mathematical formulation, simulation and draft analysis of the findings were done by Sami MS Ahamed.

3. F. G. Awad, **S. M. S. Ahamed**, P. Sibanda and M. Khumalo, The effect of thermophoresis on unsteady Oldroyd-B nanofluid flow over stretching surface, PLoS ONE, 10(8), e0135914. Doi: 10.1371/ journal.pone.0135914, 2015.

   This article represents shared research ideas with the first and other authors. We jointly proposed the mathematical formulation for a polymer nanocomposite modeled as an Oldroyd-B fluid. I wrote parts of this article such as the introductory section and performed computations simulations and provided a draft analysis of the results. This article forms Chapter 4 of the thesis.

4. **S. M. S. Ahamed**, S. Mondal, and P. Sibanda, Unsteady mixed convection flow through a permeable stretching flat surface with partial slip effects through MHD nanofluid using spectral relaxation method, Open Physics, 15, 323 - 334, 2017.
   I was responsible for the mathematical formulation of the flow model with slip conditions. I performed some computational simulations and produced draft findings and conclusions. This article forms Chapter 5 of the thesis.

5. **S. M. S. Ahamed**, S. Mondal and P. Sibanda, An unsteady moving magneto-nanofluid over a moving surface in presence of chemical reaction, Proceeding of Institute for Mathematics, Bio-informatics, Information-Technology and Computer Sciences, 5, 135 - 148, 2016.
   The introduction, computational simulations, and draft discussion was done by Sami MS Ahamed. This research is included as Chapter 6 in the thesis. The paper presented at the 10th International Conference of IMBIC on "Mathematical Sciences for Advancement of Science and Technology" (MSAST 2016) in Kolkata, India.

   In summary, the work in the published articles represents a close collaboration with my supervisor and other co-authors. I acknowledge that publication of these articles may not have been possible without assistance from co-authors, especially my supervisor Prof. P. Sibanda who played a great role in the finalizing of all the papers.

Sign: ....

Sami MS Ahamed Date

Acknowledgments

I am most grateful to Allah for his grace and mercy showered upon me to achieve all I have so far. This work could not have been completed without the assistance of a number of people, and I would like to take this opportunity to thank them for their help.

I would like to express my deepest and sincere gratitude to my supervisor Prof. P. Sibanda for his invaluable guidance, encouragement and time during the period of this work. I appreciate his knowledge in the field and his willingness to share it with me. His appetite for research and his kind and helpful nature always inspire me to work hard.

I would like also to thank Professor S. S. Motsa and Dr. Sabyasachi Mondal for their support. I extend special thanks to my lovely wife Amna for being with me there through both good and bad times; as well as my sons Almubtaghah and Almutaman. Many thanks to my family for all their good words of encouragement. I would like to thank the Sudan government for supporting me to finish this work. My special thanks go to my best friend Modather Alawad as well as Dr. Ali Satty and Dr. Mohammed Omer. Also I would like to thank Dr. Ahmed Khidir for his ideas. I would extend my thanks to my colleague Ibukun S. Oyelakin for her support.

Many thanks to my Sudanese friends in Pietermaritzburg who made me feel at home. Many thanks to the administrative staff and technicians, Christel, Bev and the others. To my friends and colleagues at the University of KwaZulu-Natal and beyond, a very big thank you to all of you.

Chapter 1

Introduction

In this Chapter, the essential terminologies, concepts and ideas important for theoretical studies on heat and mass transfer in nanofluid flows are defined. A brief historical account of boundary layer flows, porous media, the synthesis of nanofluids and their thermal properties, and heat and mass transfer is provided along with a discussion of recent solution techniques for nonlinear mathematical models. The objectives, the significance of the work and structure of the thesis are given.

1.1 Historical Overview and the Concept of a Boundary Layer

The scope of fluid mechanics is wide and has considerable applications in engineering and science, for instance in medical studies including breathing and blood flow, water supply systems, meteorology, oceanography and energy generation to name a few (Rouse and Ince [1] and Rouse [2]). Fluid flow can be steady, unsteady, compressible, incompressible, viscous or inviscid. Some of these characteristics reflect the properties of the liquid itself, and others depend on how the fluid is moving.

The Navier-Stokes equations adequately describe the flow of Newtonian fluids. The behavior of any fluid flow problems can be explained mathematically by solving these equations with appropriate boundary conditions. Unfortunately, there are only a few known analytic solutions of the Navier-Stokes equations. As a consequence, researchers tend to depend on experimental results, semi-empirical methods, and numerical techniques to solve fluid flow problems (Cebeci and Cousteix [3]).

Fluid flows are generally characterized by the presence of a large number of dimensionless parameters. The most significant dimensionless parameter is the Reynolds numbers, a ratio of inertial to viscous forces. Mathematically, this is given as

$$Re = \frac{\rho U L}{\mu}, \tag{1.1}$$

where ρ represents the fluid density, U is local flow velocity, L is characteristic dimension of the body, and μ is the fluid viscosity. The size of the Reynolds number is an important indicator of the state of the fluid flow, that is , whether the flow is laminar or turbulent. The Reynolds number is an important parameter in the study of boundary layer flows.

The boundary layer concept was first introduced by Ludwig Prandtl in 1904 (see Prandtl [4]). The concept provides an important link between ideal and real fluid flows. Prandtl proved that, at high Reynolds numbers, the flow around a solid body can be divided into two zones. The first zone, is a very thin layer in a region close to the wall called the boundary layer, where the friction plays an essential part and the velocity satisfies the no-slip condition. The second one, is the outer flow determined by the displacement of streamlines around the body. Here, the viscosity is negligible and the pressure field fully developed (Schlichting [5], Gersten et al. [6] and Kluwick [7]). There is a singnificant velocity gradient from the boundaries to the flow. The velocity gradient leads to shear stresses at the boundary that reduce the flow speed at the boundary. This region near the solid wall is called a boundary layer (White [8]). Flow of real fluids is subject to fluid viscosity and Newton's law for viscosity states that the shear stress, τ, in a fluid is proportional to the

velocity gradient across the fluid flow. This law can be written as,

$$\tau = \mu \frac{du}{dy}, \tag{1.2}$$

where the constant of proportionality μ is the coefficient of viscosity (see Schlichting [9]).

Different types of boundary layers are defined in the literature, for instance, laminar and turbulent boundary layers. Examples of specific boundary layers include the Stokes, Blasius, Falkner-Skan, atmospheric, and geophysical boundary-layers, to name a few. The laminar and turbulent boundary layers are the most studied in the literature (Kluwick [7]). The boundary layer often begins as laminar with fluid particles moving in smooth layers. Down stream, the boundary layer becomes unstable with fluid particles moving in random paths. The nature of the flow, whether laminar or turbulent, is well described in terms of the Reynolds number (Munson et al. [10]).

Ran et al. [11] studied the flow characteristics of a methane/moist-air laminar boundary layer. The study sought to analyze the effects of air/carbon ratio, water/carbon ratio, air mass flow and the wall friction on the characteristic of the boundary layer. The results showed that the velocity increased from rest to the free stream velocity. The boundary layer thickness in the case of both a micro-channel and micro-tube channel increased with the increasing plate length. Suzki et al. [12] investigated the laminar boundary layer on a flat plate using an immersed boundary-lattice Boltzmann method at a Reynolds number of about one thousand. It was found that the immersed boundary-lattice Boltzmann method gave good accuracy whether the flat plate was coincident with the lattice or not. Mager [13] studied three-dimensional laminar boundary-layer flows along flat and curved surfaces. It was found that the sharp curvature of the surface tended to cause flow separation. The separation was as a result of the cross-flow.

Shateyi and Marewo [14] investigated an axisymmetric laminar boundary layer flow of a viscous fluid and heat transfer along a stretching cylinder in a porous medium with variable conductivity. The flow equations were solved using a successive relaxation method.

They concluded that the flow properties were significantly affected by the permeability parameter. A numerical study of laminar boundary layer flow along a permeable flat plate with thermal radiation was made by Mohamed et al. [15]. They investigated the effects of Prandtl numbers, suction/injection and thermal radiation. It was found that the thermal radiation and injection parameters increased the temperature, while the reverse was noted with the suction parameter. Beratlis et al. [16] studied the flow along a flat plate with two and eight rows of dimples in a staggered arrangement. It was shown that the shear layer that forms as the flow separates over the first two rows of dimples becomes unstable.

Uddin et al. [17] investigated flow along a moving plate with a variable magnetic field and radiation. Findings showed that the heat transfer rate increases with the Prandtl numbers, velocity ratio and the magnetic field parameters. It was also found that the mass transfer rate increased with the fluid velocity, the power law index and the Schmidt numbers, but it reduced with the magnetic field effect. Avramenko et al. [18] studied heat and mass transport in a turbulent boundary layer along a flat plate. It was noted that the flow velocity decreased with increasing nanoparticle concentration at the outer edge of the boundary layer. Elsayed et al. [19] studied the effect of using helical coils on heat transfer characteristics in turbulent flow. Findings showed that tube coiling increased the heat transfer coefficient compared with a straight tube at the same Reynolds number. Wang and Zhang [20] investigated turbulent flow subject to high-velocity oscillating amplitudes in a pipe. The results showed that in a pulsating turbulent flow we can find a Womersley number at which heat transfer is optimum where the Womersley number is a dimensionless parameter in biofluid and the pulsatile flows. It is important in conserving dynamic similarity when scaling an experiment.

The Earth's surface is a boundary layer with the lowest two kilometers of the atmosphere being the region most influenced by exchanges in momentum, heat, and water vapor. It is the region most affected by the presence of surface forces. The common forces include drag, evaporation and transpiration, and terrain-induced flow modification (Roland [21],

Kaimal and Finnigan [22] and Oke [23]).

Dörenkämper et al. [24] studied the effect of the stably stratified atmospheric boundary layer on power production and wake effects in offshore wind farms. Results showed that the distance of the wind farm to the coast is an important factor for the power output of wind turbines inside the farm. Pires et al. [25] studied three different passive devices separately and in various combinations, to simulate the atmospheric boundary layer in a wind tunnel. Findings showed that, if the length of the wind tunnel is being short and the pressure loss is not so important; the best choice would be a thin screen. Wächter et al. [26] studied the small-scale intermittent properties of atmospheric flows and their effect on the wind energy conversion process. They concluded that atmospheric turbulence has a strong influence on the wind energy conversion process.

1.2 Flow in Porous Media

Transport of energy and mass in porous media occur frequently with many practical applications in the physical sciences. Many surfaces, for example, soil, sandstone, limestone, ceramics, foam, and rocks have natural pores, while other pores are made purposely, for instance those in filtering and insulation materials, which may be manufactured to have pores of a certain size. Biological tissues such as lungs, cell walls, blood vessels and kidneys; and food products such as bread are porous. Common porous media include paper, clothing, rubber, grit, activated-carbon filters, limestone, metal foams and air filters, to name a few (Bear and Bachmat [27]). In a porous medium, heat and mass transport processes take various forms, for instance, heat exchangers, petroleum reservoir engineering, metallurgy, chemical processing, catalytic reactors, industrial filtration, water purification, soil drainage and irrigation, geothermal energy production and in cores of nuclear reactors (Bear and Corapcioglu [28]).

A porous medium consists of a solid formation with interconnected gaps, which allows the

fluid and small particles to pass through (Dullien [29], Nield and Bejan [30]). The porosity λ, is the ratio of the volume of void space in a representative elementary volume (REV) to the total volume of REV, expressed as,

$$\lambda = \frac{Volume\ \ of\ \ void\ \ space\ \ in\ \ REV}{Total\ \ Volume\ \ of\ \ REV}, \tag{1.3}$$

where $1-\lambda$ is the volume fraction of the solid matrix (Bear and Bachmat [27]). Measurements of porosity in materials are often reliant on techniques such as nuclear magnetic resonance (NMR) which can be utilized to study porous materials, and diffusion in fine porous material (Mitzithras et al. [31] and Valiullin et al. [32]).

Fluid flow in a porous medium is not easily modelled using the Navier-Stokes equations owing to the complexity of the inner pore geometry. Where the boundary conditions are unknown. Because of the irregularity of a porous medium, it can best be studied by methods of statistical mechanics. A random walk model was the first attempt in the study of porous media by Scheidegger [33]. Models of porous media in the literature include the Darcy model, the Darcy-Forchheimer model, Darcy-Brinkman model, Darcy-Brinkman-Forchheimer model, power law model, Richards' model, fracture or fissured flow, Darcy Lapwood, Darcy-Lapwood-Brinkman, Darcy-Lapwood Forchheimer-Brinkman, Darcy-Forchheimer radial and Rudraiah flow models (see for example Darcy [34], Forchheimer [35], Brinkman [36] and Lauriat and Prasad [37]).

In the nineteenth century, Henry Darcy performed a pioneering experimental study of fluid flow over homogeneous and isotropic porous media. Darcy's experiments, culminated in Darcy's law, which may be stated as: "The rate of flow Q of water through a filter bed is directly proportional to the area A of the sand and to the difference $\triangle h$ in the height between the fluid heads at the inlet and outlet of the bed, and inversely proportional to the thickness L of the bed" (Darcy [34]). Mathematically, this law can be written as,

$$Q = \frac{C\,A\,\triangle h}{L}, \tag{1.4}$$

where C is a material property of the porous media. The constant C is expressed as K/μ,

where μ is the fluid viscosity and K is the permeability of the porous medium (Holst and Aziz [38]). Hence, the generalized Darcy law in terms of the total pressure is stated as (Bear [39] and Nield and Bejan [40])

$$u_f = -\frac{K}{\mu}\nabla p, \tag{1.5}$$

where u_f is the Darcy velocity, and p is the pressure.

Darcy's equation is simply an approximation of the balance of linear momentum which however ignores the effect of inertia. Darcy's law has been used to determine the magnitude and direction of discharge through an aquifer; and to get the total flux in a multi-layer system (Todd and Mays [41]).

A limitation of Darcy's law is that it represents the resistance, the friction offered by the solid particles to the fluid flow (Hsu and Cheng [42]). The Darcy flow model is restricted to laminar flow in which the viscous forces dominate over the inertia forces. At low Reynolds number the inertial forces can be ignored. However, these forces become important at high Reynolds numbers when the relation between the pressure drop and the flow motion is no longer linear (Neuman [43] and Bridgman [44]). The Darcy flow model is of order one less than the Navier-Stokes equation; and for this reason it is difficult to use the no-slip boundary condition, therefore, it is likely that a high velocity is possible at the surface (Nakshatrala and Rajagopal [45]; Wang et al. [46]). As the flow rate increases, the inertial forces become significant and the pressure drop becomes a nonlinear (Thauvin and Mohanty [47]). This flow regime is better characterized as a non-Darcy flow rather than a turbulent flow (Belhaj et al. [48]).

Historically, the classical Darcy, Fourier and Fick's laws are coupled with magnitude averaged conservation of mass and energy and other terms to derive mathematical models for transport processes in porous media (Sullivan [49]). In 1901, Philippe Forchheimer noted that, for gas flowing through coal beds, the link between the rate of flow and the potential gradient is nonlinear at high velocity (Forchheimer [35]). Forchheimer modified Darcy's

flow model (1.5) by adding a new term to model the inertia effects in the pressure drop. The modified law is called the Darcy-Forchheimer flow model, and is the earliest non-Darcian flow model (Beji and Gobin [50] and Wu et al. [51]). Mathematically this can be written as

$$\nabla p = -\frac{\mu}{K} V - \beta \rho \upsilon V, \tag{1.6}$$

where V is the velocity, ρ is the fluid density, υ is the absolute value of seepage velocity, and $C_F/\sqrt{K} = \beta > 0$ is Forchheimer' coefficient or non-Darcy coefficient, and C_F is the inertial resistance coefficient. Aulisa et al. [52] analyzed flows in a porous media that were not adequately described by Darcy's law. They concluded that the results could be used for the quantitative evaluation of some engineering parameters. Khan et al. [53] investigated the effects of homogeneous-heterogeneous reactions in flow over a stretching sheet with a nonlinear velocity and variable thickness using the Darcy-Forchheimer porous media model. Their results showed among other things that the temperature increased when Biot number was increased.

Muhammad et al. [54] investigated the flow of a nanofluid in porous media using the Darcy-Forchheimer flow model. Findings demonstrated that the heat transfer rate reduces with increasing porosity and Forchheimer parameters. Hayat et al. [55] studied the effects of Cattaneo-Christov heat flux and homogeneous-heterogeneous reactions on Darcy-Forchheimer flow for two viscoelastic fluids. They concluded that the temperature and thermal boundary layer thickness are smaller for a Cattaneo-Christov heat flux model in comparison to the classical Fourier law of heat conduction. In addition the homogeneous-heterogeneous reaction parameters enhanced the concentration level. Kishan and Maripala [56] studied the effects of thermophoresis and viscous dissipation on a magneto-hydrodynamic flow of heat and mass transfer along isothermal vertical flat plate in a porous medium. They noticed a significant increase in the temperature with viscous dispersion and the magnetic parameter.

Brinkman [57] modified Darcy's law by adding further terms to Darcy's flow model. The

Brinkman flow model is the most appropriate for fast flowing fluids in porous media. The model takes the form

$$\nabla p = -\frac{\mu}{K} V - \mu_{eff} \nabla^2 V, \tag{1.7}$$

where μ_{eff} is the effective fluid viscosity.

The generalized Darcy-Brinkman-Forchheimer flow model is based on the Darcy-Forchheimer flow model. It was originally derived in the framework of thermal dispersion in a porous medium using the method of volume averaging of the velocity and temperature deviations in the pores (Hsu and Cheng [42]). The mathematical generalization of the Darcy-Brinkman-Forchheimer flow model is (see Lauriat and Prasad [37]),

$$\rho(\frac{\partial}{\partial t} + V.\nabla)V = -\nabla p - \mu_{eff} \nabla^2 V - \frac{\mu_f}{K} V - \beta|V|V, \tag{1.8}$$

where the terms are as previously defined. In the last few decades, research using the Brinkman-Forchheimer extended Darcy model have been carried out by Vafai [58]. Jha and Kaurangini [59] studied steady flow in a channel filled with porous materials using the nonlinear Brinkman-Forchheimer extended Darcy model. They concluded that the time-dependent flow solutions approximately produced the same steady-state values. Marpu [60] studied heat transfer in a vertical cylindrical porous annulus using the Forchheimer-Brinkman extended Darcy flow model. It was found that Brinkman viscous terms led to a higher reduction in the heat transfer rate compared to the Forchheimer inertial terms.

Kumar et al. [61] studied flow in a square cavity filled with a porous medium using the Brinkman-Forchheimer-Darcy and the Brinkman-extended Darcy models. The results showed that the Brinkman-extended Darcy model gives the best performance for the flow and heat transfer rates compared to the Brinkman-Forchheimer-Darcy model. Chen et al. [62] investigated the steady flow inside a cavity filled with a porous medium. They concluded that due to higher porosity, there is high flow rate in the porous medium, thus, the heat transfer is high. Juncu [63] investigated the flow through an impermeable sphere

using the Brinkman-Forchheimer-Darcy or Brinkman Hazen-Dupuit-Darcy, model. Results showed that with a decrease in Darcy numbers, the surface vorticity increases for all Reynolds numbers.

1.3 Heat and Mass Transfer Processes

Generally, heat transfer is the transit of thermal energy due to spatial temperature differences. The three essential processes in heat transfer are conduction, convection, and radiation (Cengel and Ghajar [64]). The driving force for heat transfer is a temperature gradient. If the surface temperature differs from the ambient fluid temperature, this leads to a temperature gradient in the thermal boundary layer. This temperature gradient leads to a body force in the form of buoyancy of the fluid. Aiding flow occurs when the surface temperature is higher than the surrounding temperature. The induced pressure gradient is due to buoyancy force whilst an opposing flow happens when the surface temperature is less than the ambient temperature (Mahmood [65]).

Mass transfer happens when a high concentration of a chemical species moves toward a lower concentration relative to other chemical species in the medium. The pressure difference is the main driving force for fluid flow, whilst for mass transport it is the concentration difference (Hines and Maddox [66]). The most common mass transfer processes are through diffusion and convection. There is no mass transfer process similar to heat radiation. Heat and mass transport are kinetic processes that can be studied either together or separately. Mathematical equations are used to study diffusion and convection processes. Heat transfer by a conduction process occurs when a thermal energy exchange happens via direct interaction between molecules possessing temperature differences; that means there exists of a temperature gradient in a fixed medium (Arpaci [67] and Ahsan [68]). In fluids, the term “conduction” refers to heat transfer through a solid or a motionless fluid, whereas for mass conduction, it is better to introduce Fick’s law of diffusion which states

that the rate of diffusion of a chemical species at a point in a mixture is proportional to the concentration gradient of that species at that position (Cengel [69]).

The convection mode of heat transfer in fluids is the mechanism of heat transfer when there is a temperature difference between a surface and bulk fluid motion. In the same way, mass convection refers to the mechanism of mass transfer between a surface and a moving fluid that includes both mass conduction and bulk fluid motion (Cengel and Ghajar [70]). Some examples of convective heat transfer applications are in cooling of microelectronics, heat exchangers and cooling of car engines. Convection is divided into natural, forced and mixed convection. Natural convection processes occur when heat is carried by the fluid due to a buoyancy force, whereas in the forced convection process, heat transfer depends on forced fluid movement (Welty et al. [71]). In addition, mixed convection occurs due to the existence of both a buoyancy force and the forced flow of a fluid where the external force might be a free stream or some movable or stretching surface. In heat and mass transfer the term "convection" is used to indicate the totality of advective and diffusive transfer. The radiation mode of heat transport refers to the thermal energy transit in the form of electromagnetic waves (Modest [72]). In the case of no medium, there exists a net heat transport by radiation between two surfaces at different temperatures. Thermal radiation travels at the speed of light (Bear and Bachmat [73]). Heat and mass transfer are simultaneously affected by the medium movement. Furthermore, heat and mass transfer in most industrial and engineering applications involve the flow of fluids (Hewakandamby [74]).

A large number of studies are available on an unsteady flow heat and mass transport processes in porous media. Among these studies, Huang and Vafai [75] studied heat transfer characteristics in a channel with multiple porous blocks. The importance of inertia, Reynolds number and viscous effects were considered. Results showed that a significant increase in heat transfer could be achieved through the emplacement of porous blocks. The study of some models of fluid flow, heat and mass transfer in porous media have been made

by Su and Davidson [76], and Vafai[77].

A review of literature on heat and mass transport in porous media is given by Vadasz [78]. This gives the theory and applications in emerging fields such as bioengineering, microelectronics, and nanotechnology. Bennacer et al. [79] investigated double-diffusive, natural convection in a perpendicular porous cylinder. The influence of thermal-diffusion was considered in the analysis. The conservation equations were solved by adapting a finite volume approach. Findings showed that the cylindrical annulus allows a high thermal gradient. Davarzani et al. [80] studied heat and mass transport in porous media and the thermo-diffusion influence utilizing a volume averaging technique. They concluded that, for low Péclet numbers, the effective thermo-diffusion in porous media is similar to that in the free fluid and that it does not rely on the solid to fluid conductivity ratio. Makanda et al. [81] studied natural convection in a downward pointing cone in a viscoelastic liquid embedded in a permeable medium. The partial differential equations were solved using the successive linearization method. Findings showed that the augmenting of the viscoelastic fluid with tends to enhance the fluid temperature. The heat transport for a power law Jeffery fluid with thermal radiation was studied by Hayat et al. [82]. They studied the effect of thermal radiation, heat source, and the Deborah number. They noted that these parameters have a significant effect on fluid flow and heat transfer.

An analysis of heat and mass transport along a stretching sheet with suction or injection was undertaken by Gupta and Gupta [83]. They considered a moving surface with non-zero transverse velocity. The exact solution was obtained to the flow equations. Results showed that the temperature reduces due to increasing fluid injection. An investigation of magnetohydrodynamic mixed convection, diffusion-thermo and thermal-diffusion effects on heat and mass transport a power-law fluid along an inclined plate in a permeable medium with variable thermal conductivity, thermal radiation, Ohmic dissipation and absorption or blowing was done by Pal and Chatterjee [84]. Increasing the diffusion-thermo parameter tended to enhance the fluid temperature, while the oppositewas true for viscous dissipation.

Hayat and Qasim [85] investigated the energy and mass transport along a stretching sheet with Joule heating and thermophoresis. The findings demonstrated that increasing Joule heating and thermophoretic velocity enhances heat and mass transfer. Beg et al. [86] analyzed heat and mass transfer from a spherical body in a micropolar fluid with consideration of Soret and Dufour influences. The study showed that heat transfer rates increased with the Dufour number, while it reduces with an increase in the Soret number. In the same context, the mass transfer rates reduced with increasing Dufour numbers, but for the Soret number, the opposite was true. The results further showed that the flow moved faster with less drag compared to micropolar and Newtonian fluids. Hina et al. [87] studied the effect of a chemical reaction on an incompressible fluid flow in a channel with compliant walls. The effects of viscous dissipation were considered under small Grashof number and a long wavelength assumptions. A regular perturbation technique was used to solve the flow equations. They found that the parameters affect the velocity and temperature in a qualitatively similar manner. Hina et al. [88] studied heat and mass transfer in the peristaltic transport of a fluid in a curved channel with flexible walls. They noted that the axial velocity for a Johnson-Segalman fluid is larger than that of a Newtonian fluid. Temperature and concentration distributions were found to be higher in curved channels compared to straight channels. They concluded that the heat transfer coefficient is higher in a straight channel in comparison to a curved channel.

Rahman et al. [89] analyzed the impact of the buoyancy ratio and Lewis number on heat and mass transport over a triangular cavity with a zig-zag shaped bottom wall. The results revealed a distortion to the symmetric distribution of the temperature, and concentration fields for higher values of the Lewis number. It was further noted that increasing the buoyancy ratio and Rayleigh number leads to enhanced heat and mass transfer rates. The impact of combined heat generation/absorption and transpiration on the heat and mass transfer on a non-isothermal stretched surface was analyzed by Mabood et al. [90]. It was found that the suction/injection parameter enhanced the heat and mass transfer. Heat and mass transfer over a plate in porous media as well as chemical reaction effects were

discussed by Patil and Chamkha [91]. An implicit finite-difference scheme together with a quasi-linearization technique was used to obtain the solutions of the coupled, nonlinear partial differential equations. Results showed that polar fluids behave very differently from Newtonian fluids, and that the effects of the chemical reaction parameter and the Schmidt number are significant for the concentration distribution and the mass transfer rate.

The study by Narayana and Babu [92] focused on the effects of a chemical reaction and a heat source on magnetohydrodynamic Jeffrey fluid flow along a stretching surface with power-law temperature and concentration fields. They found that the influence of a magnetic field and thermal radiation is to increase the fluid temperature. The flow concentration reduces with increasing chemical reaction rates. Mekheimer et al. [93] discussed the peristaltic magneto-hydrodynamic second-order fluid flow within a channel, a wave frame of reference was supposed. Findings showed that the concentration distribution increased with the Hartman number, while the Eckert number enhanced the fluid temperature. Yasmin et al. [94] discussed the influence of Hall currents, viscous dissipation and Joule heating on the flow of an incompressible and electrically conducting Williamson fluid in a symmetric planar channel. An increase in the Biot number reduced the fluid temperature, while increasing the concentration of the fluid.

An analysis of heat and mass transport along an inclined plate in a permeable medium with thermophoresis was done by Postelnicu [95]. The influence of the thermophoresis parameter was analyzed for both cold and hot wall cases. The study presented numerical results of the deposition velocity at the wall due to thermophoresis in the context of porous media. The physical impact of thermophoresis and internal heat generation or absorption on hydromagnetic flow along an isothermal inclined plate was discussed by Noor et al. [96]. The model equations were solved numerically using the shooting method. Results showed that with suction, the velocity and temperature distributions are smaller than with injection, while for the concentration distribution the opposite is true. Also, with the influence of a heat source, fluid properties are reduced less compared to the case of flow with a heat sink.

The flow of a three-dimensional viscoelastic fluid along a stretching surface and the influence of diffusion-thermo and thermal-diffusion was discussed by Hayat et al. [97]. They found that the thermal-diffusion and diffusion-thermo had the opposite effect on heat and mass transfer rates. Bell et al. [98] used the Darcy model in the study of flow in a permeable spherical body. Their aim was to study the impact of the extra viscous term on the steady-state mass transfer from a sphere at low Peclet numbers. Their results showed that a larger Brinkman viscous boundary layer reduces convection. A solution for Darcy flow with a Robin boundary condition was also obtained. Pal and Mondal [99] focused on viscous dissipation, thermal-thermo diffusion, thermal radiation, and a non uniform heat source-sink together with chemical reaction on mixed convection flow, heat and mass transport over a semi-infinite nonlinear stretching sheet in porous media. They concluded that the fluid temperature increases with decreasing thermal-diffusion while the opposite was noted for the fluid concentration.

Ramesh [100] investigated the flow of a magnetohydrodynamic couple stress fluid, including heat and mass transfer over an inclined asymmetric channel in a permeable medium. The study was subject to the long wavelength and small Reynolds number approximations. It was found that the temperature and heat transfer coefficient are enhanced by increasing the Darcy number and the angle of inclination of the magnetic field. Prasad et al. [101] presented a mathematical model for the transport of an optically-dense, electrically-conducting fluid over a permeable isothermal sphere. Findings show that increasing the porosity accelerates the flow, and minimizes the fluid temperature and concentration. Increasing the Forchheimer inertial drag reduced the fluid flow, but enhanced the fluid temperature and concentration. Both the boundary layer velocity and temperature were reduced by increasing thermal radiation.

Prasad et al. [102] analyzed the heat and mass transfer in fluid flow along a vertical porous plate as well as the influences of a magnetic field, Soret and Dufour parameters. The findings were that increasing the Dufour number reduced the flow concentration but increased

the flow temperature, while the reverse is true for the Soret number. The influence of the Forchheimer parameter is to strongly decelerate the fluid flow and to increase the temperature and concentration. The effects of thermal radiation and non-uniform magnetic field were studied by Rashidi et al. [103]. The results were obtained using the homotopy analysis method to solve the conservation equations. Results showed that the impact of the magnetic field is to diminish the flow velocity and increase both the fluid temperature and concentration. Thermal radiation enhances the heat transfer coefficient. Magneto-hydrodynamic laminar flow over a moving vertical surface in a porous medium was investigated by Javaherdeh et al. [104]. The results were found using a fully implicit finite difference method. They found that the transverse magnetic field produces a resistive force which opposes the flow. This contributes to diminishing heat and mass transfer rates.

Raju et al. [105] analyzed magnetohydrodynamic Casson fluid flow over a porous surface with the thermal radiation, viscous dissipation, a heat source and chemical reaction effects. They found dual solutions and compared the results of the Casson fluid with a Newtonian fluid. It was found that the heat transfer rate increases with the strength of the heat source. In addition, it was found that the Casson fluid achieved better heat transfer performance compared with the Newtonian fluid. An analytical study of non-Darcy mixed convection due to a vertical isothermal permeable surface in a homogeneous porous medium saturated with Ostwald de-Waele type non-Newtonian fluid was carried out by Ibrahim et al. [106]. Their aim was to study the effect of surface injection or suction on heat and mass transfer. It was found that fluid flows with suction have smaller heat transfer rates. Increasing the viscosity index reduced the heat transfer rate for flows with suction or injection.

A study of the impact of a chemical reaction and viscous dissipation on flow along an isothermal porous vertical surface was done by Mahdy and Chamkha [107]. It was found that increasing both the chemical reaction rate and viscous dissipation reduces the heat transfer rate while fostering mass transfer. The investigation of non-Darcian flow on a sphere in a porous medium with a chemical reaction has been done by Rashad et al. [108].

They found that both heat and mass transfer rates are minimized by an increase in either the permeability parameter or the inertial parameter for aiding flow conditions. In addition, with an increase in the chemical reaction, the heat transfer rate diminished, while the mass transfer rate was enhanced.

The study of transport processes in a porous medium with thermal-diffusion, diffusion-thermo, chemical reaction and thermal radiation influence around a truncated cone was made by Rashad and Chamkha [109]. They found that the heat and mass transfer coefficient increases with the Darcy number and thermal radiation. They also showed that with a chemical reaction, the heat transfer rate diminished while the mass transfer rate increased. Eldabe et al. [110] studied the impact of a magnetic field on the peristaltic movement of a non-Newtonian fluid together with heat and mass transfer through a channel in a porous medium. The problem was for a modified Casson non-Newtonian constitutive model. Results showed that the impact of some physical parameters such as the magnetic field, permeability, wave number, and Casson parameter on heat and mass transfer cannot be ignored.

Bhukta et al. [111] investigated the influence of thermal radiation and viscous dissipation on a viscoelastic fluid flow along a shrinking sheet in a porous medium. Findings showed that the magnetic field, as has been shown by others before, reduces the velocity and concentration of the flow. The existence of porous matrix reduces the temperature of the fluid. They demonstrated that the rate of heat transfer is very sensitive to the existence of porous matrix and the magnetic parameter. An investigation of magneto-hydrodynamic incompressible fluid flow and heat and mass transfer along a vertical stretching sheet was done by Kandasamy and Muhaimin [112]. They predicted that the effect of a high temperature-dependent fluid viscosity parameter is to enhance both the fluid flow and the heat transfer rate. Thermophoresis particle deposition has a significant influence on the fluid flow, heat and mass transfer rates. Sheikholeslami et al. [113] analyzed micropolar fluid flow with heat and mass transfer along a channel. Findings showed that suction and injection and the

Péclet number have a direct impact on heat and mass transfer rates.

The study of suction or injection and heat generation/absorption on non-Newtonian power-law fluid flow in a porous medium was done by Chamkha and Al-Humoud [114]. Their aim was to determine the effects of the buoyancy ratio, power-law fluid index, mixed convection parameter, suction or injection parameter, heat generation or absorption parameter, and the Lewis number on the heat and mass characteristics. They found that as the buoyancy ratio was increased, both the heat and mass transfer rates were enhanced for the full range of the free and mixed convection regimes whilst they remained constant for the forced-convection regime. They further showed that the heat and mass transfer rates are reduced as the power-law fluid index was increased. Chamkha et al. [115] investigated the impact of thermal radiation and chemical reaction on natural convection over a vertical cylinder in porous media. It was found that there are additional implications on the heat and mass transfer characteristics due to the variation of fluid viscosity, thermal radiation and a chemical reaction.

Rashidi et al. [116] analyzed the effect of a chemical reaction on laminar flow along a horizontal surface. Findings showed that with increasing order of a chemical reaction, the fluid velocity, temperature and concentration are enhanced. Viscous dissipation and the Joule heating influence on the heat and mass transfer in a second grade magneto-hydrodynamic stagnation point flow along a permeable stretching cylinder was studied by Hayat et al. [117]. They found that increasing the curvature parameter both the flow velocity and the temperature were enhanced far from the cylinder. Chamkha and Aly [118] studied the impact of Soret-Dufour and a chemical reaction on stagnation-point polar flow over a stretching surface in a porous medium taking into consideration both, namely, assisting and opposing flows. It was observed that for assisting flow conditions, the heat transfer rate diminished with a high chemical reaction rate, but was enhanced in the case of opposing flow conditions.

Jumah et al. [119] investigated heat and mass transfer using the Darcy-Forchheimer model for flow in a saturated porous medium. Results demonstrated that the heat and mass transfer rates reduced with increasing porous media inertial resistance. Mallikarjuna et al. [120] studied mixed convection along rotating vertical cone. They concluded that with a large porosity and magnetic field, the rates of heat and mass transfer are increased. Over and above, the mass transfer rate rose with increasing chemical reaction rates. Thermal and mass diffusion along a vertical porous plate has been investigated by Makinde and Ogulu [121]. Findings showed that the rate of mass transfer rose with increasing chemical reaction parameter. Jashim et al. [122] studied Darcian magneto-convective slip flow over a non-isothermal continuously movable permeable radiating surface with viscous dissipation, Joule heating, and chemical reaction effects. They concluded that the flow concentration rose whilst the rate of mass transfer diminished with high mass diffusivity. The heat transfer reduced with high thermal radiation-conduction, magnetic field and viscous dissipation.

Williams and Rhyne [123] investigated unsteady flows of impulsively started wedge type flows using a new set of scaled coordinates. It was found that it is possible to calculate the initial phases of wedge type flows impulsively set into motion for an arbitrarily large adverse pressure gradient. An incompressible electrically conducting fluid flow past an impulsive stretching sheet was studied by Takhar et al. [124]. Results illustrated that the surface shear stresses and the surface heat transfer rate rose with stretching and the magnetic field effects, They noted a smooth transition from the short-time solution to the long-time solution. Xu and Liao [125] analyzed the unsteady magneto-hydrodynamic non-Newtonian fluid flow due to an impulsively stretching surface. They showed that, the magnetic field leads to an increase in the wall friction which is more pronounced for non-Newtonian fluids with larger power-law index. Liao [126] and Kechil and Hashim [127] studied the unsteady fluid flow through an impulsively stretching surface. They found accurate analytic solutions of unsteady boundary-layer flow, which they claimed were uniformly valid for all time. Viscous flow along an impulsively stretching surface was further studied by

Ali et al. [128]. They showed a smooth transition from the short-time solution to the long-time solution. The flow through a stretching or shrinking sheet was investigated by Khan et al. [129] and Lok and Pop [130]. They showed that the stretching or shrinking parameters have a significant influence on the flow and that such effects cannot be ignored.

Viscoelastic fluid flow over an impulsively started vertical surface with variable surface temperature and mass concentration was done by Kumar et al. [131]. The results showed that the viscoelasticity enhances the fluid flow but has a no impact on the fluid temperature and concentration. The effect of heat absorption or generation on unsteady electrically conducting fluid flow over a vertical infinite surface was studied by Turkyilmazoglu and Pop [132]. It was found that the heat and mass transfer rates become independent of time in the long run. Das et al. [133] studied thermal radiation and chemical reaction impact on unsteady Casson fluid flow through a vertical surface. They noted that the flow rate and the temperature fall with high values of Casson parameter whilst the concentration reduced with increasing chemical reaction rates.

Hall currents and magnetic field influences on an electrically conducting unsteady fluid flow past a stretching surface was investigated by Shateyi and Motsa [134]. The numerical solution was obtained by using the successive linearization method together with Chebyshev pseudo-spectral collocation method. It was found that the skin-friction coefficient, the heat and mass transfer rates are enhanced by high Hartmann numbers, Prandtl numbers the unsteadiness parameter, or Schmidt numbers. The Hall parameter caused the temperature and concentration levels to diminish. Chamkha et al. [135] investigated the impact of radiation and a chemical reaction on unsteady micropolar fluid flow over a infinite vertical flat plate. They showed that with an increase in the micropolar fluid vortex viscosity parameter, the heat and mass transfer rates reduced, while the opposite is true for the wall couple stress. Furthermore, with an increase in the mixed convection parameter the wall couple stress, heat and mass transfer rates rose. Chamkha and El-Kabeir [136] studied thermal and mass diffusion for an impulsively stretched vertical surface with a chemical reaction,

and Soret and Dufour influences. Findings showed that the heat transfer rates increased as either the mixed convection parameter, suction/injection parameter, or the wall temperature and concentration exponent increased, and decreased as either the Hartmann number or the chemical reaction parameter increased. With high Dufour or low Soret numbers, both the skin-friction coefficient and the heat transfer rates were reduced while the mass transfer rate was enhanced.

The influence of viscous dissipation on an incompressible electrically conducting micropolar fluid with heat and mass transfer has been investigated by Mohanty et al. [137]. They concluded that high viscous dissipation produces heat due to drag between the fluid particles, which causes an increase in the fluid temperature. They also found that the thermal buoyancy has no significant effect on both couple stress and mass transfer coefficient. Animasaun [138] studied the impact of thermophoresis, chemical reaction and radiative heat transfer on unsteady micropolar fluid flow due to a vertical porous surface with temperature dependent dynamic viscosity and constant vortex viscosity. They showed that the flow with high suction lead to an increase in both the fluid temperature and concentration levels. in addition, both heat and mass transfer rates fell with the increase in the thermophoretic parameter. The modified Boussinesq approximation gave better results for flow along vertical surface and melting heat transfer surface.

Chamkha et al. [139] studied unsteady fluid flow with heat and mass transfer over a permeable stretching surface subject to a chemical reaction influences. They showed that the heat transfer rate is enhanced by large Prandtl numbers, suction/injection, or the unsteadiness effects, and reduced as either the chemical reaction or the Schmidt number increased. Furthermore, the mass transfer rate increased as a result of increasing unsteadiness, chemical reaction, suction/injection, or the Schmidt number. Heat transfer reduced for high Prandtl numbers. Mansour et al. [140] focused their work on unsteady heat and mass transport within a porous square enclosure. It was found that the sinusoidal variations in temperature

and concentration removed the singularities which appeared in the case of fixed temperature and concentration levels. A low Darcy number reduce both the heat and mass transfer rates. In addition, an increase in the amplitude wavelength ratio tended to raise both heat and mass transfer rates. The flow of an unsteady Newtonian fluid flow due to an exponentially accelerated infinite vertical permeable surface was investigated by Rajesh and Chamkha [141]. They concluded that the heat transfer rate rose due to increase in the suction and time parameters while it reduced with an increase in the viscous dissipation both air and water. Benazir et al. [142] studied unsteady magneto-hydrodynamic Casson fluid flow transfer through a permeable surface with double dispersion, non-uniform heat source/sink and a higher order chemical reaction. Results showed that the temperature dependent heat source/sink plays a great role in controlling the heat transfer. Heat and mass transfer from an inclined surface subject to viscous dissipation, joule heating and thermophoresis has been studied by Alam and Rahman [143]. It was found that flow with viscous dissipation reduces the heat transfer rate for both suction and injection cases. Moreover, suction presented a stronger impact on wall thermophoretic deposition velocity than injection.

Free convection from an optically thin radiating fluid flow along an impulsively moving infinite permeable vertical plate subject to rotation and a chemical reaction was studied by Seth et al. [144]. It was noted that the heat transfer rate rises with thermal radiation and falls with thermal diffusion. Furthermore, chemical reaction leads to an enhanced mass transfer rate, whilst mass diffusion has the reverse effect. The diffusion-thermo and thermal-diffusion influence on heat and mass transfer along a rotating vertical cone was investigated by Chamkha and Rashad [145]. It was found that the local tangential and azimuthal skin-friction coefficients, heat and mass transfer rates were enhanced by an increase in the angular velocity of the cone. Furthermore, it was noted that high Dufour numbers tend to minimize both the heat and mass transfer rates.

Olanrewaju et al. [146] studied an electrically conducting power law flow with heat and mass transfer from a heated porous plate subject to Soret and Dufour effects. They showed

that flow with high suction and a magnetic field effect accelerates the flow of both pseudoplastic and dilatant fluids. The high Dufour number for pseudoplastic fluid raises the temperature levels across the wall plate. Ali et al. [147] analyzed an electrically conducting incompressible viscous fluid flow with the combined influence of radiation and chemical reaction along an inclined porous plate. They concluded that the heat and mass transfer rates rise with the time. Sagar et al. [148] analyzed the magneto-hydrodynamic flow of a chemically reacting and radiation absorbing Kuvshinski fluid along a semi-infinite vertical surface. It was found that the temperature levels rose with increasing radiation and radiation absorption. The thermal-thermo diffusion influence on an unsteady flow along a vertical porous surface moving through a binary mixture with *n*th-order Arrhenius type irreversible chemical reaction was studied by Makinde and Olanrewaju [149]. Results reveal that reverse flow is triggered with increasing buoyancy forces, injection, destructive chemical reaction, radiation absorption, and thermo-diffusion effect, while it reduces with the diffusion-thermal. Furthermore, the fluid temperature levels became high, while the species concentration lessened with high Soret number but reduced with the Dufour number. The suggestion is that for fluids with medium molecular weight that include hydrogen-air mixtures, the impact of Dufour and Soret terms cannot be ignored.

1.4 Nanofluids As Heat Transfer Fluids

Fluid heating and cooling is important in many industrial and commercial processes, for instance, in manufacturing, transportation, and electronics. The need for high or low heat flow processes has created considerable demand for new technologies to enhance heat transfer. Since the middle of the 20th century, micro and nano-technologies have grown tremendously. There is significant interest in enhancing the efficiency of heat transfer processes. Fluids developed by suspending nanoparticles in traditional heat transfer fluids are called nanofluids. (Choi et al. [150]; Das [151]; Das et al. [152]; Eastman et al. [153]; and Keblinski et al. [154]). Choi [155] defined nanofluids as fluids with solid particles

of sizes between 1 and 100 nanometre in diameter. Nanofluids typically utilize metal or metal oxide nanoparticles. The most common conventional fluids used as base fluids for nanofluids are de-ionized water and ethanol.

The most commonly used materials for nanoparticles are chemically stable metals such as Aluminium, Copper, Silver, Gold and Iron; non-metals such as graphite and carbon nanotubes; ceramics such as Aluminium Oxides, Copper II Oxide, Titania, Silica Oxide, Zinc Oxide or Zirconia and Sodium Oxide; metal carbides such as Silicon carbide, Titanium carbide and Boron carbide; nitrides such sa Aluminium nitride, Silicon nitride, Titanium nitride and boron nitride; and borides such as Titanium boride (Thomas [156]).

Nanofluids have enhanced thermo-physical properties like high thermal conductivity, thermal diffusivity, viscosity, density and convective heat transfer coefficients in contrast to base fluids (Choi [157]; Tyler et al. [158]; Das et al. [152]; and Liu et al. [159]). Experimental studies showed that the improvement in thermal conductivity is in the range between 15-40 % and heat transfer coefficient enhancements is up to 40% (Yu et al. [160]).

Unsteady nanofluids flow, heat and mass transfer processes in porous media have received significant interest in the last few decades with many theoretical and experimental studies. Abbasi et al. [161] explored the influence of thermal radiation, Brownian motion and thermophoresis on hydromagnetic Jeffrey fluid flow over a stretching surface with flux conditions. It was found that with increasing thermophoresis and Brownian motion, the thermal conductivity enhances which gives a higher temperature. Awad et al. [162] investigated the thermophoresis, Brownian motion and cross-diffusion impacts on magneto-nanofluid flow due to a stretching sheet. The flow equations were solved numerically using the successive linearization method. Results showed that the heat transfer rate rose in the absence of the Brownian motion and the thermophoresis.

Pal and Mandal [163] studied the influence of three types of nanoparticles, copper, alumina, and titanium dioxide in stagnation-point flow due to a permeable stretching or shrinking

surface. They concluded that a minimization of the heat transfer rate occurs with high viscous dissipation, but increases with an increase in the Schmidt number. On the other hand, the mass transfer rate rose significantly with an increase in the Schmidt number and the chemical reaction. It reduced for higher values of the nanoparticle volume fraction. Furthermore, a copper-water nanofluid showed a higher skin friction and mass transfer rate, and less heat transfer rate when compared with an alumina-water and titanium dioxide-water nanofluids. Yohannes and Shankar [164] studied the impact of a magnetic field, viscous dissipation, chemical reaction and Soret on nanofluid flow along a permeable stretching surface. The study showed that the heat transfer rate reduces with increasing nanoparticle volume fraction, magnetic field, and viscous dissipation. The copper-water nanofluid provided a higher heat transfer rate than the silver-water nanofluid. Also, the mass transfer rate increased with increasing nanoparticle volume fraction, chemical reaction, and thermal-diffusion effects. The silver-water nanofluid gave a higher mass transfer rate than a copper-water nanofluid.

Moshizi [165] investigated the influence of a uniform magnetic field on heat and mass transfer inside a porous microchannel. Findings demonstrated that with the nanoparticles the heat transfer rate was enhanced in the microchannel. In addition, the heat transfer rate rose with the Hartmann number and slip parameters. Haile and Shankar [166] considered the effect of two nanoparticles, copper and alumina on heat and mass transfer on a fluid-saturated porous medium with thermal radiation, viscous dissipation and a chemical reaction. It was noted that with large nanoparticle volume fraction the temperature was raised for both copper-water and alumina-water. Both of viscous dissipation and thermal radiation enhanced the fluid temperature. In addition, the concentration increased with the Soret number, while the chemical reaction minimized it. The influence of Brownian motion and thermophoresis on nanofluid flow due to a porous moving plate has been studied by Qasim et al. [167]. They concluded that with both Brownian motion and thermophoresis the temperature was elvated, while the fluid concentration rose with the Brownian motion and reduced due to the thermophoresis effect.

Agarwal and Bhadauria [168] investigated the thermal instability in a horizontal layer of a Newtonian nanofluid with Brownian motion, thermophoresis and rotation. It was found that the heat and mass transfer rates are enhanced by Rayleigh and Lewis numbers. Also, the modified diffusivity ratio enhanced mass transfer rate. Reddy et al. [169] studied nanofluid flow with heat and mass transfer through a semi-infinite moving vertical surface. Findings showed that the spherical shaped nanoparticles have better heat transfer performance compared with cylindrically shaped nanoparticles. Iqbal et al. [170] investigated viscous dissipation on an unsteady electrically conducting nanofluid flow between two orthogonally moving porous coaxial disks. They used a water-based nanofluid with titanium dioxide nanoparticles.

As stated earlier, there are numerous experimental and theoretical studies in the literature regarding the thermal conductivity of nanofluids; heat and mass transfer in porous and nonporous media; and fewer studies on mass transfer using nanofluid models. Numerical schemes like spectral linearization methods are not widely used to solve the equations of fluid flow models. This study investigates some mathematical models of unsteady nanofluid flow on heat and mass transfer; using the spectral methods.

This study is concerned with the numerical solution of the unsteady flow along an inclined cylinder in a porous medium saturated with nanofluids. Influences of a chemical reaction, viscous and Ohmic dissipation subject to applied transverse magnetic and electric fields on heat and mass transfer are investigated. Two different types of nanoparticles, copper, and silver were considered, with water as the base fluid. The model equations are solved using the spectral local linearization method.

The effects of viscous dissipation, internal heat generation and chemical reaction on unsteady flow through a vertically stretching cone have been investigated. Two nanoparticles, namely, the copper and titanium oxide were included with water considered as the base fluid. The numerical results are obtained using the spectral local linearization method.

A numerical solution to the equations of unsteady flow of a polymer nanocomposite represented by an Oldroyd-B nanofluid along a stretching sheet is investigated. The nanoparticle flux at the boundary surface is assumed to vanish. The spectral relaxation and quasi-linearisation methods were used to obtain the numerical results for flow equations.

Unsteady nanofluid flow, of stagnation point subject to magneto-hydrodynamic along a permeable stretching surface, was studied. The effects of Brownian motion, thermophoresis, partial slip boundary condition and internal heat source or sink were considered in the flow model. The flow equations were solved using the numerical spectral relaxation method.

Lastly, the impact of Brownian motion, thermophoresis, chemical reaction and thermal radiation on unsteady nanofluid flow along a moving surface in a porous medium is studied. The nanofluid particle fraction on the boundary was considered to be passively rather than actively controlled, and the nanoparticle flux at the boundary surface was assumed to be zero. The flow equations were solved numerically using the spectral relaxation method.

1.5 Solution Techniques for Fluid Flow Problems

In the last few decades, computational fluid mechanics has become an important subdomain of the field of fluid mechanics. Fluid flow problems are modeled using complicated equation systems. For these problems, it is not always possible to apply analytical methods directly or traditional perturbation techniques with slow or no convergence to find correct solution. Over the years, a number of computational methods have been developed to solve linear and nonlinear equations. These methods are needed to solve nonlinear systems, which are analytically difficult to solve. Several of these methods have been used in the literature and are quite efficient in terms of providing approximate solutions. However, many of these methods are not very efficient for high order systems of nonlinear ordinary and partial differential equations that arise in the study of fluid flow problems, for example, partial differential equations formulated using the transformation suggested by Williams

and Rhyne [123]. Examples of common numerical methods used include different versions of finite difference methods, finite volume and finite element methods.

A lot of literature exists on the use of various finite difference schemes to solve boundary layer flow problems described by nonlinear ordinary and partial differential equations (see Bhattacharyya [171], Patil et al. [172], Roy [173], Saikrishnan and Roy [174]; and Ponnaiah [175]). Many researchers have suggested that finite difference methods are suitable to solve partial differential equations because they are fast and easy to code (Strikwerda [176]). Finite element methods can be very accurate and suitable for complex geometries (Johnson [177]). Some authors like Argyris [178], Turner [179] and Hrennikov [180] presented some research on the development of finite element methods. Spectral methods use all available function values to generate the required approximations, which is an advantage compared to other methods (Jovanovic and Süli [181]). Spectral methods are the preferred techniques for solving nonlinear ordinary and partial differential equations because of their high accuracy in resolving problems with smooth functions (see Canuto et al. [182], Fornberg [183] and Trefethen [184]). These methods are considered to be more accurate compared to numerical methods such as the finite difference and finite elements methods.

Various spectral methods in combination with linearization techniques are used in this study. In the following sections we describe the spectral local linearization (SLLM), spectral relaxation (SRM) and spectral quasi-linearization (SQLM) methods because of their perceived higher rates of convergence, accuracy and ease of application to complicated nonlinear ordinary and partial differential equations. These methods were introduced and are more fully described in Motsa [185–187] and Motsa et al. [188].

The primary objective of using these linearization techniques coupled with the spectral methods is because they have not been used extensively in the literature and their true worth in finding solutions of fluid flow problems remains to be assessed. The methods (SLLM,

SRM, and SQLM) have been shown in a limited number of case studies to be applicable to linear and nonlinear ordinary and partial differential equations. It has also been suggested that they are easy to use and to code in Matlab. In this study, we test these claims and the accuracy of the methods by solving various nonlinear systems that model the conservation principles in the flow of fluids.

1.5.1 The Spectral Local Linearization Method

The spectral local linearization method is a modification of the quasi-linearization method originally proposed by Bellman and Kalaba [189] to solve functional equations. The spectral local linearization method (SLLM) was introduced by Motsa [185] to solve nonlinear differential equations. The spectral linearization method linearizes and decouples systems of equations using a combination of a univariate linearization technique and spectral collocation discretization. The key feature of the algorithm is that it breaks down a large coupled system of equations into a sequence of easier to solve smaller subsystems of equations. The method is accurate and gives excellent convergence, higher stability, and is very efficient when compared with other methods of solving large systems of boundary value problems (see Motsa [185]).

Motsa [186] used the method to find solutions to systems of equations for unsteady flow over an impulsively stretching surface. The method was also used to obtain solutions for natural convection in a boundary layer flow problem (Motsa et al. [190]). Sithole et al. [191] studied unsteady Maxwell nanofluid flow along a shrinking surface with convective and slip boundary conditions. The aim was to determine the effect of Brownian motion and thermophoresis. The flow equations were solved efficiently using the spectral local linearization method. They concluded that increasing particle Brownian motion leads to a reduction in the concentration profiles but concentration profiles increase with thermophoresis parameter.

Das et al. [133] investigated the effect of homogeneous-heterogeneous reactions on the steady flow of heat transfer and chemically reacting for copper-water nanofluid. The spectral local linearization method used to solve the flow equations. They showed that the heat transfer rate increases with an increase in nanoparticle volume fraction, mixed convection, thermal radiation, temperature ratio and stretching rate.

Shateyi and Marewo [192] investigated the hydromagnetic Casson fluid flow with heat and mass transfer along a stretching surface subject to thermal radiation, viscous dissipation, and a chemical reaction. The numerical solution was obtained using the spectral local linearization method. Results showed that the flow, temperature, and concentration fields are significantly influenced by the Casson parameter, magnetic parameter, velocity ratio parameter, Eckert number and chemical reaction. Shateyi and Marewo [193] studied the unsteady flow of heat and mass transfer with the influence of thermal radiation and chemical reaction. The flow equations were solved using the spectral local linearization method and the successive relaxation method. The showed that the temperature reduced by increasing values of the Prandtl number and the thermal radiation parameter. The flow velocity reduced with increasing values of chemical reaction, Schmidt number, and magnetic parameter.

1.5.2 The Spectral Relaxation Method

The main innovation in the spectral relaxation method is the decoupling of differential equations in a manner similar to the Gauss-Seidel method for algebraic equations. The Chebyshev pseudospectral collocation method is then used to integrate the decoupled system (see Canuto et al. [182], Fornberg [183] and Trefethen [184]). The spectral relaxation method for ordinary differential equations is fully described by Motsa [187]. The method was first used to obtain solutions for steady von Kármán flow subject to resistive heating and viscous dissipation by Motsa and Makukula [194]. The spectral relaxation method has further been used to solve the equations for chaotic and hyperchaotic systems (see Motsa et al. [195], and Motsa et al. [196]).

The spectral relaxation method had been extended to solve a system of nonlinear partial differential equations (Motsa et al. [188]). The findings showed that the method is effective and may work better than some popular schemes such as the Keller-box method in terms of accuracy and speed of convergence.

Oyelakin et al. [197] studied unsteady Casson nanofluid flow along stretching sheet. The aim was to investigate the influence of Dufour-Soret, thermal radiation and heat generation on heat and mass transfer. The flow equations were solved using the spectral relaxation method. The results illustrated that the fluid flow, temperature, and concentration profiles are significantly influenced by the fluid unsteadiness parameter, the Casson parameter, magnetic parameter and the velocity slip parameter. Kameswaran et al.[198] investigated unsteady nanofluid flow on heat transfer due to stretching sheet according to the influence of thermal dispersion and radiation. The numerical solution was obtained using the spectral relaxation method. The findings showed that the convergence rate of the spectral relaxation method significantly improves when the method is used in conjunction with the successive over-relaxation method.

Shateyi et al. [199] investigated the magnetohydrodynamic flow and heat transfer of a Maxwell fluid. The flow model equations were solved using the spectral relaxation method. It was found that entropy generation increased with the Reynolds number, the magnetic parameter and the dimensionless group parameter while it decreased with increasing values of Prandtl numbers. Motsa et al. [200] used the spectral relaxation method and spectral quasi-linearisation method to solve the highly nonlinear equations that describe the unsteady heat transfer in a nanofluid over a permeable stretching or shrinking surface. They concluded that the spectral quasi-linearisation method converges faster than the spectral relaxation method, while the spectral relaxation method is more accurate than the spectral quasi-linearisation method.

Rao and Rao [201] studied the steady flow of heat and mass transfer with the effect of

thermal dispersion. The solution was obtained using the spectral relaxation method. Results showed that the temperature and concentration profiles increase with an increase in Weissenberg number and power law index. Makanda and Sibanda [202] considered the impact of radiation, partial slip, cross-diffusion and viscous dissipation on Casson fluid flow in a non-Darcy porous medium. The spectral relaxation method was used to solve the flow equations. It is shown that increasing the Casson parameter decrease the fluid flow. Increasing the velocity slip parameter lead to enhance the flow while increasing the thermal and concentration slip parameters lead to reduce temperature and concentration levels respectively.

Rao and Rao [203] studied the steady flow of heat and mass transfer of power-law fluid with the impact of thermal dispersion. The nonlinear equations were solved using spectral relaxation method. It is shown that the heat and mass transfer rate increase for shear-thinning fluids compared to Newtonian fluid and shear thickening fluids. Shateyi [193] investigated magnetohydrodynamic flow and heat transfer of a Maxwell fluid using a spectral relaxation method. It was found that velocities depend strongly on the magnetic and the viscoelastic parameters while the temperature varied significantly with the Prandtl number, the magnetic parameter, the Eckert number and the heat source parameter. RamReddy [204] studied steady flow on heat and mass transfer along an exponentially stretching surface with Soret-Dufour effects. The spectral relaxation method was used to obtain the numerical solutions. It was found that the rates of heat and mass transfer were lower in the MHD Newtonian fluid compared to the Newtonian fluid without magnetic field.

1.5.3 The Spectral Quasi-linearization Method

The spectral quasi-linearization method has been used to solve a number of fluid mechanics problems (see Motsa et al. [205], Motsa and Shateyi [206]; and Awad et al [207]). In using the SQLM, the nonlinear equations are linearized using a generalization of the Newton-Raphson quasi-linearization method (QLM), developed by Bellman and Kalaba

[189], and integrated using the Chebyshev spectral collocation method. The advantage of using this method as suggested in the literature is that the SQLM gives good convergence and accuracy.

In the literature, numerous spectral quasi-linearization techniques have been used to solve systems of nonlinear ordinary and partial differential equations that arise in fluid flow models. RamReddy and Pradeepa [208] investigated the flow of a micropolar fluid along a permeable vertical plate in a porous medium. The spectral quasi-linearization method was used to solve the model equations. It was observed that the wall couple stress decreases, but the skin friction, heat and mass transfer rates increase with an increase in the Darcy parameters in both cases of flow with suction and injection. RamReddy and Pradeepa [209] presented a study of micropolar fluid flow along a vertical plate in a porous medium. The transformed flow equations were solved numerically using the spectral quasi-linearization method. It was shown that in both aiding and opposing flow cases, the skin friction coefficient, heat transfer rate, velocity, and concentration are decreased, whilst the wall couple stress and temperature increased with the Darcy parameter.

Oyelakin et al. [210] investigated the effects of thermal radiation, heat and mass transfer on the unsteady magnetohydrodynamic flow of Casson nanofluid. The flow equations were solved using the spectral quasi-linearisation method. It was noted that increasing the flow unsteadiness reduces the fluid momentum, thermal and nanoparticle volume fraction profiles.

1.6 The Objectives of The Study

The main aim of this study is use recent linearization and spectral techniques to solve nonlinear mathematical models that describe fluid flows and heat and mass transfer problems. Through the solution of systems of differential equations of varying complexity we test the accuracy, the convergence rates and robustness of these techniques. The flows are assumed

to take place in different flow configurations and with different boundary conditions. The objectives are to solve and analyze the unsteady fluid flows, and to determine how certain fluid and physical parameters affect heat and mass transfer in nanofluid flow through saturated porous media.

1.7 Thesis Layout

This study consists of seven chapters, Chapters 2 - 6 consist of published papers that form the main body of the study while Chapters 1 and 7 form the introduction and conclusion, respectively.

In Chapter 2, we study and obtain numerical solutions for unsteady nanofluid flow along an inclined cylinder permeated by an electromagnetic field. The objective is to investigate the influence of Ohmic and viscous dissipation, a chemical reaction and thermo-diffusion on heat and mass transfer coefficients. Two different types of nanoparticles, namely, copper and silver are used with water as the base fluid. Theoretical studies suggest that nanoparticles enhance the thermal conductivity and the heat transfer coefficient compared to the base fluid. The system of model equations are solved numerically using the spectral local linearization method.

In Chapter 3, we present a modified version of the model studied in Chapter 2 by analyzing the impulsive flow on heat and mass transfer along a vertically stretching cone using nanofluid. The effects of viscous dissipation, internal heat generation, and the chemical reaction have been taken into consideration. The fluid contains two types of nanoparticles, namely, copper and titanium dioxide with water used as the base fluid. The spectral local linearization method was used to get the numerical solution to the flow model equations.

In Chapter 4, we find a numerical solution to the unsteady incompressible non-Newtonian nanofluid represented by an Oldroyd-B nanofluid over a stretching surface. This study

assumes that the nanoparticle volume fraction flux at the boundary surface vanishes (see Kuznetsov and Nield [211]). The motivation is to investigate the effects of the Deborah number, Brownian motion and thermophoresis parameters on the flow. The spectral relaxation and quasi-linearization methods are used to obtain solutions to the transport equations and to show the significance of the physical and fluid parameters.

In Chapter 5, we extend the study by Nandy and Mahapatra [212] by using the revised nanofluid model in Chapter 4. We present the study of magnetohydrodynamic stagnation point flow of a nanofluid along a permeable stretching flat surface. The aim of the study is to determine the effects of important physical parameters, such as, buoyancy forces, Brownian motion, thermophoresis, internal heat source/sink and the partial slip boundary condition on heat and mass transfer. The conservation equations are solved using the spectral relaxation method.

In Chapter 6, we extend the ideas in Chapter 5 by considering a binary nanofluid, such as salty water (Kuznetsov and Nield [213]). We consider the unsteady nanofluid flow over a permeable moving surface in a magnetic field. We present the impact of inertia, thermal radiation, Brownian motion, thermophoresis, thermo-diffusion, diffusion-thermo and chemical reaction on the flow problems. The equations that describe the flow are solved numerically using the spectral relaxation method.

In Chapter 7, we present the major results and conclusions to this study we give recommendations for further studies.

Chapter 2

Thermo-diffusion effects on unsteady mixed convection in a magneto-nanofluid flow along an inclined cylinder with a heat source, ohmic and viscous dissipation

In this Chapter, we investigate unsteady fluid flow containing two types of nanoparticles namely, copper and silver nanoparticles. These increase the thermal conductivity of the fluid. The nanoparticle volume fraction flux is assumed to be not actively controlled at the boundary surface. This flow is along an inclined cylinder, with an electromagnetic field and a chemical reaction. The objectives are to investigate the significance of Ohmic and viscous dissipation, and thermo-diffusion effects on the flow. The change in fluid properties with the physical properties of the skin friction, heat and mass transfer coefficient is discussed. A unique feature of the study is the use of the spectral local linearization method to obtain solutions to the flow equations.

Copyright © 2016 American Scientific Publishers
All rights reserved
Printed in the United States of America

Journal of
Computational and Theoretical Nanoscience
Vol. 13, 1670–1684, 2016

RESEARCH ARTICLE

Thermo-Diffusion Effects on Unsteady Mixed Convection in a Magneto-Nanofluid Flow Along an Inclined Cylinder with a Heat Source, Ohmic and Viscous Dissipation

S. M. S. Ahamed, S. Mondal*, and P. Sibanda

School of Mathematics, Statistics and Computer Science, University of KwaZulu-Natal, Private Bag X01 Scottsville 3209, Pietermaritzburg, South Africa

We present a numerical solution of the unsteady nanofluid boundary-layer flow on an inclined cylinder. We investigate heat and mass transfer in the presence of a chemical reaction, viscous and Ohmic dissipation due to applied transverse magnetic and electric fields. In this study two different nanoparticles; namely copper and silver are considered with water as the base fluid. The model equations are solved using the spectral local linearization method. Results for the skin friction coefficient, the wall temperature and mass gradients as well as the velocity, temperature and concentration profiles have been obtained for various physical parameters values. The results have been benchmarked with previously published results.

Keywords: Ohmic Heating, Viscous Dissipation, Electromagnetic Flow, Thermo-Diffusion, Nanofluid, Chemical Reaction.

1. INTRODUCTION

The steady and unsteady boundary layer flow, and heat and mass transfer over a stretching or shrinking cylinder has several applications in engineering processes that involve both metal and polymer sheets. Important relevant engineering applications can be found in polymer processing, melt-spinning, hot rolling, paper production, wire and glass-fiber production, etc. In these processes, the quality of the final product depends on the rate of cooling and the rate of stretching or shrinking.[1] The flow due to a shrinking plane was first studied by Miklavčič and Wang.[14] Researchers who have studied flow owing to a stretching cylinder include, among others, Wang,[2] Ishak et al.[3] Wang and Ng,[4] Wang,[5] Ishak et al.,[6] and Fang et al.[7] The problem of the unsteady sticky influx as a consequence of an expanding, stretching cylinder provided an exact similarity solution to the Navier-Stokes equations. Fang et al.[8] obtained numerical solutions of unsteady flow over a stretching cylinder. The numerical solutions for a steady state stagnation point flow of an inviscid and incompressible fluid along a shrinking cylinder were presented by Lok and Pop.[9] Zaimia et al.[10] investigated the behaviour of the unsteady viscous flow over a shrinking cylinder with suction.

Choi[27] proposed the concept of a "nanofluid" by suspending solid nanoparticles in a base fluid in order to address challenges in thermal engineering. Currently nanofluids are made by dispersing nanometer-sized solid particles, rods or tubes in traditional heat transfer fluids such as water or oil. Investigations in the past decade have shown that nanofluids exhibit significantly enhanced thermophysical properties compared to base fluids. The full impact of nanofluid technology is still to be fully realized but is nonetheless expected to be significant in the coming years, Sudhan et al.[37]

Abu-Nada and Chamkha[23] studied mixed convection flow in an inclined square enclosure filled with an alumina-water nanofluid. Oztop and Abu-Nada[24] studied natural convection in a rectangular enclosure filled with a nanofluid containing copper, alumina, and titanium nanoparticles. They concluded that the highest value of heat transfer is obtained using copper nanoparticles.

The study of magnetic field effects has important applications in physics, chemistry and engineering. Many types of industrial equipment, such as magnetohydrodynamic (MHD) generators, pumps and bearings are affected by the interaction between the electrically conducting fluid and a magnetic field. Many studies in the literature have been made in relation to these applications. One of the basic and important problems in this area is the hydro-magnetic behaviour of boundary layers along fixed or moving surfaces. MHD boundary layers are found in various technical systems employing liquid metals and plasma flow with transverse magnetic fields.[29]

*Author to whom correspondence should be addressed.

 1546-1955/2016/13/1670/015 doi:10.1166/jctn.2016.5097

This study is focused on MHD nanofluid flow and heat transfer due to a stretching cylinder. A similar study has been made by Ashorynejad et al.[29] who found, *inter alia*, that the heat transfer coefficient increased with increases in the Reynolds number or the nanoparticle volume fraction. They also found that choosing copper nanoparticles for small values of the magnetic parameter, and alumina for large values of the magnetic parameter led to the highest system cooling performance.

The aim of this work is to investigate the two-dimensional unsteady incompressible viscous boundary layer flow with two types of nanoparticles; namely copper and silver nanoparticles with water as the base fluid. The flow is along an inclined cylinder with an applied transverse magnetic field and a chemical reaction. The nonlinear momentum, heat and mass transfer equations are solved numerically using a spectral local linearization method SLLM (see Motsa).[36]

2. MATHEMATICAL FORMULATIONS

Consider the two-dimensional laminar unsteady boundary layer flow of an viscous incompressible, electrically conducting nanofluid over an inclined cylinder of radius a embedded in a porous medium as shown in Figure 1. The flow region is exposed to a transverse magnetic field $\vec{B} = (0, B_0, 0)$ and a uniform electric field $\vec{E} = (0, 0, -E_0)$. It has been suggested in the literature that application of such electric and magnetic fields stabilizes the boundary layer flow.[22] The electric and magnetic fields satisfy Maxwell's equations $\nabla \cdot \vec{B} = 0$ and $\nabla \times \vec{E} = 0$. If the magnetic field is weak, the electric and magnetic fields obey Ohm's law $\vec{J} = \sigma(\vec{E} + \vec{q} \times \vec{B})$, where $\vec{J}$ is the Joule current, σ the magnetic permeability and $\vec{q}$ is the fluid velocity. It is assumed that the cylinder surface has temperature T_w and concentration C_w which depend on x. The uniform ambient fluid temperature and concentration are T_∞ and C_∞, respectively, where $T_w > T_\infty$ for the heated cylinder. The cylinder velocity is $u = u_w(x/\ell)$ where u_w and ℓ are the surface velocity and the characteristic length of the cylinder surface, respectively. Under these assumptions, the boundary layer equations governing the flow can be written as (see Refs. [11, 12, and 13]);

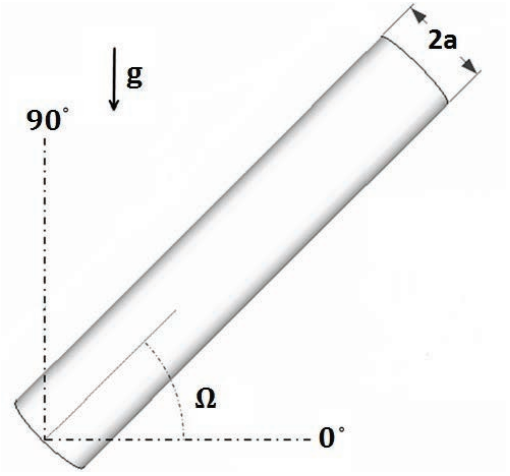

Fig. 1. Geometry and the coordinate system.

$$\frac{\partial u}{\partial x} + \frac{1}{r}\frac{\partial}{\partial r}(rv) = 0 \tag{1}$$

$$\frac{\partial u}{\partial t} + u\frac{\partial u}{\partial x} + v\frac{\partial u}{\partial r} = \frac{\nu_{nf}}{r}\frac{\partial}{\partial r}\left(r\frac{\partial u}{\partial r}\right) + \frac{\sigma}{\rho_{nf}}(E_0 B_0 - B_0^2 u) + \frac{(\rho\beta)_{nf}}{\rho_{nf}} g(T - T_\infty)\cos\Omega \tag{2}$$

$$\frac{\partial T}{\partial t} + u\frac{\partial T}{\partial x} + v\frac{\partial T}{\partial r} = \frac{\alpha_{nf}}{r}\frac{\partial}{\partial r}\left(r\frac{\partial T}{\partial r}\right) + \frac{\mu_{nf}}{(\rho C_p)_{nf}}\left(\frac{\partial u}{\partial r}\right)^2 + \frac{\sigma}{(\rho C_p)_{nf}}(B_0 u - E_0)^2 \tag{3}$$

$$\frac{\partial C}{\partial t} + u\frac{\partial C}{\partial x} + v\frac{\partial C}{\partial r} = \frac{D_m}{r}\frac{\partial}{\partial r}\left(r\frac{\partial C}{\partial r}\right) + \frac{D_S}{r}\frac{\partial}{\partial r}\left(r\frac{\partial T}{\partial r}\right) - k_0(C - C_\infty) \tag{4}$$

subject to the boundary conditions

$$\begin{aligned} &u = U, \quad v = 0, \quad T = T_w, \quad C = C_w \quad \text{at } r = a, \quad t \geq 0 \\ &u \to 0, \quad T \to T_\infty, \quad C \to C_\infty, \quad \text{as } r \to \infty, \quad t \geq 0 \end{aligned} \tag{5}$$

The corresponding initial conditions are

$$u = v = 0, \quad T = T_\infty, \quad C = C_\infty \quad \text{at } t < 0 \text{ for all } x \text{ and } r$$

where t is the time, u and v are the velocity components in the x and r directions respectively, T is the fluid temperature, C is the fluid concentration, g is the gravitational acceleration, Ω is the inclination angle, D_m is the diffusivity of the concentration, D_S is the Soret diffusivity and k_0 is the chemical reaction parameter. The effective dynamic viscosity is μ_{nf}; the kinematic viscosity is ν_{nf}; the thermal diffusivity is α_{nf}; the heat capacity is $(\rho C_p)_{nf}$; the density of fluid is ρ_{nf}; the thermal expansion coefficient is $(\rho\beta)_{nf}$ and the thermal conductivity is k_{nf} of the nanofluid. (see Ref. [24]). The other parameters are

$$\begin{aligned} \mu_{nf} &= \frac{\mu_f}{(1-\phi)^{2.5}}, \quad \nu_{nf} = \frac{\mu_{nf}}{\rho_{nf}}, \quad \alpha_{nf} = \frac{k_{nf}}{(\rho C_p)_{nf}} \\ (\rho C_p)_{nf} &= (1-\phi)(\rho C_p)_f + \phi(\rho C_p)_s \\ \rho_{nf} &= (1-\phi)\rho_f + \phi\rho_s \\ (\rho\beta)_{nf} &= (1-\phi)(\rho\beta)_f + \phi(\rho\beta)_s \\ \frac{k_{nf}}{k_f} &= \frac{(k_s + 2k_f) - 2\phi(k_f - k_s)}{(k_s + 2k_f) + \phi(k_f - k_s)} \end{aligned} \tag{6}$$

where ϕ is the nanoparticle volume fraction, μ_f is the dynamic viscosity of the base fluid, C_p the heat capacity of base fluid, ρ_f and ρ_s are the densities of the base fluid and nanoparticles volume fractions, respectively. β_f is the base fluid thermal expansion coefficient, k_f and k_s are the base fluid and nanoparticles thermal conductivity respectively. It is convenient to introduce the stream function ψ defined as

$$u = \frac{1}{r}\frac{\partial \psi}{\partial r}, \quad v = -\frac{1}{r}\frac{\partial \psi}{\partial x} \tag{7}$$

Following,[25] similarity transformations may be chosen as

$$\eta = \left[\frac{u_w}{\nu_f \ell \xi}\right]^{1/2}\left(\frac{r^2-a^2}{2a}\right), \quad f(\xi,\eta) = \frac{\psi}{ax}\left[\frac{\ell}{\nu_f u_w \xi}\right]^{1/2}$$
$$\xi = 1-e^{-\tau}, \quad \tau = \frac{u_w}{\ell}t, \quad T - T_\infty = (T_w - T_\infty)\theta(\xi,\eta)$$
$$C - C_\infty = (C_w - C_\infty)\Phi(\xi,\eta), \quad T_w = T_\infty + T_0\left(\frac{x}{\ell}\right)^m$$
$$C_w = C_\infty + C_0\left(\frac{x}{\ell}\right)^m \tag{8}$$

where ν_f is the kinematic viscosity of the base fluid, T_0 and C_0 are characteristic of temperature and concentration, respectively. Substituting the transformations of Eq. (8) into Eqs. (1)–(4) along with the boundary conditions (5), we get

$$\frac{1}{\phi_1}((1+2\eta K\sqrt{\xi})f'')' + \xi\left[ff'' - (f')^2 + \frac{\mathrm{Mn}}{\phi_2}(E_1 - f') + \frac{\phi_3}{\phi_2}\lambda\theta\cos(\Omega)\right] = (1-\xi)\left[\xi\frac{\partial f'}{\partial \xi} - \frac{1}{2}\eta f''\right] \tag{9}$$

$$\frac{k_{nf}}{k_f\phi_4 Pr}((1+2\eta K\sqrt{\xi})\theta')' + \xi\left[f\theta' - mf'\theta + \frac{MnEc}{\phi_4}(E_1 - f')^2\right] + \frac{Ec}{\phi_5}(1+2\eta K\sqrt{\xi})(f'')^2 = (1-\xi)\left[\xi\frac{\partial \theta}{\partial \xi} - \frac{1}{2}\eta\theta'\right] \tag{10}$$

$$\frac{1}{Sc}((1+2\eta K\sqrt{\xi})\Phi')' + \xi[f\Phi' - (mf' + \gamma)\Phi] + \frac{Sr}{Sc}((1+2\eta K\sqrt{\xi})\theta')' = (1-\xi)\left[\xi\frac{\partial \Phi}{\partial \xi} - \frac{1}{2}\eta\Phi'\right] \tag{11}$$

along with the boundary conditions

$$f(\xi,0) = 0, \quad f'(\xi,0) = 1, \quad \theta(\xi,0) = 1, \quad \Phi = 1, \quad \xi \in [0,1]$$
$$f'(\xi,\infty) \to 0, \quad \theta(\xi,\infty) \to 0, \quad \Phi(\xi,\infty) \to 0, \quad \xi \in [0,1] \tag{12}$$

where

$$\phi_1 = (1-\phi)^{2.5}\left[1 - \phi + \phi\left(\frac{\rho_s}{\rho_f}\right)\right]$$
$$\phi_2 = 1 - \phi + \phi\left(\frac{\rho_s}{\rho_f}\right)$$
$$\phi_3 = 1 - \phi + \phi\frac{(\rho\beta)_s}{(\rho\beta)_f}, \quad \phi_4 = 1 - \phi + \phi\frac{(\rho C_p)_s}{(\rho C_p)_f}$$
$$\phi_5 = (1-\phi)^{2.5}\left[1 - \phi + \phi\frac{(\rho C_p)_s}{(\rho C_p)_f}\right] \tag{13}$$

The primes denote differentiation with respect to η. The important parameters of primary interest are the transverse curvature K (when K approaches zero, the results for the flat plate can be recovered), the magnetic field Mn, the local electric E_1, mixed convection λ (with $\lambda > 0$ corresponding to a heated inclined cylinder; assisting flow, $\lambda < 0$ corresponding to a cooled inclined cylinder; opposing flow and $\lambda = 0$ corresponding to forced convection flow) ($T_w = T_\infty$), local Grashof number Gr_x, local Reynolds number Re_x, Prandtl number Pr, Eckret number Ec, Schmidt number Sc, chemical reaction γ and Soret number Sr, given respectively, by

$$K = \left[\frac{\nu_f \ell}{a^2 u_w}\right]^{1/2}, \quad \mathrm{Mn} = \frac{\sigma B_0^2 \ell}{\rho_f u_w}, \quad E_1 = \frac{E_0 \ell}{B_0 u_w x}$$
$$\lambda = \frac{Gr_x}{Re_x^2}, \quad Gr_x = \frac{g\beta_f(T_w - T_\infty)x^3}{\nu_f^2}, \quad Re_x = \frac{u_w x^2}{\nu_f \ell}$$
$$Pr = \frac{\mu_f (C_p)_f}{k_f}, \quad Ec = \frac{(u_w x)^2}{(C_p)_f (T_w - T_\infty)\ell^2}, \quad Sc = \frac{\nu_f}{D_m}$$
$$\gamma = \frac{k_0 \ell}{u_w}, \quad Sr = \frac{D_S(T_w - T_\infty)}{D_m(C_w - C_\infty)} \tag{14}$$

We note that when $K = \lambda = E_1 = 0$ and $\xi = 1$, the momentum boundary layer equation is partially decoupled from the energy and species equations. Integrating Eq. (9) with respect to η over the interval $[0, \eta]$ subject to boundary conditions (2) gives the exact solution

$$f(1,\eta) = \frac{1 - \exp(-\kappa\eta)}{\kappa} \tag{15}$$

where κ is a parameter associated with the nanoparticle volume fraction, the magnetic field parameter, the fluid density and the nanoparticle density. This satisfies the equation

$$\kappa = \sqrt{\phi_1\left(1 + \frac{\mathrm{Mn}}{\phi_2}\right)} \tag{16}$$

When $\phi = 0$, Eq. (16) reduces to $\kappa = \sqrt{1 + \mathrm{Mn}}$, the result reported by Vajravelu et al.[35] for clear fluids. The physical quantities of engineering interest in heat and mass transport problems are the skin friction coefficient C_f, the local Nusselt number Nu_x and the local Sherwood number

Sh_x. These parameters respectively characterize the surface drag, wall heat and mass transfer rates, which are defined as

$$C_f = \frac{2\tau_w}{\rho_f u_\infty^2}, Nu_x = \frac{xq_w}{k_f(T_w - T_\infty)}, Sh_x = \frac{xq_m}{D_m(C_w - C_\infty)} \tag{17}$$

where τ_w is the shear stress at the surface of the cylinder, q_w and q_m are the heat and mass flux from the surface of the cylinder respectively, which are given by

$$\tau_w = -\mu_{nf}\left(\frac{\partial u}{\partial r}\right)_{r=a}, \quad q_w = -k_{nf}\left(\frac{\partial T}{\partial r}\right)_{r=a}$$
$$q_m = -D_m\left(\frac{\partial C}{\partial r}\right)_{r=a} \tag{18}$$

Using (6) into (17) and (20), we gain

$$(1-\phi)^{2.5}\sqrt{Re_x\xi}C_f = -2f''(\xi,0)$$
$$\frac{k_f}{k_{nf}}\sqrt{\frac{\xi}{Re_x}}Nu_x = -\theta'(\xi,0) \tag{19}$$
$$\sqrt{\frac{\xi}{Re_x}}Sh_x = -\Phi'(\xi,0)$$

3. METHOD OF SOLUTION

The spectral local linearization method was used to solve the system of non-similar Eqs. (9)–(11). In the method, the Eqs. (9)–(11) are linearized using a Gauss Seidel approach. In the frame work of SLLM, we obtain the following iterative scheme

$$f'_{r+1} = u_{r+1} \tag{20}$$
$$(1+2\eta K\sqrt{\xi})u''_{r+1} + a_{1,r}u'_{r+1} + a_{2,r}u_{r+1} + a_{3,r} = a_{4,r}\frac{\partial u_{r+1}}{\partial \xi} \tag{21}$$
$$\frac{k_{nf}}{k_f}\frac{1}{Pr}(1+2\eta K\sqrt{\xi})\theta''_{r+1} + b_{1,r}\theta'_{r+1} + b_{2,r}\theta_{r+1} + b_{3,r} = b_{4,r}\frac{\partial \theta_{r+1}}{\partial \xi} \tag{22}$$
$$(1+2\eta K\sqrt{\xi})\Phi''_{r+1} + c_{1,r}\Phi'_{r+1} + c_{2,r}\Phi_{r+1} + c_{3,r} = c_{4,r}\frac{\partial \Phi_{r+1}}{\partial \xi} \tag{23}$$

The boundary conditions for the above iteration scheme are

$$f_{r+1}(\xi,0) = 0, \quad u_{r+1}(\xi,0) = 1,$$
$$\theta_{r+1}(\xi,0) = 1, \quad \Phi_{r+1}(\xi,0) = 1$$
$$u_{r+1}(\xi,\infty) \to 0, \quad \theta_{r+1}(\xi,\infty) \to 0, \tag{24}$$
$$\Phi_{r+1}(\xi,\infty) \to 0$$

where

$$a_{1,r} = 2K\sqrt{\xi} + \phi_1\left[\frac{1}{2}(1-\xi)\eta + \xi f_r\right]$$
$$a_{2,r} = -\phi_1\xi\left[\frac{\mathrm{Mn}}{\phi_2} + 2u_r\right]$$
$$a_{3,r} = \phi_1\xi\left[\frac{\mathrm{Mn}E_1}{\phi_2} + u_r^2 + \frac{\phi_3}{\phi_2}\lambda\theta_r\cos(\Omega)\right] \tag{25}$$
$$a_{4,r} = \phi_1\xi(1-\xi)$$
$$b_{1,r} = \frac{k_{nf}}{k_f}\frac{1}{Pr}(2K\sqrt{\xi}) + \phi_4\left[\frac{1}{2}(1-\xi)\eta + \xi f_{r+1}\right]$$
$$b_{2,r} = -m\phi_4\xi u_{r+1}$$
$$b_{3,r} = \xi\mathrm{Mn}Ec(u_{r+1} - E_1)^2 + \frac{\phi_4}{\phi_5}(1+2\eta K\sqrt{\xi})Ecu_r'^2 \tag{26}$$
$$b_{4,r} = \phi_4\xi(1-\xi)$$

$$c_{1,r} = 2K\sqrt{\xi} + Sc\left[\frac{1}{2}(1-\xi)\eta + \xi f_{r+1}\right]$$
$$c_{2,r} = -Sc\xi[mu_{r+1} + \gamma] \tag{27}$$
$$c_{3,r} = Sr((1+2\eta K\sqrt{\xi})\theta'_{r+1})'$$
$$c_{4,r} = Sc\xi(1-\xi)$$

In the above equations, indices r and $r+1$ denote the previous and current iteration levels, respectively. Starting from an initial approximation denoted by f_0, u_0, θ_0, and φ_0, Eqs. (9)–(11) are solved iteratively for $f_{r+1}(\xi,\eta)$, $u_{r+1}(\xi,\eta)$, $\theta_{r+1}(\xi,\eta)$, and $\Phi_{r+1}(\xi,\eta)$ $(r = 0,1,2,\ldots)$. The Eqs. (9)–(11) are discretized using the Chebyshev spectral collocation method in the η direction while the discretization in ξ direction is done using the implicit finite difference method. We thus obtain

$$\mathbf{A}_1 f_{r+1}^{n+1} = u_r^n \tag{28}$$
$$\mathbf{A}_2 u_{r+1}^{n+1} = \mathbf{B}_2 u_{r+1^n} + \mathbf{K}_2 \tag{29}$$
$$\mathbf{A}_3\theta_{r+1}^{n+1} = \mathbf{B}_3\theta_{r+1}^{n} + \mathbf{K}_3 \tag{30}$$
$$\mathbf{A}_4\Phi_{r+1}^{n+1} = \mathbf{B}_4\Phi_{r+1}^{n} + \mathbf{K}_4 \tag{31}$$

where

$$\mathbf{A}_1 = \mathbf{D} \tag{32}$$
$$\mathbf{A}_2 = \left[\frac{1}{2}([(1+2\eta K\sqrt{\xi})]_{\mathbf{d}}\mathbf{D}^2 + [a_{1,r}^{n+(1/2)}]_{\mathbf{d}}\mathbf{D} + [a_{2,r}^{n+(1/2)}]_{\mathbf{d}}) - \frac{a_{4,r}^{n+(1/2)}}{\Delta\xi}\mathbf{I}\right]$$
$$\mathbf{B}_2 = \left[-\frac{1}{2}\left([(1+2\eta K\sqrt{\xi})]_{\mathbf{d}}\mathbf{D}^2 + [a_{1,r}^{n+(1/2)}]_{\mathbf{d}}\mathbf{D} + [a_{2,r}^{n+(1/2)}]_{\mathbf{d}}\right) - \frac{a_{4,r}^{n+(1/2)}}{\Delta\xi}\mathbf{I}\right]$$

RESEARCH ARTICLE

$$\mathbf{K}_2 = -a_{3,r}^{n+(1/2)} \tag{33}$$

$$\mathbf{A}_3 = \left[\frac{1}{2}\left(\frac{k_{nf}}{k_f}\frac{1}{Pr}[(1+2\eta K\sqrt{\xi})]_{\mathbf{d}}\mathbf{D}^2 + [b_{1,r}^{n+(1/2)}]_{\mathbf{d}}\mathbf{D} + [b_{2,r}^{n+(1/2)}]_{\mathbf{d}}\right) - \frac{b_{4,r}^{n+(1/2)}}{\Delta\xi}\mathbf{I}\right]$$

$$\mathbf{B}_3 = \left[-\frac{1}{2}\left(\frac{k_{nf}}{k_f}\frac{1}{Pr}[(1+2\eta K\sqrt{\xi})]_{\mathbf{d}}\mathbf{D}^2 + [b_{1,r}^{n+(1/2)}]_{\mathbf{d}}\mathbf{D} + [b_{2,r}^{n+(1/2)}]_{\mathbf{d}}\right) - \frac{b_{4,r}^{n+(1/2)}}{\Delta\xi}\mathbf{I}\right]$$

$$\mathbf{K}_3 = -b_{3,r}^{n+(1/2)} \tag{34}$$

$$\mathbf{A}_4 = \left[\frac{1}{2}([(1+2\eta K\sqrt{\xi})]_{\mathbf{d}}\mathbf{D}^2 + [c_{1,r}^{n+(1/2)}]_{\mathbf{d}}\mathbf{D} + [c_{2,r}^{n+(1/2)}]_{\mathbf{d}}) - \frac{c_{3,r}^{n+(1/2)}}{\Delta\xi}\mathbf{I}\right]$$

$$\mathbf{B}_4 = \left[-\frac{1}{2}([(1+2\eta K\sqrt{\xi})]_{\mathbf{d}}\mathbf{D}^2 + [c_{1,r}^{n+(1/2)}]_{\mathbf{d}}\mathbf{D} + [c_{2,r}^{n+(1/2)}]_{\mathbf{d}}) - \frac{c_{3,r}^{n+(1/2)}}{\Delta\xi}\mathbf{I}\right]$$

$$\mathbf{K}_4 = -c_{3,r}^{n+(1/2)} \tag{35}$$

where $\mathbf{I}$ is an $(N+1)\times(N+1)$ identity matrix, and $[(\cdot)]_{\mathbf{d}}$ are diagonal matrices of order $(N+1)\times(N+1)$.

In applying the SLLM the computational domain of extent $L=30$ is chosen in the η-direction. Through numerical experimentation, this value is found to give accurate results for all the selected physical parameters used in the generation of results. Increasing the value of η did not change the results to a significant extent. The number of collocation points used in the spectral method discretization was $N_x = 100$ in all cases. We note that the SLLM algorithm is based on the computation of the value of some quantity, say F_{r+1}^{n+1}, at each time step. This is achieved by iterating using the local linearization method using a known value at the previous time step n as initial approximation. The calculations are carried until some desired tolerance level, ε, is attained. In this study, the tolerance level was set to be $\varepsilon = 10^{-6}$. The tolerance level is defined as the maximum values of the infinity norm of the difference between the values of the calculated quantities, that is

$$\max\{\|f_{r+1}^{n+1} - f_r^{n+1}\|_\infty, \|\theta_{r+1}^{n+1} - \theta_r^{n+1}\|_\infty, \|\Phi_{r+1}^{n+1} - \Phi_r^{n+1}\|_\infty\} < \varepsilon$$

To ensure the accuracy of the results, a sufficiently small step size $\Delta\xi$ was used. The step size was chosen to be small enough such that further reduction did not change the results for the flow properties of interest.

4. RESULTS AND DISCUSSION

The unsteady governing Eqs. (1)–(4) with boundary conditions Eq. (5) were simplified using the similarity transformations (8). The numerical solutions of the reduced nonlinear differential Eqs. (9)–(11) were obtained using the spectral local linearization method (SLLM), see Motsa[36] for a detailed description of this method.

The questions answered in this study relate to the significance of the various physical parameters on the heat and mass transfer properties and the behaviour of the fluid. Results were obtained for various physical parameters such as the nanoparticle volume fraction, the transverse curvature, magnetic field, the local electric, the Eckret number, the chemical reaction and the Soret number. The default parameter values (unless otherwise stated differently) are as follows; $\phi = 0.1$, $K = 0.1$, $Mn = 0.1$, $E_1 = 0.1$, $\lambda = 0.1$, $\Omega = \pi/4$, $m = 2$, $Ec = 0.4$, $Sc = 1$, $\gamma = 0.1$ and $Sr = 0.2$.[30–34]

The results are presented in Figures 2–14 and Tables II–VI. Two types of nanoparticles, namely copper (Cu) and silver (Ag) with water as the base fluid are considered. The thermophysical properties of the base fluid and the nanoparticles are listed in Table I (see Oztop and Abu-Nada).[24]

To determine the accuracy of our numerical method, a comparison of the skin friction coefficient $-f''(0,1)$ with previous work by Vajravelu et al.[35] for different values of K and Mn is given in Table II when $\xi = 1$, $\phi = 0$, $\lambda = 0$, $E_1 = 0$ and $\Omega = 0$. Table III shows a comparison of the skin friction coefficient $-f''(1,0)$ for various nanoparticle volume fraction values ϕ and the magnetic field parameter Mn when $K = E_1 = \lambda = 0$ and $\Omega = 0$, and $\xi = 1$. Comparison of the wall temperature gradient $-\theta'(1,0)$ for various values of Pr when $K = \mathrm{Mn} = E_1 = \lambda = \Omega = Ec = \phi = 0$ and $m = 1$ is given in Table IV. The comparison of the current results is found, in all instances, to be in a good agreement with existing literature values.

Table V shows the skin fraction coefficient $-f''(\xi,0)$ for both Cu-water and Ag-water nanofluids for various values of K, Mn and ϕ when $E_1 = 0.1$, $\lambda = 0.1$, $\Omega = \pi/4$, $Pr = 7.0$, $m = 2$, $Ec = 0.4$, $Sc = 1$, $\gamma = 0.1$ and $Sr = 0.2$. The skin friction coefficient increases with ϕ for any value of ξ. Again, the skin friction coefficient increases with increasing K, Mn only for $\xi = 0.5$ and 1.0 due to a Lorentz drag force which enhances the values of skin friction coefficient.

Table VI displays the computed skin fraction coefficient for both Cu-water and Ag-water nanofluids for various values of E_1 and λ when $K = 0.1$, $\mathrm{Mn} = 0.1$, $\Omega = \pi/4$, $Pr = 7.0$, $m = 2$, $Ec = 0.4$, $Sc = 1$, $\gamma = 0.1$, $Sr = 0.2$ and $\phi = 0.1$. We note that there is no change in the value of the skin friction for any value of E_1 and λ when $\xi = 0.0$. However, the skin friction coefficient decreases with increasing E_1 and λ.

The evolution of the horizontal velocity (f'), temperature (θ) and concentration (Φ) profiles is shown in Figure 2

RESEARCH ARTICLE

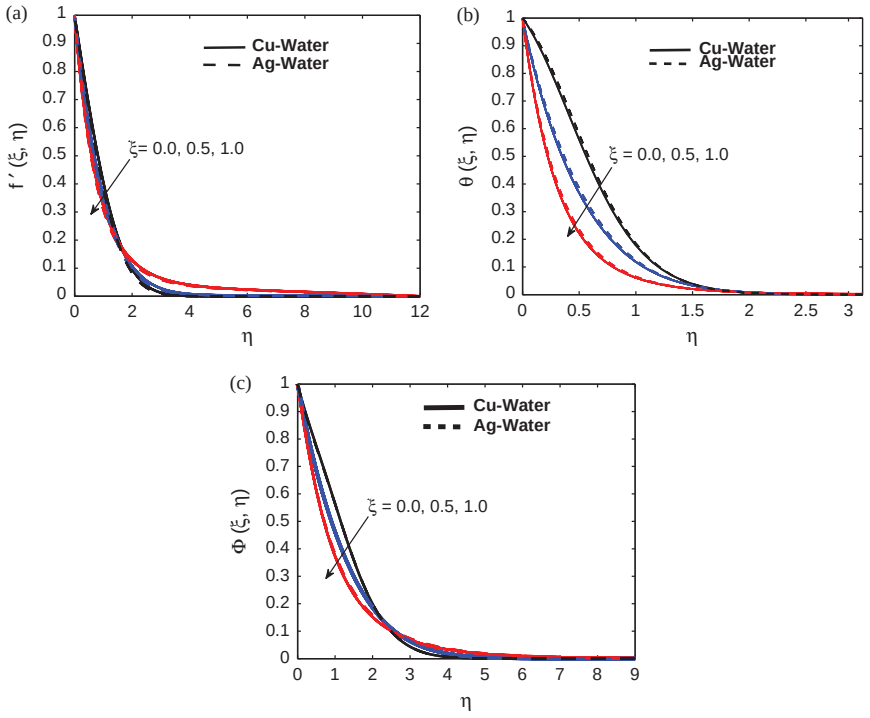

Fig. 2. Effects of the dimensionless time ξ on (a) horizontal velocity, (b) temperature and (c) concentration profiles.

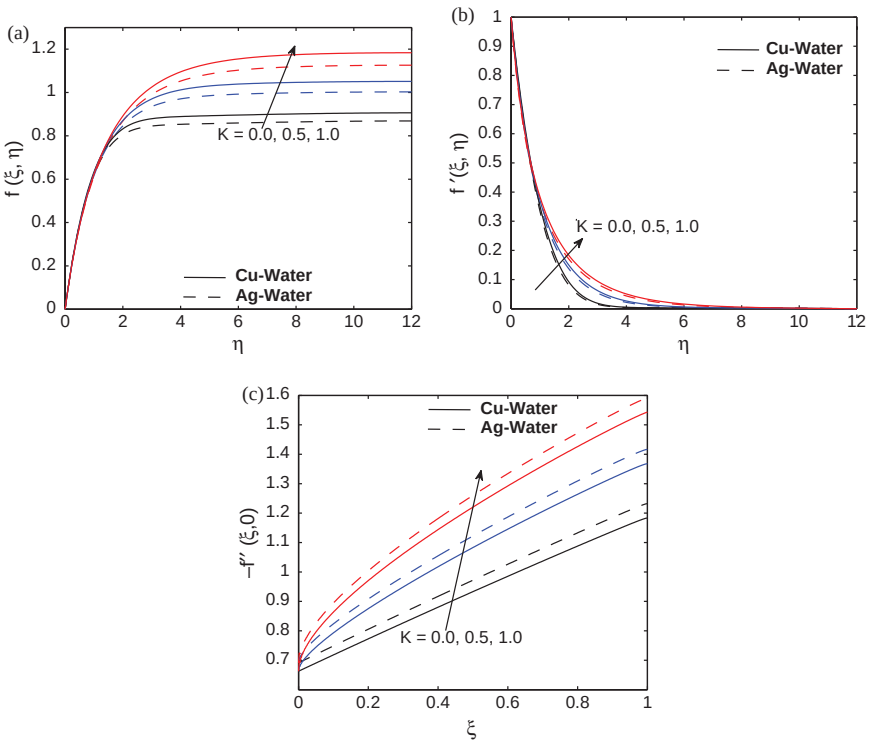

Fig. 3. Effects of the transverse curvature parameter K on (a) transverse velocity profiles, (b) horizontal velocity profiles and (c) skin friction coefficient.

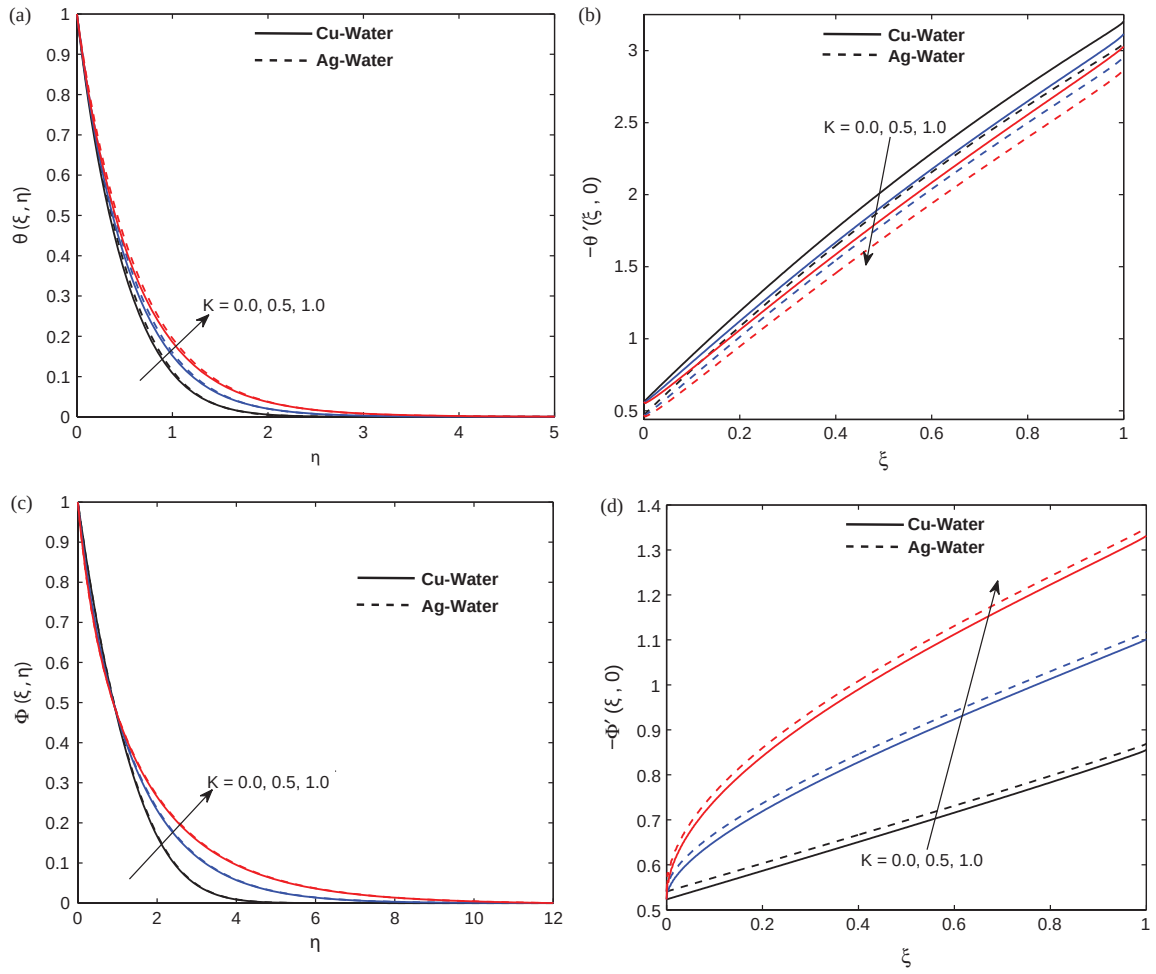

Fig. 4. Effects of the transverse curvature parameter K on (a) temperature profiles, (b) wall heat transfer coefficient, (c) concentration profiles and (d) wall mass transfer coefficient.

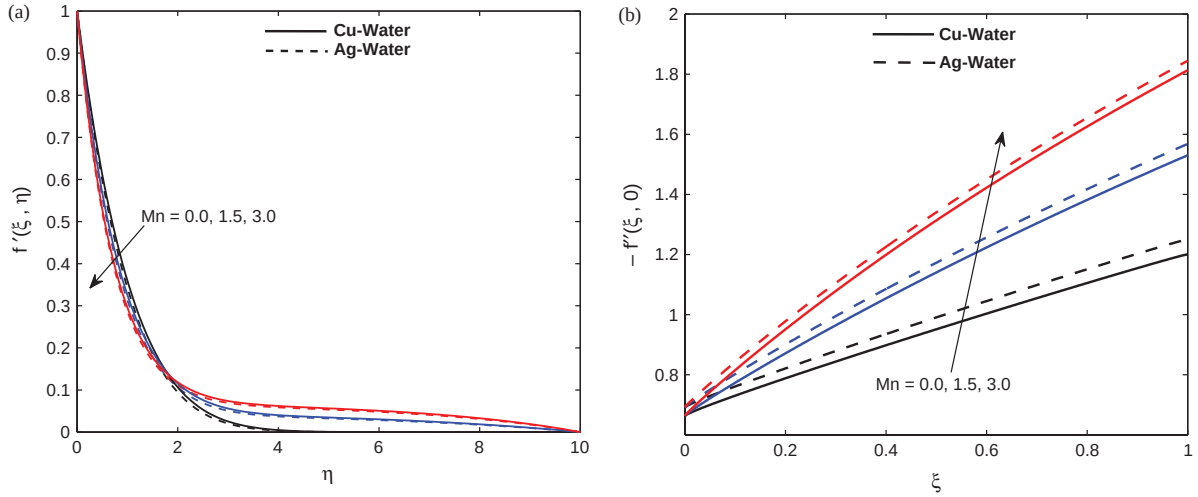

Fig. 5. Effects of the magnetic field parameter Mn on (a) horizontal velocity profiles and (b) skin friction coefficient.

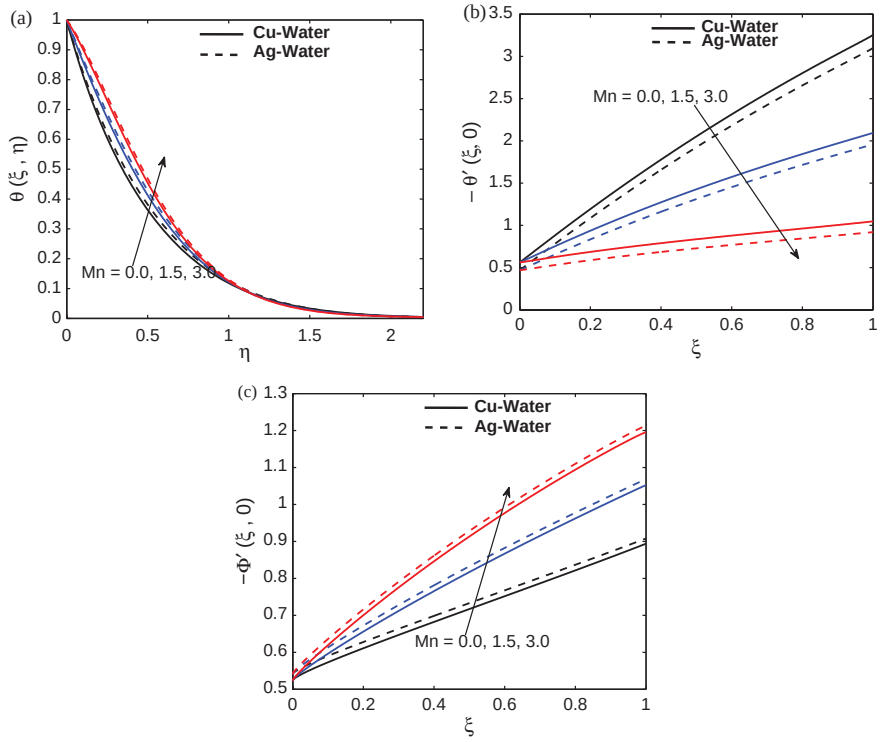

Fig. 6. Effects of the magnetic field parameter Mn on (a) temperature profiles, (b) wall heat transfer coefficient and (c) wall mass transfer coefficient.

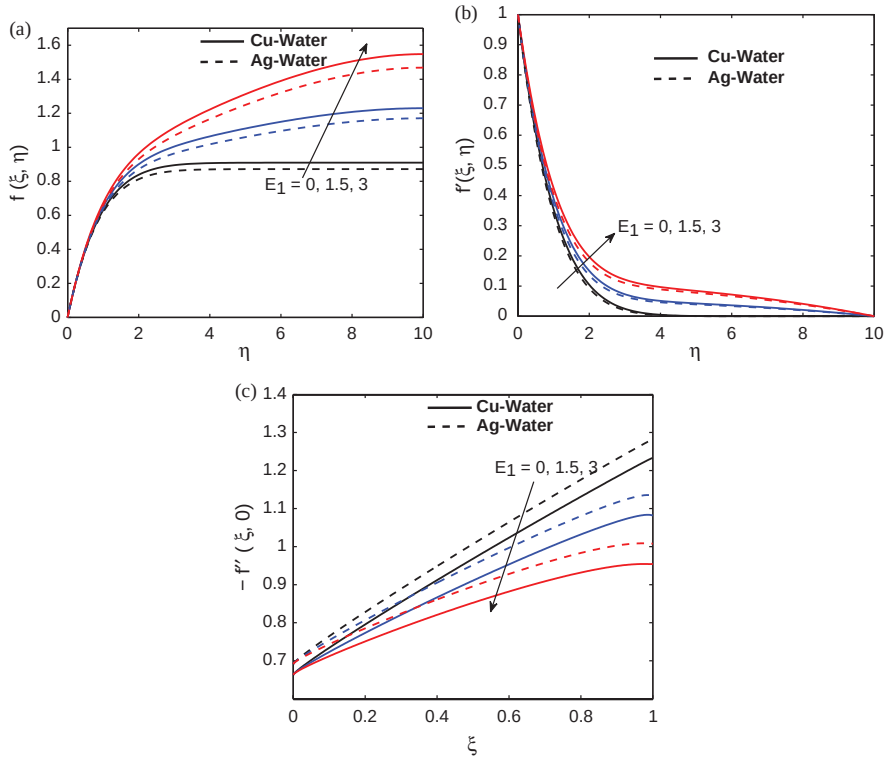

Fig. 7. Effects of the local electric parameter E_1 on (a) transverse velocity profiles, (b) horizontal velocity profiles and (c) skin friction coefficient.

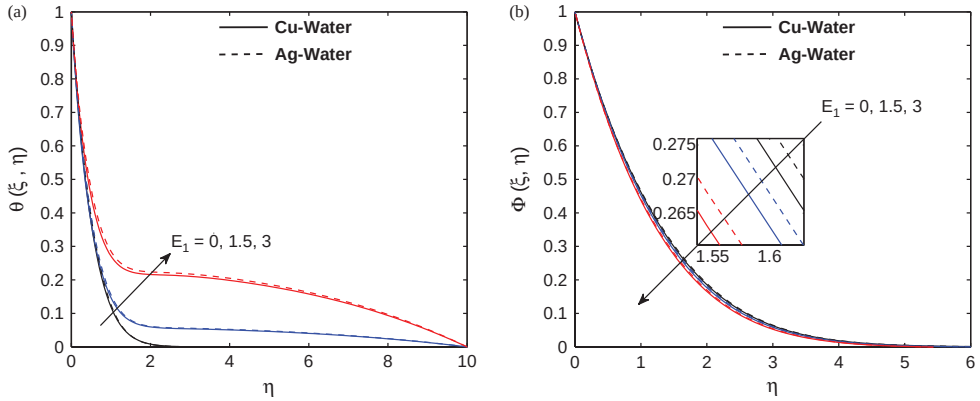

Fig. 8. Effects of the local electric parameter E_1 on (a) temperature and (b) concentration profiles.

for Cu-water and Ag-water nanofluids for different values of ξ. The velocity and concentration profiles first decrease with increases in ξ near the inclined cylinder surface up to a certain value of η. Beyond this point, the opposite trend is observed far from the inclined cylinder surface where the momentum and concentration boundary-layer thicknesses decrease. The nanofluid temperature profiles decrease with increasing ξ. The conductivity of the nanofluid in the case of a Ag nanoparticles is higher than the case of Cu nanoparticles.

The effects of the transverse curvature parameter K on the transverse velocity (f), streamwise velocity (f'), temperature (θ) and concentration (Φ) profiles and skin friction coefficient $(-f''(\xi,0))$, wall heat transfer coefficient $-\theta'(\xi,0)$ and wall mass transfer coefficient $-\Phi'(\xi,0)$ are shown in Figures 3 and 4. Physically $K=0$

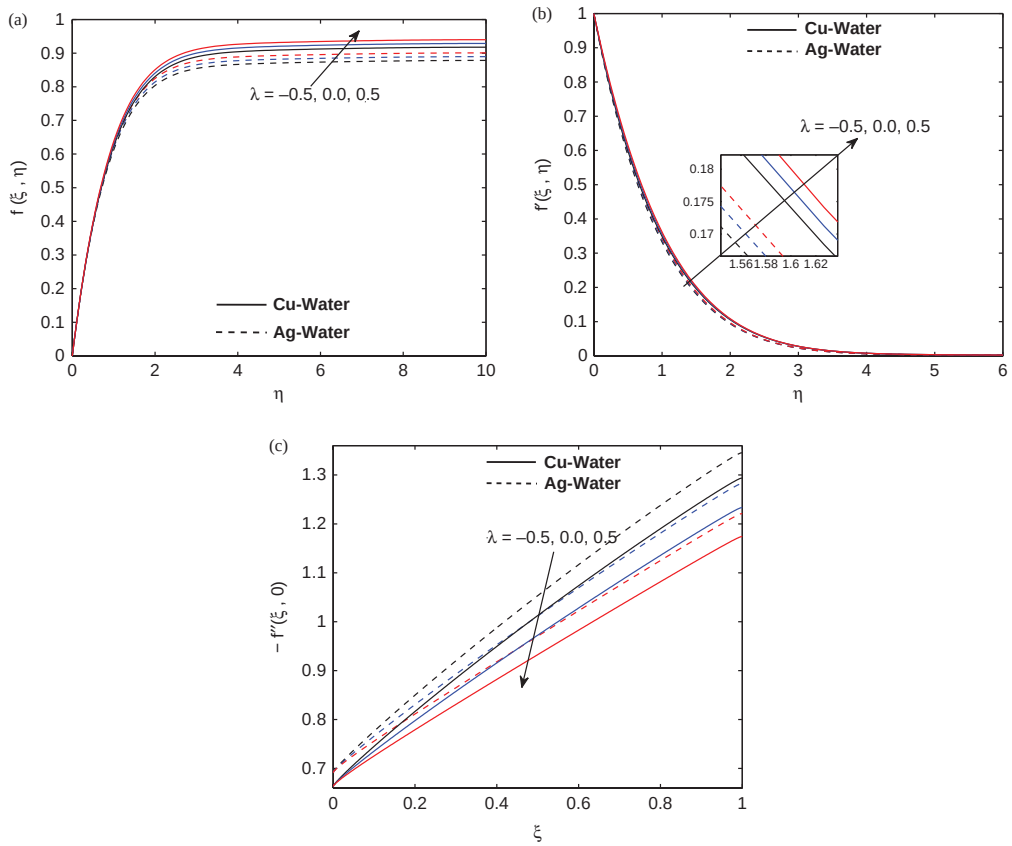

Fig. 9. Effects of the mixed convection parameter λ on (a) transverse velocity profiles, (b) horizontal velocity profiles and (c) skin friction coefficient.

means the inclined cylinder's outer surface behaves like a stretching flat surface. The viscosity effect reduces due to the fact that the contact area of the surface with the fluid tends to the tangential position as $K \to 1$. From Figure 3(b), it can be observed that the effect of the transverse curvature parameter on the horizontal velocity is very limited within approximately the range $[0, 0.75]$. This streamwise velocity approaches zero asymptotically in the region $[0.75, \infty)$. In this case, the streamwise velocity is the free stream velocity within $[0.75, \infty)$, and in this region the velocity increases with the increasing value of K.

Increasing the transverse curvature parameter increases the nanofluid velocity, temperature and concentration profiles and skin friction coefficient and wall mass transfer coefficient at the inclined cylinder surface. This is due to the increasing momentum, thermal and concentration boundary layer thicknesses. We may conclude that the curvature parameter enhances the nanofluid temperature which means we gain higher thermal conductivity due to high concentration of the nanoparticles. The wall temperature gradient decreases with increases in the curvature parameter. Furthermore, it is clear that the velocity components and the wall temperature gradient are higher in the case of Cu-water nanofluids than for Ag-water nanofluids. However, the opposite trends are observed for the nanofluid thermal conductivity, concentration profile, skin friction coefficient and wall mass transfer coefficient.

Physically, negative values of f'' imply that the surface exerts a higher drag force on the nanofluid in the case of Ag-water nanofluid as compared to the Cu-water nanofluid, this findings is similar to Hamad.[38]

Figures 5 and 6 illustrate the influence of the magnetic field parameter (Mn) on the horizontal velocity f' and temperature (θ) profiles and skin friction coefficient $(-f''(\xi, 0))$, wall heat transfer coefficient $(-\theta'(\xi, 0))$ and wall mass transfer coefficient $(-\Phi'(\xi, 0))$ on Cu-water and Ag-water nanofluids. We have noticed from these figures that the Ag-water nanofluid present higher conductivity for the temperature, skin friction coefficient and the wall mass gradient than Cu-water nanofluid. But the reverse is true for the horizontal velocity and wall temperature gradient. So, we get the higher shear stress in case of Ag-water than Cu-water nanofluids with increasing values of the magnetic field (Mn) parameter. The horizontal velocity profile decrease up to a certain distance from the boundary layer and after that opposite trend is observed. Again, the momentum boundary layer decrease at the beginning

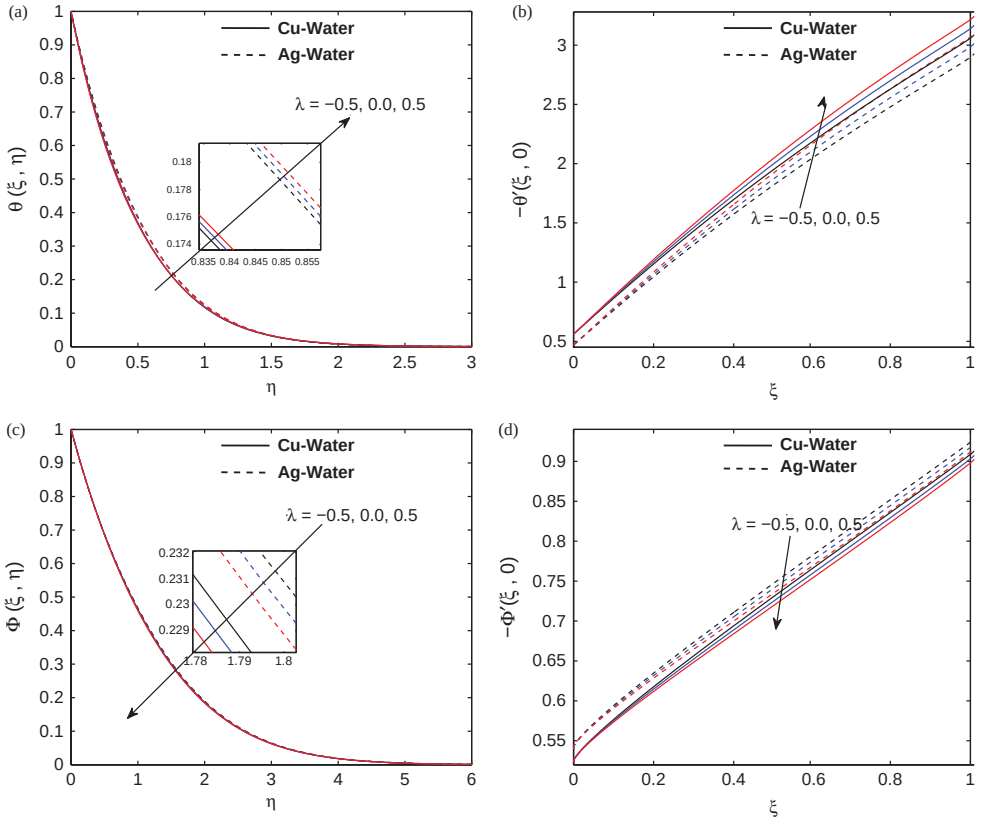

Fig. 10. Effects of the mixed convection parameter λ on (a) temperature profiles, (b) wall heat transfer coefficient, (c) concentration profiles and (d) wall mass transfer coefficient.

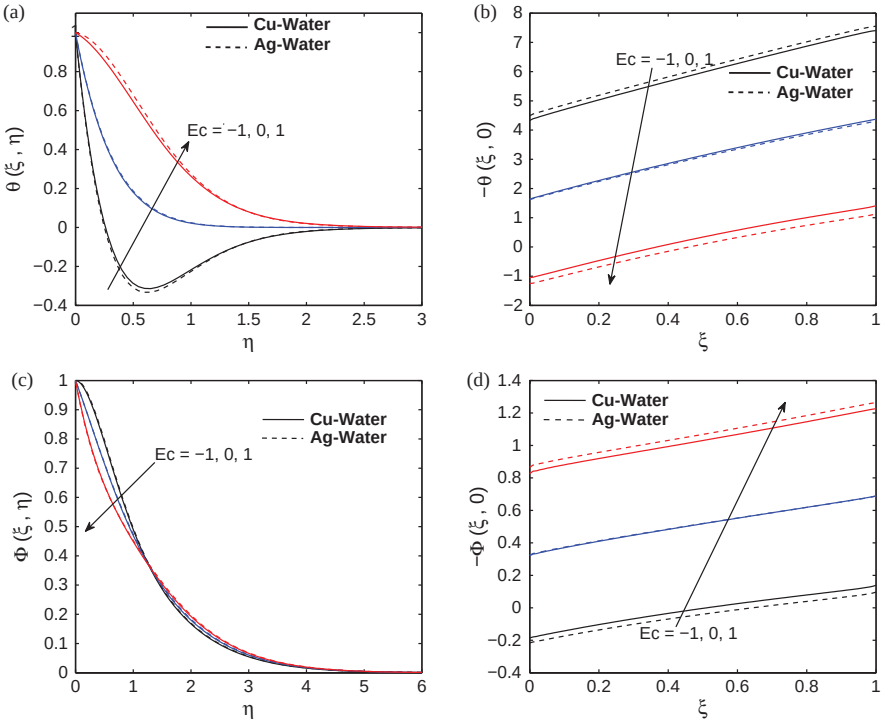

Fig. 11. Effects of the Eckret number *Ec* on (a) temperature profiles, (b) wall heat transfer coefficient, (c) concentration profiles and (d) wall mass transfer coefficient.

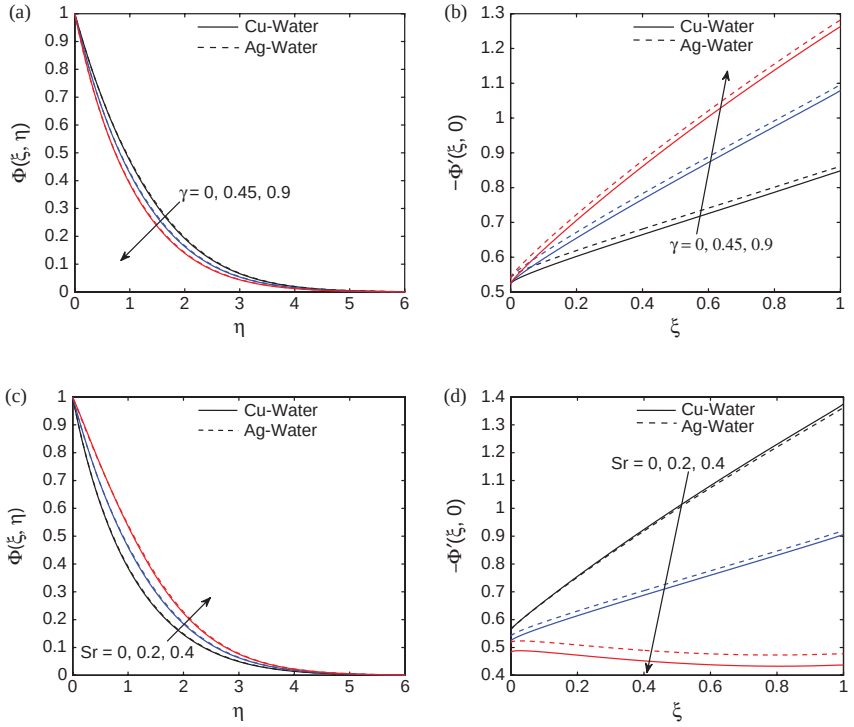

Fig. 12. Effects of (a) the chemical reaction parameter γ on concentration profiles, (b) the chemical reaction parameter γ on wall mass transfer coefficient, (c) the Soret number *Sr* on concentration profiles, and (d) the Soret number *Sr* on wall mass transfer coefficient.

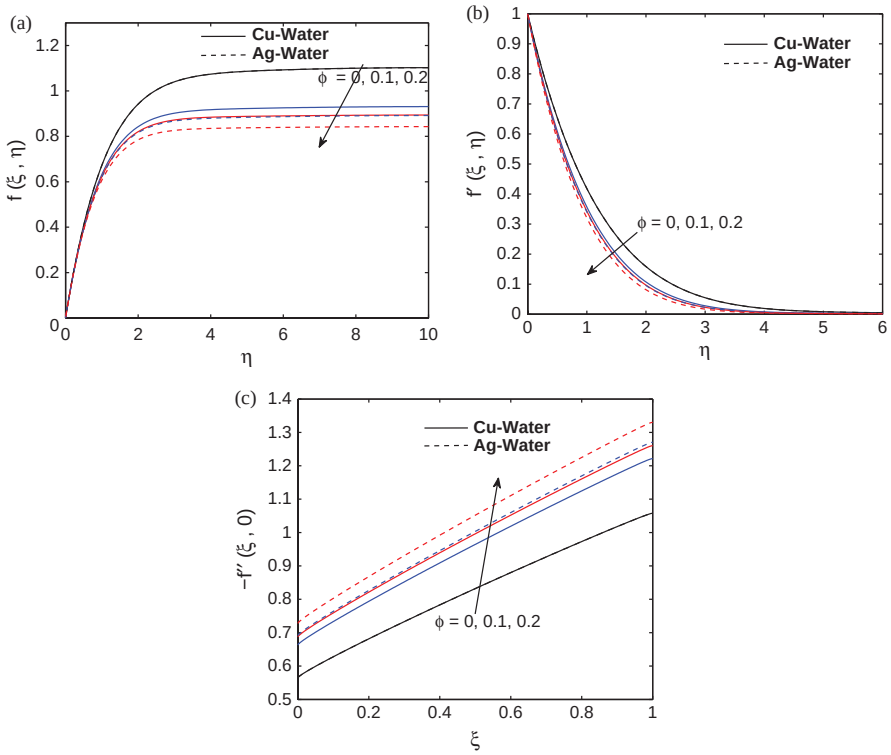

Fig. 13. Effects of the nanoparticle volume fraction ϕ on (a) transverse velocity profiles, (b) horizontal velocity profiles and (c) skin friction coefficient.

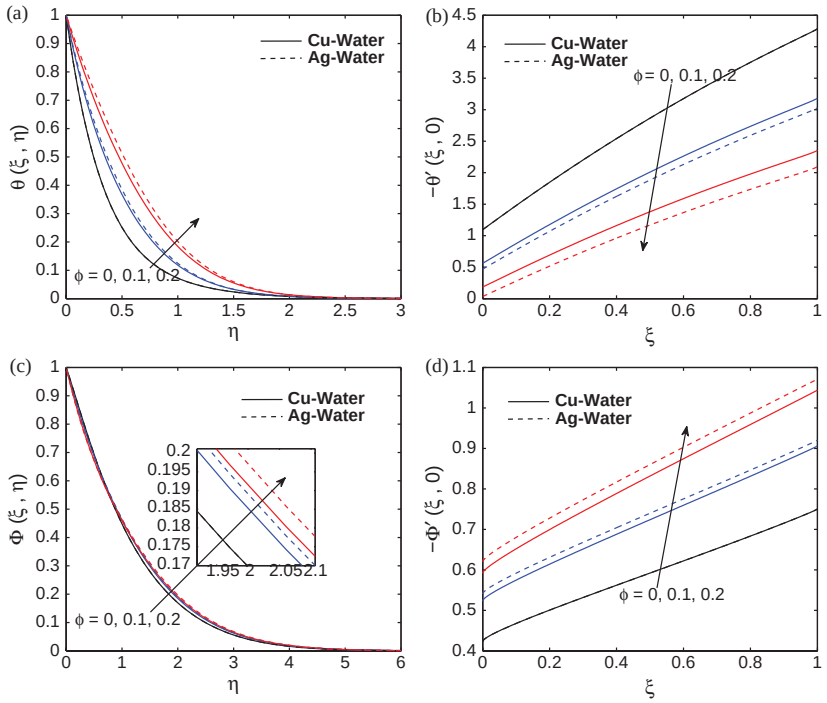

Fig. 14. Effects of the nanoparticle volume fraction ϕ on (a) temperature profiles, (b) wall heat transfer coefficient, (c) concentration profiles and (d) wall mass transfer coefficient.

RESEARCH ARTICLE

Table I. Thermophysical properties of the base fluid and the nanoparticles[24].

	Physical properties			
	C_p (J/kg K)	ρ (Kg/m^3)	k (W/m K)	$\beta \times 10^5$ (K^{-1})
Pure water (H_2O)	4179	997.1	0.613	21
Copper (Cu)	385	8933	401	1.67
Silver (Ag)	235	10500	429	1.89

and then it increase with increase in the magnetic field parameter. More than that, the increasing value of the magnetic field parameter enhance the temperature profile, skin friction coefficient and the wall mass gradient increase while it reduces the wall temperature gradient. That means the effect of the increasing values of the magnetic field leads to accelerating the thermal boundary thickness. This behavior is true even for all values of the magnetic parameter which in turn causes the enhancement of the temperature field.

Figures 7 and 8 show the transverse velocity (f), the horizontal velocity (f'), temperature (θ), concentration (Φ) profiles and skin friction coefficient $(-f''(\xi,0))$ for various values of local electric parameter E_1. An analysis of the results reveals that the impact of Ag nanoparticles is stronger than Cu nanoparticles for the thermal conductivity, concentration and skin friction coefficient but the reverse is true for the velocities. In fact the Ag-water nanofluid gives a higher shear stress than a Cu-water nanofluid. The effect of the local electric parameter E_1 on velocities is to increase its effect throughout the boundary layer. Also, increasing the local electric parameter is to increase the velocity and temperature profiles. On the other hand, nanoparticle concentration and the skin friction coefficient decreases with increasing E_1. This is because the Lorentz force increases due to the electric field which acts as an accelerating force in reducing frictional resistance.

Table II. Comparison of $-f''(1,0)$ for various values of K and Mn when $E_1 = \lambda = \Omega = \phi = 0$ and $Pr = 6.2$.

K	Mn	Vajravelu et al.[35]	Present results
0.00	0.0	1.000001	1.000241
	0.5	1.224745	1.224747
	1.0	1.414214	1.414213
	1.5	1.581139	1.581139
	2.0	1.732051	1.732051
0.25	0.0	1.091826	1.092879
	0.5	1.328505	1.328570
	1.0	1.523163	1.523179
	1.5	–	1.693041
	2.0	–	1.845871
0.50	0.0	1.182410	1.184654
	0.5	1.427151	1.427488
	1.0	1.626496	1.626577
	1.5	–	1.799346
	2.0	–	1.954208
0.75	0.0	1.271145	1.274994
	0.5	1.521975	1.522824
	1.0	1.725576	1.725815
	1.5	–	1.901384
	2.0	–	2.058310
1.00	0.0	1.358198	1.363888
	0.5	1.613858	1.615435
	1.0	1.821302	1.821816
	1.5	–	2.000026
	2.0	–	2.158992

Table III. Comparison of $-f''(1,0)$ for various values of Mn and ϕ when $K = E_1 = \lambda = \Omega = 0$ and $Pr = 6.2$.

		Hamad[38]		Present results	
Mn	ϕ	Cu-water	Ag-water	Cu-water	Ag-water
0.0	0.05	1.10892	1.13966	1.109188	1.139935
	0.10	1.17475	1.22507	1.175030	1.225364
	0.15	1.20886	1.27215	1.209154	1.272460
	0.20	1.21804	1.28979	1.218338	1.290099
0.5	0.05	1.29210	1.31858	1.292113	1.318593
	0.10	1.32825	1.37296	1.328276	1.372991
	0.15	1.33955	1.39694	1.339598	1.396992
	0.20	1.33036	1.39634	1.330417	1.396419
1.0	0.05	1.45236	1.47597	1.452360	1.475964
	0.10	1.46576	1.50640	1.465764	1.506396
	0.15	1.45858	1.51145	1.458585	1.511459
	0.20	1.43390	1.49532	1.433908	1.495337
2.0	0.05	1.72887	1.74875	1.728873	1.748748
	0.10	1.70789	1.74289	1.707892	1.742888
	0.15	1.67140	1.71773	1.671398	1.717730
	0.20	1.62126	1.67583	1.621264	1.675834

The results are presented in Figures 2–14 and Tables II–VI. Two types of nanoparticles, namely copper (Cu) and silver (Ag) with water as the base fluid are considered. The thermophysical properties of the base fluid and the nanoparticles are listed in Table I (see Oztop and Abu-Nada).[24]

The impact of various λ on the transverse velocity (f), horizontal velocity (f'), temperature (θ) and concentration (Φ) profiles and skin friction coefficient $(-f''(\xi,0))$, wall heat transfer coefficient $(-\theta'(\xi,0))$ and wall mass transfer coefficient $(-\Phi'(\xi,0))$ are presented in Figures 9 and 10. It is clear that increasing the buoyancy force parameter increases the temperature profiles and the wall temperature gradient whereas it reduces the concentration profiles, skin friction coefficient and wall mass transfer

Table IV. Comparison of $-\theta'(1,0)$ for various values of Pr when $\mathrm{Mn} = E_1 = \lambda = \Omega = Ec = \phi = 0$ and $m = 1$.

		39	40	41	35	Present values
K	Pr	$-\theta'(1,0)$	$-\theta'(1,0)$	$-\theta'(1,0)$	$-\theta'(1,0)$	$-\theta'(1,0)$
0	1	1.0000	0.9961	1.0000	1.00002	1.00024
	10	3.7207	3.7006	3.7207	3.72078	3.72057

Table V. Computed values of skin fraction coefficient $-f''(\xi,0)$ for both cases of nanoparticles Cu-water and Ag-water with various values of K, Mn and ϕ when $E_1 = 0.1$, $\lambda = 0.1$, $\Omega = \pi/4$, $Pr = 7.0$, $m = 2$, $Ec = 0.4$, $Sc = 1$, $\gamma = 0.1$ and $Sr = 0.2$.

			$\xi = 0.0$		$\xi = 0.5$		$\xi = 1.0$	
K	Mn	ϕ	Cu	Ag	Cu	Ag	Cu	Ag
0.1	0.1	0.00	0.564190	0.564190	0.832073	0.832073	1.056906	1.056906
		0.05	0.625641	0.642984	0.914590	0.938293	1.158847	1.188455
		0.10	0.662779	0.691171	0.964444	1.003377	1.220578	1.269348
		0.20	0.687208	0.727685	0.996243	1.051916	1.259533	1.329421
0.1	0.0	0.1	0.662779	0.691171	0.951325	0.990797	1.200246	1.250094
	0.1		0.662779	0.691171	0.964444	1.003377	1.220578	1.269348
	1.5		0.662779	0.691171	1.140240	1.172568	1.530073	1.567786
	3.0		0.662779	0.691171	1.313344	1.340295	1.813264	1.844855
0.0	0.1	0.1	0.662779	0.691171	0.933130	0.972047	1.182630	1.231515
0.1			0.662779	0.691171	0.964444	1.003377	1.220578	1.269348
0.5			0.662779	0.691171	1.082979	1.122192	1.367693	1.416254
1.0			0.662779	0.691171	1.220348	1.260148	1.543161	1.591563

coefficient. In the case of a Ag-water nanofluid, the temperature and concentration profiles, skin friction coefficient and wall mass gradient are higher than for a Cu-water nanofluid. It is interesting to note that the buoyancy opposing force reduces the magnitude of the velocity considerably within the boundary layer for an inclined cylinder surface for opposing buoyancy flow. Increasing the buoyancy parameter increases the thermal boundary layer. Also, it is observed that the magnitude of the temperature profiles increase considerably within the thermal boundary layer.

The effect of Ec on the temperature profiles, concentration profiles, wall temperature and mass gradient are shown in Figure 11 for both Cu-water and Ag-water nanofluids. The effect of the viscous dissipation parameter is to generate more heat in the boundary layer region and to reduce the wall heat transfer coefficient. Hence, the thermal boundary layer thickness increases as the viscous dissipation parameter increases. The results demonstrate that an increase in the viscous dissipation parameter reduces the concentration profile near the inclined cylinder surface and then increases far from the surface.

Table VI. Computed values of skin fraction coefficient $-f''(\xi,0)$ for both cases of nanoparticles Cu-water and Ag-water with various values of E_1 and λ when $K = 0.1$, $\mathrm{Mn} = 0.1$, $\Omega = \pi/4$, $Pr = 7.0$, $m = 2$, $Ec = 0.4$, $Sc = 1$, $\gamma = 0.1$, $Sr = 0.2$ and $\phi = 0.1$.

		$\xi = 0.0$		$\xi = 0.5$		$\xi = 1.0$	
E_1	λ	Cu	Ag	Cu	Ag	Cu	Ag
0.0	0.1	0.662779	0.691171	0.968269	1.007049	1.233064	1.281562
0.1		0.662779	0.691171	0.964444	1.003377	1.220578	1.269348
1.5		0.662779	0.691171	0.910450	0.951514	1.077625	1.128901
3.0		0.662779	0.691171	0.851710	0.895010	0.949903	1.003648
0.1-0.5		0.662779	0.691171	1.012532	1.053215	1.292718	1.344492
	0.0	0.662779	0.691171	0.972429	1.011652	1.232492	1.281748
	0.5	0.662779	0.691171	0.932618	0.970405	1.173334	1.220210
	1.0	0.662779	0.691171	0.893087	0.929461	1.115152	1.159764

The variation of the concentration profiles and wall mass gradient with the chemical reaction γ and the Soret number Sr are shown in Figure 12 for both Cu-water and Ag-water nanofluids. It is seen that the Cu-water nanofluid generally has lower values than the Ag-water nanofluid except when $Sr = 0$. Also, we observe in this figure that the concentration profiles increase with increasing values Soret number and decreases with increasing in the values of the chemical reaction parameters. The increasing values of Sr increase the temperature gradient. It is seen that the wall mass gradient is an increasing function of time except when $Sr = 0.4$.

Figures 13 and 14 demonstrate the effect of the nanoparticle volume fraction (ϕ) on the transverse velocity (f) and the horizontal velocity (f'), temperature (θ) and concentration (Φ) profiles and skin friction coefficient ($-f''(\xi,0)$), wall heat transfer coefficient ($-\theta'(\xi,0)$) and wall mass transfer coefficient ($-\Phi'(\xi,0)$), in the case of a Cu-water and Ag-water nanofluids. It is seen that the increasing value of nanoparticle volume fraction decrease the nanofluid flow and wall temperature gradients while it increase the temperature, concentration, skin friction coefficient and wall mass gradient. Increasing the volume fraction of nanoparticles increases the momentum and thermal conductivity of the nanofluid due to the enhancement of the momentum and thermal boundary layer. We also notice that the velocity and wall temperature gradient in the case of a Ag-water nanofluid are relatively less than that of a Cu-water nanofluid. In the same context, we also perceive that the temperature and concentration distribution as well as the skin friction coefficient and wall mass transfer coefficient in a Ag-water nanofluid are higher than that of Cu-water nanofluid since the conductivity of silver is more than that of copper. In addition to that the concentration boundary layer thickness increases for both types of nanofluids with an enhancement in the nanoparticle volume fraction.

5. CONCLUSIONS

The unsteady flow due to the inclined cylinder immersed in a magneto-nanofluid in the presence of chemical reaction, viscous and ohmic dissipations in terms of heat and mass transfer characteristics are investigated. The governing non-dimensional equations are solved numerically using a spectral local linearization method. The results are illustrated graphically and discussed for two types of nanoparticles; namely, copper and silver nanoparticles. We note that the combine effects of the buoyancy force, viscous and Ohmic dissipations is to enhance the nanofluid temperature within the boundary layer. The nanofluid concentration reduces while the wall mass gradient increased with increases in the chemical reaction parameter, buoyancy force, viscous and Ohmic dissipations. The opposite trend is observed for the thermodiffusion parameter. The buoyancy force and Ohmic dissipations enhance the transport phenomena within the boundary layer region.

Conflict of Interest

The authors declare that there is no conflict of interests regarding the publication of this article.

Acknowledgments: The authors are grateful for financial support from the University of KwaZulu-Natal and the Claude Leon Foundation.

References

1. N. Bachok, A. Ishak, and I. Pop, *Int. J. Heat Mass Transf.* 55, 8122 **(2012)**.
2. C. Y. Wang, *Phys Fluids* 31, 466 **(1988)**.
3. A. Ishak, R. Nazar, and I. Pop, *Appl. Math. Model* 32, 2059 **(2008)**.
4. C. Y. Wang and C. Ng, *Int. J. Non-linear Mech.* 46, 1191 **(2011)**.
5. C. Y. Wang, *Commun. Non-Linear Sci. Numer. Simul.* 17, 1098 **(2012)**.
6. A. Ishak, R. Nazar, and I. Pop, *Energy Convers. Manage.* 49, 3265 **(2008)**.
7. T. Fang, J. Zhang, Y. Zhong, and H. Tao, *Chin. Phys. Lett.* 28 **(2011)**.
8. T. Fang, J. Zhang, and Y. Zhong, *Commun. Nonlinear Sci. Numer. Simul.* 17, 3124 **(2012)**.
9. Y. Y. Lok and I. Pop, *Phys. Fluids* 23 **(2011)**.
10. W. M. K. A. W. Zaimia, A. Ishakb, and I. Pop, *J. King Saud University Sci.* 25, 143 **(2013)**.
11. S. Munawar, A. Mehmood, and A. Ali, *Chinese J. Phys.* 50, 828 **(2012)**.
12. D. Pal and H. Mondal, *Int. J. Nonlinear Sci.* 14, 115 **(2012)**.
13. M. S. Abel, E. Sanjayanand, and M. M. Nandeppanavar, *Communications in Nonlinear Sci. Numerical Simul.* 13, 1808 **(2008)**.
14. M. Miklavčič and C. Y. Wang, *Quart. Appl. Math.* 64, 283 **(2006)**.
15. W. J. McCroskey, *ASME J. Fluid Engg.* 99, 8 **(1977)**.
16. K. Stewartson, *Adv. Appl. Mech.* 6, 1 **(1960)**.
17. J. T. Stuart, Unsteady boundary layers, Laminar Boundary Layers, edited by L. Rosenhead, Oxford **(1964)**, p. 349.
18. N. Riley, Unsteady laminar boundary layers, SIAM Review **(1975)**, Vol. 17, p. 274.
19. N. Riley, Unsteady viscous flows, Sci. Progress, Oxford **(1990)**, Vol. 74, p. 361.
20. D. P. Telionis, Unsteady Viscous Flows, Springer, New York **(1981)**.
21. C. Y. Wang, *Appl. Mech. Rev.* 42, 269 **(1989)**.
22. B. S. Dandapat and A. Mukhopadhyay, *Int. J. Appl. Mech. Engg.* 8, 379 **(2003)**.
23. E. Abu-Nada and A. J. Chamkha, *Eur. J. Mech. B/Fluids* 29, 472 **(2010)**.
24. H. F. Oztop and E. Abu-Nada, *Int. J. Heat Fluid Flow* 29, 1326 **(2008)**.
25. J. C. Williams and T. H. Rhyne, *SIAM J. Appl. Math.* 38, 215 **(1980)**.
26. L. Tham, R. Nazar, and I. Pop, *Int. J. Numerical Methods for Heat and Fluid Flow* 22, 576 **(2012)**.
27. S. U. S. Choi, *J. ASME FED.* 23, 1 **(1995)**.
28. T. Mahmood and J. H. Merkin, *J. Engg. Math.* 22, 73 **(1988)**.
29. H. R. Ashorynejad, M. Sheikholeslami, I. Pop, and D. D. Ganji, *Heat Mass Transf.* 49, 427 **(2013)**.
30. P. K. Kameswaran, M. Narayana, P. Sibanda, and P. V. S. N. Murthy, *Int. J. Heat Mass Transf.* 55, 7587 **(2012)**.
31. M. Ramzan, M. Farooq, T. Hayat, A. Alsaedi, and J. Cao, *J. Cent. South. Univ.* 22, 707 **(2015)**.
32. S. Khalili, A. Khalili, S. Kafashian, and A. Abbassi, *J. Porous Media* 16, 967 **(2013)**.
33. S. Shateyi and S. S. Motsa, *The Canadian J. Chemical Engg.* 89, 1388 **(2011)**.
34. T. Hayat, M. Farooq, and A. Alsaedi, *Z. Naturforsch* 70, 317 **(2015)**.
35. K. Vajravelu, K. V. Prasad, and S. R. Santhi, *Applied Mathematics and Computation* 219, 3993 **(2012)**.
36. S. S. Motsa, *J. Applied Math.* 15 **(2013)**, http://dx.doi.org/10.1155/2013/423628.
37. E. P. J. Sudhan and K. S. Meenakshi, *Indian J. Science and Tech.* 4, 417 **(2011)**.
38. M. A. A. Hamad, *Int. Commun. Heat Mass Transf.* 38, 487 **(2011)**.
39. L. G. Grubka and K. M. Bobba, *ASME-J. Heat Transf.* 107, 248 **(1985)**.
40. M. E. Ali, *Heat Mass Transf.* 29, 227 **(1994)**.
41. A. Ishak and R. Nazar, *Euro J. Sci. Res.* 36, 22 **(2009)**.

Received: 1 November 2015. Accepted: 22 November 2015.

Chapter 3

Impulsive nanofluid flow along a vertical stretching cone

In this chapter, we modified the study in Chapter 2 by considering the unsteady nanofluid flow and heat and mass transfer along a vertically stretching cone subject to impulsive motion. The flow involves two kinds of nanoparticles, namely copper and titanium dioxide. The aim is to study the effects of physical parameters such as the stretching or shrinking parameter, nanoparticle volume fraction, the magnetic field, chemical reaction and viscous dissipation. The flow equations are solved using the spectral local linearization method.

IJHT INTERNATIONAL JOURNAL OF HEAT AND TECHNOLOGY

ISSN: 0392-8764
Vol. 35, No.4, December 2017, pp. 1005-1014
DOI: 10.18280/ijht.350437
Licensed under CC BY-NC 4.0

A publication of IIETA

IIETA International Information and Engineering Technology Association
Advancing the World of Information and Engineering
http://www.iieta.org/Journals/IJHT

Impulsive nanofluid flow along a vertical stretching cone

Sami M.S. Ahamed[1], Sabyasachi Mondal[2*], Precious Sibanda[1]

[1] School of Mathematics, Statistics and Computer Science, University of KwaZulu-Natal Private Bag X01 Scottsville 3209, South Africa
[2] Department of Mathematics, Amity University, Kolkata, Newtown-700135, West Bengal, India

Email: sabya.mondal.2007@gmail.com

ABSTRACT

We study the unsteady convective flow of two water-based nanofluids containing Copper and Titanium oxide along a vertical stretching or shrinking cone with viscous dissipation and internal heat generation. The problem is transformed to two-dimensional flow over a cone using Mangler's transformation. The coupled nonlinear conservation equations are solved numerically using the spectral local linearization method. We present an analysis of how some physical parameters affect the flow structure, the heat and mass transfer rates and the fluid properties. The accuracy of the results is determined by comparison with previously published studies, for some limiting cases.

Keywords: Chemical Reaction, Nanofluid Flow, Stretching or Shrinking Cone, Spectral Local Linearization Method.

1. INTRODUCTION

Common fluids such as water, ethylene glycol and oil have low heat transfer characteristic owing to their poor thermal conductivities. It is now understood that the thermo-physical properties of these fluids can be significantly enhanced by suspending nano-sized metallic particles such as Aluminum, titanium, Gold, Copper, Iron or their oxides, resulting in what is commonly called a nanofluid, see Choi and Eastman [1].

During the last several years many authors have studied the boundary layer flow of nanofluid fluids through different geometries and with different conditions. Examples include Kameswaran et al. [2] who studied hydromagnetic nanofluid flow due to a stretching or shrinking sheet and Kameswaran et al. [3] who found solutions for the equations for the stagnation-point flow of a nanofluid over a stretching surface. The steady nanofluid boundary layer flow along a vertical cone in a porous medium was investigated by Fauzi et al. [4]. Boutra et al. [5] studied free convection enhancement within a nanofluid' filled enclosure with square heaters and Ambethkar and Kumar [6] examined solutions of 2-D unsteady incompressible flow with heat transfer in a driven square cavity sing streamfunction-vorticity formulation. Cheng [7] discussed natural convection in boundary layer flow over a truncated cone embedded in a porous medium. Chamkha et al. [8] considered the problem of steady, laminar, mixed convection boundary-layer flow over a vertical cone embedded in a porous medium with thermal radiation while Nadeem and Saleem [9] investigated unsteady nanofluid flow in a rotating cone subject to an applied magnetic field. In this study we investigate the flow of a nanofluid along a vertical stretching cone. Early studies of boundary layer over a cone-shaped surface include those of Heiring and Grosh [10] who studied natural convection along a non-isothermal cone. Tien and Tsuji [11] gave a theoretical analysis of the forced convection flow due to a rotating cone. Koh and Price [12] investigated heat transfer past a rotating cone. Convection in gas flow over an isothermal vertical cone was studied by Takhar et al. [13]. Turkyilmazoglu [14] presented analytical a solution of the equations for steady laminar flow of a Newtonian fluid over a rotating cone. Lately, several researchers such as Sivaraj and Kumar [15], Srinivasa et al. [16] and Roy et al. [17] have presented studies focussing on the flow and heat transfer to or from cone shaped bodies under different assumed conditions. Boundary layer studies of stretching surfaces have a rich history starting with the work of Crane [18]. More recent studies include Mahapatra et al. [19], Salem and abd El-Aziz [20] and Noor et al. [21]. The interest in boundary layer stretching sheet flow problems has partly been driven by industrial processes where such flows occur or may apply. Often cited examples include extrusion processes, the manufacture of plastic products, polymers and rubber sheets, wire and fibre coating, glass and optical fibre production, hot rolling production, metal spinning, food processing and many others.

Notwithstanding the number of studies on both stretching and cone-shaped bodies so far, we study here nanofluid along a vertical stretching or shrinking cone with dissipative heat loss and heat generation. The base fluid is water containing a

stable suspension of Cu and TiO_2 nanoparticles. The axisymmetric flow problem is transformed to a two-dimensional problem and the equations are solved numerically using a spectral local linearization method (SLLM). We give an analysis of the impact of changes in flow parameters on the skin friction, heat transfer and the fluid properties. To validate the results, we give a comparison with the earlier work of Kameswaran et al. [3], Wang [22], Jafar et al. [23].

2. MATHEMATICAL FORMULATION

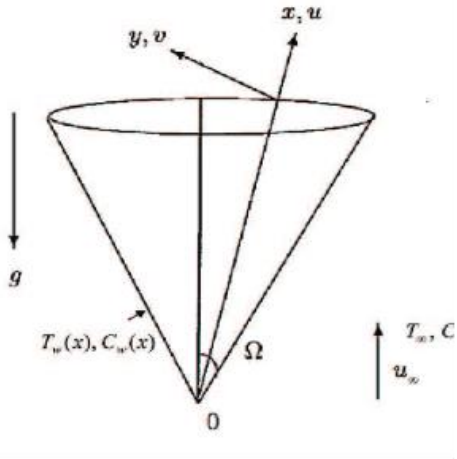

Figure 1. Geometry and the coordinate system

We consider a two-dimensional unsteady boundary layer flow of an incompressible viscous nanofluid along a vertical stretching or shrinking cone embedded in a porous medium. The coordinate system and the physical model are shown in Fig. 1. The cone stretches or shrinks with velocity $U_0 = u_0 x^{m/3}$ where m is an exponent. Mangler's transformation is used (see Schlichting, [24]) to reduce the axisymmetric system to a two-dimensional problem. Then equations can be written as,

$$\frac{\partial u}{\partial x}+\frac{\partial v}{\partial y}=0 \tag{1}$$

$$\frac{\partial u}{\partial t}+u\frac{\partial u}{\partial x}+v\frac{\partial u}{\partial y}=-\frac{1}{\rho_{nf}}\frac{\partial p}{\partial x}+\nu_{nf}\left(\frac{\partial^2 u}{\partial y^2}\right)+\frac{(\rho\beta)_{nf}}{\rho_{nf}}(T-T_\infty)g\cos\Omega-\frac{\sigma B_0^2}{\rho_{nf}}u \tag{2}$$

$$\frac{\partial T}{\partial t}+u\frac{\partial T}{\partial x}+v\frac{\partial T}{\partial y}=\alpha_{nf}\frac{\partial^2 T}{\partial y^2}+\frac{Q}{(\rho c_p)_{nf}}(T-T_\infty)+\frac{\mu_{nf}}{(\rho c_p)_{nf}}\left(\frac{\partial u}{\partial y}\right)^2 \tag{3}$$

$$\frac{\partial C}{\partial t}+u\frac{\partial C}{\partial x}+v\frac{\partial C}{\partial y}=D_m\frac{\partial^2 C}{\partial y^2}-R(C-C_\infty)$$

The boudary conditions are given by

$u = U_0 = u_0 x^{m/3}$, $v = 0$, $T = T_w$, $C = C_w$, at $y = 0$ and $t > 0$,
$u \to U_\infty = u_\infty x^{m/3}$, $T \to T_\infty$, $C \to C_\infty$, as $y \to \infty$ and $t > 0$. (5)

subject to the initial conditions

$u = v = 0$, $T = T_\infty$, $C = C\infty$ for $t < 0$.

The parameters are the effective dynamic viscosity μ_{nf}, the kinematic viscosity ν_{nf}, the thermal diffusivity α_{nf}, the heat capacity $(\rho c_p)_{nf}$, the density ρ_{nf}, the thermal expansion coefficient $(\rho\beta)_{nf}$ and the thermal conductivity k_{nf} of nanofluid, which are given by (see Oztop and Abu-Nada [25]),

$$\begin{aligned}
&\mu_{nf}=\frac{\mu_f}{(1-\phi)^{2.5}},\ \nu_{nf}=\frac{\mu_{nf}}{\rho_{nf}},\ \alpha_{nf}=\frac{k_{nf}}{(\rho c_p)_{nf}},\\
&(\rho c_p)_{nf}=(1-\phi)(\rho c_p)_f+\phi(\rho c_p)_s,\ \rho_{nf}=(1-\phi)\rho_f+\phi\rho_s,\\
&(\rho\beta)_{nf}=(1-\phi)(\rho\beta)_f+\phi(\rho\beta)_s,\ \frac{k_{nf}}{k_f}=\frac{(k_s+2k_f)-2\phi(k_f-k_s)}{(k_s+2k_f)+\phi(k_f-k_s)}.
\end{aligned} \tag{6}$$

We introduce the following transformations,

$$\begin{aligned}
&\eta=\sqrt{\frac{U_\infty}{\nu_f x\xi}}\,y,\ f(\eta,\xi)=\frac{\psi}{\sqrt{\nu_f U_\infty x\xi}},\\
&\xi=1-e^{-\tau},\ \tau=\frac{U_\infty}{x}t,\ \theta(\eta,\xi)=\frac{T-T_\infty}{T_w-T_\infty},\\
&\Phi(\eta,\xi)=\frac{C-C_\infty}{C_w-C_\infty},\ T_w=T_\infty+T_0\,x^{\frac{(2m-3)}{3}},\\
&C_w=C_\infty+C_0\,x^{\frac{(2m-3)}{3}},
\end{aligned} \tag{7}$$

And the stream function ψ is chosen such that

$$u = \partial\psi/\partial y,\ v = -\partial\psi/\partial x. \tag{8}$$

Substituting the transformations (7) into Eqs. (1) - (4), the (1) is automatically satisfied and Eqs. (2)-(4) reduce to

$$\begin{aligned}
&f'''+\phi_1\left\{\frac{1}{2}(1-\xi)\eta f''+f_1 ff''+\xi\left[\left(\frac{m}{3}\right)(1-(f')^2)+\frac{\mathrm{Mn}^2}{\phi_2}(1-f')+\frac{\phi_3}{\phi_2}\lambda\theta\right]\right\}\\
&=\phi_1\xi(1-\xi)\left\{f_2 f''\frac{\partial f}{\partial\xi}+(1-f_2 f')\frac{\partial f'}{\partial\xi}\right\}
\end{aligned} \tag{9}$$

$$\begin{aligned}
&\theta''+\frac{k_f}{k_{nf}}Pr\phi_4\left\{\frac{1}{2}(1-\xi)\eta\theta'+f_1 f\theta'-\xi\left[\left(\frac{2m-3}{3}\right)f'\theta-\frac{\delta}{\phi_4}\theta\right]+\frac{Ec}{\phi_5}f''^2\right\}\\
&=\frac{k_f}{k_{nf}}Pr\phi_4\xi(1-\xi)\left\{f_2\theta'\frac{\partial f}{\partial\xi}+(1-f_2 f')\frac{\partial\theta}{\partial\xi}\right\}
\end{aligned} \tag{10}$$

$$\begin{aligned}
&\Phi''+Sc\left\{\frac{1}{2}(1-\xi)\eta\Phi'+f_1 f\Phi'-\xi\left[\left(\frac{2m-3}{3}\right)f'\Phi+\gamma\Phi\right]\right\}\\
&=Sc\,\xi(1-\xi)\left\{f_2\Phi'\frac{\partial f}{\partial\xi}+(1-f_2 f')\frac{\partial\Phi}{\partial\xi}\right\}
\end{aligned} \tag{11}$$

The boundary conditions in Eq. (5) are transformed to

$f = 0$, $f' = \varepsilon$, $\theta = \Phi = 1$ at $\eta = 0$, $1 \geq \xi \geq 0$,
$f' = 1$, $\theta = \Phi = 0$ as $\eta \to \infty$, $1 \geq \xi \geq 0$, (12)

where

$$\begin{aligned}
&f_1=\xi\left(\frac{m+3}{6}\right)-\left(\frac{m-3}{6}\right)(1-\xi)\log(1-\xi),\ f_2=\left(\frac{m-3}{3}\right)\log(1-\xi),\\
&\phi_1=(1-\phi)^{2.5}\left[1-\phi+\phi\left(\frac{\rho_s}{\rho_f}\right)\right],\ \phi_2=\left[1-\phi+\phi\frac{\rho_s}{\rho_f}\right],\ \phi_3=\left[1-\phi+\phi\frac{(\rho\beta)_s}{(\rho\beta)_f}\right],\\
&\phi_4=\left[1-\phi+\phi\frac{(\rho c_p)_s}{(\rho c_p)_f}\right],\ \phi_5=(1-\phi)^{2.5}\left[1-\phi+\phi\frac{(\rho c_p)_s}{(\rho c_p)_f}\right]
\end{aligned} \tag{13}$$

In the above equations, the prime denotes differentiation with respect to η. The parameters are defined as

$$Mn = \sqrt{\frac{\sigma B_0^2 x}{\rho_f U_\infty}}, ?\lambda = \frac{Gr_x}{Re_x^2}, ?Gr_x = \frac{g\beta_f (T_w - T_\infty) x^3 \cos\Omega}{\nu_f^2}, ?$$

$$Re_x = \frac{U_\infty x}{\nu_f}, ?Pr = \frac{\nu_f (\rho c_p)_f}{k_f}, ?\delta = \frac{Q x}{(\rho c_p)_f U_\infty}, ?$$

$$Ec = \frac{U_\infty^2}{(c_p)_f (T_w - T_\infty)}, ?Sc = \frac{\nu_f}{D_m}, ?\gamma = \frac{R x}{U_\infty}, ?\varepsilon = \frac{u_0}{u_\infty} \quad \text{.....(14)}$$

where *Rex* is the local Reynolds number and *Grx* is the local Grashof number (see Gangadhar et al. [26], Mahdy [27]). It must be noted that $\lambda > 0$ corresponds to the case of buoyancy assisting the flow while $\lambda < 0$ corresponds to buoyancy opposing the flow and $\lambda = 0$ suggests pure forced convection. When $\xi = 0$ and $\phi = 0$ (regular fluid), Eq. (9) reduces to the ordinary differential equation,

$$f''' + 1/2\ \eta f'' = 0, \tag{15}$$

with boundary conditions (when $\varepsilon = 0$) are

$$f(0, 0) = 0,\ f'(0, 0) = 0,\ f'(1, 0) = 1$$

In studies of this nature, we also often interested in the skin friction coefficient *Cfx* , the Nusselt number *Nux* and the Sherwood number *Shx*. These defined as

$$C_{fx} = 2\tau_w/\rho_f U^2_\infty,\ Nu_x = x q_w / k_f (T_w - T_\infty),$$
$$Sh_x = x q_m / D_m (C_w - C_\infty)\ . \tag{16}$$

where τ_w is the shear stress at the cone surface, q_w and q_m are the heat and mass flux from the cone surface, respectively,

$$\tau_w = \mu_{nf} \left(\frac{\partial u}{\partial y}\right)_{y=0}, ?q_w = -k_{nf} \left(\frac{\partial T}{\partial y}\right)_{y=0}, q_m = -D_m \left(\frac{\partial C}{\partial y}\right)_{y=0} \tag{17}$$

and substituting (6) into (16) and (17), we get

$$\frac{1}{2}\sqrt{Re_x}\, C_{f_x} = \frac{(1-\phi)^{-2.5}}{\sqrt{\xi}} f''(0, \xi), ?$$

$$Re_x^{-1/2}\, Nu_x = -\frac{1}{\sqrt{\xi}} \frac{k_{nf}}{k_f} \theta'(0, \xi), ? \tag{18}$$

$$Re_x^{-1/2} Sh_x = -\frac{1}{\sqrt{\xi}} \Phi'(0, \xi)$$

3. SOLUTION METHOD

We use the spectral local linearization method (SLLM) to solve the system of equations (9)-(11). Eqs. (9) - (11) are linearized using the Gauss-Seidel approach (see Motsa [28]). The principle of the SLLM algorithm is to linearize and decouple the system of equations. Nonetheless, this method has only been used in a limited number of studies, hence its general validation in complex systems remains to be made. The detail derivation of SLLM algorithm is described in [28].

Here, the computational domain in the η-direction is chosen so that $L = 30$. This value was found to give accurate results for all selected physical parameters. Increasing η does not change the results to a significant extent. The number of collocation points used in the spectral method discretization is $N_x = 100$ in all cases. We note that the computation of some quantity, say $F^{n+1}{}_{r+1}$, at each time step is achieved by iterating using the local linearization method using a known value at the previous time step *n* as the initial approximation. The calculations were carried out until the desired tolerance level $\epsilon = 10^{-6}$ was attained. The tolerance level is the maximum value of the infinity norm of the difference between the values of the calculated quantities, that is to ensure the accuracy of the results, a sufficiently small step size $\Delta\xi$ was used. The step size was chosen to be small enough such that further reduction did not change the results.

4. RESULTS AND DISCUSSION

The nanofluid velocity profiles $f'(\eta, \xi)$ for different values of the nanoparticle volume fraction ϕ and stretching or shrinking parameter ε are given in Fig. 2. Fig. 2(a) shows that the nanofluid velocity decreases when the nanoparticle volume fraction increases. Fig. 2(b) shows that the TiO_2-water nanofluid has marginally higher values increasing stretching parameter values $\varepsilon > 0$ while opposite trend is observed for a shrinking parameter $\varepsilon < 0$. The stretching or shrinking is due to the impulsive force that acts in *x*-direction (*+ve* or *-ve*). The findings in the case of *Cu*-water nanofluid are similar to the result obtained by Grosan and Pop [29].

The unsteady boundary layer flow of two water based nanofluids along a vertical stretching or shrinking cone was studied. The flow was subject to viscous dissipation, internal heat generation and a chemical reaction. The non-similar partial differential equations were solved using the spectral local linearization method. We have investigated the effects of the nanoparticle volume fraction (ϕ), magnetic field parameter (*Mn*), buoyancy parameter (λ), stretching or shrinking parameter (ε), heat generation parameter (δ), Eckert number (*Ec*), chemical reaction parameter (γ) on the nanofluid velocity, temperature and concentration profiles as well as the skin friction coefficient, heat and mass transfer coefficients. We have used the values $m = 4$, $Pr = 6.7$ and $Sc = 1$ unless otherwise stated. We have considered Copper (*Cu*) and Titanium oxide (TiO_2) nanoparticles with water as the base fluid. We note that $\epsilon < 0$ for a shrinking cone and $\epsilon > 0$ indicates that the cone is stretching. The thermophysical properties of the base fluid and the nanoparticles are listed in Table 1. To determine the accuracy of the numerical method, solutions for some special cases are presented in Tables 2 and 3. The results are in excellent agreement with the work of Kameswaran et al. [3], Wang [22] and Jafar et al. [23].

Table 1. Thermophysical properties of the base fluid and the nanoparticles Oztop and Abu-Nada [25]

Physical properties	*Cp* (*J/kgK*)	*P* (*Kg/m*^{3})	*K* (*W/mK*)	β $\times 10^5$ (*K*$^{-1}$)
Pure water (H_2O)	4179	997.1	0.613	21
Copper (*Cu*)	385	8933	401	1.67
Titanium Oxide (TiO_2)	686.2	4250	8.9538	0.9

Table 2. Comparison of the skin friction coefficient $f''(0, 1)$ and heat transfer rate $-\theta'(0, 1)$, for various values of stretching or shrinking parameter ε when Mn = λ = δ = Ec = 0,m = 3, Pr = 1 and ϕ = 0.

	Suali et al. [30]		Present results	SLL Method
ϵ	$f''(0, 1)$	$-\theta'(0, 1)$	$f''(0, 1)$	$-\theta'(0, 1)$
4	-7.086378	2.116738	-7.086378	2.116738
3	-4.276545	1.870671	-4.276542	1.870671
0.2	1.051130	0.913303	1.051130	0.913303
0.1	1.146561	0.863452	1.146561	0.863452
-0.2	1.373886	0.501448	1.373886	0.698748
-0.5	1.495672	0.501448	1.495670	0.501447
-1.15	1.082232	-0.2979953	1.082491	-0.297346

Table 3. Comparison of the skin friction coefficient $f''(0, 1)$ for various values of stretching or shrinking parameter ε when Mn = λ = 0,m = 3 and ϕ = 0.

	Wang [22]	Jafar et al. [23]	Kameswaran et al. [3]	Present results
ϵ	$f''(0, 1)$	$f''(0, 1)$	$f''(0, 1)$	$f''(0, 1)$
0.0	1.232588	1.2326	1.232588	1.232588
0.1	1.14656	1.1466	1.146561	1.146561
0.2	1.05113	1.0511	1.051130	1.051130
0.5	0.71330	0.7133	0.713295	0.713295
1.0	0.00000	0.0000	0.000000	0.000000
2.0	-1.88731	-1.8873	-1.887307	-1.887307
5.0	-10.26475	-10.2648	-10.264749	-10.264751

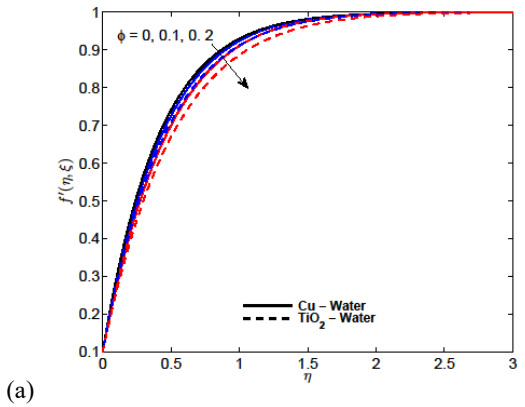

(a)

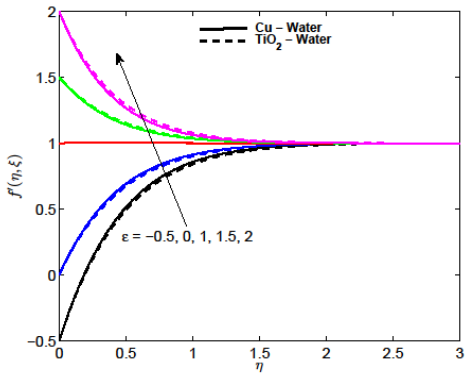

(b)

Figure 2. a) Effect of various nanoparticle volume fraction (ϕ). (b) Effect of stretching or shrinking parameter (ε) on velocity profiles

Figs. 3 and 4 illustrate the effects of nanoparticle volume fraction (ϕ), stretching or shrinking parameter (ε), heat generation parameter (δ) and Eckert number (Ec) on the temperature profiles $\theta(\xi,\eta)$ for both Cu-water and TiO_2-water nanofluids. The temperature profiles increase with increases in ϕ, δ and Ec. We note that an increase in the nanoparticle volume fraction increases the thermal conductivity of the nanofluid significantly, and that internal heat generation increases the temperature of the nanofluid. An increase in the Eckert number increases dissipation due to fluid viscosity or frictional heating. The surface gets cooler when the dissipation increases and as a result there is a transfer of heat from the surface to the nanofluid which causes the temperature to increase. On the other hand, the Cu-water nanofluid temperature decreases with increasing stretching parameter $\varepsilon > 0$ and increases with shrinking parameter $\varepsilon < 0$.

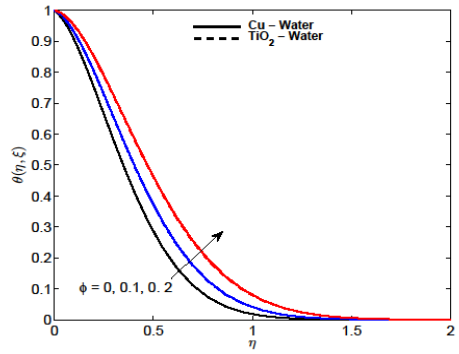

(a)

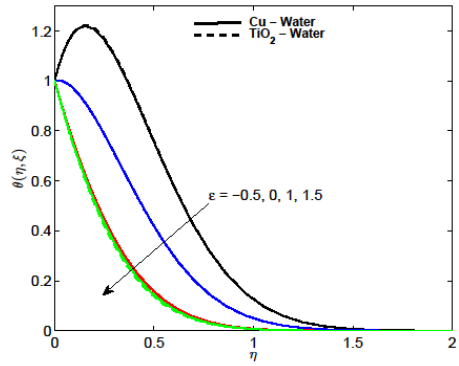

(b)

Figure 3. (a) Effect of nanoparticle volume fraction (ϕ). (b) Effect of stretching or shrinking parameter (ε) on temperature profiles.

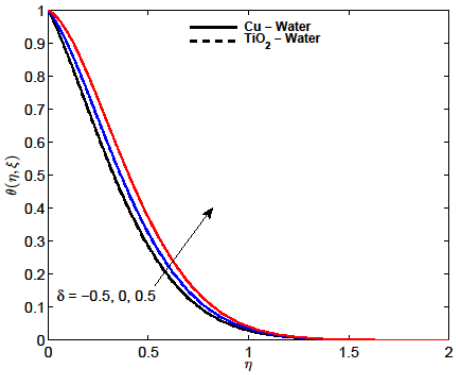

(a)

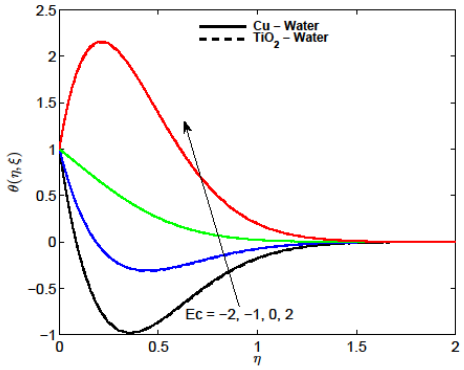

(b)

Figure 4. (a) Effect of heat generation parameter (δ). (b) Effect of Eckert number (Ec) on temperature profiles.

Fig.5 shows that the concentration profiles increase with nanoparticle volume fraction but reduce with stretching. It is observed from Fig. 6 that the concentration profiles decrease with Mn, λ and γ for both nanofluids. It is observed in Fig.7(a) that the Cu-water nanofluid has higher skin friction coefficient values compared to the TiO_2-water nanofluid for the increasing values of ξ. Fig.7(b) shows that the value of the skin friction coefficient of a Cu-water nanofluid are higher than for TiO_2- *water* nanofluid when $\epsilon > 0$ but the opposite trend is observed for $\epsilon < 0$. These results show that the skin friction coefficient decreases with increasing nanoparticle volume friction and stretching or shrinking parameters.

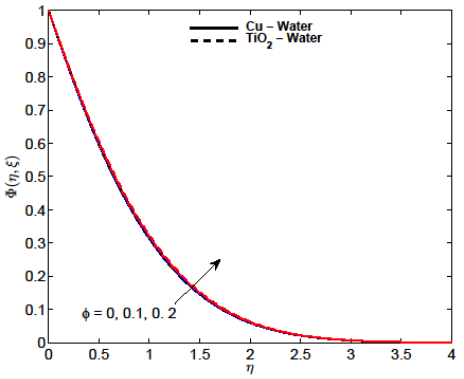

(a)

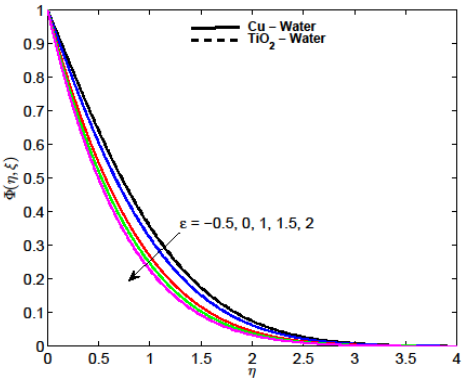

(b)

Figure 5. (a) Effect of nanoparticle volume fraction (ϕ). (b) Effect of stretching or shrinking parameter (ε) on concentration profiles

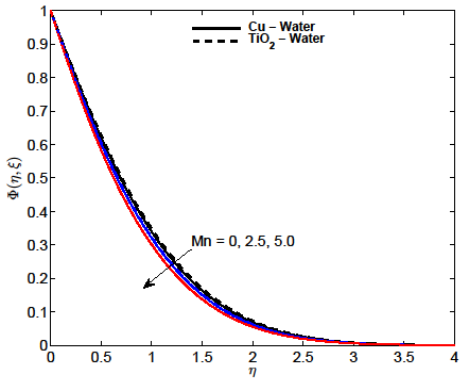

(a)

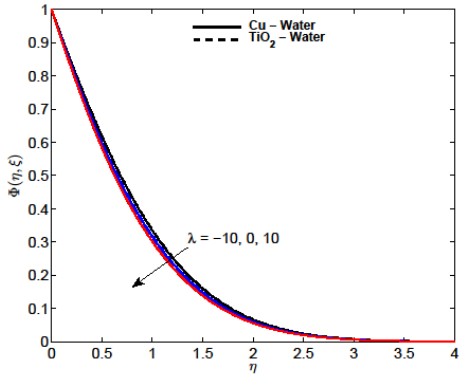

(b)

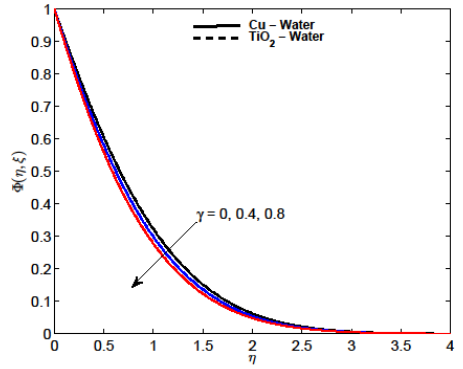

(c)

Figure 6. a) Effect of magnetic field parameter (Mn), (b) Effect of buoyancy parameter (λ), (c) Effect of chemical reaction parameter (γ) on concentration profiles.

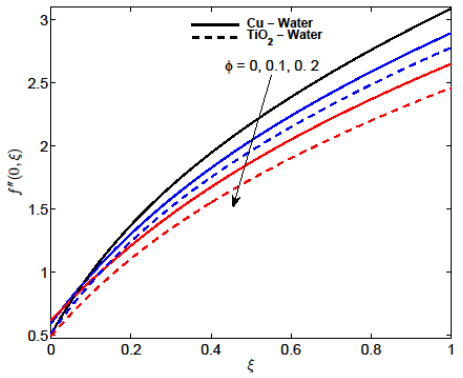

(a)

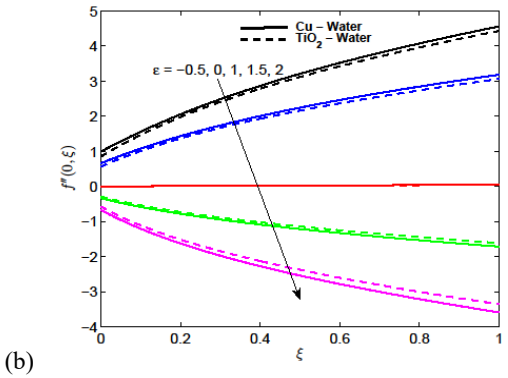

(b)

Figure 7. (a) Effect of nanoparticle volume fraction (ϕ). (b) Effect of stretching or shrinking parameter (ε) on skin friction coefficients.

Fig. 8(a) shows that the heat transfer rate for a *Cu*-water nanofluid is smaller compared to the TiO_2-water nanofluid at the surface of the cone as the nanoparticle volume friction increases. We observe from Figs. 8 (a) and (b) that the heat transfer rate decreases with the increasing ϕ but the opposite trend is observed for ϵ. The *Cu*-water gives a smaller heat transfer rate in comparison to the TiO_2-water nanofluid for increasing δ. Again, we note that δ, *Ec* reduce the heat transfer rate in both Figs. 9 (a) and (b).

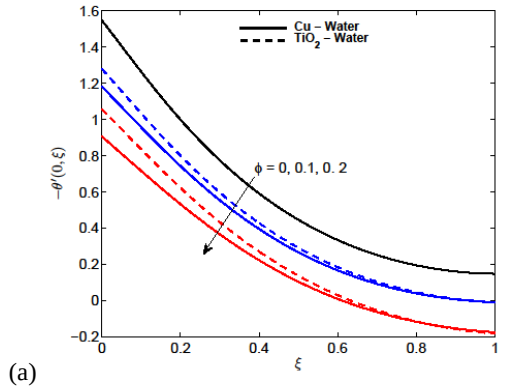

(a)

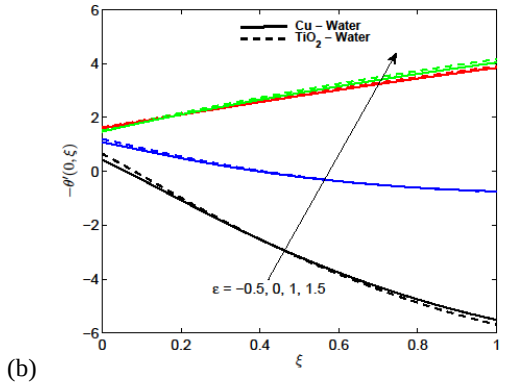

(b)

Figure 8. (a) Effect of nanoparticle volume fraction (ϕ). (b) Effect of stretching or shrinking parameter (ε) on heat transfer rate

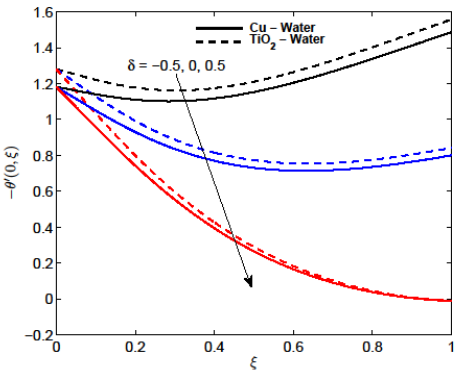

(a)

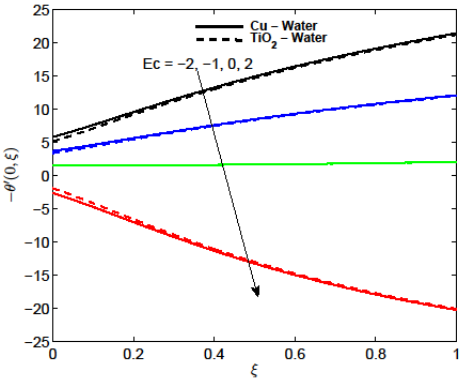

(b)

Figure 9. (a) Effect of heat generation parameter (δ). (b) Effect of Eckert number (*Ec*) on heat transfer rate.

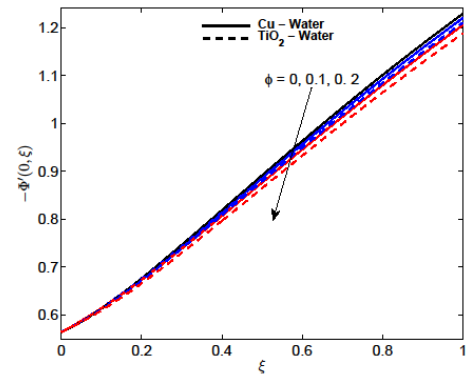

(a)

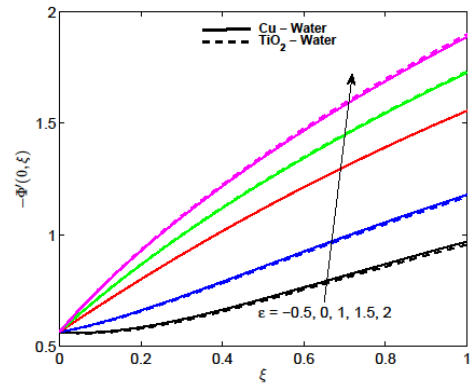

(b)

Figure 10. (a) Effect of nanoparticle volume fraction (ϕ). (b) Effect of stretching or shrinking parameter (ε) on mass transfer rate

The impact of increasing the nanoparticle volume fraction, stretching or shrinking parameters, magnetic field, buoyancy force parameter and chemical reaction parameters on the mass transfer rate at the cone surface is shown in Fig. 10. Fig. 10 (a) shows that the *Cu*-water nanofluid takes higher values than the TiO_2-water nanofluid for the increasing value of ϕ. The mass transfer rate reduces with increasing ϕ for both nano fluids but the opposite trend is observed in Fig. 10 (b).

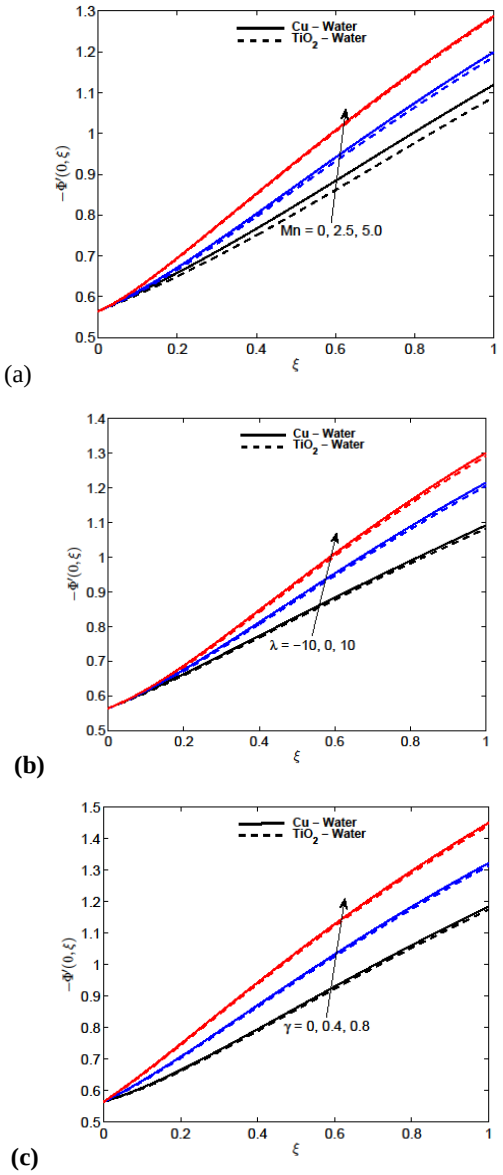

Figure 11. (a) Effect of magnetic field parameter (Mn), (b) Effect of buoyancy parameter (λ), (c) Effect of chemical reaction parameter (γ) on mass transfer rate.

Fig. 11 shows that the mass transfer rate increases with increasing *Mn,* λ and γ for both nanofluids. The effects of magnetic field parameter *Mn* and buoyancy force parameter λ on the velocity and the skin friction coefficient are shown in Figs. 12 and 13 respectively. We note that the *Cu*-water nanofluid assumes higher velocity and skin friction coefficient than the TiO_2-water nanofluid for the increasing values of *Mn,* λ.

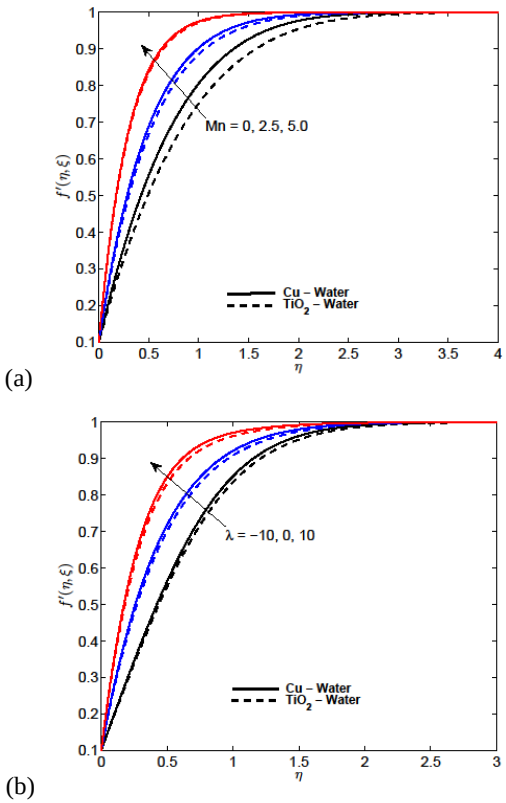

Figure 12. a) Effect of magnetic field parameter (Mn), (b) Effect of buoyancy parameter (λ) on velocity profiles.

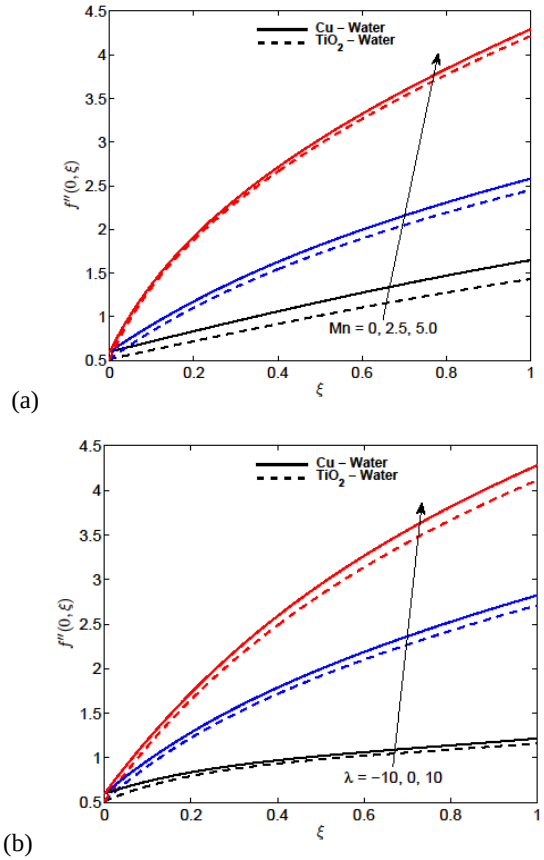

Figure 13. (a) Effect of magnetic field parameter (Mn), (b) Effect of buoyancy parameter (λ) on skin friction coefficients.

The influence of the magnetic field and buoyancy force parameters on the nanofluid temperature and the local Nusselt number are captured in Figs. 14 and 15, respectively. It is noted from Fig. 15 that a *Cu*-water nanofluid has smaller values of the local Nusselt number than a TiO_2-water nanofluid for the increasing value of *Mn*, λ. We further observe that the local Nusselt number decreases with increases in *Mn* and λ.

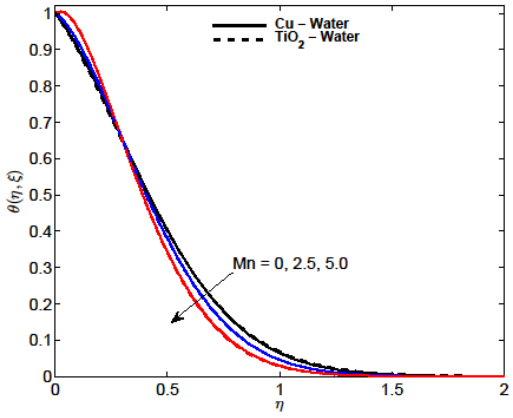

(a)

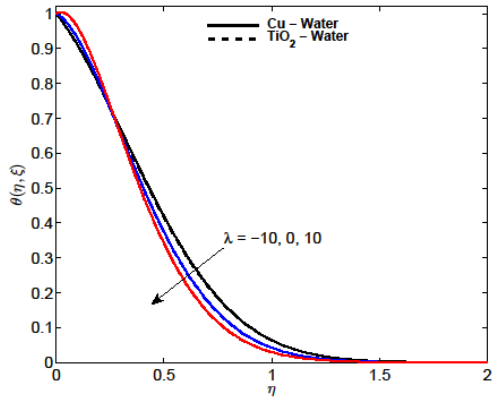

(b)

Figure 14. (a) Effect of magnetic field parameter (Mn), (b) Effect of buoyancy parameter (λ) on temperature profiles

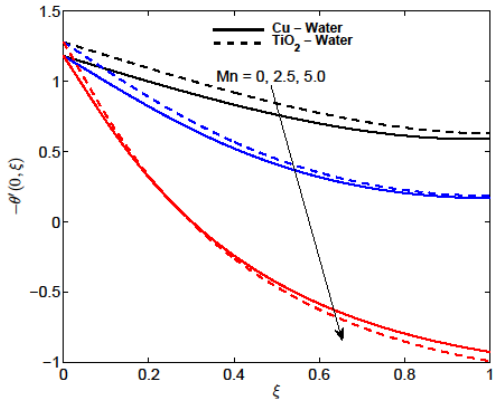

(a)

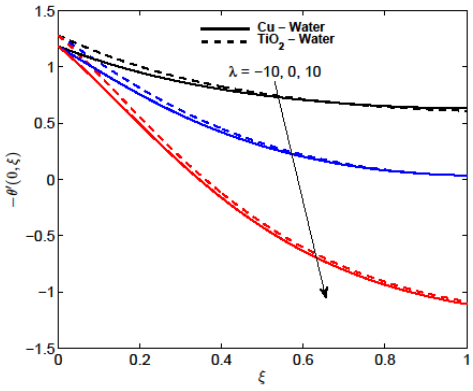

(b)

Figure 15. (a) Effect of magnetic field parameter (Mn), (b) Effect of buoyancy parameter (λ) on heat transfer rate.

Fig. 16 shows the effect of the Prandtl number on the temperature profiles. The temperature profiles and the thermal boundary layer thickness quickly decreases with increasing Prandtl numbers. The Prandtl number is a means to increase fluid viscosity resulting in a reduction in the flow velocity and temperature. Here, the thermal boundary layer thickness decreases with increasing Prandtl number, which is consistent with the findings of various researchers. Fig 17 shows the streamlines for different value of ϵ when the other values are fixed.

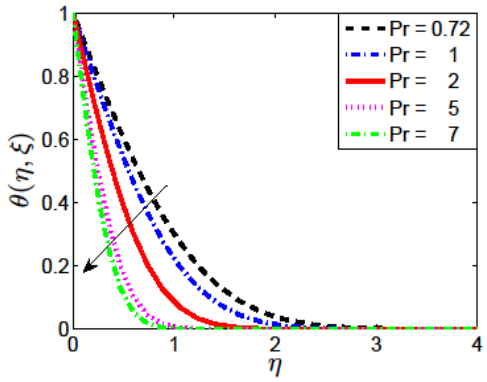

Figure 16. Effect of (*Pr*) on temperature profiles

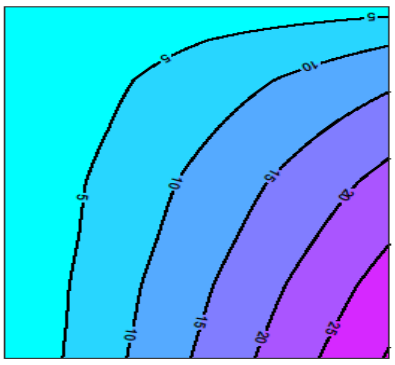

(a)

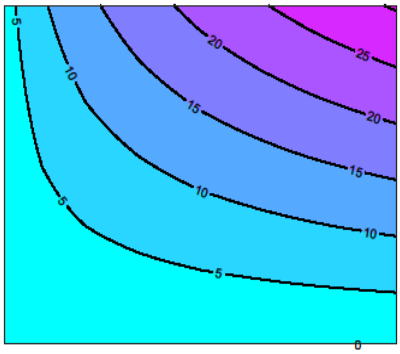

b)

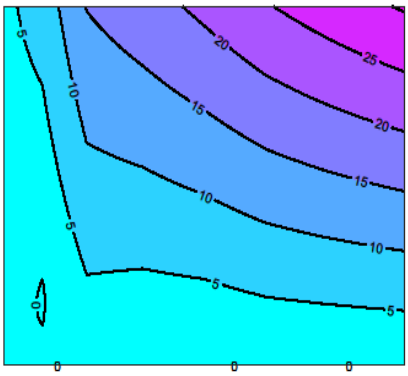

(c)

Figure 17. Streamlines for (a) ϵ = - 1.2, (b) ϵ = 1.0, (c) ϵ = 2.0 when the other parameters are fixed.

5. CONCLUSIONS

The unsteady boundary layer flow of a viscous, incompressible fluid along a vertical stretching or shrinking cone was investigated. The effects of viscous dissipation, internal heat generation and a chemically reactive species have been taken into account for *Cu*-water and *TiO*2-water nanofluids.

It was found that the viscous dissipation has the effect of increasing the nanofluid temperature within the boundary layer region while the rate of heat transfer from the surface decreases with an increase in viscous dissipation. The internal heat generation has the tendency to increase the nanofluid temperature and reduce the rate of heat transfer at the surface of the cone. The nanoparticle concentration decreases while the wall mass transfer rate increases with the increase in the strength of a chemical reaction.

ACKNOWLEDGEMENTS

All the authors are thankful to University of KwaZulu-Natal, South Africa and Amity University, Kolkata, India for the necessary support.

REFERENCES

[1] Choi S.U.S., Eastman J.A. (1995). Enhancing thermal conductivity of fluids with nanoparticles, San Francisco, *ASME International Mechanical Engineering Congress and Exposition*, Vol. 231, pp. 99-103.

[2] Kameswaran P.K., Narayana M., Sibanda P., Murthy P.V.S.N. (2012). Hydromagnetic nanofluid flow due to a stretching or shrinking sheet with viscous dissipation and chemical reaction effects, *International Journal of Heat and Mass Transfer*, Vol. 55, pp. 7587-7595. DOI: 10.1016/j.ijheatmasstransfer.2012.07.065

[3] Kameswaran P.K., Sibanda P., Ramreddy C., Murthy P.V.S.N. (2013). Dual solutions of stagnation-point flow of a nanofluid over a stretching surface, *Boundary Value Problems*, Vol. 188, pp. 1-12. DOI: 10.1186/1687-2770-2013-188

[4] Fauzi E.L.A., Ahmad S., Pop I. (2012). Mixed convection boundary layer flow from a vertical cone in a porous medium filled with a nanofluid, *World Academy of Science, Engineering and Technology*, Vol. 6, pp. 15-18. DOI: scholar.waset.org/1307-6892/13549

[5] Boutra A., Ragui K., Labsi N., Benkahla Y.K. (2017). Free convection enhancement within a nanofluid' filled enclosure with square heaters, *International Journal of Heat and Technology*, Vol. 35, pp. 447-458. DOI: 10.18280/ijht.350302

[6] Ambethkar V., Kumar M. (2017). Numerical solutions of 2-D unsteady incompressible flow with heat transfer in a driven square cavity using streamfunction-vorticityformulation, *International Journal of Heat and Technology*, Vol. 35, pp. 459-473. DOI: 10.18280/ijht.350303

[7] Cheng C. (2012). Natural convection boundary layer flow over a truncated cone in a porous medium saturated by a nanofluid, *Int. Commun. Heat Mass Transf.* Vol. 39, pp. 231-235. DOI: 10.1016/j.icheatmasstransfer.2011.11.002

[8] Chamkha A.J., Abbasbandy S., Rashad A.M., Vajravelu K. (2013). Radiation effects on mixed convection about a cone embedded in a porous medium filled with a nanofluid, *Meccanica*, Vol. 48, pp. 275-285. DOI: 10.1007/s11012-012-9599-1

[9] Nadeem S., Saleem S. (2014). Unsteady mixed convection flow of nanofluid on a rotating cone with magnetic field, *Appl. Nanosci*., Vol. 4, pp. 405-414. DOI: 10.1007/s13204-013-0213-1

[10] Hering R.G., Grosh R.J. (1963). Laminar combined convection from a rotating cone, *ASME J. Heat Transfer* 85, pp. 29-34. DOI: 10.1115/1.3614336

[11] Tien C.L., Tsuji I.J. (1965). A theoretical analysis of laminar forced flow and heat transfer about a rotating cone, *ASME J. Heat Transfer*, Vol. 87, pp. 184-190. DOI: 10.1115/1.3689069

[12] Koh J.C.Y., Price J.F. (1967). Non-similar boundary layer heat transfer of a rotating cone in forced flow, *ASME J. Heat Transfer*, Vol. 89, pp. 139-145. DOI: 10.1115/1.3614336

[13] Takhar H.S., Chamkha A.J., Nath G. (2004). Effect of thermophysical quantities on the natural convection flow of gases over a vertical cone, *International Journal of Engineering Science*, Vol. 42, pp. 243-256. DOI: 10.1016/j.ijengsci.2003.07.005

[14] Turkyilmazoglu M. (2009). On the purely analytic computation of laminar boundary layer flow over a rotating cone, *International Journal of Engineering*

Science, Vol. 47, pp. 875-882. DOI: 10.1016/j.ijengsci.2009.05.008

[15] Sivaraj R., Kumar B.R. (2003). Viscoelastic fluid flow over a moving vertical cone and flat plate with variable electric conductivity, *International Journal of Heat and Mass Transfer*, Vol. 61, pp. 119-128. DOI: 10.1016/j.ijheatmasstransfer.2013.01.060

[16] Srinivasa A.H., Eswara A.T. (2013). Unsteady free convection flow and heat transfer from an isothermal truncated cone with variable viscosity, *International Journal of Heat and Mass Transfer*, Vol. 57, pp. 411-420. DOI: 10.1016/j.ijheatmasstransfer.2012.10.054

[17] Roy S., Datta P., Mahanti N.C. (2007). Non-similar solution of an unsteady mixed convection flow over a vertical cone with suction or injection, *International Journal of Heat and Mass Transfer*, Vol. 50, pp. 181-187. DOI: 10.1016/j.ijheatmasstransfer.2006.06.024

[18] Crane L.J. (1970). Flow past a stretching plate, *Zeit. Angew. Math. Phys.*, Vol. 21, pp. 645-647. DOI: 10.1007/BF01587695

[19] Mahapatra T.R., Pal D., Mondal S. (2012). Heat transfer due to Magnetohydrodynamic stagnation-point flow of a Power-law fluid towards a stretching surface in the presence of thermal radiation and suction/injection, *ISRN Thermodynamics*, Article ID 465864, pp. 1-9, DOI: 10.5402/2012/465864

[20] Salem A.M., Abd El-Aziz M. (2008). Effect of Hall currents and chemical reaction on hydromagnetic flow of a stretching vertical surface with internal heat generation/absorption, *Applied Mathematical Modelling*, Vol. 32, pp. 1236-1254. DOI: 10.1016/j.apm.2007.03.008

[21] Noor N.F.M., Kechil S.A., Hashim I. (2010). Simple non-perturbative solution for MHD viscous flow due to a shrinking sheet, *Commun. Nonlinear Sci. Numer. Simul.*, Vol. 15, pp. 144-148. DOI: 10.1016/j.cnsns.2009.03.034

[22] Wang C.Y. (2008). Stagnation flow towards a shrinking sheet, *Int. J. Non-Linear Mech*., Vol. 43, pp. 377-382. DOI: 10.1016/j.ijnonlinmec.2007.12.021

[23] Jafar K., Nazar R., Ishak A., Pop I. (2012). MHD flow and heat transfer over stretching/shrinking sheets with external magnetic field, viscous dissipation and joule effects, *Can. J. Chem. Eng*., Vol. 90, pp. 1336-1346. DOI: 10.1002/cjce.20609

[24] Schlichting H., Gersten K. (2003). *Boundary Layer Theory*, 8th edition, Springer, pp. 86-89. DOI: 10.1007/978-3-662-52919-5

[25] Oztop H.F., Abu-Nada E. (2008). Numerical study of natural convection in partially heated rectangular enclosures filled with nanofluids, *Int. J. Heat Fluid Flow*, Vol. 29, pp. 1326-1336. DOI: 10.1016/j.ijheatfluidflow.2008.04.009

[26] Gangadhar K., RangaRao T., Subhakar M.J., Sekhar T.V.S. (2014). MHD and mixed convection flow of Maxwell fluid on heat transfer near a stagnation point flow, *IOSR Journal of Mathematics*, Vol. 10, No. 2, pp. 60-68. DOI: 10.9790/5728-10216068

[27] Mahdy A. (2012). Unsteady mixed convection boundary layer flow and heat transfer of nanofluids due to stretching sheet, *Nuclear Engineering and Design*, Vol. 249, pp. 248-255. DOI: 10.1016/j.nucengdes.2012.03.025

[28] Motsa S.S. (2013). A new spectral local linearization method for nonlinear boundary layer flow problems, *J. Appl. Math*., 2013, pp. 1-15. DOI: 10.1155/2013/423628

[29] Grosan T., Pop T. (2011). Axisymmetric mixed convection boundary layer flow past a vertical cylinder in a nanofluid, *International Journal of Heat and Mass Transfer*, Vol. 54, pp. 3139-3145. DOI: 10.1016/j.ijheatmasstransfer.2011.04.018

[30] Suali M., Long N.M.A.N., Ishak A. (2012). Unsteady stagnation point flow and heat transfer over a stretching/shrinking sheet with prescribed surface heat flux, *App. Math. and Comp. Intel*., Vol. 1, pp. 1-11.

Chapter 4

The effect of thermophoresis on unsteady Oldroyd-B nanofluid flow over stretching surface

In this Chapter we investigate the unsteady flow of an Oldroyd-B nanofluid. Many investigators have demonstrated that the Oldroyd-B fluid theory has applications in many fields, including bio-rheology, geophysics, chemical and petroleum industries. The main objective of this study is to present a numerical investigation of unsteady flow over a stretching surface subject to the influence of physical parameters, such as Deborah numbers, thermophoresis and Brownian motion. We assume zero nanoparticle flux at the boundary surface. The coupled nonlinear partial differential equations for the flow are solved using both the spectral relaxation and quasi-linearization methods.

PLOS | ONE

RESEARCH ARTICLE

The Effect of Thermophoresis on Unsteady Oldroyd-B Nanofluid Flow over Stretching Surface

Faiz G. Awad[1], Sami M. S. Ahamed[2], Precious Sibanda[2]*, Melusi Khumalo[1]

1 Department of Mathematics, University of Johannesburg, P.O. Box 17011, Doornfontein 2028, South Africa, **2** University of KwaZulu-Natal, School of Mathematics, Statistics and Computer Science, Private Bag X01, Scottsville, Pietermaritzburg 3209, South Africa

* sibandap@ukzn.ac.za

CrossMark
click for updates

OPEN ACCESS

Citation: Awad FG, Ahamed SMS, Sibanda P, Khumalo M (2015) The Effect of Thermophoresis on Unsteady Oldroyd-B Nanofluid Flow over Stretching Surface. PLoS ONE 10(8): e0135914. doi:10.1371/journal.pone.0135914

Editor: Ming Dao, Massachusetts Institute Of Technology, UNITED STATES

Received: October 4, 2014

Accepted: July 28, 2015

Published: August 27, 2015

Copyright: © 2015 Awad et al. This is an open access article distributed under the terms of the Creative Commons Attribution License, which permits unrestricted use, distribution, and reproduction in any medium, provided the original author and source are credited.

Data Availability Statement: All relevant data are within the paper.

Funding: The authors are grateful for funding from the universities of KwaZulu-Natal and Johannesburg.

Competing Interests: The authors have declared that no competing interests exist.

Abstract

There are currently only a few theoretical studies on convective heat transfer in polymer nanocomposites. In this paper, the unsteady incompressible flow of a polymer nanocomposite represented by an Oldroyd-B nanofluid along a stretching sheet is investigated. Recent studies have assumed that the nanoparticle fraction can be actively controlled on the boundary, similar to the temperature. However, in practice, such control presents significant challenges and in this study the nanoparticle flux at the boundary surface is assumed to be zero. We have used a relatively novel numerical scheme; the spectral relaxation method to solve the momentum, heat and mass transport equations. The accuracy of the solutions has been determined by benchmarking the results against the quasilinearisation method. We have conducted a parametric study to determine the influence of the fluid parameters on the heat and mass transfer coefficients.

Introduction

A wide variety of fluids, such as polymer solutions, plastics, pulps, emulsions, blood plasma, chocolate, tomato sauce, mustard, mayonnaise, toothpaste, asphalt, some greases and sewage, petroleum products, oils, etc., are non-Newtonian in character. Such fluids have a non-linear shear stress-strain rate relationship. The equations that model the flow of these fluids are generally of a higher order than the Navier-Stokes equations. During the last several decades, the study of flow of non-Newtonian fluids, has received considerable amount of research interest, due to the relevance of non-Newtonian flows to a large number of engineering and manufactural applications such as in the processing of synthetic fibers, food, polymers melts and pharmaceutical products.

The unsteady boundary layer flow of non-Newtonian fluids due to stretching surface is an important field of research in fluid mechanics. In many practical problems, the flow could be unsteady due to a time dependent free stream velocity. There are several transport processes with surface mass transfer where the buoyancy force arises from thermal diffusion caused by

the temperature gradient. It is interesting as well as useful to investigate the combined effects of thermal diffusion and surface mass transfer on a stretching surface where the free stream velocity varies arbitrarily with time. The stretched boundary layer flow with heat transfer has numerous applications in engineering and industrial processes such as when polymer sheets are extruded continuously from a dye, in the annealing and thinning of copper wires, paper production and glass blowing, aerodynamic extrusion of plastic sheets and the cooling of infinite metallic plates in cooling baths. Mixed convection or buoyancy driven flows over a surface occur naturally in geothermal and petroleum recovery processes, solid matrix heat exchanges, the cooling of nuclear reactors and other practical problems. Historically, the study of a boundary layer flow along a stretching surface has its origins in the work of Sakiadis [1]. Tsou et al. [2] presented a combined experimental and analytical study of the stretching flow, which, in essence demonstrated that such a flow is physically possible. Crane [3] further extended the Sakiadis study to a linearly stretching plate in a quiescent fluid and presented an exact analytic solution. Subsequent work has looked at various aspects of the stretching sheet problem, but most have been concerned with how the flow is affected by or responds to changes in various fluid and surface parameters, see for instance, [4–9].

Conventional fluids such as water, ethylene glycol and oil have low heat transfer characteristics owing to their low thermal conductivity. A recent technique to enhance the thermal conductivity of these base fluids is to suspend nano-sized metallic particles such as aluminum, titanium, gold, copper, iron or their oxides in the conventional base fluids resulting in what has come to be name as a "nanofluid," Choi [10]. Nanofluids have considerably improved thermophysical properties such as thermal conductivity, thermal diffusivity, viscosity and convective heat transfer coefficient compared to base fluids. In the last few years the flow of nanofluid through different geometries, and under various physical assumptions have been studied by several authors such as [11–14].

The Oldroyd-B constitutive model describes a subclass of non-Newtonian fluids that adequately describe the behaviour of some viscoelastic fluids such as dilute polymer solutions. The Oldroyd-B fluid can describe stress-relaxation, creep and the normal stress differences but it cannot describe either shear thinning or shear thickening, a phenomenon that is exhibited by many polymer materials. Nonetheless, this model is perhaps one of the most successful models for describing the response of some polymeric liquids [15]. Some investigations of Oldroyd-B fluids have been done, by, among others, Hayat et al. [16] who presented a study of the three-dimensional flow of an Oldroyd-B fluid due to a stretching surface with convective boundary conditions. Siddiqui et al. [17] investigated the unsteady flow of an incompressible Oldroyd-B fluid between two infinite parallel plates subject to slip between the plates and the fluid. Jamil et al. [18] further studied the unsteady flow of an Oldroyd-B fluid and solved the model equations using finite Hankel transforms. Sohail et al. [19] investigated the two-dimensional steady incompressible Oldroyd-B nanofluid flow past a stretching sheet. The thermophoresis and radiation effects on Heat and mass transfer characteristics in three-dimensional flow of an Oldroyd-B fluid due to a bi-directional stretching surface were investigated by Shehzad et al. [20]. Related studies include, among others, [21–25]. Excellent survey papers on Oldroyd-B fluids can be found in studies by Rajagopal and his colleagues [26–28].

There are currently only a few theoretical studies on the convective boundary layer flow and heat transfer in an Oldroyd-B nanofluid over a stretching surface. Including nanoparticles in dilute polymer solutions imparts improved thermophysical properties to the polymer materials. This could, for example, include improved electrical, mechanical and optical properties, Chao [29]. Recent exception is the study by Khan et al. [30]. These studies all assumed that the nanoparticle volume fraction at the boundary is actively controlled. To the best of the authors' knowledge, there are as yet no studies of convective heat transport in polymer nanocomposites

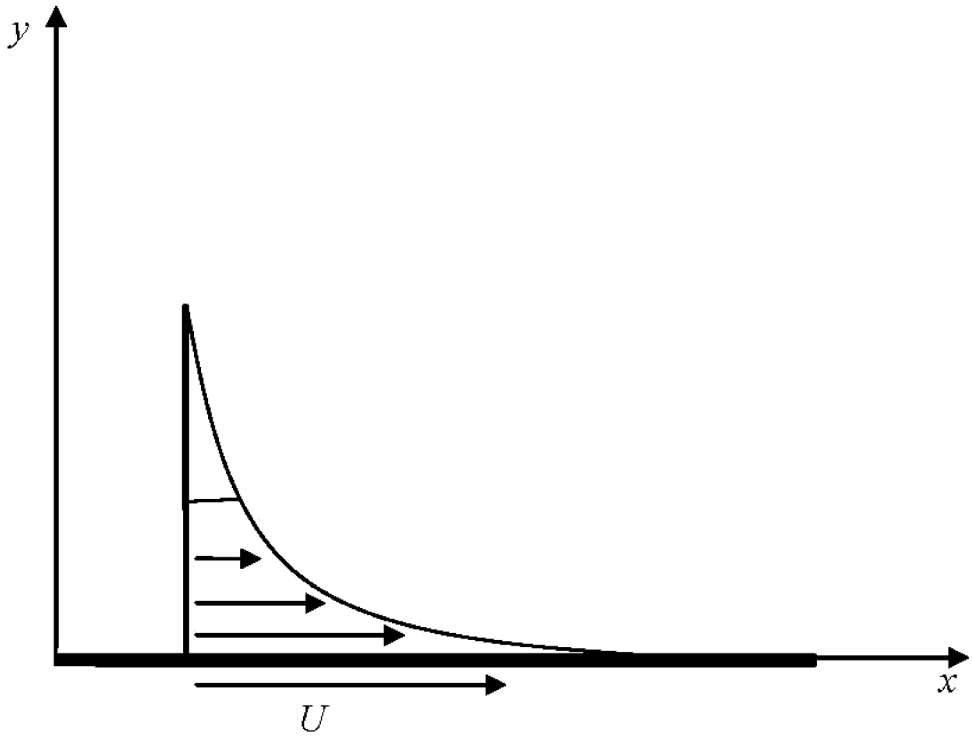

Fig 1. Geometry and the coordinate system.

doi:10.1371/journal.pone.0135914.g001

such as an Oldroyd-B nanofluid flow in which the nanofluid particle fraction on the boundary is not actively managed. The objective of this study is therefore to investigate thermophoresis effects in unsteady Oldroyd-B nanofluid flow along a stretching surface. The problem is formulated under the assumption that the nanoparticle volume fraction at the boundary is not actively controlled, see Nield and Kuznetsov [31–34]. The highly non-linear momentum, heat and mass transfer equations are solved numerically using the spectral relaxation and quasi-linearization methods, see Motsa et al. [35, 36].

1 Mathematical Formulation

Consider the unsteady two-dimensional Oldroyd-B nanofluid flow over a stretching surface. The sheet stretches along the plane $y = 0$ with the flow confined in the region $y > 0$. The nanoparticle flux at the boundary surface is assumed to be zero. The surface is stretched with a velocity $U = bx/(1-at)$ where a and b are positive constants. Both the nanofluid and the surface are kept at a constant temperature T_w where $T_w > T_\infty$ is for a heated surface and $T_w < T_\infty$ corresponds to a cooled surface. The geometry of the problem is shown in Fig 1. Applying the Oberbeck-Boussinesq and the boundary layer approximations to the basic equations of an incompressible non-Newtonian fluid, we obtain

$$\nabla \cdot \mathbf{V} = 0, \tag{1}$$

$$\rho \frac{d\mathbf{V}}{dt} = \nabla \cdot \tau, \tag{2}$$

$$(\rho c)_f\left(\frac{\partial T}{\partial t}+\mathbf{V}\cdot\nabla T\right) = (\rho c)_p\left[D_B\nabla C\cdot\nabla T+\left(\frac{D_T}{T_\infty}\right)\nabla T\cdot\nabla T\right] +k\nabla^2 T, \tag{3}$$

$$\frac{\partial C}{\partial t}+\mathbf{V}\cdot\nabla C=D_B\nabla^2 C+\left(\frac{D_T}{T_\infty}\right)\nabla^2 T. \tag{4}$$

The Cauchy stress tensor τ and extra stress tensor $\mathbf{S}$ are defined as

$$\tau=-p\mathbf{I}+\mathbf{S} \quad \text{and} \quad \mathbf{S}+\hat{\delta}_1(t)\frac{D\mathbf{S}}{Dt}=\mu\left(\mathbf{A}+\hat{\delta}_2(t)\frac{D\mathbf{A}}{Dt}\right), \tag{5}$$

where

$$\frac{D}{Dt}=\frac{\partial(\cdot)}{\partial t}+(V\cdot\nabla)(\cdot)-(\nabla V)(\cdot)-(\cdot)(\nabla V)^*,$$

is the covariant differentiation, the * denotes the matrix transpose, $\hat{\delta}_1(t)$ and $\hat{\delta}_2(t)$ are the relaxation and retardation times respectively. The velocity field is

$$\mathbf{V}=(u(x,y,t),v(x,y,t)),$$

where u and v are the velocity components along the x and y directions respectively. The first Rivlin-Ericksen tensor $\mathbf{A}$ is defined as

$$\mathbf{A}=\nabla\mathbf{V}+(\nabla\mathbf{V})^*.$$

The governing equations take the form (see Nadeem et al. [19])

$$\frac{\partial u}{\partial x}+\frac{\partial v}{\partial y} = 0, \tag{6}$$

$$\begin{aligned}
&\frac{\partial u}{\partial t}+u\frac{\partial u}{\partial x}+v\frac{\partial u}{\partial y}+\hat{\delta}_1(t)\left[\frac{\partial^2 u}{\partial t^2}+\frac{\partial}{\partial t}\left(u\frac{\partial u}{\partial x}+v\frac{\partial u}{\partial y}\right)+u\frac{\partial^2 u}{\partial t\partial x}+v\frac{\partial^2 u}{\partial t\partial y}\right.\\
&\left.-\frac{\partial u}{\partial t}\frac{\partial u}{\partial x}-\frac{\partial v}{\partial t}\frac{\partial u}{\partial y}+u^2\frac{\partial^2 u}{\partial x^2}+v^2\frac{\partial^2 u}{\partial y^2}+2uv\frac{\partial^2 u}{\partial x\partial y}\right]=\nu\frac{\partial^2 u}{\partial y^2}\\
&+\nu\hat{\delta}_2(t)\left[\frac{\partial^3 u}{\partial t\partial y^2}+u\frac{\partial^3 u}{\partial x\partial y^2}+v\frac{\partial^3 u}{\partial y^3}-\frac{\partial u}{\partial x}\frac{\partial^2 u}{\partial y^2}-\frac{\partial u}{\partial y}\frac{\partial^2 v}{\partial y^2}\right],\\
&\frac{\partial T}{\partial t}+u\frac{\partial T}{\partial x}+v\frac{\partial T}{\partial y}=\alpha_m\frac{\partial^2 T}{\partial y^2}+\tau\left[D_B\frac{\partial C}{\partial y}\frac{\partial T}{\partial y}+\frac{D_T}{T_\infty}\left(\frac{\partial T}{\partial y}\right)^2\right],
\end{aligned} \tag{7}$$

$$\frac{\partial C}{\partial t}+u\frac{\partial C}{\partial x}+v\frac{\partial C}{\partial y}=D_B\frac{\partial^2 C}{\partial y^2}+\frac{D_T}{T_\infty}\frac{\partial^2 T}{\partial y^2}, \tag{8}$$

subject to the boundary conditions

$$u=\mathrm{U},\quad v=0,\quad T=T_\mathrm{w},\quad D_B\frac{\partial C}{\partial y}+\frac{D_T}{T_\infty}\frac{\partial T}{\partial y}=0 \quad \text{on} \quad y=0, \tag{9}$$

$$u\to 0,\quad T\to T_\infty,\quad C=C_\infty \quad \text{as} \quad y\to\infty, \tag{10}$$

where ν is the kinematic viscosity, T and $\hat{\phi}$ are the local fluid temperature and concentration volume fraction, T_∞ and $\hat{\phi}_\infty$ are the fluid temperature and ambient concentration volume fraction respectively, α_m is the effective thermal diffusivity, D_B is the Brownian diffusion coefficient, D_T is thermophoresis diffusion coefficient, $\tau = (\rho c)_f/(\rho c)_P$ is the ratio between the effective heat capacity of the nanoparticle material and heat capacity of the fluid.

We introduce the following similarity transformations

$$\begin{aligned}\psi(x,y,t) &= \sqrt{\frac{b\nu}{1-at}}xf(\eta), \qquad \eta = \sqrt{\frac{b}{\nu(1-at)}}\,y,\\ T(x,y,t) &= T_\infty + T_{ref}\left[\frac{bx^2}{2\nu}\right](1-at)^{-\frac{3}{2}}\theta(\eta),\\ C(x,y,t) &= C_\infty + C_{ref}\left[\frac{bx^2}{2\nu}\right](1-at)^{-\frac{3}{2}}\phi(\eta),\end{aligned}$$

where θ and ϕ are the dimensionless temperature and nanoparticle volume fraction respectively and η is a similarity variable. The physical stream function $\psi(x, y, t)$ automatically ensures that mass conservation given in Eq (6). The velocity components are readily obtained as

$$u = \frac{\partial\psi}{\partial y} = \frac{bx}{(1-at)}f'(\eta), v = -\frac{\partial\psi}{\partial x} = -\sqrt{\frac{\nu b}{(1-at)}}f(\eta), \tag{11}$$

where f' is the dimensionless velocity. Eqs (7)–(8) can be presented as

$$\begin{aligned}&f''' + ff'' - f'^2 - S\left(f' + \frac{1}{2}\eta\, f''\right) + \beta_1(2ff'f'' - f^2f''') + \beta_2(f''^2 - ff'''')\\ &+ \beta_2 S\left(2f''' + \frac{1}{2}\eta f''''\right) - \beta_1 S^2\left(2f' + \frac{7}{4}\eta f'' + \frac{1}{4}\eta^2 f'''\right)\\ &- \beta_1 S\left(2f'^2 - 3ff'' + \frac{3}{2}\eta f'f'' - \frac{1}{2}\eta ff'' - \eta ff''''\right) = 0,\end{aligned} \tag{12}$$

$$\theta'' + Pr\left[f\theta' - 2f'\theta - \frac{S}{2}(3\theta + \eta\theta')\right] + N_b\phi'\theta' + N_t\theta'^2 = 0, \tag{13}$$

$$\phi'' + Le\left[f\phi' - 2f'\phi - \frac{S}{2}(3\phi + \eta\phi')\right] + \frac{N_t}{N_b}\theta'' = 0, \tag{14}$$

with the boundary conditions

$$f' = 1, \quad f = 0, \quad \theta = 1, \quad N_b\phi' + N_t\theta' = 0 \quad \text{at} \quad \eta = 0, \tag{15}$$

$$f' \to 0, \quad \theta' \to 0, \quad \phi \to 0 \quad \text{as} \quad \eta \to \infty, \tag{16}$$

where S is the dimensionless measure of the unsteadiness, β_1 and β_2 are the Deborah numbers in terms of relaxation and retardation times, respectively, the Prandtl number Pr, the Brownian motion parameter N_b, the thermophoresis parameter N_t, the Lewis number Le. These

parameters are defined as

$$S = \frac{a}{b},\ \beta_1 = \delta_1 b,\ \beta_2 = \delta_2 b,\ Pr = \frac{\nu}{\alpha_m},\ Le = \frac{\nu}{D_B},$$

$$N_t = \frac{\tau D_T (T_{(w} - T_\infty)}{T_\infty \alpha_m},\quad Nb = \frac{\tau D_B C_{ref}\left[\frac{bx^2}{2\nu}\right]}{\alpha_m}(1-at)^{-\frac{3}{2}}.$$

The non-dimensional form of the Nusselt number and Sherwood number that describe the heat and nanoparticle volume fraction transfer at the surface are

$$Nu_x/Re_x^{\frac{1}{2}} = -\theta'(0) \quad \text{and} \quad Shw_x/Re_x^{\frac{1}{2}} = -\phi'(0),$$

where $Re_x = Ux/\nu$ is the local Reynolds number.

2 Method of Solution

To solve Eqs (12)–(14) along with the boundary conditions Eqs (15)–(16), the spectral relaxation method (SRM) was used, see Motsa et al. [37–39]. This method is preferred since it has been shown to be accurate and generally easier to use compared to other common numerical methods such as finite differences.

We start by reducing the order of Eq (12) from fourth to third order. To this end, we set $f' = g$, so that Eq (12) becomes

$$\begin{aligned} & f' = g, \\ & g'' + fg' - g^2 - S\left[g + \frac{1}{2}\eta g'\right] + \beta_1(2fgg' - f^2 g'') \\ & \quad + \beta_2(g'^2 - fg''') + \beta_2 S\left(2g'' + \frac{1}{2}\eta g'''\right) - \beta_1 S^2\left(2g + \frac{7}{4}\eta g' + \frac{1}{4}\eta^2 g''\right) \\ & \quad - \beta_1 S\left(2g^2 - 3fg' + \frac{3}{2}\eta gg' - \frac{1}{2}\eta fg' - \eta fg''\right) = 0. \end{aligned} \tag{17}$$

The spectral relaxation algorithm decouples the system of governing Eqs (12)–(14). From the decoupled equations an iteration scheme is developed by evaluating linear terms at the current iteration level $r+1$ and the nonlinear terms at the previous iteration level r. Applying the SRM to Eqs (13)–(14) and (17)–(17) gives the following linear ordinary differential equations;

$$a_1 g'''_{r+1} + a_2 g''_{r+1} + a_3 g'_{r+1} + a_4 g_{r+1} + a_5 = 0, \tag{18}$$

$$f'_{r+1} = g_{r+1},\quad f_{r+1}(0) = 0, \tag{19}$$

$$\theta''_{r+1} + b_1\theta'_{r+1} + b_2\theta_{r+1} + b_3 = 0, \tag{20}$$

$$\phi''_{r+1} + c_1\phi'_{r+1} + c_2\phi_{r+1} + c_3 = 0, \tag{21}$$

$$g_{r+1}(0) = 1,\ \theta_{r+1}(0) = 1,\ N_b\phi'_{r+1}(0) + N_t\theta'_{r+1}(0) = 0, \tag{22}$$

$$g_{r+1}(\infty) = 0,\ \theta_{r+1}(\infty) = 0,\ \phi_{r+1}(\infty) = 0, \tag{23}$$

where a_i, b_i and c_i ($i = 1, 2, \ldots$) are given by

$$\begin{aligned}
a_1 &= \beta_2\left(\frac{1}{2}S\eta - f_{r+1}\right),\\
a_2 &= 1-\beta_1\left(f_{r+1}^2+\frac{1}{4}S^2\eta^2 - S\eta f_{r+1}\right)+2\beta_2 S,\\
a_3 &= f_{r+1}-\frac{1}{2}S\eta+\beta_1\left(2f_{r+1}g_r-\frac{7}{4}S^2\eta+3Sf_{r+1}-\frac{3}{2}S\eta g_r+\frac{1}{2}S\eta f_{r+1}\right)\\
&\quad +2\beta_2 g_r',\\
a_4 &= -\left[2g_r+S-\beta_1\left(2f_{r+1}g_r'-s^2-4Sg_r-\frac{3}{2}S\eta g_r'\right)\right],\\
a_5 &= -\left[g_r^2-\beta_1\left(2f_{r+1}g_rg_r'-2Sg_r^2-\frac{3}{2}S\eta g_rg_r'\right)-\beta_2 g_r'2\right],
\end{aligned}$$

$$\begin{aligned}
b_1 &= Pr\left(f_{r+1}-\frac{1}{2}S\eta+N_b\phi_r'\right), \quad b_2 = -Pr\left(2g_{r+1}+\frac{3}{2}S\right),\\
b_3 &= -N_t\theta_r'^2, \quad c_1 = Le\left(f_{r+1}-\frac{1}{2}S\eta\right),\\
c_2 &= -Le\left(2g_{r+1}+\frac{3}{2}S\right), \quad c_3 = \frac{N_t}{N_b}\theta_r''.
\end{aligned}$$

Starting from given initial approximations f_0, g_0, θ_0 and ϕ_0, Eqs (18)–(21) can be solved iteratively using any suitable numerical method. We opt to use the spectral collocation methods for its accuracy. We find the unknown function at collocation points by requiring that Eqs (18)–(21) be satisfied exactly at these points. A convenient set of collocation points is the Gauss-Lobatto points defined by

$$\omega_j = \cos\frac{\pi j}{N}, \quad j = 0, 1, \ldots, N. \tag{24}$$

For convenience, in numerical computations the semi-infinite domain is approximated by the truncated domain $[0, L]$. Then using the linear transformation $\eta = L(\omega + 1)/2$, we convert $[0, L]$ into the interval $[-1, 1]$ in which the spectral method can be used, where $L = \eta_\infty$ is a finite number selected to be large enough to represent the behaviour of the flow properties when η is very large. The derivatives are defined as

$$\frac{df}{d\eta} = \sum_{k=0}^{N}\mathbf{D}_{jk}f(\omega_k) = \mathbf{D}f, \quad j = 0, 1, \ldots, N, \tag{25}$$

where $N + 1$ is the number of collocation points, $\mathbf{D} = 2D/L$ and $\mathrm{f} = [f(\omega_0), f(\omega_1), \ldots, f(\omega_N)]^T$ is the vector of unknown functions at the collocation points. Applying the Chebyshev spectral collocation method to the system Eqs (18)–(21), we obtain the following matrix equations

$$\mathbf{A}_{1,r}g_{r+1} = \mathbf{R}_{1,r}, \;\; g_{r+1}(\omega_N) = 1, \;\; g_{r+1}(\omega_0) = 0, \tag{26}$$

$$\mathbf{D}f_{r+1} = g_{r+1}, \;\; f_{r+1}(\omega_N) = 0, \tag{27}$$

$$\mathbf{A}_{2,r}\theta_{r+1} = \mathbf{R}_{2,r}, \quad \theta_{r+1}(\omega_N) = 1, \quad \theta_{r+1}(\omega_0) = 0, \tag{28}$$

$$\mathbf{A}_{3,r}\phi_{r+1} = \mathbf{R}_{3,r}, \quad N_b\phi_{r+1}(\omega_N) + N_t\theta_{r+1}(\omega_N), \quad \phi_{r+1}(\omega_0) = 0, \tag{29}$$

where

$$\begin{aligned} \mathbf{A}_{1,r} &= \text{diag}[a_1]\mathbf{D}^3 + \text{diag}[a_2]\mathbf{D}^2 + \text{diag}[a_3]\mathbf{D} + \text{diag}[a_4]\mathbf{I}, \\ \mathbf{R}_{1,r} &= -a_5, \end{aligned} \tag{30}$$

$$\mathbf{A}_{2,r} = \mathbf{D}^2 + \text{diag}[b_1]\mathbf{D} + \text{diag}[b_2]\mathbf{I}, \quad \mathbf{R}_{2,r} = -b_3, \tag{31}$$

$$\mathbf{A}_{3,r} = \mathbf{D}^2 + \text{diag}[c_1]\mathbf{D} + \text{diag}[c_2]\mathbf{I}, \quad \mathbf{R}_{3,r} = -c_3. \tag{32}$$

Here I is an $(N+1)\times(N+1)$ diagonal matrix, diag[·] denotes a diagonal matrix. We choose suitable initial guesses f_0, g_0, θ_0 and ϕ_0 which satisfy the boundary conditions of governing equations as

$$f_0 = 1 - e^{-\eta}, \quad g_0 = e^{-\eta}, \quad \theta_0 = e^{-\eta}, \quad \phi_0 = -\frac{N_t}{N_b}e^{-\eta}. \tag{33}$$

3 Results and Discussion

Eqs (12)–(14) along with the boundary conditions Eqs (15)–(16), were solved numerically using both the spectral relaxation method (SRM) and the quasi-linearization method (QLM), see Bellman and Kalaba [40]. Here the QLM has been used as a benchmarking tool to test the accuracy, and hence the reliability of the SRM results.

The results showing the effects of various parameters on the skin-friction coefficient and the heat transfer rate on the unsteady Oldroyd-B nanofluid are given in Tables 1–3.

Table 1 gives a comparison between the present results and the results obtained by Sharidan [41] and Pal [42] for the skin friction. There is a good agreement between the two sets of results with the SRM having converged at the fifth order up to six decimal places. The SRM results are further validated by comparison with results generated using a quasilinearisation method. The quasilinearisation method has also been used recently, albeit in a slightly different form, by Ibrahim and Shanker [43]

Table 1. Comparison of results for the $-f''(0)$ with $\beta_1 = 0$ and $\beta_2 = 0$.

				present results		
S	Sharidan [41]	Elbashbeshy [47]	Pal [42]	Ord 4	Ord 5	Ord 6
0.0	—	1.0000	—	1.000000	1.000000	1.000000
0.2	—	—	—	1.068015	1.068012	1.068012
0.4	—	—	—	1.134688	1.134686	1.134686
0.6	—	—	—	1.199113	1.199119	1.199119
0.8	1.261042	1.3345	1.261043	1.261039	1.261043	1.261043
1.2	1.377722	1.4535	1.377724	1.377722	1.377724	1.377724
1.4	—	—	—	1.432835	1.432836	1.432836
2.0	1.587362	1.6828	1.587366	1.587365	1.587366	1.587366

doi:10.1371/journal.pone.0135914.t001

Table 2. Comparison of the skin friction coefficient $-f''(0)$ for various values of dimensionless unsteadiness S, the Deborah numbers β_1 and β_2, when $N_t = 0.5$, $N_b = 0.5$, $Pr = 7$ and $Le = 10$.

			SRM			QLM
S	β_1	β_2	Ord 5	Ord 6	Ord 7	Ord 8
0.2	0.3	0.4	0.962067	0.962066	0.962066	0.962066
0.4	0.3	0.4	1.014081	1.014081	1.014081	1.014081
0.6	0.3	0.4	1.064909	1.064909	1.064909	1.064909
0.8	0.3	0.4	1.114378	1.114377	1.114377	1.114377
1.0	0.3	0.4	1.162441	1.162441	1.162441	1.162441
1.2	0.3	0.4	1.209120	1.209120	1.209120	1.209120
1.4	0.3	0.4	1.254465	1.254465	1.254465	1.254465
1.6	0.3	0.4	1.298547	1.298546	1.298546	1.298546
0.2	0.1	0.4	0.979541	0.979541	0.979541	0.979541
0.2	0.2	0.4	1.049256	1.049256	1.049256	1.049256
0.2	0.3	0.4	1.114378	1.114377	1.114377	1.114377
0.2	0.4	0.4	1.175721	1.175720	1.175720	1.175720
0.2	0.5	0.4	1.233884	1.233883	1.233883	1.233883
0.2	0.6	0.4	1.289322	1.289320	1.289320	1.289320
0.2	0.7	0.4	1.342389	1.342387	1.342387	1.342387
0.2	0.8	0.4	1.393369	1.393366	1.393366	1.393366
0.2	0.3	0.1	0.979541	0.979541	0.979541	0.979541
0.2	0.3	0.4	1.175721	1.175720	1.175720	1.175720
0.2	0.3	0.7	1.342389	1.342387	1.342387	1.342387
0.2	0.3	1.0	1.489952	1.489947	1.489947	1.489947
0.2	0.3	1.4	1.665997	1.665990	1.665990	1.665990
0.2	0.3	1.7	1.786444	1.786435	1.786435	1.786435
0.2	0.3	2.0	1.899127	1.899117	1.899117	1.899117
0.2	0.3	2.5	2.073154	2.073142	2.073142	2.073142

doi:10.1371/journal.pone.0135914.t002

Table 2 shows a further comparison of the spectral relaxation and quasilinearisation results for the skin friction coefficient while Table 3 shows the variation of the heat transfer rate for different values of dimensionless unsteadiness parameter and Deborah numbers. The comparison of the two methods shows an excellent agreement between the numerical results obtained by the spectral relaxation and the quasilinearisation methods. In addition, Table 2 shows that the skin friction coefficient increases with increasing values of the unsteadiness parameter S and the relaxation time in terms of the Deborah number β_1 and decreases with increasing retardation time or Deborah number β_2. The heat transfer coefficient $-\theta'(0)$ is however shown to decrease with β_1 in Table 3. he increase in the skin friction coefficient with the flow unsteadiness has also been observed in earlier studies, such as in Ibrahim and Shanker [43] and Mukhopadhyay et al. [44]. It has been suggested in Mukhopadhyay et al. [44] that a decrease in the skin friction coefficient may be important in coating processes where higher stretching speeds may be achieved for smaller pulling forces. The study by Mukhopadhyay et al. [44] was on unsteady flow in a Casson fluid and further showed that for Casson fluids, the temperature decreased significantly with unsteadiness.

We observe further that heat transfer coefficient increases with increased unsteadiness and β_2. The negative values of the nanoparticle profile are due to the fact that the effect of

Table 3. Comparison of heat transfer rate $-\theta'(0)$ for various values of dimensionless unsteadiness S, the Deborah numbers β_1 and β_2, when $N_t = 0.5$, $N_b = 0.5$, $Pr = 7$ and $Le = 10$.

			SRM			QLM
S	β_1	β_2	Ord 5	Ord 7	Ord 8	
0.2	0.3	0.4	4.039516	4.039531	4.039531	4.039531
0.4	0.3	0.4	4.232584	4.232585	4.232585	4.232585
0.6	0.3	0.4	4.418677	4.418690	4.418690	4.418690
0.8	0.3	0.4	4.598443	4.598455	4.598455	4.598455
1.0	0.3	0.4	4.772377	4.772390	4.772390	4.772390
1.2	0.3	0.4	4.940927	4.940940	4.940940	4.940940
1.4	0.3	0.4	5.104494	5.104507	5.104507	5.104507
1.6	0.3	0.4	5.263439	5.263453	5.263453	5.263453
0.2	0.1	0.4	4.620580	4.620593	4.620593	4.620593
0.2	0.3	0.4	4.598443	4.598455	4.598455	4.598455
0.2	0.5	0.4	4.579026	4.579036	4.579036	4.579036
0.2	0.7	0.4	4.561566	4.561574	4.561574	4.561574
0.2	0.5	0.1	4.620580	4.620593	4.620593	4.620593
0.2	0.5	0.4	4.588452	4.588463	4.588463	4.588463
0.2	0.5	0.7	4.561566	4.561574	4.561574	4.561574
0.2	0.5	1.0	4.538087	4.538091	4.538091	4.538091

doi:10.1371/journal.pone.0135914.t003

thermophoresis is such that an elevation above the ambient surface temperature leads to a reduction in the relative value of the nanoparticle fraction at the surface (see Kuznetsov and Nield [34]).

Figs 2 and 3 show the velocity profiles for different values of the unsteadiness parameter. We observe that the velocity distribution and the momentum boundary layer thicknesses reduce with an increase in the unsteadiness parameter. This finding is in line with the earlier findings of Ibrahim and Shanker [43], and shows that even in the absence of an applied magnetic field, the velocity profiles decrease with the unsteadiness parameter. Figs 4 and 5 show the dimensionless temperature and concentration volume fraction profiles respectively for selected values of S. The steepness in both the temperature and concentration profiles decreases reducing the thicknesses of both the thermal and concentration volume fraction boundary layers. These results also follow a similar trend as observed by Ibrahim and Shanker [43] and Mukhopadhyay et al. [44]. Further, it may be pointed out that the concentration volume fraction increases from negative to positive values until boundary layer separation occurs. The magnitude of the volume fraction concentration increases up to a critical point and then decreases to zero.

Figs 6 and 7 show the influence of the Deborah numbers β_1 and β_2 on the velocity profiles. Higher Deborah numbers are indicative that the Oldroyd-B nanofluid is stretched. The nanofluid velocity $f'(\eta)$ and the momentum boundary layer thickness decrease with increasing β_1 which is not an unexpected result since it is well known that the viscoelastic fluid resists the motion of the fluid.

Figs 8 and 9 show the effects of β_1 on the temperature and concentration profiles, respectively. As β_1 increases, both the nanofluid temperature and the concentration volume fraction increase enhancing both the thermal and the concentration boundary layer thicknesses.

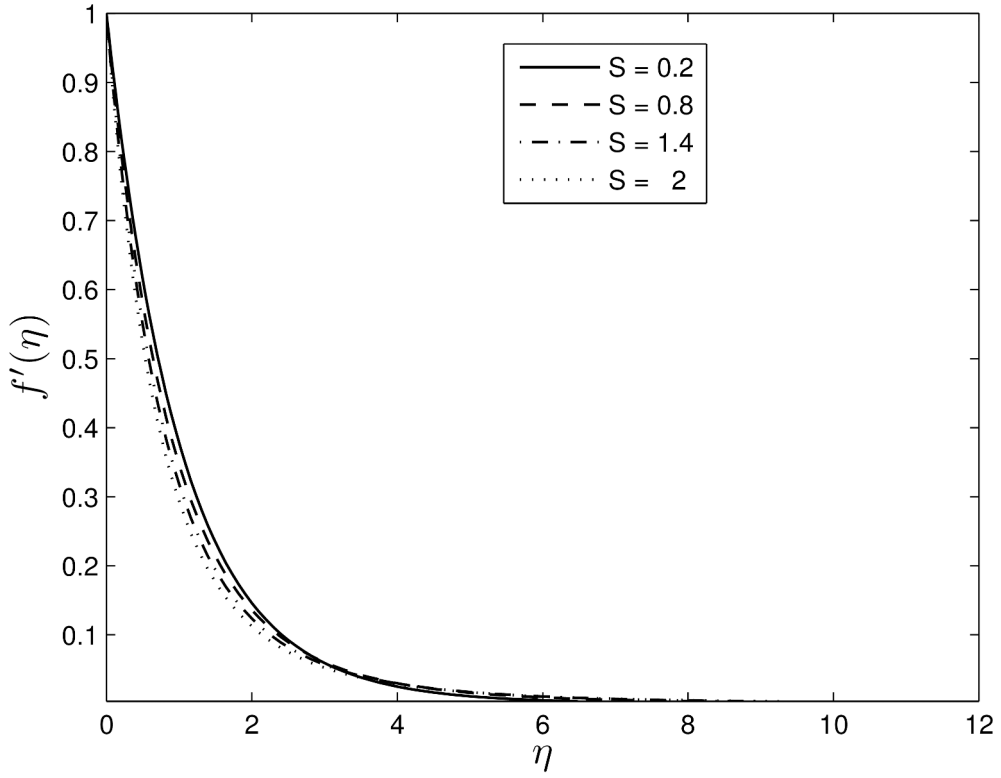

Fig 2. Effect of the unsteadiness parameter *S* on the velocity $f'(\eta)$ when $\beta_1 = 0.3$, $\beta_2 = 0.4$ *Le* = 10, *Pr* = 5, *Nt* = 0.5 and *Nb* = 0.5.

doi:10.1371/journal.pone.0135914.g002

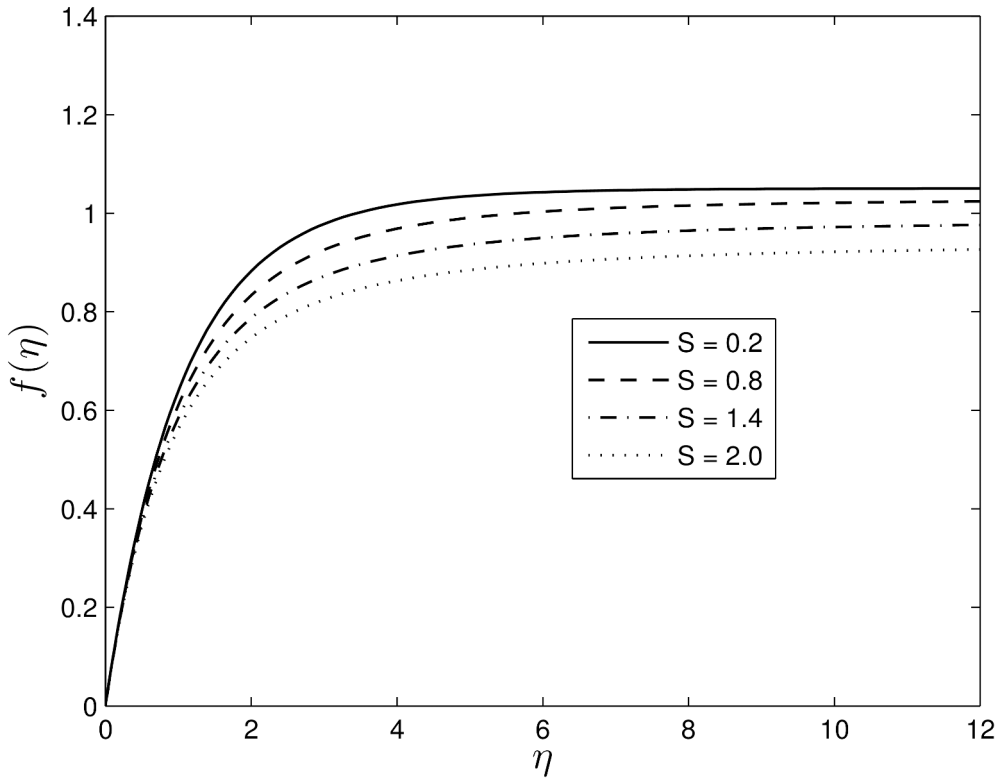

Fig 3. Effect of the unsteadiness parameter *S* on the velocity $f'(\eta)$, when $\beta_1 = 0.3$, $\beta_2 = 0.4$ *Le* = 10, *Pr* = 5, *Nt* = 0.5 and *Nb* = 0.5.

doi:10.1371/journal.pone.0135914.g003

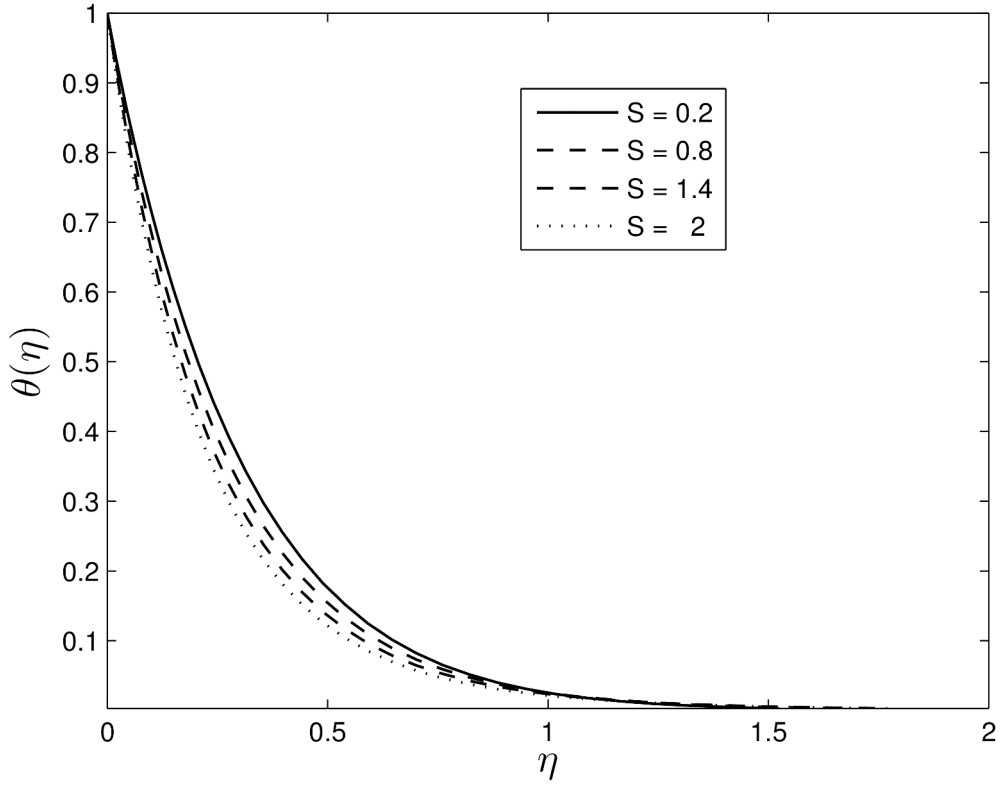

Fig 4. Effect of the unsteadiness parameter *S* on $\theta(\eta)$ when $\beta_1 = 0.3$, $\beta_2 = 0.4$ *Le* = 10, *Pr* = 5, *Nt* = 0.5 and *Nb* = 0.5.

doi:10.1371/journal.pone.0135914.g004

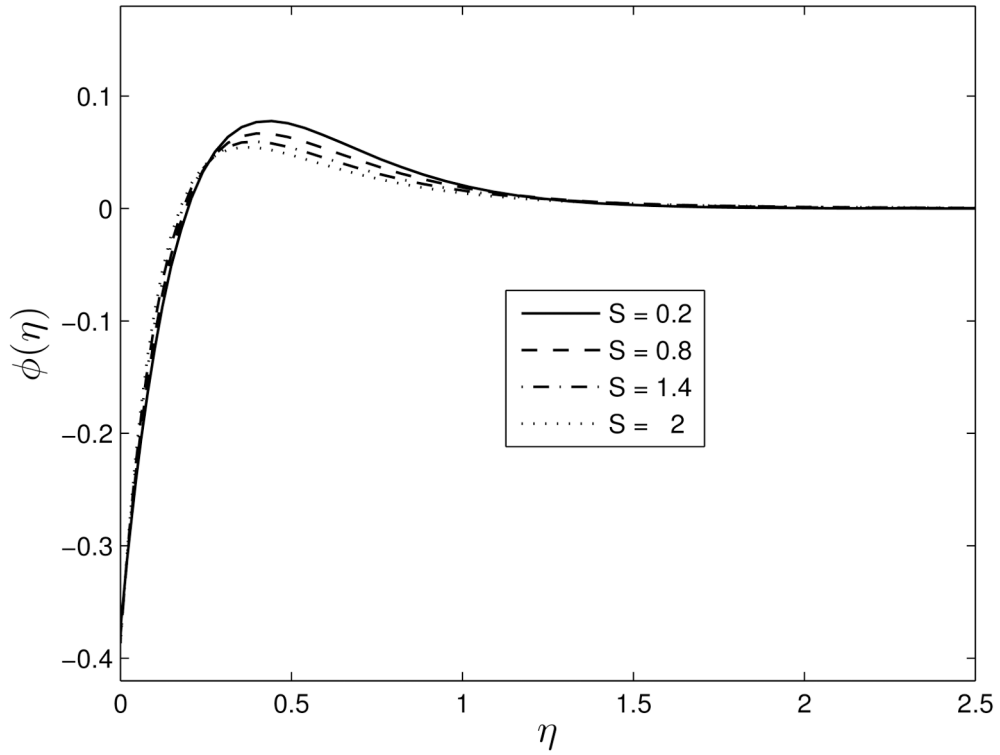

Fig 5. Effect of the unsteadiness parameter *S* on $\phi(\eta)$ for $\beta_1 = 0.3$, $\beta_2 = 0.4$ *Le* = 10, *Pr* = 5, *Nt* = 0.5 and *Nb* = 0.5.

doi:10.1371/journal.pone.0135914.g005

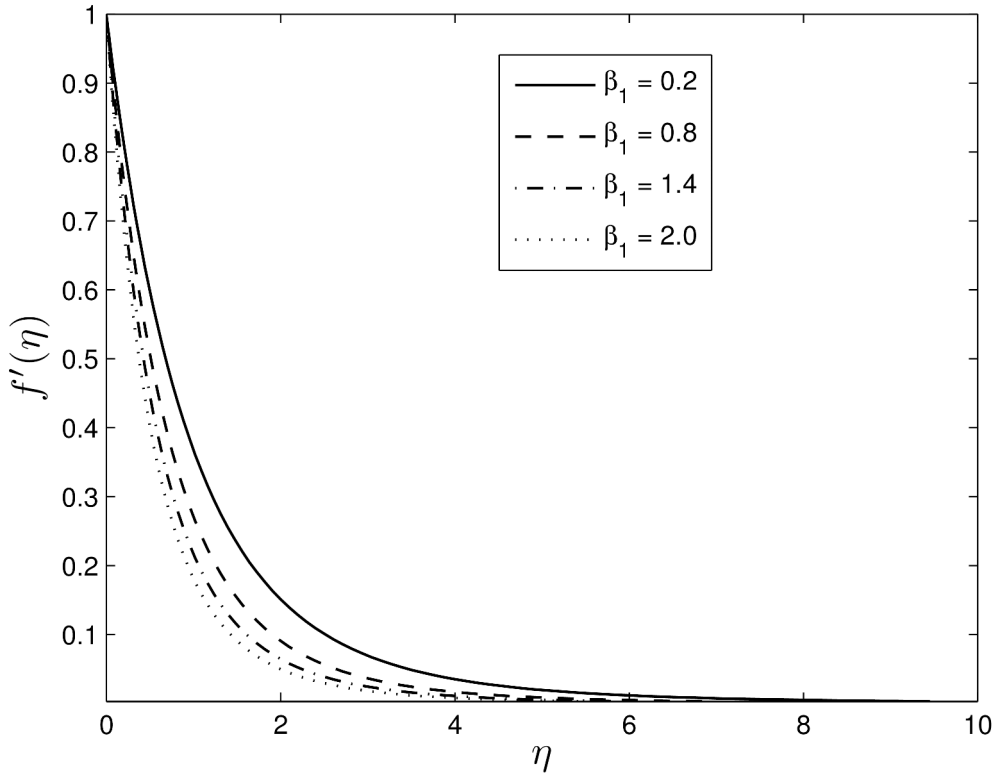

Fig 6. Effect of β_1 on velocity component $f'(\eta)$ for $S = 0.8$, $Le = 10$, $Pr = 5$, $Nt = 0.5$ and $Nb = 0.5$.

doi:10.1371/journal.pone.0135914.g006

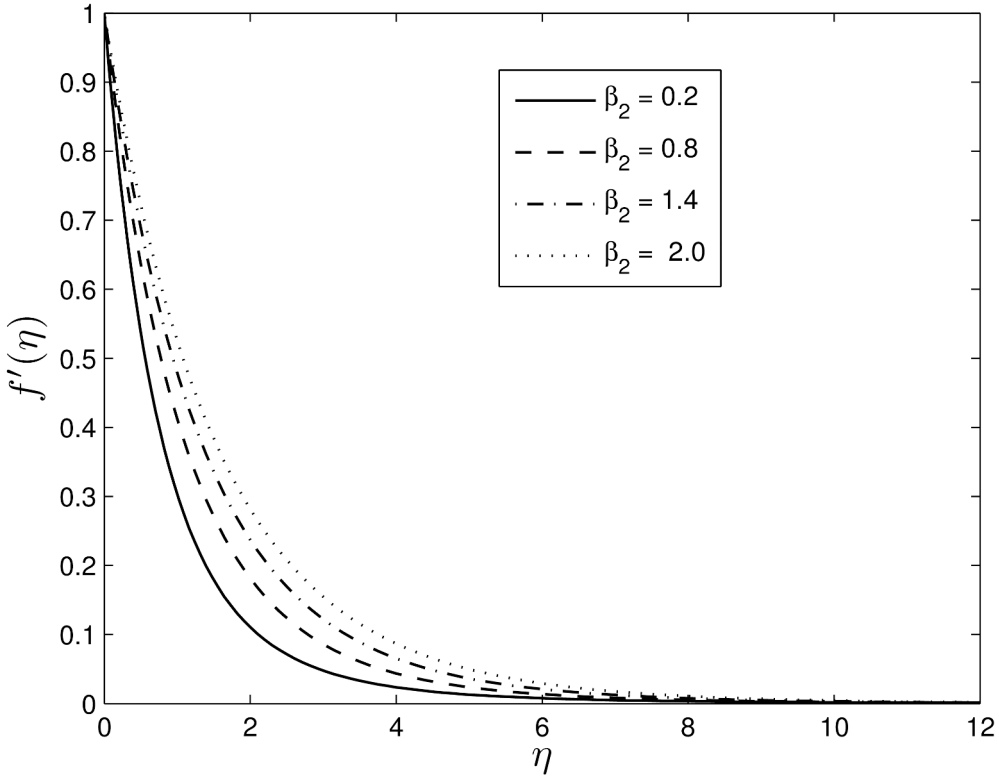

Fig 7. Effect of β_2 on velocity component $f'(\eta)$ for $S = 0.8$, $Le = 10$, $Pr = 5$, $Nt = 0.5$ and $Nb = 0.5$.

doi:10.1371/journal.pone.0135914.g007

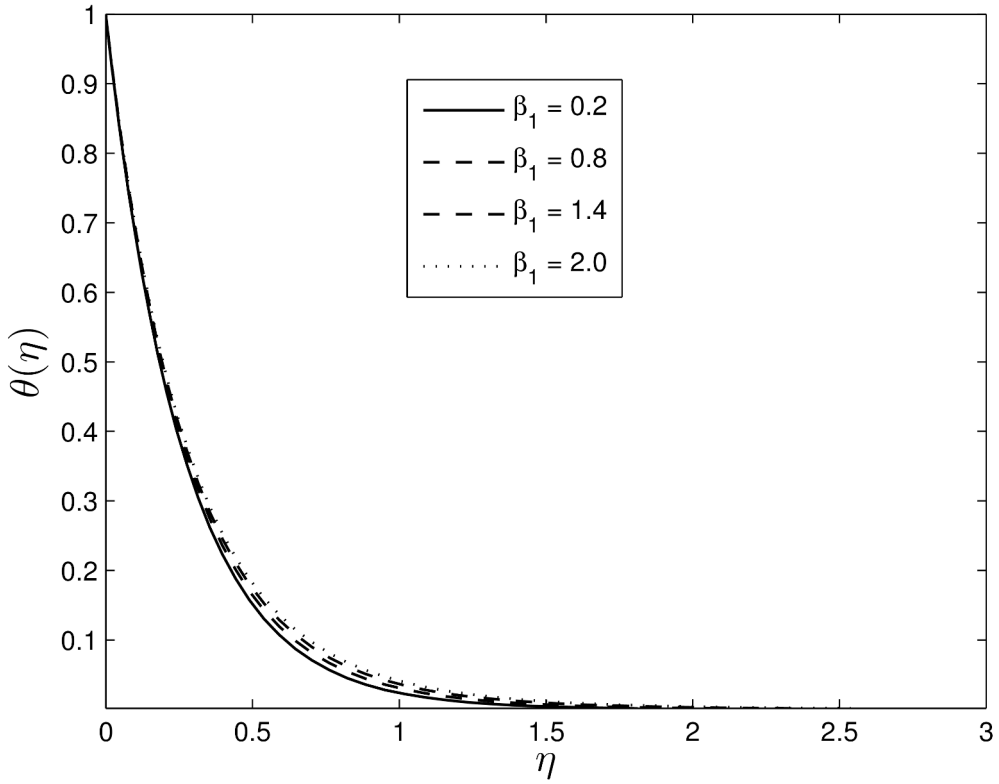

Fig 8. Effect of the unsteadiness parameter β_1 on $\theta(\eta)$ for $S = 0.8$, $\beta_2 = 0.4$ $Le = 10$, $Pr = 5$, $Nt = 0.5$ and $Nb = 0.5$.

doi:10.1371/journal.pone.0135914.g008

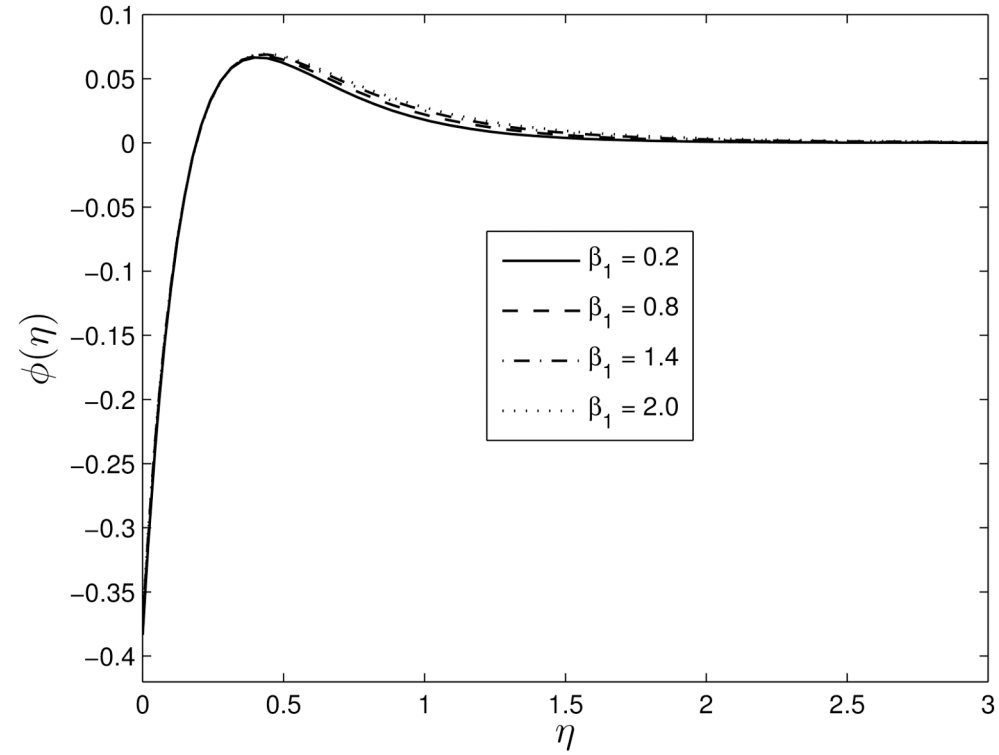

Fig 9. Effect of the unsteadiness parameter β_1 on $\phi(\eta)$ for $S = 0.8$, $\beta_2 = 0.4$ $Le = 10$, $Pr = 5$, $Nt = 0.5$ and $Nb = 0.5$.

doi:10.1371/journal.pone.0135914.g009

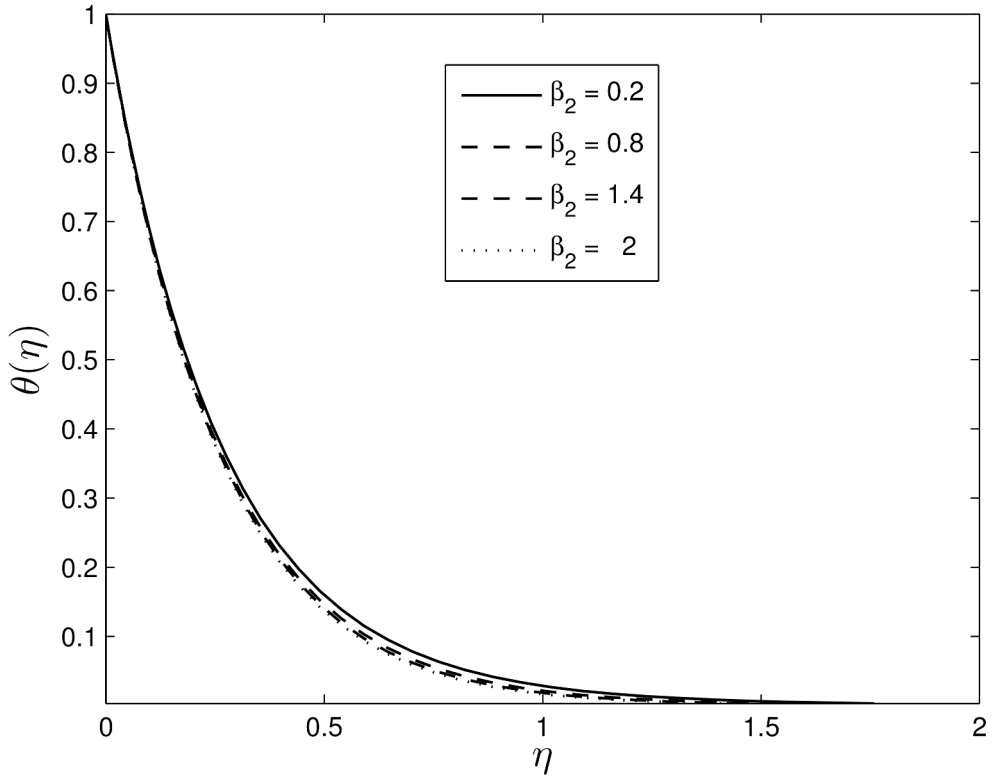

Fig 10. Effect of the unsteadiness parameter β_2 on $\theta(\eta)$ for $\beta_1 = 0.3$, $S = 0.8$ $Le = 10$, $Pr = 5$, $Nt = 0.5$ and $Nb = 0.5$.

doi:10.1371/journal.pone.0135914.g010

Figs 10 and 11 show the variation of the temperature and concentration volume fraction profiles for difference values of the retardation Deborah number β_2. It can be seen that when β_2 increases, both the temperature and concentration volume fraction distributions decrease thus diminishing the thicknesses of both the thermal and volume fraction boundary layers.

Figs 12 and 13 show the effect of the thermophoresis parameter Nt on $\theta(\eta)$ and $\phi(\eta)$ for fixed S, β_1, β_2, Le and Nb. The temperature gradients in the boundary layer induces a thermophoretic force on the nanoparticles and that leads to a fast flow away from the stretching surface. Hence more fluid is heated away from the surface, and consequently, as N_t increases, the temperature within the boundary layer increases. The fast flow from the stretching sheet carries with it nanoparticles leading to an increase in the mass volume fraction boundary layer thickness. It can also be observed that with an increase in the thermophoretic force, the nanoparticle fraction concentration profiles increase in the boundary layer before reducing to zero far from the surface. Here boundary layer separation occurs early at the stretching surface.

Figs 14 and 15 show the influences of the random particle motion (represented by the parameter N_b) and the Lewis number Le on the nanoparticle volume fraction profiles. The nanoparticle Brownian motion at the molecular level plays a significant role in determining the thermal behaviour of the nanoparticle-fluid suspensions, Jang and Choi [45]. It is obvious that the nanoparticle volume fraction increases close to the stretching surface with increased Brownian motion and Lewis numbers before the boundary layer separation point. However, after the separation point the concentration volume fraction profiles decrease with an increase in both N_b and Le.

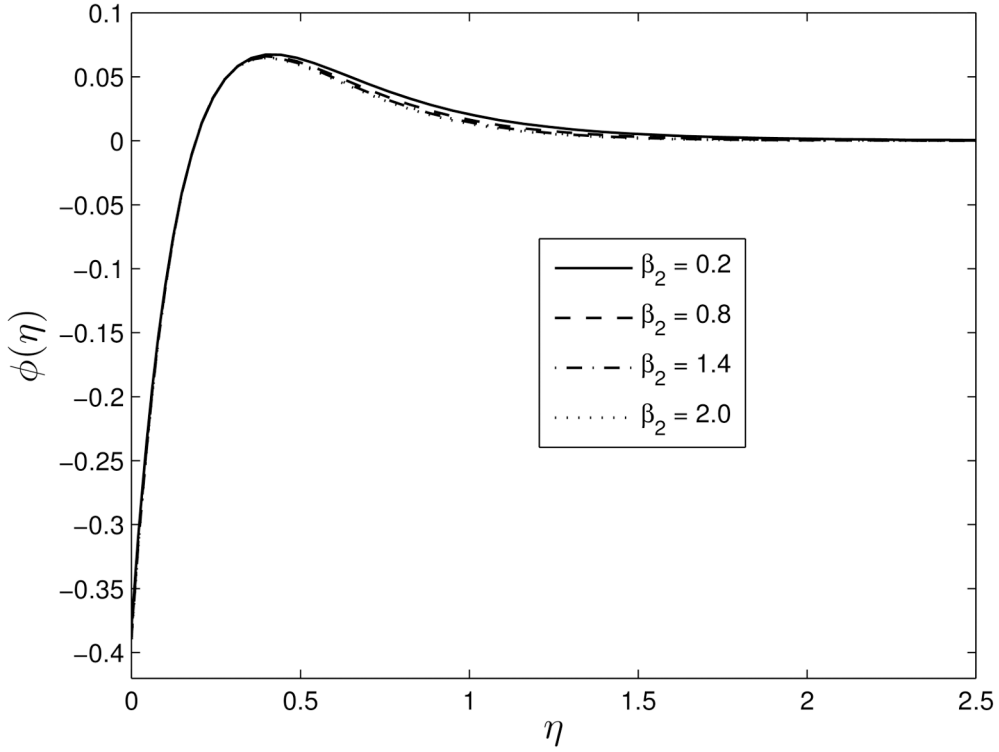

Fig 11. Effect of the unsteadiness parameter β_2 on $\phi(\eta)$ for $\beta_1 = 0.3$, $S = 0.8$ $Le = 10$, $Pr = 5$, $Nt = 0.5$ and $Nb = 0.5$.

doi:10.1371/journal.pone.0135914.g011

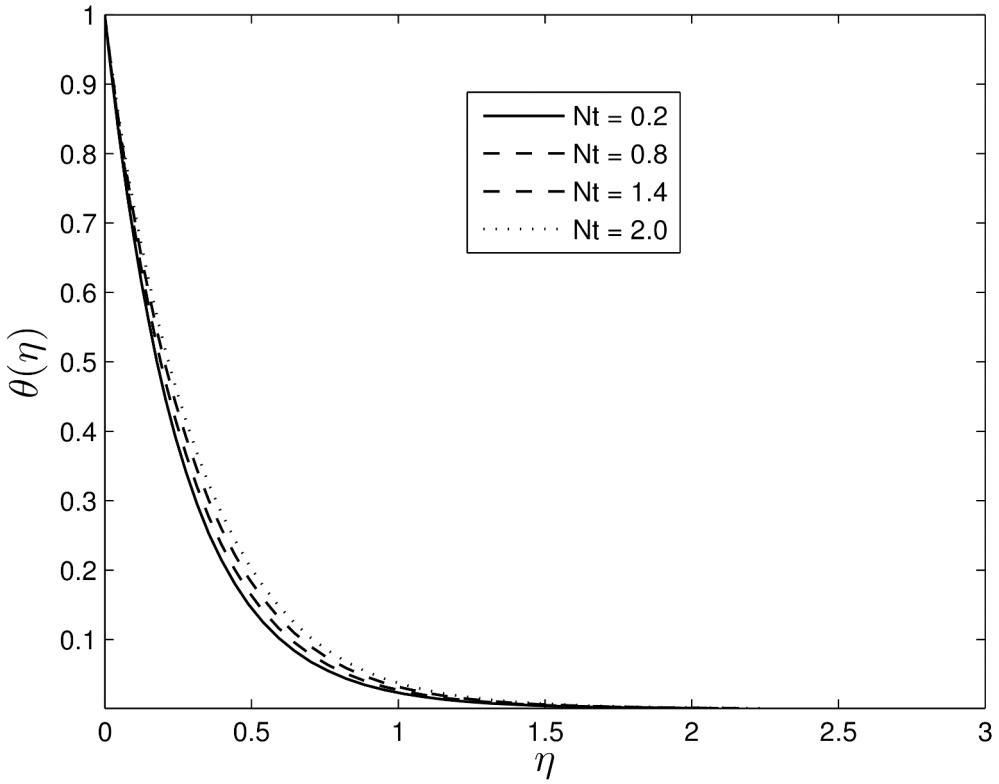

Fig 12. Effect of the thermophoresis parameter Nt on $\theta(\eta)$ for $S = 0.2$, $\beta_1 = 0.3$, $\beta_2 = 0.4$ $Le = 10$, $Pr = 5$ and $Nb = 0.5$.

doi:10.1371/journal.pone.0135914.g012

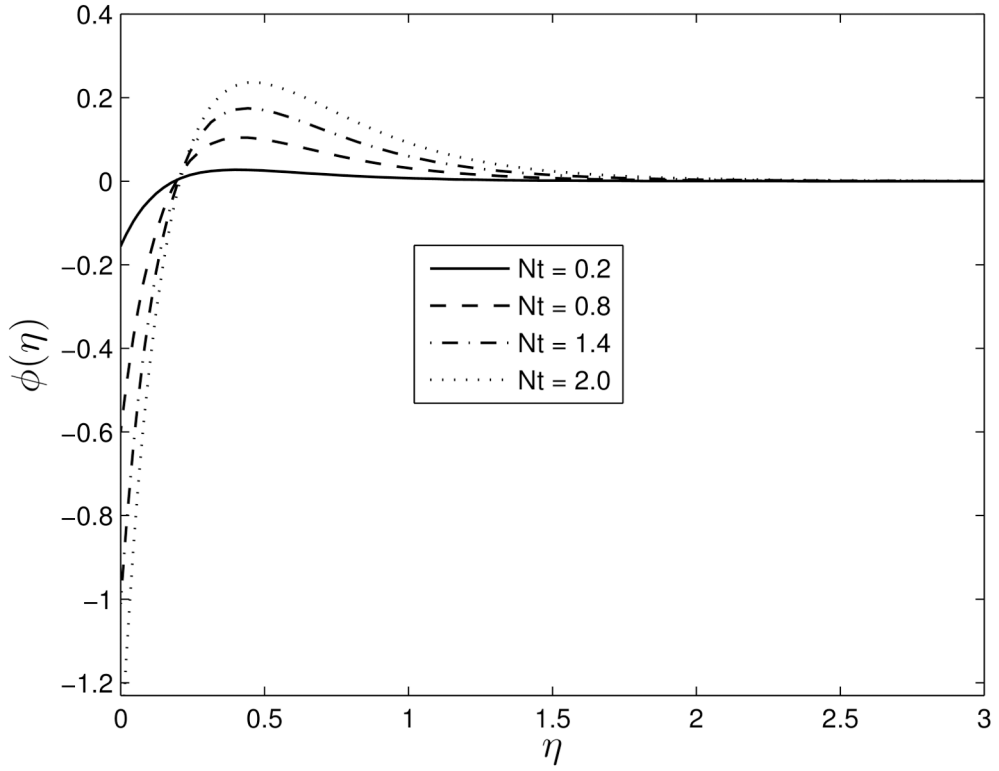

Fig 13. Effect of thermophoresis *Nt* on $\phi(\eta)$ for $S = 0.2$, $\beta_1 = 0.3$, $\beta_2 = 0.4$ $Le = 10$, $Pr = 5$ and $Nb = 0.5$.

doi:10.1371/journal.pone.0135914.g013

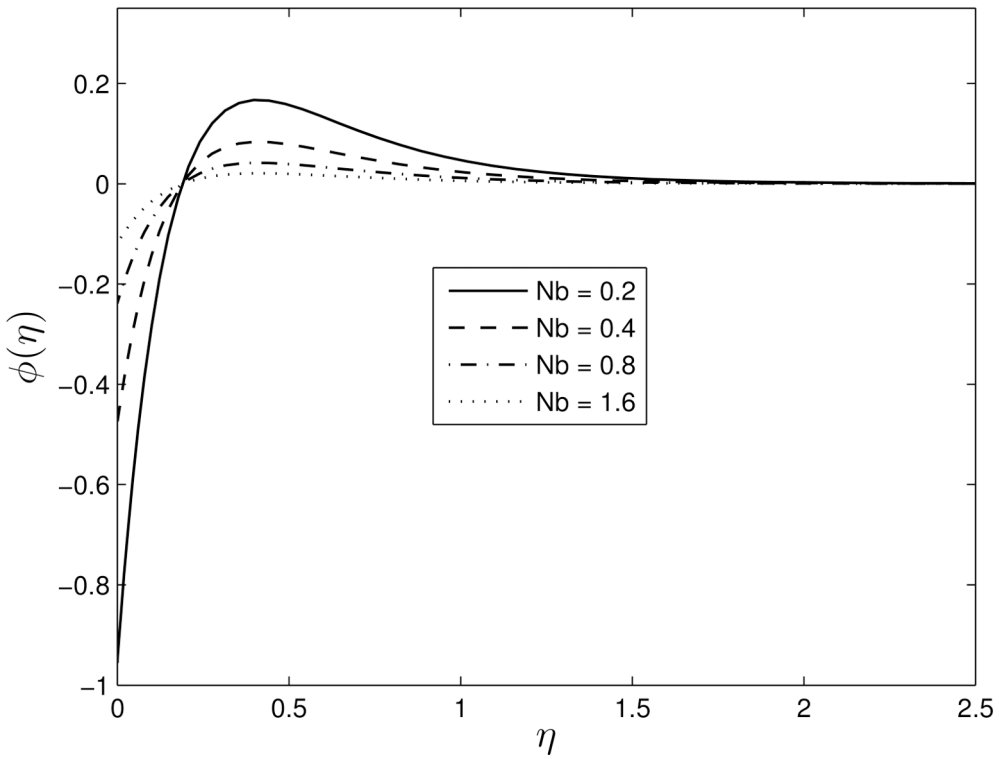

Fig 14. Effect of the Brownian motion *Nb* on $\phi(\eta)$ for $\beta_1 = 0.3$, $\beta_2 = 0.4$ $Pr = 7$, $Nt = 0.5$.

doi:10.1371/journal.pone.0135914.g014

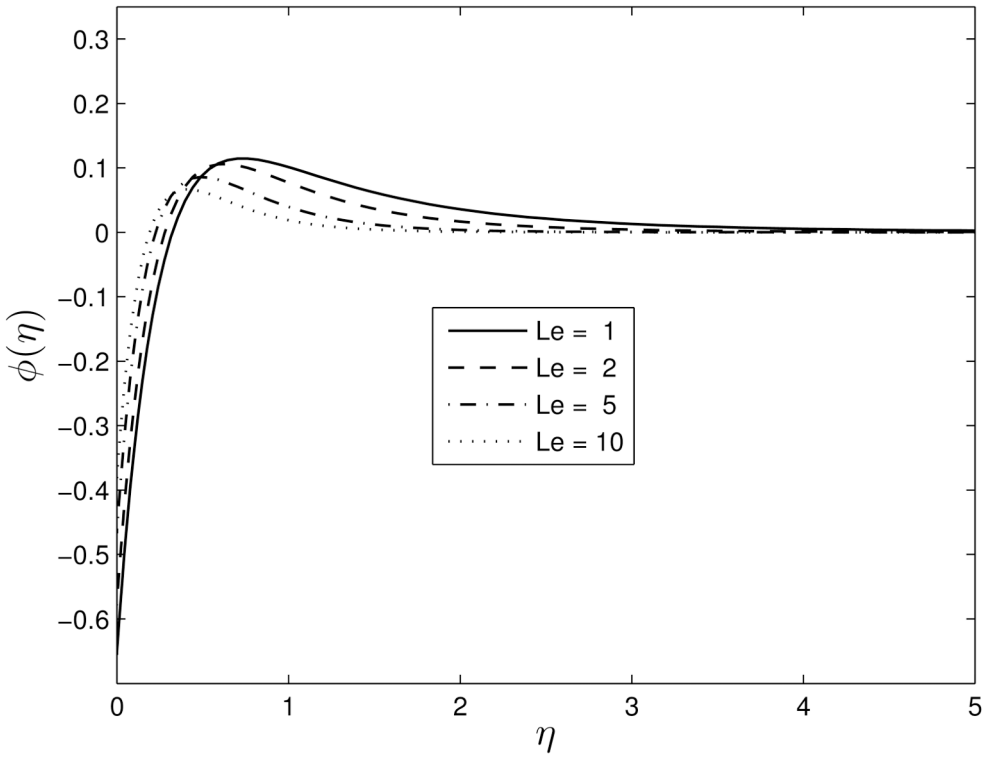

Fig 15. Effect of the Lewis number *Le* on $\phi(\eta)$ for $\beta_1 = 0.3$, $\beta_2 = 0.4$ *Pr* = 7, *Nt* = 0.5.

doi:10.1371/journal.pone.0135914.g015

Figs 16 and 17 show the effects of Deborah numbers β_1 and β_2 on skin friction and heat transfer coefficients. The skin friction coefficient increases with increasing β_1 leading to higher surface shear stresses, while increases in the skin-friction coefficient takes place with increasing β_2. We observe that increasing β_1 leads to a decrease in $-\theta'(0)$ whereas increasing β_2 enhances the rate of heat transfer.

The variation of heat transfer coefficients with the thermophoresis parameter *Nt* is shown in Fig 18. It is clear that the thermal boundary layer thickness increases when the thermophoresis parameter *N*t increases, and hence reducing the rate of heat transfer.

In order to apply the linear regression formula used by Kuznetsov and Nield [46], we used a set of 125 values of *S*, *Nb* and *Nt* with each *S*, *Nb*, *Nt* restricted to the space [0, 0.5] with a maximum error of less than 1%. Table 4 shows the linear regression coefficients and error bounds for the reduced Nusselt number. Here C_s, C_b, C_t, are the coefficients in the linear regression estimate

$$Nu_{est}/Ra_x^{1/2} = Nu_{PKB} + C_s S + C_b Nb + C_t Nt,$$

and ε is the maximum relative error defined by $\varepsilon = |(Nu_{est} - Nu)/Nu|$. In this study, the minimum error occurs for small values of *S*, *Nb* and *Nt*.

4 Conclusions

In this paper we have studied the unsteady Oldroyd nanofluid flow over stretching surface. The classical boundary condition in which both the nanoparticle volume fraction and the

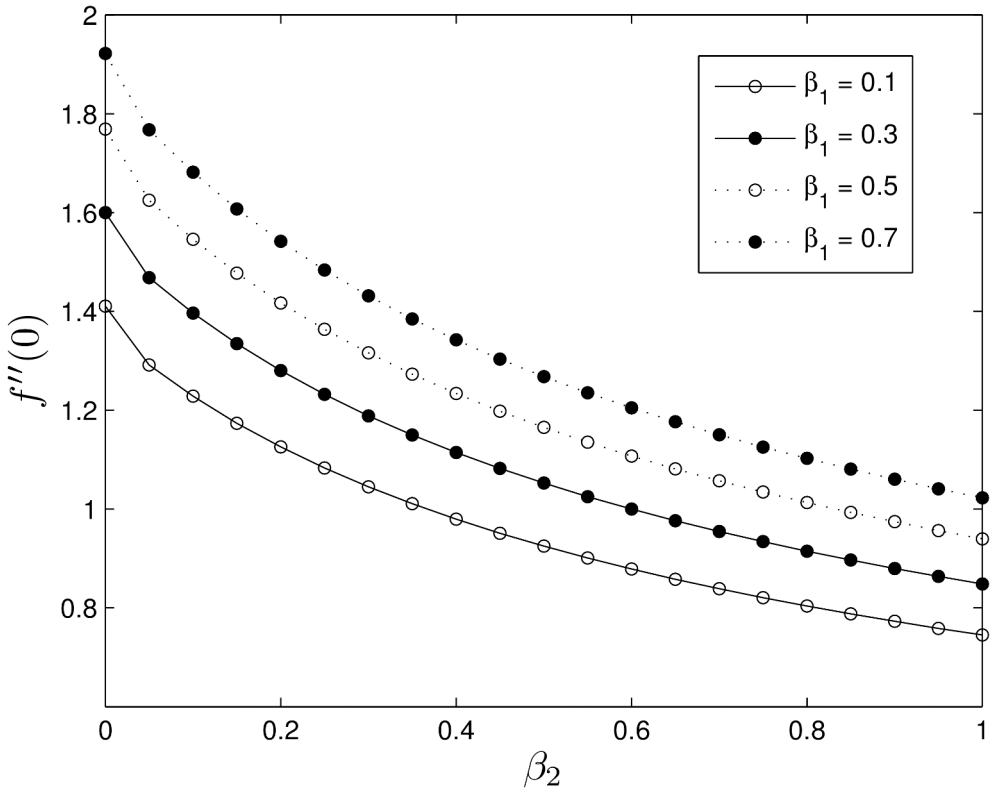

Fig 16. Effect of the Deborah numbers β_1 and β_2 on $f''(0)$ for $S = 0.8$, $Le = 10$, $Pr = 5$, $Nt = 0.5$ and $Nb = 0.5$.

doi:10.1371/journal.pone.0135914.g016

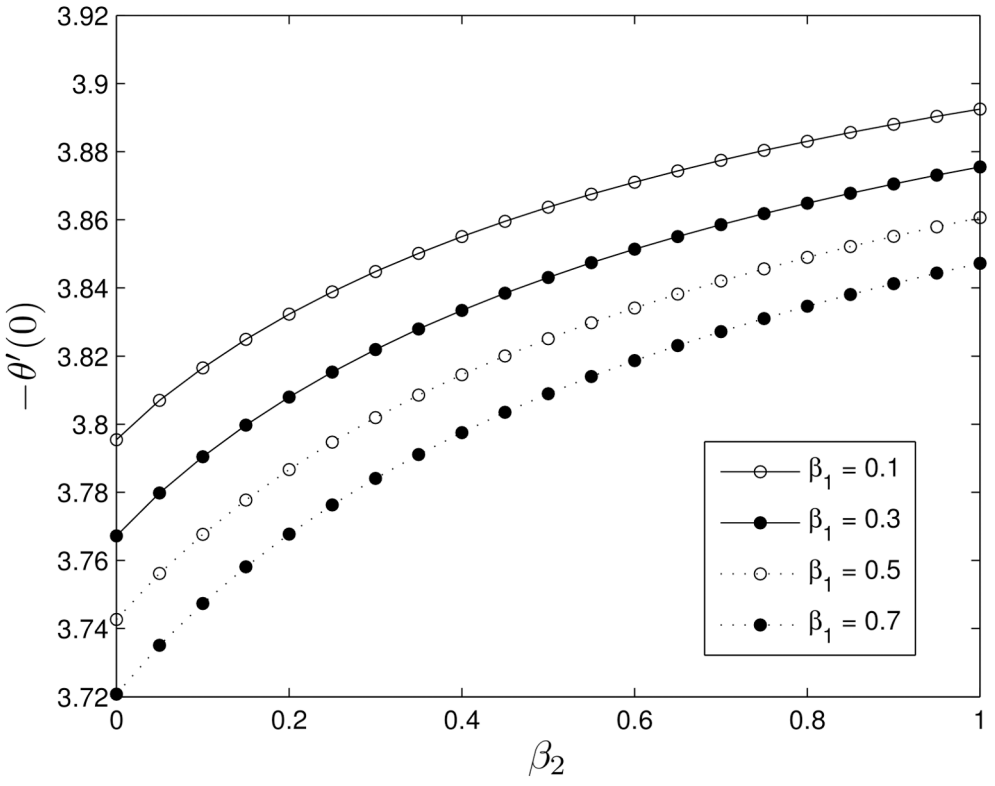

Fig 17. Effect of the Deborah numbers β_1 and β_2 on $-\theta'(0)$ for $S = 0.8$, $Le = 10$, $Pr = 5$, $Nt = 0.5$ and $Nb = 0.5$.

doi:10.1371/journal.pone.0135914.g017

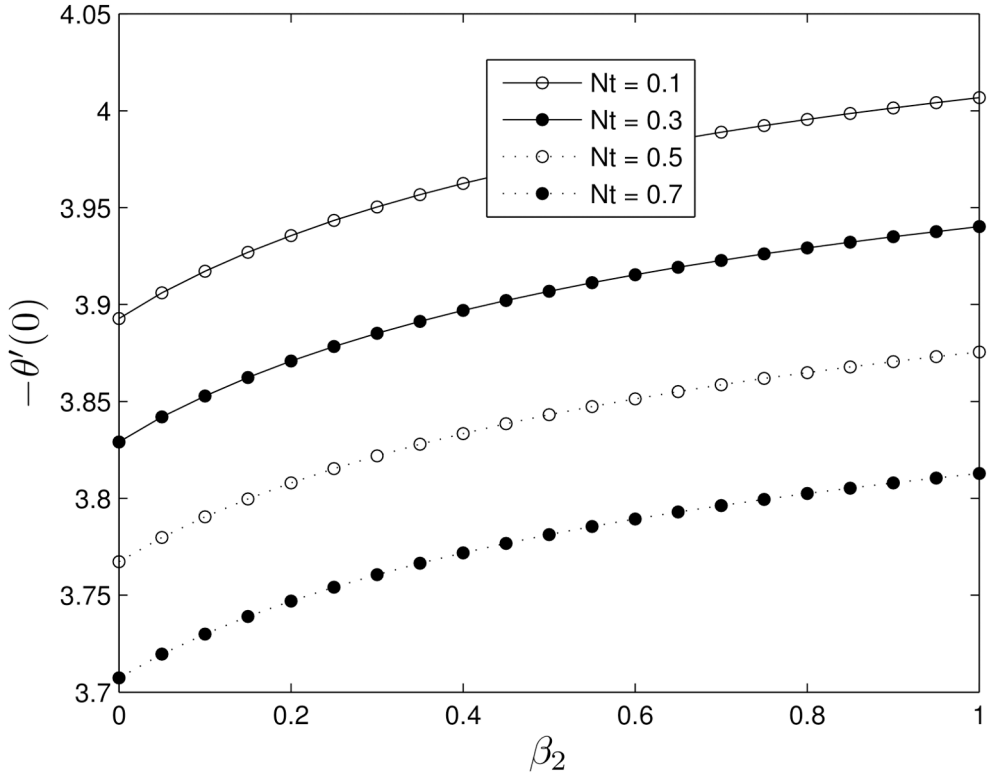

Fig 18. Effect of the thermophoresis number *Nt* on $-\theta'(0)$ for $\beta_1 = 0.3$, *Le* = 10, *Pr* = 5, *Nt* = 0.5 and *Nb* = 0.5.

doi:10.1371/journal.pone.0135914.g018

Table 4. Linear regression coefficients and error bounds for the reduced Nusselt number.

C_s	C_b	C_t	*Pr*	ε
-0.347	-0.111	-0.225	1	0.001
-0.360	-0.128	-0.239	2	0.001
-0.390	-0.141	-0.251	5	0.001
-0.400	-0.167	-0.270	10	0.001
-0.412	-0.197	-0.281	100	0.001

doi:10.1371/journal.pone.0135914.t004

temperature are actively controlled has been substituted by the more realistic condition where the nanoparticle volume fraction is not controlled an the boundary. The effects of the governing parameters such as the unsteadiness parameter, the Deborah numbers in terms of relaxation and retardation times, the Prandtl number, the Brownian motion parameter, the thermophoresis parameter, the Lewis number on skin friction, heat transfer coefficients and fluid flow characteristics have been studied. Here β_1 represents the viscoelastic properties of the fluid and resists the motion of the fluid. The effects of the Brownian motion on the rate of heat transfer are negligible. The comparison between results obtained using the SRM and the QLM for skin friction and heat transfer coefficients showed a good agreement, with the SRM having converged at the sixth order up to six decimal places.

Author Contributions

Conceived and designed the experiments: FGA SMA PS. Performed the experiments: FGA SMA PS. Analyzed the data: FGA PS. Wrote the paper: MK PS FGA SMA.

References

1. Sakiadis BC (1961) Boundary-layer behavior on continuous solid surface: I. Boundary- layer equations for two-dimensional and axisymmetric flow, *J Am Inst Chem Eng*, 7: 26–28.
2. Tsou FK (1967) Sparrow EM, Goldstein RJ, Flow and heat transfer in the boundary layer on a continuous moving surface, *Int J Heat Mass Transfer*, 10: 219–235. doi: 10.1016/0017-9310(67)90100-7
3. Crane L (1970) Flow past a stretching plate, *Z Angew Math Phys*, 21: 645–647. doi: 10.1007/BF01587695
4. Abel MS, Datti PS, Mahesha N (2009) Flow and heat transfer in a power-law fluid over a stretching sheet with variable thermal conductivity and non-uniform heat source, *Int J Heat and Mass Transfer*, 52: 2902–2913. doi: 10.1016/j.ijheatmasstransfer.2008.08.042
5. Cortell R (2007) Viscous flow and heat transfer over a nonlinearly stretching sheet, *Applied Mathematics and Computation*, 184: 864–873. doi: 10.1016/j.amc.2006.06.077
6. Kechil SA, Hashim I (2008) Series solution of flow over nonlinearly stretching sheet with chemical reaction and magnetic field, *Physics Letters A*, 372: 2258–2263. doi: 10.1016/j.physleta.2007.11.027
7. Prasad KV, Pal D, Datti PS (2009) MHD power-law fluid flow and heat transfer over a non-isothermal stretching sheet, *Commun Nonlinear Sci Numer Simulat*, 14: 2178–2189. doi: 10.1016/j.cnsns.2008.06.021
8. Salleh MZ, Nazar R, Pop I (2010) Boundary layer flow and heat transfer over a stretching sheet with Newtonian heating, *J Taiwan Institute of Chemical Engineers*, 41, 651–655. doi: 10.1016/j.jtice.2010.01.013
9. Pal D, Mondal H (2013) Influence of Soret and Dufour on MHD buoyancy-driven heat and mass transfer over a stretching sheet in porous media with temperature-dependent viscosity, *Nuclear Engineering and Design*, 256: 350–357. doi: 10.1016/j.nucengdes.2012.08.015
10. Choi US (1995) Enhancing thermal conductivity of fluids with nanoparticles, *ASME FED*, 231: 99–103.
11. Bachok N, Ishak A, Pop I (2012) Unsteady boundary-layer flow and heat transfer of a nanofluid over a permeable stretching/shrinking sheet, *Int J Heat and Mass Transfer*, 55, 2102–2109. doi: 10.1016/j.ijheatmasstransfer.2012.06.050
12. Mustafa M, Hayat T and Alsaedi A (2013) Unsteady boundary layer flow of nanofluid past an impulsively stretching sheet, *J Mechanics*, 29: 423–432. doi: 10.1017/jmech.2013.9
13. Cheng CY (2012) Natural convection boundary layer flow over a truncated cone in a porous medium saturated by a nanofluid, *Int Commun Heat and Mass Transfer*, 39: 231–235. doi: 10.1016/j.icheatmasstransfer.2012.08.004
14. Zaimi K, Ishak A, Pop I (2014) Unsteady flow due to a contracting cylinder in a nanofluid using Buongiornos model, *Int J Heat and Mass Transfer*, 68, 509–513. doi: 10.1016/j.ijheatmasstransfer.2013.09.047
15. Jamil M (2012) Some exact solution for Oldroyd-B fluid due to time dependent prescribed shear stress, *J Theoretical and Applied Mechanics*, 50: 549–562.
16. Hayat T, Shehzad SA, Alsaedi A, Alhothuali MS (2013) Three-dimensional flow of Oldroyd-B fluid over surface with convective boundary conditions, *Appl Math Mech-Engl Ed*, 34: 489–500. doi: 10.1007/s10483-013-1685-9
17. Siddiqui AM, Haroon T, Zahid M and Shahzad A (2011) Effect of slip condition on unsteady flows of an Oldroyd-B fluid between parallel plates, *World Applied Sciences Journal*, 13: 2282–2287.
18. Jamil M, Fetecau C, Imran M (2011) Unsteady helical flows of Oldroyd-B fluids, *Commun Nonlinear Sci Numer Simulat*, 16: 1378–1386. doi: 10.1016/j.cnsns.2010.07.004
19. Nadeem S, Haq R. Ul, Akbar NS, Lee C, Khan ZH (2013) Numerical study of boundary layer flow and heat transfer of Oldroyd-B nanofluid towards a stretching sheet, *PLoS ONE*, 8: e69811. doi: 10.1371/journal.pone.0069811 PMID: 24015172
20. Shehzad SA, Alsaedi A, Hayat T, Alhuthali MS (2014) Thermophoresis particle deposition in mixed convection three-dimensional radiative flow of an Oldroyd-B fluid, *J Taiwan Institute of Chemical Engineers*, 45: 787–794. doi: 10.1016/j.jtice.2013.08.022

21. Qi H, Jin H (2009) Unsteady helical flows of generalized Oldroyd-B fluid with fractioanl derivative, *Nonlinear Anal Real World Appl*, 10: 2700–2708. doi: 10.1016/j.nonrwa.2008.07.008

22. Tong D, Zhang X, Zhang X, Unsteady helical flows of generalized Oldroyd-B fluid, *J Non-Newtonian Fluid Mech*, 156, 75–83 (2009). doi: 10.1016/j.jnnfm.2008.07.004

23. Hayat T, Shehzad SA, Mustafa M, Hendi AA (2012) MHD flow of an Oldroyd-B fluid thorough a porous channel, *Int J Chemical Reactor Engineering*, 10:A8. doi: 10.1515/1542-6580.2655

24. Jamil M, and Khan NA (2011) Axial Couette flow of an Oldroyd-B fluid in an annulus, *Theoretical and Applied Mechanics Letters*, 2: 012001. doi: 10.1063/2.1201201

25. Hayat T and Alsaedi A (2011) On thermal radiation and Joule heating effects on MHD flow of an Oldroyd-B fluid with thermophoresis, *Arabian J Science and Engineering*, 36: 1113–1124. doi: 10.1007/s13369-011-0066-4

26. Rajagopal KR (1995) On boundary conditions for fluids of the differential type. *Navier-Stokes equations and related non-linear problems* (ed. Sequria A.), Plenum Press, New York, 273–278.

27. Rajagopal KR (1982) Boundedness and uniqueness of fluids of the differential type. *Acta Cienca Indica*, 18: 1–11.

28. Rajagopal KR (1986) Szeri AZ and Troy W, An existence theorem for the flow of a non-Newtonian fluid past an infinite porous plate. *Int J Non-Linear Mech*., 21: 279–289. doi: 10.1016/0020-7462(86)90035-1

29. Chao H, Hagberg BA and Riggleman RA (2014) The distribution of homogeneously grafted nanoparticles in polymer thin films and blends, *The Royal Society of Chemistry*, DOI: 10.1039/c4sm01188k

30. Khan WA, Khan M, and Malik R (2014) Three-dimensional flow of an Oldroyd-B nanofluid towards stretching surface with heat generation/absorption, *PLoS ONE* 9(8): e105107. doi: 10.1371/journal.pone.0105107 PMID: 25170945

31. Nield DA, Kuznetsov AV 2014 Thermal instability in a porous medium layer saturated by a nanofluid: A revised model, *Int JHeat and Mass Transfer*, 68: 211–214. doi: 10.1016/j.ijheatmasstransfer.2013.09.026

32. Nield DA, Kuznetsov AV (2014) Forced convection in a parallel-plate channel occupied by a nanofluid or a porous medium saturated by a nanofluid, *Int J Heat and Mass Transfer*, 70: 430–433. doi: 10.1016/j.ijheatmasstransfer.2013.11.016

33. Nield DA, Kuznetsov AV (2014) The onset of convection in a horizontal nanofluid layer of finite depth: A revised model, *Int J Heat and Mass Transfer*, 77: 915–918. doi: 10.1016/j.ijheatmasstransfer.2014.06.020

34. Kuznetsov AV, Nield DA (2014) Natural convective boundary-layer flow of a nanofluid past a vertical plate: A revised model, *Int J Thermal Sciences*, 77: 126–129. doi: 10.1016/j.ijthermalsci.2013.10.007

35. Motsa SS, A new spectral relaxation method for similarity variable nonlinear boundary layer flow systems, *Chemical Engineering Communications*, DOI: 10.1080/00986445.2013.766882

36. Motsa SS, Sibanda P and Shateyi S (2011) On a new quasi-linearization method for systems of nonlinear boundary value problems, *Math Meth Appl Sci* 34: 1406–1413. doi: 10.1002/mma.1449

37. Motsa SS, Dlamini PG, and Khumalo M (2012) Solving hyperchaotic systems using the spectral relaxation method, *Abstract and Applied Analysis*, vol. 2012, Article ID 203461, 18 pages. doi: 10.1155/2012/203461

38. Motsa SS, Dlamini P, and Khumalo M (2013) A new multistage spectral relaxation method for solving chaotic initial value systems, *Nonlinear Dynamics*, 72: 265–283. doi: 10.1007/s11071-012-0712-8

39. Motsa SS and Makukula ZG (2013) On spectral relaxation method approach for steady von Krmn flow of a Reiner-Rivlin fluid with Joule heating, viscous dissipation and suction/injection, *Centr Eur J Phys*, 11: 363–374.

40. Bellman R and Kalaba R (1965) Quasilinearization and nonlinear boundary value problems, Elsivier, New York.

41. Sharidan S, Mahmood T, Pop I (2006) Similarity solutions for the unsteady boundary layer flow and heat transfer due to a stretching sheet, *Int J Appl Mech Eng*, 11: 647–654.

42. Pal D (2011) Combined effects of non-uniform heat source/sink and thermal radiation on heat transfer over an unsteady stretching permeable surface, *Commun Nonlinear Sci Numer Simulat*, 16: 1890–1904. doi: 10.1016/j.cnsns.2010.08.023

43. Ibrahim W, Shanker B (2012) Unsteady MHD boundary-layer flow and heat transfer due to stretching sheet in the presence of heat source or sink by quasi-linearization technique, *Int J Appl Math and Mech* 8(7): 18–30.

44. Mukhopadhyay M, De Ranjan P, Bhattacharyya, Layek GC (2013) Casson fluid flow over an unsteady stretching surface, *Ain Shams Engin Phys Math*, 4: 933–938. doi: 10.1016/j.asej.2013.04.004

45. Jang SP and Choi SUS (2004) Role of Brownian motion in the enhanced thermal conductivity of nanofluids, *Appl Phys Lett*, 84: 4316 (2004). doi: 10.1063/1.1756684

46. Kuznetsov AV, Nield DA (2010) Natural convective boundary-layer flow of a nanofluid past a vertical plate, *Int J Thermal Sciences*, 49: 243–247. doi: 10.1016/j.ijthermalsci.2009.07.015

47. Elbashbeshy Elsayed M.A., Aldawody Dalia A (2010) Heat transfer over an unsteady stretching surface with variable heat flux in the presence of a heat source or sink, *Comp Appl Math*, 60: 2806–2811. doi: 10.1016/j.camwa.2010.09.035

Chapter 5

Unsteady mixed convection flow through a permeable stretching flat plate with partial slip effects through MHD nanofluid using the spectral relaxation method

In this Chapter, we extend the study by Nandy and Mahapatra [212] by using the revised nanofluid model in Chapter 4. Here we study the unsteady magnetohydrodynamic stagnation point nanofluid flow along a permeable stretching flat plate. There have been several theoretical models developed to describe slip flow over a surface. However, to the best of knowledge, no investigation has as yet been done to analyze the impact of unsteady slip flow on heat and mass transfer in a nanofluid flow past a non-linear stretching permeable surface. The purpose of this study is to investigate the combined effects of partial slip, internal heat source/sink, thermophoresis and Brownian motion on fluid properties and the impact on heat and mass transfer. The results may have engineering applications such as in MHD micro pumps.

Research Article Open Access

Sami M. Ahamed, Sabyasachi Mondal*, and Precious Sibanda

Unsteady mixed convection flow through a permeable stretching flat surface with partial slip effects through MHD nanofluid using spectral relaxation method

DOI 10.1515/phys-2017-0036
Received January 30, 2016; accepted November 8, 2016

Abstract: An unsteady, laminar, mixed convective stagnation point nanofluid flow through a permeable stretching flat surface using internal heat source or sink and partial slip is investigated. The effects of thermophoresis and Brownian motion parameters are revised on the traditional model of nanofluid for which nanofluid particle volume fraction is passively controlled on the boundary. Spectral relaxation method is applied here to solve the non-dimensional conservation equations. The results show the illustration of the impact of skin friction coefficient, different physical parameters, and the heat transfer rate. The nanofluid motion is enhanced with increase in the value of the internal heat sink or source. On the other hand, the rate of heat transfer on the stretching sheet and the skin friction coefficient are reduced by an increase in internal heat generation. This study further shows that the velocity slip increases with decrease in the rate of heat transfer. The outcome results are benchmarked with previously published results.

Keywords: MHD nanofluid; Slip condition; Internal heat source/sink; Spectral relaxation method; Permeable stretching surface

PACS: 02.60.Cb, 02.60.Lj, 02.70.Hm

Sami M. Ahamed: School of Mathematics, Statistics and Computer Science, University of KwaZulu-Natal, Pietermaritzburg-3209, South Africa, E-mail: samimusa81@yahoo.com
***Corresponding Author: Sabyasachi Mondal:** School of Mathematics, Statistics and Computer Science, University of KwaZulu-Natal, Pietermaritzburg-3209, South Africa, E-mail: sabya.mondal.2007@gmail.com
Precious Sibanda: School of Mathematics, Statistics and Computer Science, University of KwaZulu-Natal, Pietermaritzburg-3209, South Africa, E-mail: sibandap@ukzn.ac.za

© 2017 Sami M. Ahamed et al., published by De Gruyter Open.
This work is licensed under the Creative Commons Attribution-NonCommercial-NoDerivs 3.0 License.

1 Introduction

Cooling and heating of liquids are significant in many engineering applications and transportation industries. In general, many common heat transfer fluids such as ethylene glycol, oil and water are not efficient heat transfer fluids for their low thermal conductivities and poor physical and chemical characteristics [1]. In contrast, fluids with added nanometer sized metals such as titanium, aluminum, gold, silver, copper and iron or their oxides and composite materials have significantly higher thermal conductivities than these base fluids. The nanoparticles are commonly made by a high-energy-pulsed process from a conductive material. For these reasons, it is prudent to combine base fluids with nanoparticles to achieve both the characteristics of a base fluid and the physical properties of the nanoparticles [2, 3]. Suspending nanoparticles affects the base fluid's homogeneity and the randomness of molecular motion leading to higher conductive rates and better convective heat transfer performances compared to base fluids [4–7]. There are however mechanisms, which include particle agglomeration, particle shape/surface area, nanoparticle size, temperature and liquid layering on the nanoparticle liquid interface that still need to be fully understood.

Nanofluids have large application in industries, like micro-electro-mechanical or microprocessors electronic systems as well as in the field of biotechnology [8]. Several authors, for instance, [9, 10] conducted theoretical and experimental investigations to demonstrate that nanofluids increased the heat transfer properties of base fluid. The numerical solution of the equations that describe the combined effects of thermophoresis and Brownian motion on the nanofluid flow through a flat surface in a saturated porous medium was examined by Nield and Kuznetsov [11]. Kuznetsov and Nield [12] examined a problem on natural convection boundary layer nanofluid flow with showing the effects of thermophoresis and Brownian mo-

Authenticated | sabya.mondal.2007@gmail.com author's copy
Download Date | 6/2/17 8:52 AM

tion. Buongiorno [13] studied that particle diffusion and thermophoresis play an important role in the flow of a nanofluid. The classical concept of a boundary layer corresponds to a thin region next to a solid surface where viscous forces are important, Blasius [14]. Viscous forces play an essential role in processes such as glass fiber drawing, crystal growing and plastic extrusion. For the case of the Blasius problem, Sakiadis [15] focused on the concept of a boundary layer flow induced by a moving plate in a quiescent ambient fluid. Further studies in this area were made by Schlichting and Gersten [16], Bejan [17], White [18] and Mukhopadhyay [19, 20].

The magnetohydrodynamic (MHD) boundary layer flow of a viscous incompressible fluid which is electrically conducted has huge applications in industry and technological sectors, like cooling of nuclear reactors, the extrusion of plastics, textile industry, purification of crude oil, polymer technology, geothermal energy extractions, metallurgy, drug delivery and biological transportation [21, 22]. The application of the magnetic field produces a Lorentz force that increase the mixing processes as an active micro mixing mechanism. The transport system of conductive biological fluids in the micro systems will be benefitted from research [23]. The simultaneous occurrence of buoyancy and magnetic field forces on fluid flow were investigated by many researchers [24–28]. In these investigations, many authors have used a no-slip boundary condition. Recently, some researchers have investigated boundary layer flow assuming a slip condition at the boundary [29–35].

Stagnation point flow, illustrating the fluid motion near a stagnation region, exists near solid bodies in that fluid flow. Chiam [36] studied fluid flow on a steady stagnation-point through an elastic surface with equal free stream and stretching velocities.

The mail focus of this study is to expand the work of Nandy and Mahapatra [37] to unsteady flow over a permeable stretching flat plate with an internal heat source or sink. For the nanoparticles we have used the boundary condition suggested recently by Kuznetsov and Nield [38] where active control of the nanoparticle volume fraction at the surface is not possible. Appropriate similarity transformations reduce the conservation equations to a set of nonlinear ordinary differential equations. These equations are solved by using a spectral relaxation method, numerically (see Motsa *et al.* [39]).

2 Problem formulations

Consider an unsteady, viscous, incompressible, laminar nanofluid flow past a stretching flat plate. The flow is restricted to the area $y \geq 0$, y and x are the coordinate system normal to the stretching flat plate and along the stretching surface, respectively. The concentration and temperature on the surface are ϕ_w and T_w, respectively, and away from the surface the values are ϕ_∞ and T_∞, respectively. We assume that at a time $t \geq 0$, the plate stretching velocity is $u_w = bx$. The free stream velocity is $u_\infty = ax$. Here, b is constant with $b > 0$ corresponding to a stretching plate and $b < 0$ to a shrinking plate. The fluid flow is subjected to a uniform magnetic field of strength B_0 which is applied in a normal direction to the plane $y = 0$ and to the heat source/sink. The fluid is electrically conducting with constant properties, except for the density in the buoyancy term in the momentum equation. With these assumptions, the Oberbeck-Boussinesq and the boundary layer approximations, the unsteady momentum, energy and concentration equations can be described as (see Nandy and Mahapatra [37]);

$$\frac{\partial u}{\partial x} + \frac{\partial v}{\partial y} = 0, \tag{1}$$

$$\rho_f \left(\frac{\partial u}{\partial t} + u\frac{\partial u}{\partial x} + v\frac{\partial u}{\partial y} - u_\infty \frac{du_\infty}{dx} \right) = \mu_f \frac{\partial^2 u}{\partial y^2} + \sigma B_0^2 (u_\infty - u) + (1 - \phi_\infty)\rho_{f\infty}\beta(T - T_\infty)g - (\rho_p - \rho_{f\infty})(\phi - \phi_\infty)g, \tag{2}$$

$$\frac{\partial T}{\partial t} + u\frac{\partial T}{\partial x} + v\frac{\partial T}{\partial y} = \alpha_f \frac{\partial^2 T}{\partial y^2} + \frac{1}{(\rho c_p)_f} q''' + \tau \left\{ D_B \frac{\partial \phi}{\partial y}\frac{\partial T}{\partial y} + \frac{D_T}{T_\infty}\left(\frac{\partial T}{\partial y}\right)^2 \right\}, \tag{3}$$

$$\frac{\partial \phi}{\partial t} + u\frac{\partial \phi}{\partial x} + v\frac{\partial \phi}{\partial y} = D_B \frac{\partial^2 \phi}{\partial y^2} + \left(\frac{D_T}{T_\infty}\right)\frac{\partial^2 T}{\partial y^2}, \tag{4}$$

where t, u and v represent the time, the fluid velocity components along the x and y axis, respectively, ν_f is the fluid kinematic viscosity, σ is the fluid electrical conductivity, $\rho_{f\infty}$ is the density far from the plate surface, g is the acceleration due to gravity, ρ_f is the fluid density, T is the fluid temperature, β is the coefficient of thermal expansion, ρ_p is the density of the particles, $(\rho c_p)_f$ is fluid heat capacity, ϕ is nanoparticle volume fraction, α_f is thermal diffusivity, q''' is the rate of internal heat sink (< 0) or heat source (> 0) coefficient, The ratio of the effective heat capacity of nanoparticle material with the heat capacity of the fluid is τ, D_T denotes the thermophoresis diffusion coefficient and D_B is the Brownian diffusion coefficient.

Authenticated | sabya.mondal.2007@gmail.com author's copy
Download Date | 6/2/17 8:52 AM

The boundary conditions are (see Kuznetsov and Nield [12], Nandy and Mahapatra [37] and Kuznetsov and Nield [38])

$$\begin{aligned} &v = V_w, u = u_w + L\frac{\partial u}{\partial y}, \quad \text{at} \quad y = 0, t \geq 0, \\ &T = T_w, D_B\frac{\partial \phi}{\partial y} + \frac{D_T}{T_\infty}\frac{\partial T}{\partial y} = 0 \quad \text{at} \quad y = 0, t \geq 0, \\ &u \to u_\infty,\ T \to T_\infty,\ \phi \to \phi_\infty \quad \text{as} \quad y \to \infty, t \geq 0 \end{aligned} \tag{5}$$

with the initial conditions

$$u \to 0,\ T \to T_\infty,\ \phi \to \phi_\infty \quad \text{at} \quad t < 0,$$

where L is a proportionality constant. V_w denotes the surface mass flux. Negative values of V_w imply fluid suction and positive values of V_w imply injection. Also, $V_w = 0$ corresponds to an impermeable plate.

q''' is defined according as follows, (see [40–42])

$$q''' = \left(\frac{k\, u_w}{x\nu_f}\right)[A^*(T_w - T_\infty)e^{-\eta} + B^*(T - T_\infty)], \tag{6}$$

where B^* and A^* are temperature-dependent internal heat source/sink and coefficients of space-dependent, respectively and η is a dimensionless variable defined in Eq. (7). The first term in the Eq. (6) represents the dependence of the internal heat sink or source on the space coordinates while the second term represents its dependence on the temperature. Now, for the case when the case $A^* < 0$ and $B^* < 0$, indicates to internal heat sink while both $A^* > 0$ and $B^* > 0$, indicates to internal heat source.

We introduce non-dimensional variables given by

$$\begin{aligned} &\eta = \sqrt{\frac{b}{\nu_f \xi}}y, \xi = 1 - e^{-\hat{\tau}}, \psi = \sqrt{b\,\nu_f \xi}\, x\, f(\eta, \xi), \\ &\theta(\eta, \xi) = \frac{T - T_\infty}{T_w - T_\infty}, \hat{\tau} = bt, \Phi(\eta, \xi) = \frac{\phi - \phi_\infty}{\phi_\infty}, \end{aligned} \tag{7}$$

where $\theta(\eta, \xi)$ and $\Phi(\eta, \xi)$ are the non-dimensional temperature and concentration, respectively and the stream function ψ is defined as

$$u = \frac{\partial \psi}{\partial y} \text{ and } v = -\frac{\partial \psi}{\partial x}.$$

Substituting (7) into Eqs. (1) - (4) gives

$$\begin{aligned} &f''' + \frac{1}{2}(1 - \xi)\eta f'' + \xi \\ &\left[ff'' - f'^2 + M\left(\varepsilon - f'\right) + \varepsilon^2 + \lambda(\theta - Nr\Phi)\right] \\ &= \xi(1 - \xi)\frac{\partial f'}{\partial \xi}, \\ &\theta'' + Pr\left[\frac{1}{2}(1 - \xi)\eta\theta' + \xi f\theta' + N_b\Phi'\theta' + N_t\theta'^2\right] \\ &+\xi\left(A^* e^{-\eta} + B^*\theta\right) = Pr\xi(1 - \xi)\frac{\partial \theta}{\partial \xi}, \end{aligned} \tag{8}$$

$$\begin{aligned} &\Phi'' + Le\left[\frac{1}{2}(1 - \xi)\eta\Phi' + \xi f\Phi'\right] + \frac{N_t}{N_b}\theta'' \\ &= Le\ \xi(1 - \xi)\frac{\partial \Phi}{\partial \xi}, \end{aligned} \tag{9}$$

$$\tag{10}$$

with boundary conditions

$$\begin{aligned} &f(0, \xi) = S, f'(0, \xi) = 1 + \gamma f''(0, \xi), \\ &\theta(0, \xi) = 1, \Phi'(0, \xi) + \frac{N_t}{N_b}\theta'(0, \xi) = 0, \\ &f'(\infty, \xi) \to \varepsilon, \theta(\infty, \xi) \to 0, \Phi(\infty, \xi) \to 0, \end{aligned} \tag{11}$$

where the differentiation with respect to η is denoted as prime, S is the dimensionless suction/blowing parameter, γ is the dimensionless slip factor, and the stretching parameter is ε where

$$S = -\frac{V_w}{\sqrt{b\,\nu_f \xi}},\ \gamma = L\sqrt{\frac{b}{\nu_f \xi}} \quad \text{and} \quad \varepsilon = \frac{a}{b}.$$

In Eqs. (8)-(11) the parameters are the magnetic parameter M, the buoyancy parameter λ, Gr_x is the local Grashof number, Pr is the Prandtl number, Re_x is the local Reynolds number, N_t is the thermophoresis parameter, Nr is the buoyancy ratio parameter, N_b is the Brownian motion parameter, and Le is the Lewis number. These parameters are defined as:

$$\begin{aligned} &M = \frac{\sigma B_0^2}{\rho_f b}, \lambda = \frac{Gr_x}{Re_x^2}, Re_x = \frac{x u_w}{\nu_f}, N_b = \frac{\tau D_B \phi_\infty}{\nu_f}, \\ &Gr_x = \frac{(1 - \phi_\infty)\rho_{f\infty}}{\rho_f}\frac{g\beta(T_w - T_\infty)x^3}{\nu_f^2}, \\ &Nr = \frac{(\rho_p - \rho_{f\infty})}{(1 - \phi_\infty)\rho_{f\infty}}\frac{\phi_\infty}{\beta(T_w - T_\infty)}, Pr = \frac{\nu_f}{\alpha_f}, \\ &N_t = \frac{\tau D_T(T_w - T_\infty)}{T_\infty \nu_f}, Le = \frac{\nu_f}{D_B}. \end{aligned} \tag{12}$$

We note that in the case of assisting flow $\lambda > 0$, and for opposing flow $\lambda < 0$, $\lambda = 0$ corresponds to free convection. The skin friction coefficient C_f and the local Nusselt number Nu_x are defined as

$$C_f = \frac{\tau_w}{\rho_f u_w^2},\ Nu_x = \frac{x q_w}{k_f\,(T_w - T_\infty)}, \tag{13}$$

where τ_w is the shear stress along the stretching surface, q_w is the wall heat flux, respectively defined as

$$\tau_w = -\mu_f\left(\frac{\partial u}{\partial y}\right)_{y=0},\ q_w = -k_f\left(\frac{\partial T}{\partial y}\right)_{y=0}. \tag{14}$$

Hence using Eq.(14) we get

$$\sqrt{\xi Re_x}\ C_f = -f''(0, \xi),\ \sqrt{\frac{\xi}{Re_x}}\ Nu_x = -\theta'(0, \xi). \tag{15}$$

Authenticated | sabya.mondal.2007@gmail.com author's copy
Download Date | 6/2/17 8:52 AM

With the revised boundary condition, the Sherwood number which represents the dimensionless mass flux is identically zero (see Kuznetsov and Nield [12], Kuznetsov and Nield [38]).

3 Method of solution

The spectral relaxation method (see [39]) was used to solve the system of non-similar equations (8)–(10) with the boundary conditions (11). In the SRM framework, we obtain the iterative scheme

$$f'_{r+1} = u_{r+1}, \tag{16}$$

$$u''_{r+1} + a_{1,r}u'_{r+1} + a_{2,r}u_{r+1} + a_{3,r} = a_{4,r}\frac{\partial u_{r+1}}{\partial \xi}, \tag{17}$$

$$\theta''_{r+1} + b_{1,r}\theta'_{r+1} + b_{2,r}\theta_{r+1} + b_{3,r} = b_{4,r}\frac{\partial \theta_{r+1}}{\partial \xi}, \tag{18}$$

$$\Phi''_{r+1} + c_{1,r}\Phi'_{r+1} + c_{2,r} = c_{3,r}\frac{\partial \Phi_{r+1}}{\partial \xi}, \tag{19}$$

with boundary conditions

$$\begin{aligned} &f_{r+1}(0,\xi) = S,\ u_{r+1}(0,\xi) = 1 + \gamma f''(0,\xi),\ \theta_{r+1}(0,\xi) = 1,\\ &N_b\Phi'_{r+1}(0,\xi) + N_t\theta'_{r+1}(0,\xi) = 0,\\ &u_{r+1}(\infty,\xi) \to \varepsilon,\ \theta_{r+1}(\infty,\xi) \to 0,\ \Phi_{r+1}(\infty,\xi) \to 0, \end{aligned} \tag{20}$$

where

$$\begin{aligned} &a_{1,r} = \frac{1}{2}(1-\xi)\eta + \xi f_r,\ a_{2,r} = -\xi \mathrm{M},\\ &a_{3,r} = \xi\left[\varepsilon^2 + \mathrm{M}\varepsilon - u_r^2 + \lambda(\theta_r - Nr\Phi_r)\right],\ a_{4,r} = \xi(1-\xi) \end{aligned} \tag{21}$$

$$\begin{aligned} &b_{1,r} = Pr\left[\frac{1}{2}(1-\xi)\eta + \xi f_{r+1} + N_b\Phi'_r\right],\ b_{2,r} = \xi B^*\\ &b_{3,r} = \xi A^* e^{-\eta} + PrN_t\theta'^2_r,\ b_{4,r} = Pr\xi(1-\xi) \end{aligned} \tag{22}$$

$$\begin{aligned} &c_{1,r} = Le\left[\frac{1}{2}(1-\xi)\eta + \xi f_{r+1}\right],\ c_{2,r} = \frac{N_t}{N_b}\theta''_{r+1},\\ &c_{3,r} = Le\ \xi(1-\xi). \end{aligned} \tag{23}$$

In Equations (16)–(23) the indices r and $r+1$ denote the previous and current iteration levels, respectively. Starting from initial approximations denoted by f_0, u_0, θ_0, and Φ_0, equations (9)–(11) are solved iteratively for $f_{r+1}(\eta,\xi)$, $u_{r+1}(\eta,\xi)$, $\theta_{r+1}(\eta,\xi)$, and $\Phi_{r+1}(\eta,\xi)$ ($r = 0, 1, 2, \ldots$). Equations (8)–(10) were discretized using the Chebyshev spectral collocation method in the η direction while the discretization in the ξ direction uses the implicit finite difference method. This leads to a system of linear equations of the form

$$\mathbf{A}_1 \mathrm{f}^{\mathrm{n+1}}_{\mathrm{r+1}} = \mathrm{u}^{\mathrm{n}}_{\mathrm{r}}, \tag{24}$$

$$\mathbf{A}_2 \mathrm{u}^{\mathrm{n+1}}_{\mathrm{r+1}} = \mathbf{B}_2 \mathrm{u}^{\mathrm{n}}_{\mathrm{r+1}} + \mathbf{K}_2, \tag{25}$$

$$\mathbf{A}_3 \theta^{\mathrm{n+1}}_{\mathrm{r+1}} = \mathbf{B}_3 \theta^{\mathrm{n}}_{\mathrm{r+1}} + \mathbf{K}_3, \tag{26}$$

$$\mathbf{A}_4 \Phi^{\mathrm{n+1}}_{\mathrm{r+1}} = \mathbf{B}_4 \Phi^{\mathrm{n}}_{\mathrm{r+1}} + \mathbf{K}_4, \tag{27}$$

where

$$\mathbf{A}_1 = \mathbf{D}, \tag{28}$$

$$\mathbf{A}_2 = \left[\frac{1}{2}\left(\mathbf{D}^2 + [a^{n+\frac{1}{2}}_{1,r}]_{\mathbf{d}}\mathbf{D} + a^{n+\frac{1}{2}}_{2,r}\mathbf{I}\right) - \frac{a^{n+\frac{1}{2}}_{4,r}}{\Delta\xi}\mathbf{I}\right],$$

$$\mathbf{B}_2 = \left[-\frac{1}{2}\left(\mathbf{D}^2 + [a^{n+\frac{1}{2}}_{1,r}]_{\mathbf{d}}\mathbf{D} + a^{n+\frac{1}{2}}_{2,r}\mathbf{I}\right) - \frac{a^{n+\frac{1}{2}}_{4,r}}{\Delta\xi}\mathbf{I}\right],$$

$$\mathbf{K_2} = -a^{n+\frac{1}{2}}_{3,r}, \tag{29}$$

$$\mathbf{A}_3 = \left[\frac{1}{2}\left(\mathbf{D}^2 + [b^{n+\frac{1}{2}}_{1,r}]_{\mathbf{d}}\mathbf{D} + b^{n+\frac{1}{2}}_{2,r}\mathbf{I}\right) - \frac{b^{n+\frac{1}{2}}_{4,r}}{\Delta\xi}\mathbf{I}\right],$$

$$\mathbf{B}_3 = \left[-\frac{1}{2}\left(\mathbf{D}^2 + [b^{n+\frac{1}{2}}_{1,r}]_{\mathbf{d}}\mathbf{D} + b^{n+\frac{1}{2}}_{2,r}\mathbf{I}\right) - \frac{b^{n+\frac{1}{2}}_{4,r}}{\Delta\xi}\mathbf{I}\right],$$

$$\mathbf{K_3} = -b^{n+\frac{1}{2}}_{3,r}, \tag{30}$$

$$\mathbf{A}_4 = \left[\frac{1}{2}\left(\mathbf{D}^2 + [c^{n+\frac{1}{2}}_{1,r}]_{\mathbf{d}}\mathbf{D}\right) - \frac{c^{n+\frac{1}{2}}_{3,r}}{\Delta\xi}\mathbf{I}\right],$$

$$\mathbf{B}_4 = \left[-\frac{1}{2}\left(\mathbf{D}^2 + [c^{n+\frac{1}{2}}_{1,r}]_{\mathbf{d}}\mathbf{D}\right) - \frac{c^{n+\frac{1}{2}}_{3,r}}{\Delta\xi}\mathbf{I}\right],$$

$$\mathbf{K}_4 = -c^{n+\frac{1}{2}}_{2,r}. \tag{31}$$

Here $\mathbf{I}$ is an $(N+1)\times(N+1)$ identity matrix, and $[\,.\,]_{\mathbf{d}}$ are diagonal matrices of order $(N+1)\times(N+1)$.

In applying the SRM a computational domain of extent $L = 20$ was chosen in the η-direction. Through numerical experimentation, this value was found to give accurate results for all the selected physical parameters. Increasing the value of η do not change the results to a significant extent. The number of collocation points is used in the spectral method discretization is $N_x = 100$ in all cases. The calculations are carried until some desired, tolerance level ϵ is attained. The tolerance level was defined to be the maximum infinity norm of the difference between the values of the calculated quantities, that is

$$\max\left\{\|f^{n+1}_{r+1} - f^{n+1}_r\|_\infty, \|\theta^{n+1}_{r+1} - \theta^{n+1}_r\|_\infty, \|\Phi^{n+1}_{r+1} - \Phi^{n+1}_r\|_\infty\right\} < \epsilon.$$

To ensure the accuracy of the results, a sufficiently small step size $\Delta\xi$ was used. The step size was chosen to be small enough such that further reduction in step size did not change the results of the flow properties.

Authenticated | sabya.mondal.2007@gmail.com author's copy
Download Date | 6/2/17 8:52 AM

4 Results and discussion

The transformed system of coupled nonlinear ordinary differential equations (8)-(10) including boundary conditions (11) are solved numerically using the spectral relaxation method. The numerical results are presented here to show the velocity, concentration and temperature profiles, the rate of heat transfer and the skin friction coefficient for different physical parameter values. These results are presented both graphically and in tabular form. In the numerical simulations the default parameter values used are, unless otherwise specified; $Pr = 6.8$, $\varepsilon = 0.5$, $\lambda = 0.5$, $M = 0.1$, $Nr = 0.5$, $A^{\star} = 2.0$, $N_b = 0.5$, $B^{\star} = 1.0$, $N_t = 0.5$, $S = 0.1$, $Le = 10$, $\gamma = 0.1$ and $\xi = 0.5$.

To verify the accuracy of our numerical scheme, a comparison of the computed skin friction coefficient is made with earlier results of Anwar *et al.* [43] in Table 1. Here we observe an excellent agreement validating the accuracy of the current numerical results. The residual error in the numerical simulations against the number of iterations for different values of γ, ε, S and M is shown in Figure 1. These results again confirm that the numerical method used in this study converges.

Table 1: Comparison of the reduced skin friction coefficient $-f''(0,1)$ when $\lambda = Nr = \gamma = 0$

			Anwar et al. [43]	Present Results
M	ε	S	$-f''(0,1)$	$-f''(0,1)$
0.1	0.1	0.1	1.0568	1.056803
2.5			1.7660	1.765967
0.1	0.6	0.1	0.5921	0.592079
	1.1		-0.1728	-0.172795
	1.6		–	-1.165587
2.5	1.1		-0.2328	-0.232839
0.1	0.1	-0.5	0.8050	0.804972
	1.1	-0.5	–	-0.141738
	0.1	0.5	1.2638	1.263785
	1.1	0.5	-0.1963	-0.196310

Figure 2(a) displays the variation of f' with respect to η for several values of γ when $\varepsilon < 1$, $\varepsilon = 1$ and $\varepsilon > 1$. Here we note that f' increases with γ when $\varepsilon > 1$ while the opposite is true when $\varepsilon < 1$. An increase in the slip pa-

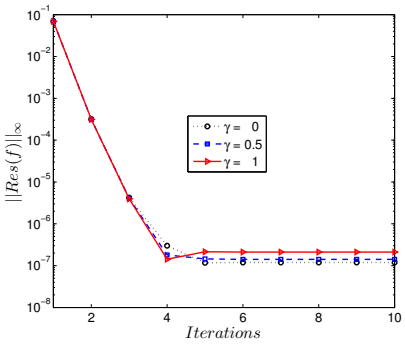

(a)

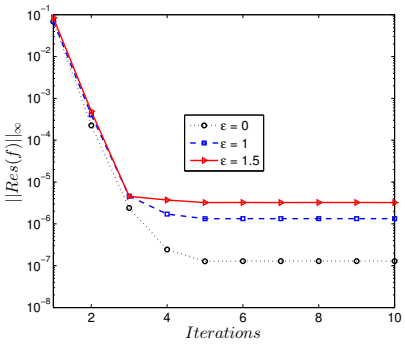

(b)

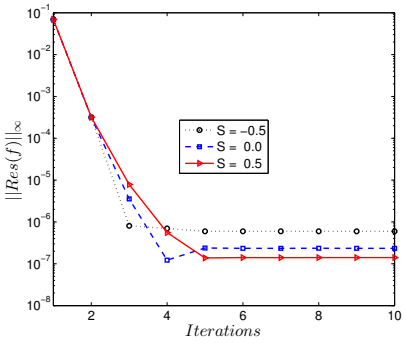

(c)

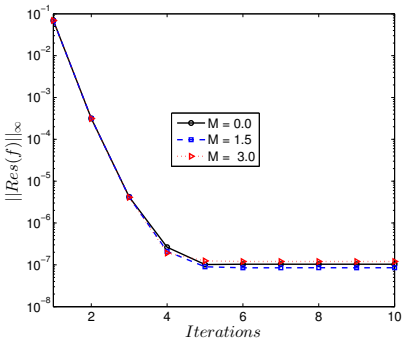

(d)

Figure 1: Residual error for different values of (a) dimensionless slip,(b) stretching or shrinking, (c) suction or injection, (d) magnetic field parameters on velocity profile

Authenticated | sabya.mondal.2007@gmail.com author's copy
Download Date | 6/2/17 8:52 AM

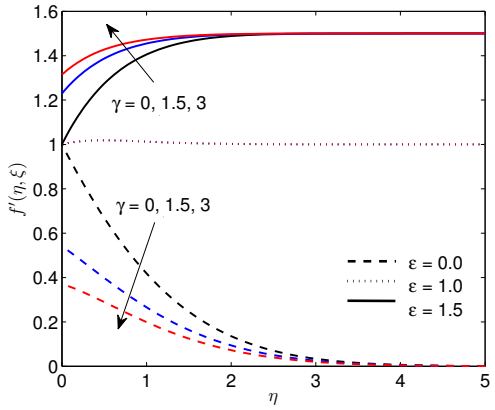

(a) Velocity profiles

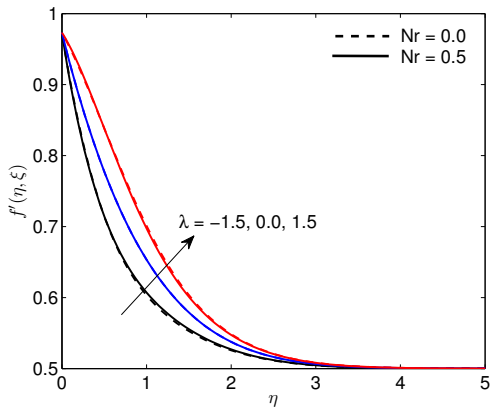

(b) Velocity profiles

Figure 2: (a) Effects of dimensionless slip factor γ and stretching parameter ε,(b) Effects of buoyancy force λ and buoyancy force ratio Nr parameters, on velocity profiles

rameter has the effect of reducing the velocity at the wall. The velocity decreases asymptotically to zero at the edge of the boundary layer. The boundary layer thickness decreases as γ increases. We note that when $\varepsilon = 1$, increasing γ gives no further changes in the velocity profiles because at this stage the external stream velocity becomes equal to the stretching velocity. This causes a frictionless Hiemenz flow [44].

Figure 2(b) explores the effect of λ and Nr on the velocity profiles. It is seen that the velocity increases as the buoyancy force parameter increases. This is due to the fact that the assisting flow ($\lambda > 0$) induces a favorable pressure gradient which enhances the fluid flow in the boundary layer and as a result the momentum boundary layer increases whereas the reverse occurs for the opposing flow when $\lambda < 0$.

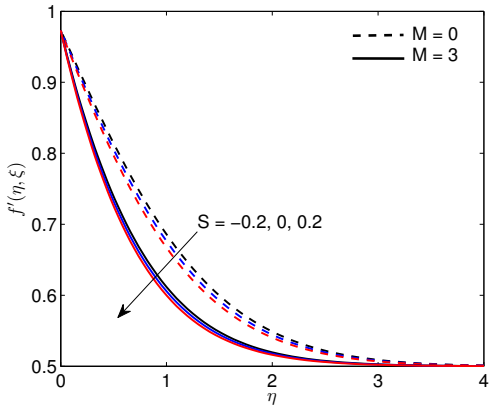

Figure 3: Effects of dimensionless suction/injection S and magnetic M parameters on velocity profiles

Figure 3 shows the effects of S and M on f' with respect to η. Here we note that $f'(\eta,\xi)$ decreases with increasing values of S and M. This behaviour is due to the fact that M increases the resistive forces on the flat plate which in turn reduces the fluid velocity and hence the motion of the fluid is slowed down. It is known that the wall suction ($S > 0$) has the tendency to decrease the momentum boundary layer thickness which is the cause of reduction in the velocity. But the the opposite behaviour can be seen for fluid injection ($S < 0$).

The internal heat source or sink in the boundary layer has an influence on the temperature fields as illustrated in Figure 4(a). It is clear that increasing $A^\star$ and $B^\star$ increases the temperature distribution within the fluid and the thermal boundary layer thickness increases. Figure 4(b) shows the variation of the temperature profiles for various values of the slip and stretching parameters. The temperature profiles increase with increasing γ when $\varepsilon < 1$ but the opposite trend is observed when $\varepsilon > 1$ as the thermal boundary layer thickness decreases.

Figure 5(a) depicts the effect of λ and Nr on the temperature profiles. We note that with the increasing value of buoyancy force parameter decreases the nanofluid temperature. Moreover, positive λ values induce a favorable pressure gradient that enhances the nanofluid temperature in the boundary layer when Nr increases. Consequently, the thermal boundary layer increases while the opposite is observed for negative λ values. Figure 5(b) demonstrates the influence of Le on the temperature distribution within the boundary layer in the presence of magnetic influence, buoyancy force, heat sink/source, thermophoresis/Brownian motion. It is observed that the temperature profiles including the thickness of the tempera-

Authenticated | sabya.mondal.2007@gmail.com author's copy
Download Date | 6/2/17 8:52 AM

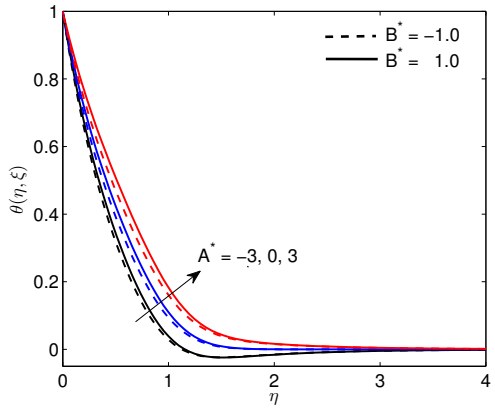

(a) Temperature profiles

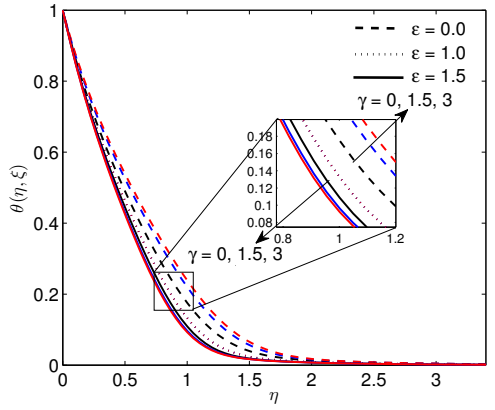

(b) Temperature profiles

Figure 4: (a) Effects of space-dependant $A^\star$ and temperature-dependent $B^\star$ parameters, (b) Effects of dimensionless slip factor γ and stretching parameter ε, on temperature profiles

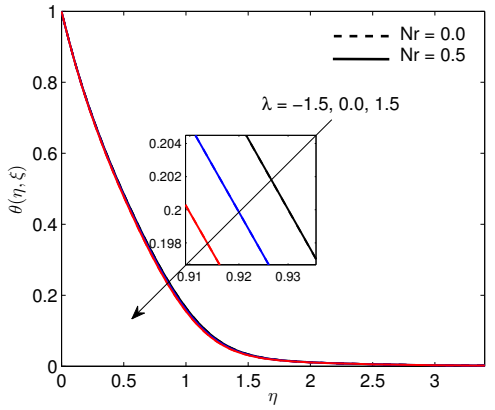

(a) Temperature profiles

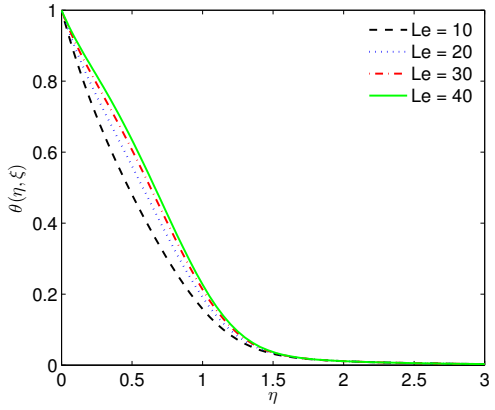

(b) Temperature profiles

Figure 5: (a) Effects of buoyancy force λ and buoyancy force ratio Nr parameters,(b) Effects of Lewis number Le, on temperature profiles

ture boundary layer increases with increases in the values of Le.

Figure 6(a) suggests that, in so far as the boundary layer temperature is concerned, thermophoresis plays the same role as the fluid Brownian motion. Thus, the fluid temperature increases with both N_t and N_b in the boundary layer region. The physical reason for this behaviour is that increased random motion of the nanoparticles increases the fluid temperature which enhances the thickness of the thermal boundary layer profiles. Figure 6(b) depicts the response of the temperature profiles to changing suction and magnetic field parameter values. Moreover, as would be expected, we note that the fluid temperature decreases with increase in suction but is higher in the case of injection.

The traditional model is revised such that the nanofluid particle volume fraction on the boundary is passively controlled. The effect of this change in boundary conditions can be seen in Figures 7 to 9 for different parameters. The impact of heat sink/source parameters $B^\star$ and $A^\star$ on the concentration profiles is presented in Figure 7(a). It can be seen that, away from the boundary, the concentration profiles increase with an increase in the values of $A^\star$ and $B^\star$. The effect of γ and ε on nanoparticle concentration is shown in Figure 7(b). An increase in the value of partial slip parameter value leads to an increase in the nanoparticle concentration when $\varepsilon < 1$ while the opposite trend is observed for $\varepsilon > 1$. In addition, the concentration increases and attains its highest value in the vicinity of the stretching plate near $\eta = 0.9$ and then decreases to the zero. Figure 8(a) displays the effect of λ and Nr on the nanoparticle concentration profile distributions. The nanoparticle concentration decreases asymptotically with increasing values of λ. Furthermore, in the case of opposing flow, the nanoparticle concentration decreases

Authenticated | sabya.mondal.2007@gmail.com author's copy
Download Date | 6/2/17 8:52 AM

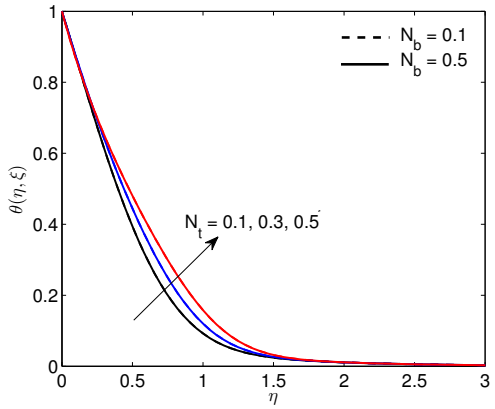

(a) Temperature profiles

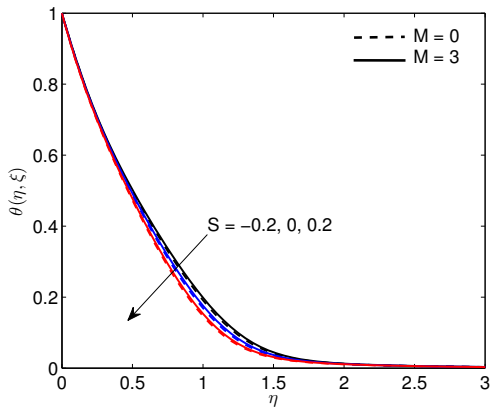

(b) Temperature profiles

Figure 6: (a) Effects of thermophoresis N_t and Brownian motion N_b parameters, (b) Effects of dimensionless suction/blowing S and magnetic M parameters, on temperature profiles

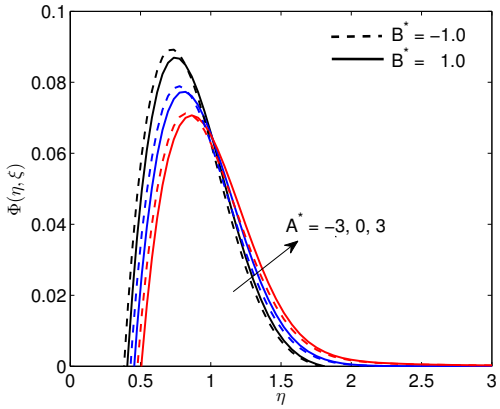

(a) Concentration profiles

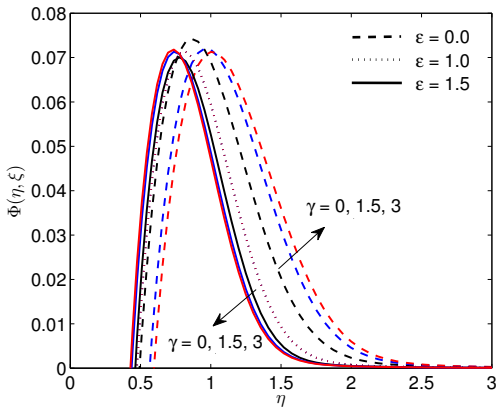

(b) Concentration profiles

Figure 7: (a) Effects of temperature-dependent B^* and space-dependent A^* parameters, (b) Effects of dimensionless slip γ and stretching ε parameters, on concentration profiles

with increasing Nr. Figure 8(b) shows the nanoparticle concentration profiles for several values of Le. It is seen that the nanoparticle volume fraction decreases with increases in Le and this manifested through the reduction in the thickness of the concentration boundary layer. Additionally, the nanoparticle concentration profiles decrease asymptotically to zero at the edge of the boundary layer.

The nanoparticle concentration profiles are presented in Figure 9(a) for various values of the thermophoresis parameter. The results show that the nanoparticle concentration profiles increase with increasing N_t away the boundary layer region. It is interesting to note that the distinctive peaks in the profiles occur in regions adjacent to the surface for higher values of thermophoresis parameter. This means that the nanoparticle concentration profile takes higher value near the plate. Figure 9(b) shows that the nanoparticle concentration profiles increase with increasing M up to a certain value of η, beyond which the opposite trend is observed. It is clear that as S increases the concentration profiles increase to the highest value in the vicinity of the plate and then decreases to zero in the quiescent fluid. As a result, the concentration boundary layer thickness increases close to the plate surface and decreases far from the surface with increasing S. Figure 9(c) shows that the concentration profile for various values of N_b. It is seen that the concentration profiles decrease with increasing N_b. The concentration profiles attain their maximum value near the $\eta = 1.0$.

Figure 10(a) shows the variation of the skin friction coefficient with ξ in response to changes in $A^\star$ and $B^\star$. The skin friction coefficient decreases with increases in both $A^\star$ and $B^\star$ when ξ increases. This suggests that $A^\star$ and $B^\star$ can be useful parameters for reducing the drag coefficient. Variations of the skin friction coefficient as a function of ξ

Authenticated | sabya.mondal.2007@gmail.com author's copy
Download Date | 6/2/17 8:52 AM

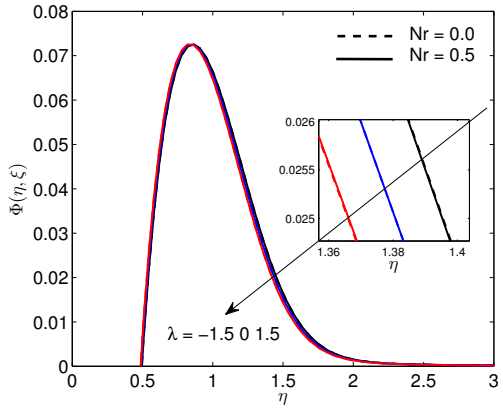

(a) Concentration profiles

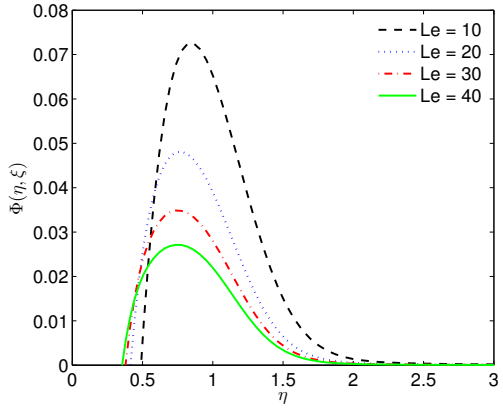

(b) Concentration profiles

Figure 8: (a) Effects of buoyancy force λ and buoyancy force ratio Nr parameters, (b) Effects of Lewis number Le, on concentration profiles

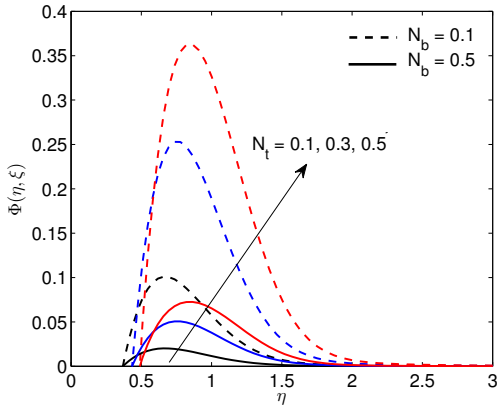

(a) Concentration profiles

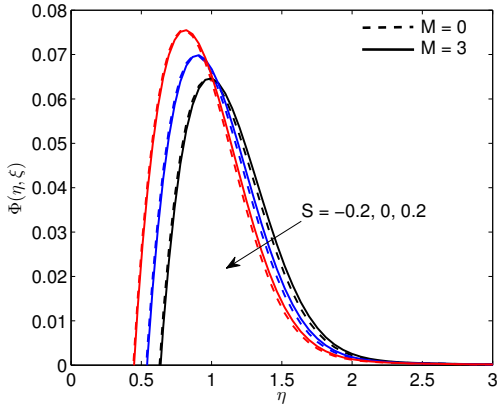

(b) Concentration profiles

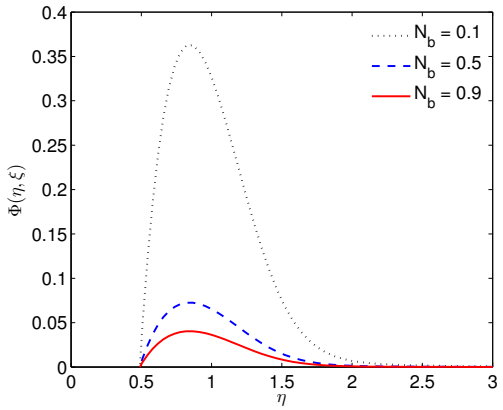

(c) Concentration profiles

Figure 9: (a) Effects of thermophoresis N_t parameter, (b) Effects of suction/injection S and magnetic M parameters, and (b) Effects of Brownian motion N_b parameters, on concentration profiles

for different values of the slip γ and stretching ε parameters are shown in Figure 10(b). We note that when $\varepsilon < 1$ the skin friction coefficient increases with increasing ξ, and decreases with increasing γ. The highest surface shear stress occurs with the no-slip velocity condition.

The variation of skin friction coefficient with λ and Nr is shown in Figure 11(a). We observe that the skin friction coefficient decreases with increasing λ. In the case of opposing flow, the skin friction coefficient increases with ξ and decreases with an increase in Nr. Figure 11 (b) shows that the skin friction coefficient decreases with increasing Lewis numbers but increases with increasing ξ.

Figure 12(a) shows the variation of the skin friction coefficient with different values of N_t and N_b. The skin friction coefficient decreases as N_t and N_b increase but increases with increasing ξ. Figure 12(b) shows the skin friction coefficient with respect to ξ for different values of M

Authenticated | sabya.mondal.2007@gmail.com author's copy
Download Date | 6/2/17 8:52 AM

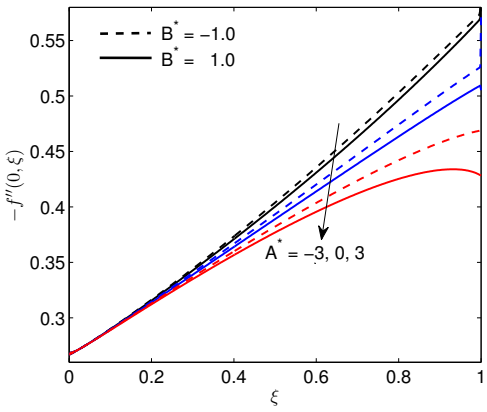

(a) Skin friction coefficient

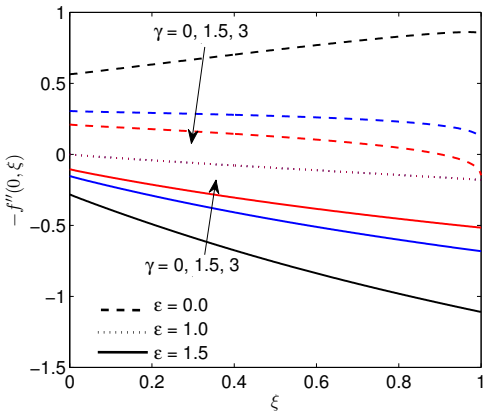

(b) Skin friction coefficient

Figure 10: (a) Effects of space-dependent A^* and temperature-dependent B^* parameters, (b) Effects of dimensionless slip γ and stretching ε parameters, on skin friction coefficient

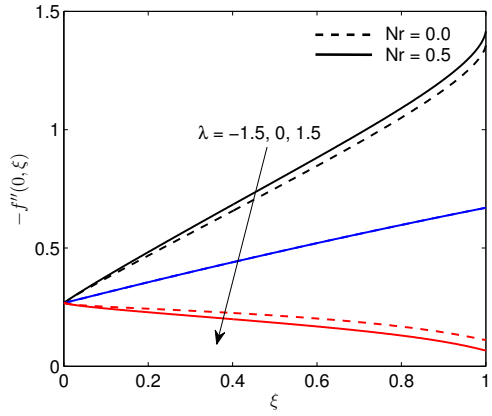

(a) Skin friction coefficient

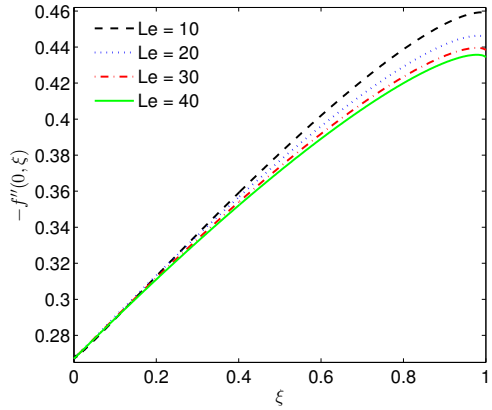

(b) Skin friction coefficient

Figure 11: (a) Effects of buoyancy force λ and buoyancy force ratio Nr parameters, (b) Effects of Lewis number Le on skin friction coefficient

and S. The skin friction coefficient increases with increasing M and S. Figures 13 - 14 show the effect of Pr on temperature and concentration profiles with same values of other parameters where dashed line indicates $Nb = 0.1$ and solid line for $Nb = 0.5$. The nature of those figures are similar to the Figures 4 (a) and 9 (b).

5 Conclusions

In this work, the unsteady stagnation boundary layer flow of a magnetohydrodynamic nanofluid over a stretching flat plate with velocity slip was investigated. The equations that model the boundary layer equations were solved numerically using the spectral relaxation method. A parametric study was performed to explore the impact of various physical parameters on the flow, and heat and mass transfer characteristics. The internal heat source or sink is shown to enhance the nanofluid motion while reducing the skin friction coefficient and the rate of heat transfer at the stretching surface.

In this study we have shown that increasing the Brownian motion parameter and the Lewis number reduces nanoparticle concentration profiles near the boundary layer region due to increasing mass transfer. The velocity, temperature and concentration profiles and the heat and mass transfer rate on the stretching plate are strongly influenced by the slip parameter. Heat transfer rates decrease with increasing velocity slip parameter values.

Acknowledgement: The authors are grateful to the Claude Leon Foundation and the University of KwaZulu-Natal, South Africa for the financial support.

Authenticated | sabya.mondal.2007@gmail.com author's copy
Download Date | 6/2/17 8:52 AM

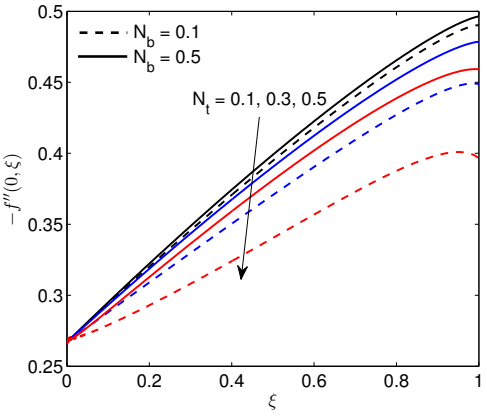

(a) Skin friction coefficient

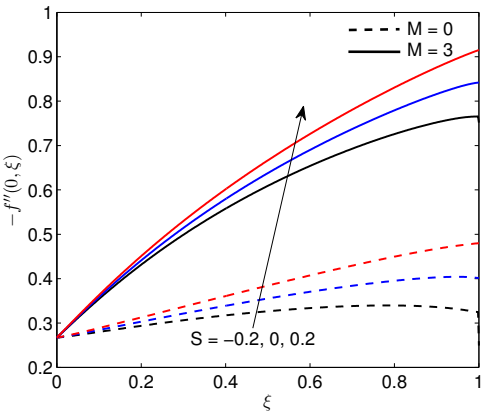

(b) Skin friction coefficient

Figure 12: (a) Effects of thermophoresis N_t and Brownian motion N_b parameters, (b) Effects of suction/injection S and magnetic M parameters on skin friction coefficient on skin friction coefficient

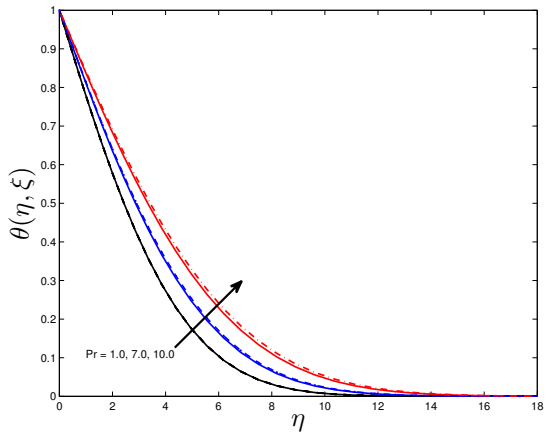

(a)

Figure 13: Effect of Pr on temperature profile for with same values of other parameters (dashed line for $Nb = 0.1$, solid line for $Nb = 0.5$)

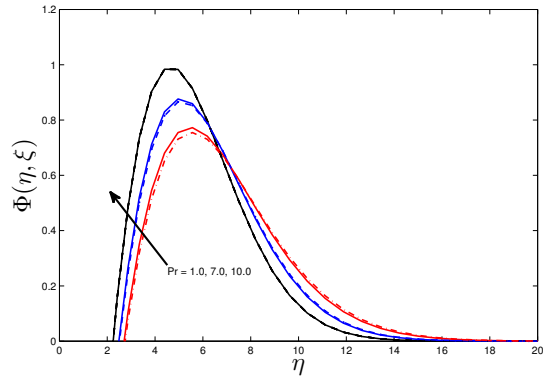

(a)

Figure 14: Effect of Pr on concentration profile with same values of other parameters (dashed line for $Nb = 0.1$, solid line for $Nb = 0.5$)

References

[1] Choi S.U.S., Nanofluids: from vision to reality through research, J. of Heat Transf, 2009, 131, 1 - 9.

[2] Choi S.U.S., Enhancing thermal conductivity of fluids with nanoparticles, ASME Fluids Eng. Div., 1995, 231, 99 - 105.

[3] Wang X.,Xu X., Choi S.U.S., Thermal conductivity of nanoparticle-fluid mixture, J. Therm. Phys. Heat Transfer, 1999, 13, 474 - 480.

[4] Akbarinia A., Abdolzadeh M., Laur R., Critical investigation of heat transfer enhancement using nanofluids in microchannels with slip and non-slip flow regimes, Appl Therm Eng., 2011, 31, 556 - 65.

[5] Murshed S.M.S., A review of boiling and convective heat transfer with nanofluids, Renewable and Sustainable Energy Reviews, 2011, 15, 2342 - 2354.

[6] Yu W., France D.M., Routbort J.L., Choi S.U.S., Review and comparison of nanofluid thermal conductivity and heat transfer enhancements, Heat Transfer Engineering, 2008, 29, 432 - 460.

[7] Wong K.V., de Leon O., Applications of nanofluids: current and future, Advances in Mechanical Engineering, 2010, Article ID 519659, 11 pages.

[8] Kiblinski P., Phillpot S.R., Choi S.U.S., Eastman J.A., Mechanism of heat flow is suspensions of nano-sized particles (nanofluids), Int. J. Heat Mass Transfer, 2002, 45, 855 - 863.

[9] Choi S.U.S., Zhang Z.G., Yu W., wood F.E.L., Grulke E.A., Anomalous thermal conductivity enhancement in nanotube suspensions, Applied Physics Letters, 2001, 79, 2252 - 2254.

[10] Eastman J.A., Choi S.U.S., Li S., Yu W., Thompson L.J., Anomalously increased effective thermal conductivities of ethylene glycol-based nanofluids containing copper nanoparticles, Applied Physics Letters, 2001, 78, 718 - 720.

[11] Nield D.A., Kuznetsov A.V., The Cheng-Minkowycz problem for natural convective boundary-layer flow in a porous medium saturated by a nanofluid, Int. J. Heat Mass Transfer, 2009, 52, 5792 - 5795.

Authenticated | sabya.mondal.2007@gmail.com author's copy
Download Date | 6/2/17 8:52 AM

[12] Kuznetsov A.V., Nield D.A., Natural convective boundary-layer flow of a nanofluid past a vertical plate, Int. J. Therm. Sci., 2010, 49, 243 - 247.
[13] Buongiorno J., Convective transport in nanofluids, ASME J. Heat Transfer, 2006, 128, 240 - 250.
[14] Blasius H., Grenzschichten in Flü ssigkeiten mit kleiner Reibung, Z. Math. Phys., 1908, 56, 1 - 37.
[15] Sakiadis B.C., Boundary-layer behaviour on continuous solid surfaces. I. Boundary-layer equations for two-dimensional and axisymmetric flow, AIChE, 1961, 7, 1 - 2.
[16] Schlichting H., Gersten K., Boundary Layer Theory, Springer Berlin, 2000.
[17] Bejan A., Entropy Generation Minimization, CRC Boca Raton, 1996.
[18] White F.M., Viscous Fluid Flow, McGraw-Hill, New York, 2006.
[19] Mukhopadhyay S., MHD boundary layer flow and heat transfer over an exponentially stretching sheet embedded in a thermally stratified medium, Alex. Eng. J., 2013, 52, 259 - 265.
[20] Mukhopadhyay S., Analysis of boundary layer flow over a porous nonlinearly stretching sheet with partial slip at the boundary, Alex. Eng. J., 2013, 52, 607 - 613.
[21] Capretto L., Cheng W., Hill M., Zhang X., Micromixing within microfluidic devices, Top Curr. Chem., 2011, 304, 27 - 68.
[22] Kleinstreuer C., Li J., Koo J., Microfluidics of nano-drug delivery, Int. J. Heat Mass Transfer, 2008, 51, 5590 - 5597.
[23] Yazdi M.H., Abdullah S., Hashim I., Sopian K., Slip MHD liquid flow and heat transfer over non-linear permeable stretching surface with chemical reaction, Int. J. Heat Mass Transfer, 2011, 54, 3214 - 3225.
[24] Singh K.R., Cowling T.G., Effect of magnetic field on free convective flow of electrically conducting fluids past a semiinfinite flat plate, Quarterly Journal of Mechanics and Applied Mathematics, 1963, 16, 1 - 15.
[25] Ahmmed S.F., Sarker A., MHD natural convection flow of viscous incompressible fluid from a vertical flat plate, Journal of Physical Sciences, 2009, 13, 77 - 85.
[26] Devi S.P.A., Kayalvizhi M., Analytical solution of MHDflow with radiation over a stretching sheet embedded in a porous medium, International Journal of Applied Mathematics and Mechanics, 2010, 6, 82 - 106.
[27] Rajesh V., Radiation effects on MHD free convection flow near a vertical plate with ramped wall temperature, International Journal of Applied Mathematics and Mechanics, 2010, 6, 60 - 677.
[28] Reddy M.G., Reddy N.B., Soret and Dufour effects on steady MHD free convection flow past a semi-infinite moving vertical plate in a porous medium with viscous dissipation, International Journal of Applied Mathematics and Mechanics, 2010, 6, 1 - 12.
[29] Devi S.P.A., Raj J.W.S., Thermo-diffusion effects on unsteady hydromagnetic free convection flow with heat and mass transfer past a moving vertical plate with time dependent suction and heat source in a slip flow regime, International Journal of Applied Mathematics and Mechanics, 2010, 7, 20 - 51.
[30] Makinde O.D., Computational modelling of MHD unsteady flow and heat transfer toward a flat plate with navier slip and newtonian heating, Brazilian Journal of Chemical Engineering, 2012, 29, 159 - 166.
[31] Mukhopadhyay S., Md Uddin S., Layek G.C., Lie group analysis on MHD boundary layer slip flow past a heated stretching sheet in presence of heat source/sink, International Journal of Applied Mathematics and Mechanic, 2012, 8, 51 - 66.
[32] Eldesoky I.M.I., Influence of slip condition on peristaltic transport of a compressible Maxwell fluid through porous medium in a tube, International Journal of Applied Mathematics and Mechanics, 2012, 8, 99 - 117.
[33] El-Shehawy E.F., El-Dabe N.T., ElDesoky I.M.I., Slip effects on the peristaltic flow of a non-Newtonian Maxwellian fluid, Acta Mechanica, 2006, 186, 141 - 159.
[34] Eldesoky I.M.I., Kamel M.H., Abumandour R. M., Numerical study of slip effect of unsteady MHD pulsatile flow through porous medium in an artery using generalized differential quadrature method (comparative study), Wor. J. Eng. Techno., 2014, 2,131 - 148.
[35] Eldesoky I.M.I., Unsteady MHD pulsatile blood flow through porous medium in stenotic channel with slip at permeable walls subjected to time dependent velocity (injection/suction), Walailak J. Sci. Techno., 2014, 11, 901 - 922.
[36] Chiam T.C., Stagnation point flow towards a stretching plate, Journal of the Physical Society of Japan., 1994, 63, 2443 - 2444.
[37] Nandy S.K., Mahapatra T.R., Effects of slip and heat generation/absorption on MHD stagnation flow of nanofluid past a stretching/shrinking surface with convective boundary conditions, International Journal of Heat and Mass Transfer, 2013, 64, 1091 - 1100.
[38] Kuznetsov A., Nield D., The Cheng-Minkowycz problem for natural convective boundry layer flow in a porous medium saturated by a nanofluid: A revised model, Int. J. Heat Mass Trans., 2013, 65, 682 - 685.
[39] Motsa S.S., Dlamini P.G., Khumalo M., Spetral relaxation method and spectral quasilinarization method for solving unsteady boundary layer flow problems, Advances in Mathematial Physics, 2014, Article ID 341964, 12 pages.
[40] Cheng P., Minkowycz W.J., Free convection about a vertical flat embedded in a porous medium with application to heat transfer from a dike, J. Geophysical Research, 1977, 82, 2040 - 2044.
[41] Bataller R.C., Viscoelastic fluid flow and heat transfer over a stretchng sheet under the effects of a non-uniform heat source, viscous dissipatio and thermal radiation, Int. J. Heat Mass Tran., 2007, 50, 3152 - 3162.
[42] Pal D., Mondal H., Effect of variable viscosity on MHD non-Darcy mixed convective heat transfer over a stretching sheet embedded in a porous medium with non-uniform heat source/sink, Commun. Nonlinear Sci. Numer. Simulat., 2010, 15, 1553 - 1564.
[43] Anwar I., Kasim A.R.M., Ismail Z., Salleh M.Z., Shafie S., Chemical reaction and uniform heat generation or absorption effects on MHD stagnation-point flow of a nanofluid over a porous sheet, World Applied Sciences Journal, 2013, 24, 1390 - 1398.
[44] Sahoo B., Flow and heat transfer of a non-Newtonian fluid past a stretching sheet with partial slip, Communications in Nonlinear Science and Numerical Simulation, 2009, doi: 10.1016/j.cnsns.2009.04.032.

Authenticated | sabya.mondal.2007@gmail.com author's copy
Download Date | 6/2/17 8:52 AM

Chapter 6

An unsteady moving magneto-nanofluid over a moving surface in presence of chemical reaction

In this Chapter, we extend the work in Chapter 5 by considering a binary nanofluid (see Kuznetsov and Nield [213]). Here we study the unsteady magneto-nanofluid flow over a moving surface. The aim is to investigate the influence of thermophoresis, Brownian motion, thermal radiation, chemical reaction and inertia on the flow model. The nanoparticle flux is assumed to vanish at the boundary surface. The model equations are solved numerically using the spectral relaxation method.

An unsteady moving magneto-nanofluid over a moving surface in presence of chemical reaction

Sami M.S. Ahamed, Sabyasachi Mondal *, Precious Sibanda
School of Mathematics, Statistics and Computer Science
University of KwaZulu-Natal, Pietermaritzburg
Private Bag X01, Scottsville 3209, South Africa
* Corresponding author's e-mail : sabya.mondal.2007@gmail.com

Abstract

The double-diffusive convection of unsteady flow in porous medium appeased by a moving nanofluid, in the presence of chemical reaction and thermal radiation effects over a moving surface has been investigated. Two different types of concentration profiles i.e., solutal concentration profile as well as nanoparticle concentration profile are chosen here. This study includes the effects of Brownian motion and thermophoresis. The nanofluid particles fraction on the boundary have been passively rather than actively controlled with the nanoparticle flux at the boundary surface assumed to vanish. The governing equations are solved using the spectral relaxation method. The numerical results are discussed and demonstrated graphically and in tabular forms for the velocity, temperature, solutal concentration, and nanoparticle concentration; as well as the skin friction coefficient, heat and mass transfer rate. A comparative study between previously published and the present results for some limiting cases shows an excellent agreement between the results.

Keywords: Magneto-Nanofluid, Moving surface, Chemical reaction, Spectral relaxation method.

1 Introduction:

The study of laminar boundary layer flow, heat and mass transfer in Newtonian and nanofluid flows over a moving surface, have received considerable research attention in the past a few decades. Fluid flow on a moving surface has many engineering and industrial applications in electro-chemistry and chemical engineering processes, including metallurgical processes, polymer extrusion and the cooling of fused fluids that have being stretched into a cooling system. Other applications can be found in glass blowing, crystal growing, and paper production. In the early twentieth century, Blasius [1] pioneered the study of the steady state boundary layer flow with a uniform free stream. Howarth [2] provided additional results to the Blasius problem. After that so many work had been done in recent past years([3] -[12])

Liquids such as oil, water, ethylene glycol, toluene and toluene di-isocyanate have low thermal conductivities. To enhance the thermal conductivity of such fluids, nano-scale metallic particles, for instance, aluminum, titanium, gold, copper, iron or their oxides are added to these fluids. Choi [13] coined the term nanofluid for such fluids with suspended nanoparticles. The main role of nanoparticles is to enhance the fluid's thermal conductivity and heat transfer coefficient. In the literature, many authors have studied problems related to a stretching surface with nanofluid flow. Khan and Pop [14] were among the first researchers to work on nanofluid flow due to a stretching sheet. A numerical study of boundary layer flow over a linear stretching sheet, combined with Brownian motion and thermophoresis influences was undertaken by

Makinde and Aziz [15]. A theoretical study of the unsteady boundary layer flow of a nanofluid over a permeable stretching/shrinking sheet was carried out by Bachok et al. [16]. Rohni et al. [17] gave a numerical solution for the unsteady flow over a continuously shrinking surface with wall mass suction in a nanofluid by using the nanofluid model proposed by Buongiorno [18].

The main objective of this work is to study double-diffusion effects on an unsteady, two-dimensional laminar flow of a moving viscous nanofluid with a chemical reaction and thermal radiation effects. The nanoparticle boundary condition assumes that the flush vanishes at the wall. The model equations are solved numerically using the spectral relaxation method, [19]. Numerical results for the velocity and temperature, concentration and nanoparticles volume fraction profiles are presented graphically and in tabular form for various physical parametric conditions.

2 Mathematical Formulation

Consider the two-dimensional flow of an unsteady viscous incompressible Newtonian nanofluid, over a surface moving with a velocity $U_{\rm w}$, in the same or opposite direction to the free stream velocity U_∞ as shown in Figure 1. The coordinate systems are assumed to be the x-axis, which extends parallel to the surface, while the y-axis extends normal to the surface. The surface temperature and solute concentration are $T_{\rm w} = T_\infty + T_0 x^\kappa$ and $C_{\rm w} = C_\infty + C_0 x^\kappa$, where T_0 and C_0 are positive real numbers and κ is the temperature and concentration power index. The ambient temperature and concentration values are T_∞ and C_∞, respectively. It assumed that the nanoparticle flux vanishes at the moving surface. The governing equations are the continuity, momentum, energy, concentration and nanoparticle volume fraction, written as (see Kuznetsov and Nield [20], Yih [21])

$$\frac{\partial u}{\partial x} + \frac{\partial v}{\partial y} = 0, \tag{1}$$

$$\frac{\partial u}{\partial t} + u\frac{\partial u}{\partial x} + v\frac{\partial u}{\partial y} = U_\infty \frac{dU_\infty}{dx} + \nu_f \frac{\partial^2 u}{\partial y^2} - \left[\frac{\nu_f}{K} + \frac{\sigma B_0^2}{\rho_f}\right](u - U_\infty) - C^*\varepsilon^2\, u^2, \tag{2}$$

$$\begin{aligned}\frac{\partial T}{\partial t} + u\frac{\partial T}{\partial x} + v\frac{\partial T}{\partial y} &= \frac{k_f}{(\rho c_p)_f}\frac{\partial^2 T}{\partial y^2} - \frac{1}{(\rho c_p)_f}\frac{\partial q_r}{\partial y} \\ &\quad + \frac{(\rho c_p)_{np}}{(\rho c_p)_f}\left\{D_B \frac{\partial \phi}{\partial y}\frac{\partial T}{\partial y} + \frac{D_T}{T_\infty}\left(\frac{\partial T}{\partial y}\right)^2\right\} + D_{TC}\frac{\partial^2 C}{\partial y^2},\end{aligned} \tag{3}$$

$$\frac{\partial C}{\partial t} + u\frac{\partial C}{\partial x} + v\frac{\partial C}{\partial y} = D_S\frac{\partial^2 C}{\partial y^2} + D_{CT}\frac{\partial^2 T}{\partial y^2} - R(C - C_\infty), \tag{4}$$

$$\frac{\partial \phi}{\partial t} + u\frac{\partial \phi}{\partial x} + v\frac{\partial \phi}{\partial y} = D_B\frac{\partial^2 \phi}{\partial y^2} + \frac{D_T}{T_\infty}\frac{\partial^2 T}{\partial y^2}, \tag{5}$$

where t is the time, u and v are the fluids' velocity components along x and y axis, respectively. ν_f is the fluids' kinematic viscosity, K is the permeability of porous medium, σ is an electrical conductivity, B_0 is an uniform magnetic field strength, ρ_f is the fluid's density, $C^*\varepsilon^2$ is an inertia parameter, T is the fluid's temperature, k_f is the is the fluids' thermal conductivity, $(\rho c_p)_f$ is the fluid's heat capacity, α_f is the thermal diffusivity or is the ratio of the fluids' thermal conductivity to fluid's heat capacity, $(\rho c_p)_{np}$ is the effective nanoparticle's material heat capacity, τ is the ratio of the effective nanoparticle's material heat capacity to fluid's heat capacity, D_B stand for the Brownian diffusion coefficient, D_T stand for thermophoretic diffusion coefficient, D_{TC} is the Dufour-type diffusivity, C is the fluid's solutal concentration, D_S is the

solutal diffusivity, D_{CT} is the Soret-type diffusivity, R is the chemical reaction parameter and ϕ is the nanoparticle volume fraction. The radiation heat flux q_r under Rosseland approximation [22] is stated as

$$q_r = -\frac{4\sigma^*}{3K^*}\frac{\partial T^4}{\partial y} \tag{6}$$

where σ^* is the Stephen-Boltzmann constant, K^* is the Rosseland mean spectral absorption coefficient. The temperature differences within the flow are assumed to be sufficiently small such that T^4 may be expressed as a linear function of temperature T. The term T^4 is expanded in a Taylor series about T_∞ as

$$T^4 \cong T_\infty^4 + 4T_\infty^3(T - T_\infty) + 6T_\infty^2(T - T_\infty)^2 + ... \tag{7}$$

Neglecting higher order terms in Eq. (7) above the first degree in $(T - T_\infty)$, we get

$$T^4 \cong 4T_\infty^3 T - 3T_\infty^4. \tag{8}$$

The initial conditions are

$$u = v = 0, \;\; T = T_\infty, \; C = C_\infty, \; \phi = \phi_\infty \quad \forall \; x, y, \; t < 0, \tag{9}$$

with boundary conditions

$$\begin{aligned} &v = 0, u = U_{\rm w} = ax, T = T_{\rm w}, C = C_{\rm w}, D_B\frac{\partial \phi}{\partial y} + \frac{D_T}{T_\infty}\frac{\partial T}{\partial y} = 0 \quad \text{at} \quad y = 0, t \geq 0, \\ &u \to \; U_\infty = bx, \; T \; \to T_\infty, \; C \to C_\infty, \; \phi \to \phi_\infty \quad \text{as} \quad y \to \infty, t \geq 0. \end{aligned} \tag{10}$$

We introduce the following non-dimensional similarity variables

$$\begin{aligned} &\eta = \sqrt{\frac{U}{\alpha_f x \xi}}, \; \xi = 1 - \exp(-t^*), \quad t^* = \frac{U}{x}t, \psi = \sqrt{Ux\alpha_f \xi}\; f(\xi, \eta), \\ &\theta(\xi, \eta) = \frac{T - T_\infty}{T_{\rm w} - T_\infty}, \; \varphi(\xi, \eta) = \frac{C - C_\infty}{C_{\rm w} - C_\infty}, \Phi(\xi, \eta) = \frac{\phi - \phi_\infty}{\phi_{\rm w}}, \end{aligned} \tag{11}$$

where $U = U_{\rm w} + U_\infty = cx$ is a composite velocity; and a, b and c are positive real numbers. The stream function ψ defined as

$$u = \frac{\partial \psi}{\partial y}, \quad v = -\frac{\partial \psi}{\partial x}, \tag{12}$$

Equations (1) - (5) are reduced into the following forms

$$Prf''' + \xi\left[ff'' - (1+\Lambda)f'^2 + (\Omega + M^2)(\lambda - f') + \lambda^2\right] + (1-\xi)\left[\frac{1}{2}\eta f'' - \xi\frac{\partial f'}{\partial \xi}\right] = 0, \tag{13}$$

$$(1 + Nr)\,\theta'' \; + \; \xi\left[f\theta' - \kappa f'\theta\right] + (1-\xi)\left[\frac{1}{2}\eta\theta' - \xi\frac{\partial \theta}{\partial \xi}\right] + N_b\Phi'\theta' + N_t\theta'^2 + N_d\varphi'' = 0, \tag{14}$$

$$\varphi'' \; + \; Le\left[\xi\left[f\varphi' - \kappa f'\varphi - \gamma\varphi\right] + (1-\xi)\left[\frac{1}{2}\eta\varphi' - \xi\frac{\partial \varphi}{\partial \xi}\right]\right] + Ld\;\theta'' = 0, \tag{15}$$

$$\Phi'' \; + \; Ln\left[\xi f\Phi' + (1-\xi)\left[\frac{1}{2}\eta\Phi' - \xi\frac{\partial \Phi}{\partial \xi}\right]\right] + \frac{N_t}{N_b}\theta'' = 0, \tag{16}$$

The boundary conditions (10) become

$$\begin{aligned} &f = 0, \; f' = 1 - \lambda, \; \theta = 1, \; \varphi = 1, \; N_b\Phi' + N_t\theta' = 0 \;\; at \;\; \eta = 0, \;\; \xi \in [0, 1] \\ &f' = \lambda, \; \theta = 0, \; \varphi = 0, \; \Phi = 0 \;\; as \;\; \eta \to \infty, \;\; \xi \in [0, 1], \end{aligned} \tag{17}$$

where the primes denote differentiation with respect to η; and $\lambda = \frac{b}{c}$ is the ratio of free stream velocity to the composite reference velocity parameter. The Blasius problem can be recovered when $\lambda = 1$ (i.e. for $U_{\rm w} = 0$) while the Sakiadis flow problem is recovered when $\lambda = 0$ (i.e. $U_\infty = 0$), [23]. The nanofluid movement is more rapid than the surface motion when $1 > \lambda > 0.5$ while the surface motion is quicker than the nanofluid movement when $0 < \lambda < 0.5$. The nanofluid and the surface are moving in the opposite direction when $\lambda > 1$, [24].

The important parameters in Eqs. (13)-(16) are the Prandtl number Pr, the permeability parameter Ω, the Hartmann number M, the dimensionless porous media inertia parameter Λ, the thermal radiation parameter Nr, Brownian motion parameter N_b, thermophoresis parameter N_t, modified Dufour parameter N_d, Lewis number Le, chemical reaction parameter γ, Dufour-Lewis number Ld and nanofluid Lewis number Ln defined as

$$\begin{aligned}
&Pr = \frac{\nu_f}{\alpha_f},\ \Omega = \frac{\nu_f}{c\ K}\ ,\ M = \sqrt{\frac{\sigma B_0^2}{\rho_f\ c}},\ \Lambda = C^*\varepsilon^2 x,\ Nr = \frac{16\sigma^* T_\infty^3}{3k_f K^*},\\
&N_b = \frac{\tau D_B \phi_\infty}{\alpha_f},\ N_t = \frac{\tau D_T (T_{\rm w} - T_\infty)}{T_\infty \alpha_f},\ N_d = \frac{D_{TC}(C_{\rm w} - C_\infty)}{\alpha_f (T_{\rm w} - T_\infty)},\\
&Le = \frac{\alpha_f}{D_S},\ \gamma = \frac{R}{c},\ Ld = \frac{D_{CT}(T_{\rm w} - T_\infty)}{D_S (C_{\rm w} - C_\infty)},\ Ln = \frac{\alpha_f}{D_B}.
\end{aligned} \tag{18}$$

The skin friction coefficient C_f, the local Nusselt number Nu_x and the local Sherwood number Sh_x of solutal concentration are defined as

$$C_f = \frac{\tau_{\rm w}}{\frac{1}{2}\rho_f U^2},\quad Nu_x = \frac{x q_{\rm w}}{k_f\,(T_{\rm w} - T_\infty)},\quad Sh_x = \frac{x q_{\rm m}}{D_S\,(C_{\rm w} - C_\infty)}, \tag{19}$$

where $\tau_{\rm w}$, $q_{\rm w}$ and $q_{\rm m}$ are the wall shear stress, surface heat and mass fluxes, respectively. defined as

$$\tau_{\rm w} = \mu_f \left(\frac{\partial u}{\partial y}\right)_{y=0},\quad q_{\rm w} = -\left(k_f + \frac{16\sigma^* T_\infty^3}{3K^*}\right)\left(\frac{\partial T}{\partial y}\right)_{y=0},\quad q_{\rm m} = -D_S \left(\frac{\partial C}{\partial y}\right)_{y=0}. \tag{20}$$

Using Eq.(20) and quantity (19), along with (11) we get

$$0.5\sqrt{\frac{\xi Re_x}{Pr}}\ C_f = f''(\xi,0),\ \sqrt{\frac{\xi}{Pe_x}}\ Nu_x = -\,(1+Nr)\,\theta'(\xi,0),\ \sqrt{\frac{\xi}{Pe_x}}\ Sh_x = -\varphi'(\xi,0), \tag{21}$$

where $Re_x = \frac{cx^2}{\nu}$ is the Reynolds number, $Pe_x = \frac{cx^2}{\alpha}$ is the local Peclet number.

We cannot calculate the Sherwood number for nanoparticle concentration equation because the nanoparticle flux at the boundary surface assumed to vanish due to the revised boundary condition.

3 Solution Technique

The spectral relaxation method [19] was used to solve the system of non-similar equations (13) - (16) with boundary conditions (17). In the frame work of the spectral relaxation method, we obtain the following iterative scheme

$$f'_{r+1} = u_{r+1} \tag{22}$$

$$Pr\ u''_{r+1} + a_{1,r}u'_{r+1} + a_{2,r}u_{r+1} + a_{3,r} = a_{4,r}\frac{\partial u_{r+1}}{\partial \xi} \tag{23}$$

$$(1+Nr)\theta''_{r+1} + b_{1,r}\theta'_{r+1} + b_{2,r}\theta_{r+1} + b_{3,r} = b_{4,r}\frac{\partial \theta_{r+1}}{\partial \xi} \tag{24}$$

$$\varphi''_{r+1} + c_{1,r}\varphi'_{r+1} + c_{2,r}\varphi_{r+1} + c_{3,r} = c_{4,r}\frac{\partial \varphi_{r+1}}{\partial \xi} \tag{25}$$

$$\Phi''_{r+1} + d_{1,r}\Phi'_{r+1} + d_{2,r} = d_{3,r}\frac{\partial \Phi_{r+1}}{\partial \xi}. \tag{26}$$

The boundary conditions for the above iteration scheme are

$$\begin{aligned}
&f_{r+1}(\xi,0)=0,\ u_{r+1}(\xi,0)=1-\lambda,\ \theta_{r+1}(\xi,0)=1,\ \varphi_{r+1}(\xi,0)=1\\
&N_b\Phi'_{r+1}(\xi,0)+N_t\theta'_{r+1}(\xi,0)=0\\
&u_{r+1}(\xi,\infty)=\lambda,\ \theta_{r+1}(\xi,\infty)=0,\ \varphi_{r+1}(\xi,\infty)=0,\ \Phi_{r+1}(\xi,\infty)=0
\end{aligned} \tag{27}$$

where

$$\begin{aligned}
a_{1,r}&=\frac{1}{2}(1-\xi)\eta+\xi f_r\\
a_{2,r}&=-\xi(\Omega+\mathrm{M}^2)\\
a_{3,r}&=\xi\left[\lambda^2+(\Omega+\mathrm{M}^2)\lambda-(1+\Lambda)u_r^2\right]\\
a_{4,r}&=\xi(1-\xi)
\end{aligned} \tag{28}$$

$$\begin{aligned}
b_{1,r}&=\frac{1}{2}(1-\xi)\eta+\xi f_{r+1}+N_b\Phi'_r\\
b_{2,r}&=-\kappa\ \xi\ u_{r+1}\\
b_{3,r}&=N_t\theta'^2_r+N_d\varphi''_r\\
b_{4,r}&=\xi(1-\xi)
\end{aligned} \tag{29}$$

$$\begin{aligned}
c_{1,r}&=Le\left[\frac{1}{2}(1-\xi)\eta+\xi f_{r+1}\right]\\
c_{2,r}&=-Le\ \xi(\kappa\ u_{r+1}+\gamma)\\
c_{3,r}&=Ld\ \theta''_r\\
c_{4,r}&=Le\ \xi(1-\xi)
\end{aligned} \tag{30}$$

$$\begin{aligned}
d_{1,r}&=Ln\left[\frac{1}{2}(1-\xi)\eta+\xi f_{r+1}\right]\\
d_{2,r}&=\frac{N_t}{N_b}\theta''_{r+1}\\
d_{3,r}&=Ln\ \xi(1-\xi).
\end{aligned} \tag{31}$$

The indices (r) and $(r+1)$ denote the previous and current iteration levels, respectively. Starting from initial approximations denoted by f_0, u_0, θ_0, φ_0 and Φ_0 the equations (13)-(16) are solved iteratively for $f_{r+1}(\xi,\eta)$, $u_{r+1}(\xi,\eta)$, $\theta_{r+1}(\xi,\eta)$, $\varphi_{r+1}(\xi,\eta)$ and $\Phi_{r+1}(\xi,\eta)$ $(r=0,1,2,...)$. Here, $f_0=1+\lambda(\eta-1)-(1-\lambda+\lambda\eta)e^{-\eta}$. The equations are discretized using the Chebyshev spectral collocation method in the η direction while the discretization in the ξ direction is done using the implicit finite difference method. To ensure accuracy of the results, a sufficiently small step size $\Delta\xi$ is used. The step size was chosen to be small enough such that further reduction did not change the results for the flow properties of interest. The total number of iteration to reach a good approximate result is 10 here.

4 Results and Discussions

Eqs. (13)-(16) subject to the boundary conditions (17) have been solved numerically using the spectral relaxation method. The results given below demonstrate the influence of fluid and physical parameters on the fluid properties. The velocity profiles, temperature profiles, solutal and nanoparticle concentration profiles, skin friction coefficient and Sherwood number for solutal concentration profile are given in Figures 1 - 13 for different parameters values. In the numerical calculations, the default parameter values utilized are, unless otherwise specified; $Pr=10$, $\Lambda=0.1$, $\Omega=1.0$, $M=3.0$, $\lambda=0.3$ and 0.7, $Nr=0.5$, $\kappa=2.0$, $N_b=0.5$, $N_t=0.5$, $N_d=0.2$, $Le=2.0$, $\gamma=0.1$, $Ld=0.2$, $Ln=10$ and $\xi=0.5$ [20, 21, 25].

To validate the accuracy of the current results, and the solution procedure, we have compared the skin friction coefficient with [21, 26, 27] using the same parameter values in Table 1. We note that a good agreement is achieved with the results in the literature.

Figure 2 indicates that when the surface motion is quicker than nanofluid movement, the velocity profiles and skin friction coefficient at the wall decrease with the increasing permeability parameter. Again, when the surface motion is slower than the nanofluid movement within the boundary layer, the velocity profiles and skin friction coefficient increase as Ω increases.

Figure 3 demonstrates that the fluid is accelerated faster than the surface with increasing value of Hartmann number, the velocity profiles as well as the skin friction coefficient increase, but the temperature, solutal concentration and nanoparticle concentration profiles decrease. Figure 4 is plotted to demonstrate the influence of thermal radiation parameter on the temperature and nanoparticle concentration profiles for different values of λ. It is noted that the temperature in the moving boundary layer increases with increase in the value of the thermal radiation parameter. This is due to the fact that, the divergence of the radiative heat flux $\partial q_r/\partial y$ increases as the Rosseland mean spectral absorption coefficient K^* decreases which increases the rate of radiative heat transfer to the nanofluid which causes the enhancement of the nanofluid temperature. In view of this fact, the effect of radiation becomes more significant for large value of Nr and the radiation effect can be neglected when $Nr = 0$. Thereupon, the thermal boundary layer thickness increases as thermal radiation parameter increases. The nanoparticle concentration profile decreases upto a certain value of η and then turn to increases. This is due to the revise nanofluid boundary condition. Furthermore, the temperature is higher when the nanofluid's motion is faster than surface's motion, near to the surface.

Figure 5 demonstrates the effect of the Brownian motion parameter of the nanoparticles suspended in the fluid on the nanoparticle concentration profiles. As the Brownian motion of the nanoparticles increases the nanoparticle concentration profiles decrease. Thence, the boundary layer of the nanoparticle volume fraction thickness decreases.

Figure 6 shows the influence of the regular Lewis number on solutal concentration, Sheerwod number of solutal concentration and nanoparticle concentration profiles for different values of λ. We note that, increasing the Lewis number reduces the solutal concentration profiles gradually, this corresponds to weaker molecular diffusivity and decrease the boundary layer thickness. On the other hand The nanoparticle concentration profiles decrease upto a certain value of η and beyond that point, opposite trend is observed. It is seen from this figure that the Sheerwood number for solutal concentration is increases with increasing both in Le and λ.

Figure 7 illustrates the effects of chemical reaction parameter on solutal concentration profile. The concentration profiles decrease with increasing values of the chemical reaction parameter, that is, the concentration field decreases for a destructive chemical reaction.

Figure 8 shows the effects of the nanofluid Lewis number on the nanoparticle volume fraction profiles. It can be seen that the nanoparticle concentration profile increases near the surface and decreases away from the surface within the moving boundary layer. This phenomena is observed for the nanofluid model with passive control of nanoparticles at the boundary.

Conclusion : This study was concerned with double-diffusion convection in the unsteady flow of a moving magneto-nanofluid over a moving surface embedded in porous media with thermal radiation and chemical reaction effects. The model nonlinear equations are solved numerically using the spectral relaxation method. Numerical results for the velocity, temperature, solutal and nanoparticles concentration profiles have been presented graphically for various physical parametric conditions.

Furthermore, the nanofluid velocity decrease with an increase in the values of permeability parameter and the Hartmann number. The temperature profiles are reduced by increasing Hartmann numbers. In addition, the nanofluid temperature increased with an increase in thermal radiation parameter. The solutal concentration decreased as the chemical reaction parameters increased.

Acknowledgements : The authors are grateful to the University of KwaZulu-Natal, South Africa and and the Claude Leon Foundation, South Africa for financial support.

References

[1] H. Blasius, Grenzschichten in Flussigkeiten Mit Kleiner Reibung, *Zeitschrift fr Angewandte Mathematik und Physik*, 56(1908) 1 - 37.

[2] L. Howarth, On the Solution of the Laminar Boundary Layer Equations, *Proceedings of the Society of London*, 164(1938) 547 - 579.

[3] T. R. Mahapatra, S. Mondal, D. Pal, Heat transfer due to magnetohydrodynamic stagnation-point flow of a power-law fluid towards a stretching surface in presence of thermal radiation and suction/injection, *ISRN Thermodynamics*, Article ID 465864, (2012), 1-9.

[4] N. A. Haroun, P. Sibanda, S. Mondal, S. S. Motsa, On unsteady MHD mixed convection in a nanofluid due to a stretching/shrinking surface with suction/injection using the spectral relaxation method, *Boundary Value Problems*, 24 (2015), 1-17.

[5] N. A. H. Haroun, P. Sibanda, S. Mondal, S. S. Motsa, M. M. Rashidi, Heat and mass transfer of nanouid through an impulsively vertical stretching surface using the spectral relaxation method, *Boundary Value Problems*, 2015 (2015) 161, 1-16.

[6] S. Mondal, N. A. H. Haroun, P. Sibanda, The effects of thermal radiation on an unsteady MHD axisymmetric stagnation- point flow over a shrinking sheet in presence of temperature dependent thermal conductivity with Navier slip,*PlOS ONE*, 10(9): e0138355. doi:10.1371/journal. pone.0138355 (2015).

[7] T.M. Agbaje, S. Mondal, Z.G. Makukula, S.S. Motsa, P. Sibanda, A new numerical approach to MHD stagnation point flow and heat transfer towards a stretching Sheet, *Ain Shams Eng. Journal*, 2016

[8] N. A.H. Haroun, S. Mondal, P. Sibanda Unsteady natural convective boundary-layer flow of MHD nanofluid over a stretching surfaces with chemical reaction using the spectral relaxation method: A revised model, *Procedia Engineering*, 127 (2015) 18 - 24

[9] I. S. Oyelakin, S. Mondal, P. Sibanda, Unsteady Casson nanofluid flow over a stretching sheet with thermal radiation, convective and slip boundary conditions, *Alexandria Eng. Journal*, 55 (2016) 1025 - 1035.

[10] S. M. S. Ahamed, S. Mondal, P. Sibanda, Thermo-diffusion effects on unsteady mixed convection in a magneto-nanofluid flow along an inclined cylinder with a heat source, Ohmic and viscous dissipation, *J. Comp. Theo. Nanoscience*, 13(3) (2016) 1-15.

[11] N. A.H Haroun, S. Mondal, P. Sibanda, Hydromagnetic Nanofluids flow through porous media with thermal radiation, chemical reaction and viscous dissipation using spectral relaxation method, *The 7th International Conference on Computational Methods (ICCM2016)*, University of California at Berkeley, Sutardja Dai Hall, California, U.S.A, 1-4 August, 2016, pp. 73-86.

[12] S. Mondal, S.P. Goqo, P. Sibanda, S.S. Motsa, Efficient multi-domain bivariate spectral collocation solution for MHD laminar natural convection flow from a vertical permeable flat plate with uniform surface temperature and thermal radiation, *The 7th International Conference on Computational Methods (ICCM2016)*, University of California at Berkeley, Sutardja Dai Hall, California, U.S.A, 1-4 August, 2016, pp. 850-866.

[13] S. U. S. Choi, Enhancing Thermal Conductivity of Fluids with Nanoparticle, In: D. A. Siginer, H. P. Wang *Eds. Developments and Applications of Non-Newtonian Flows*, 231(1995), pp. 99 - 105.

[14] W. A. Khan and I. Pop, Boundary layer flow of a nanofluid past a stretching sheet, *Int. J. Heat Mass Transf.*, 53(2010), 2477 - 2483.

[15] O. D. Makinde and A. Aziz, Boundary layer flow of a nanofluid past a stretching sheet with a convective boundary condition, *Int. J. Therm. Sci*, 50(2011), 1326 - 1332.

[16] N. Bachok , A. Ishak and I. Pop, Unsteady boundary-layer flow and heat transfer of a nanofluid over a permeable stretching/shrinking sheet, *International Journal of Heat and Mass Transfer*, 55 (2012) 2102 - 2109.

[17] A. M. Rohni, S. Ahmad, A. I. Md. Ismail and I. Pop, Flow and heat transfer over an unsteady shrinking sheet with suction in a nanofluid using Buongiorno's model, *International Communications in Heat and Mass Transfer*, 43 (2013), 75 - 80.

[18] J. Buongiorno, Convective transport in nanofluids, *ASME Journal of Heat Transfer*, 128(2006) 240 - 250.

[19] S. S. Motsa, P. G. Dlamini and M. Khumalo, Spectral Relaxation Method and Spectral Quasilinearization Method for Solving Unsteady Boundary Layer Flow Problems, *Advances in Mathematical Physics*, Volume 2014, Article ID 341964, 12 pages.

[20] A. V. Kuznetsov, D. A. Nield, Double-diffusive natural convective boundary-layer flow of a nanofluid past a vertical plate, *International Journal of Thermal Sciences*, 50 (2011) 712 - 717.

[21] K. A. Yih, The effect of uniform suction/blowing on heat transfer of magnetohydrodynamic Hiemenz flow through porous media, *Acta Mechanica*, 130 (1998) 147 - 158.

[22] A. Raptis, C. Perdikis, H. S. Takhar, Effect of thermal radiation on MHD flow, *Appl. Math. Comput.*, 153(2004) 645 - 9.

[23] S. Ahmad, A. M. Rohni, I. Pop, Blasius and Sakiadis problems in nanofluids, *Acta Mech.*, 218(2011) 195 - 204.

[24] T. G. Motsumi, O. D. Makinde, Effects of thermal radiation and viscous dissipation on boundary layer flow of nanofluids over a permeable moving flat plate, *Phys. Scr.*, 86(2012) 045003 (8pp).

[25] R. Cortell, Flow and heat transfer in a moving fluid over a moving flat surface, *Theor. Comput. Fluid Dyn.*, 21(2007) 435 - 446.

[26] P. D. Ariel, Hiemenz flow in hydromagnetics, Acta Mechanica 103(1994) 31 - 43.

[27] E. M. Sparrow, E. R. G. Eckert and W. J. Minkowycz, Transpiration cooling in a magnetohydrodynamic stagnation-point flow, *Appl. sci. Res.*, Vol. 11 (1963).

Table 1: Comparison of $f''(1,0)$ for various values of M when $Pr = 1.0$, $\Lambda = \Omega = 0$ and $\lambda = 1.0$.

M	Sparrow et al. [27]	Ariel [26]	Yih [21]	Present Results
0.0	1.231	1.232588	1.232588	1.232530
0.5	1.418	-	-	1.329396
0.6	-	1.369884	-	1.369879
1.0	1.584	1.585331	1.585331	1.585331
1.4	-	1.862848	-	1.862848
2.0	1.871	2.346663	2.346663	2.346663
4.0	2.345	-	-	4.183576
5.0	-	5.147965	5.147964	5.147965
10.0	-	10.074741	10.074741	10.074742

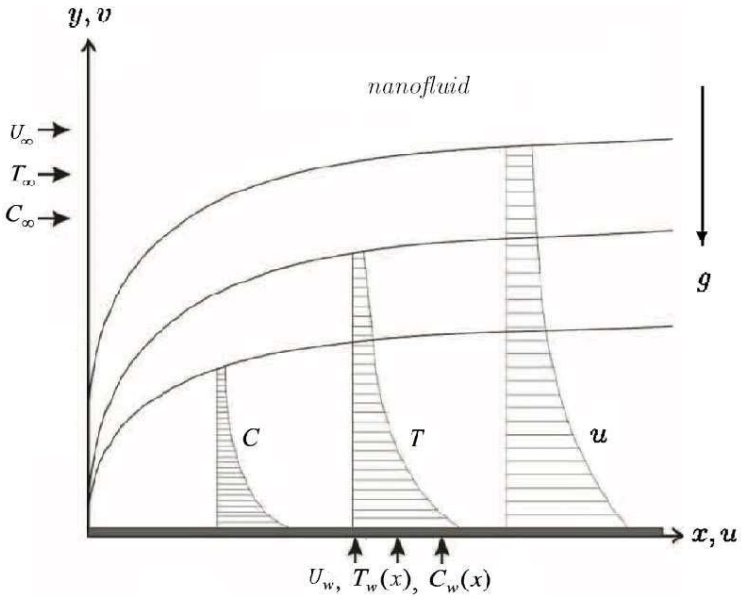

Figure 1: Geometry and the coordinate system.

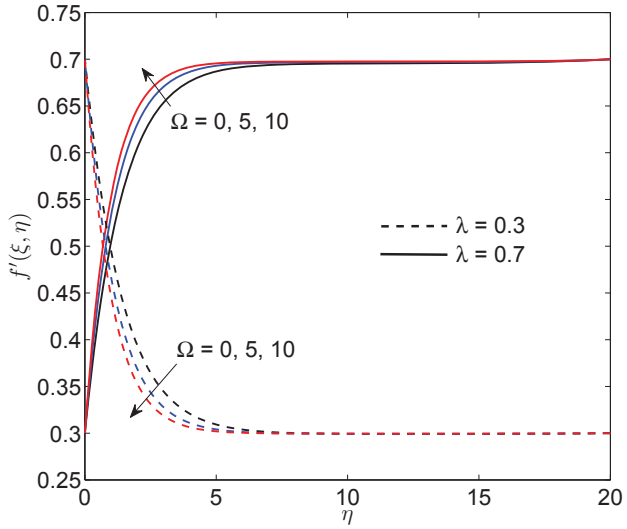

(a)

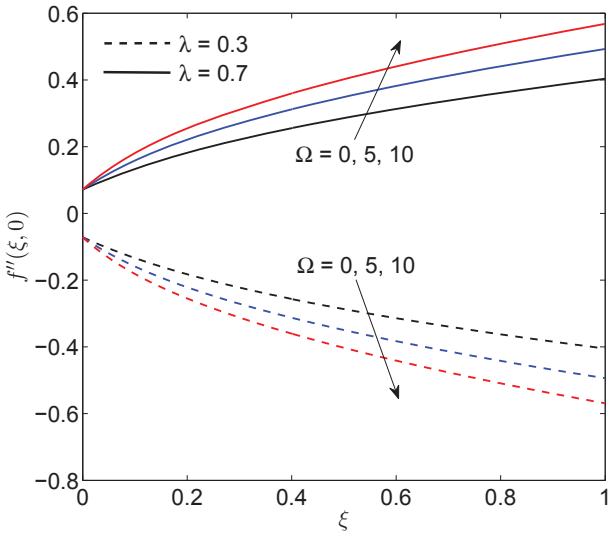

(b)

Figure 2: Influence of permeability parameter Ω on (a) tangential velocity profiles and (b) skin friction coefficient.

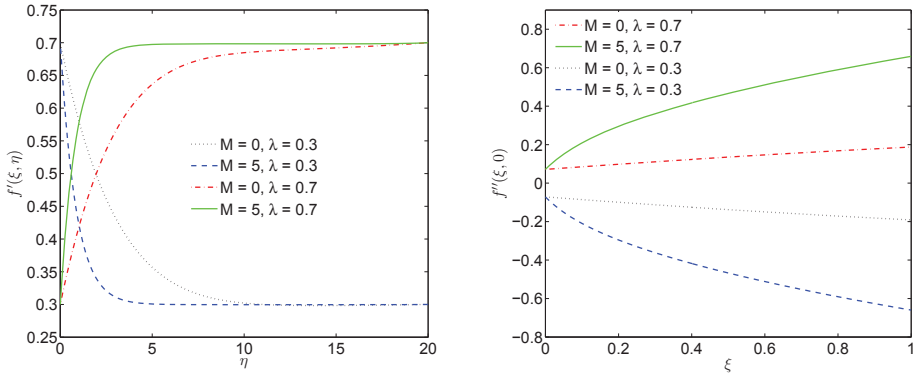

(a)

(b)

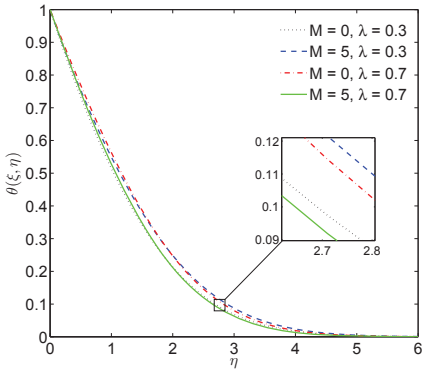

(c)

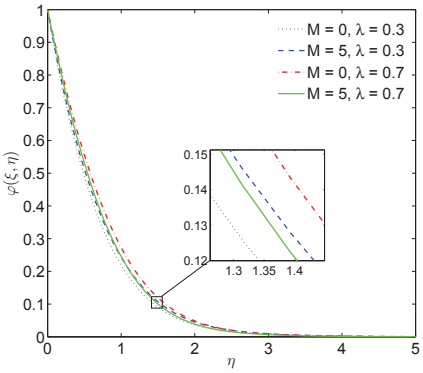

(d)

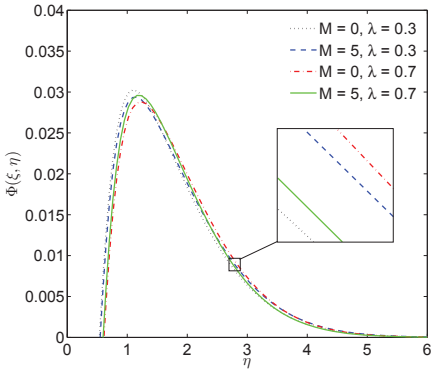

(e)

Figure 3: Influence of Hartmann number M on (a) tangential velocity profiles, (b) skin friction coefficient, (c) temperature profiles, (d) solutal concentration profiles, and (e) nanoparticle volume fraction profiles.

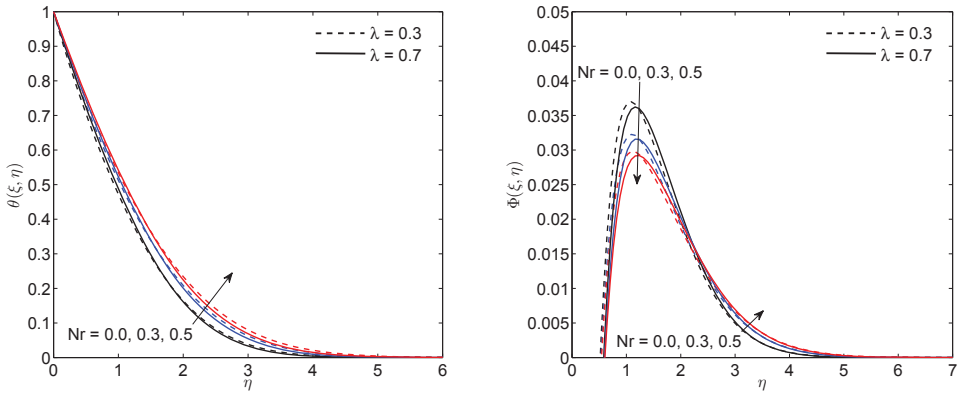

Figure 4: Influence of thermal radiation parameter Nr on (a) temperature and (b) nanoparticle volume fraction profiles.

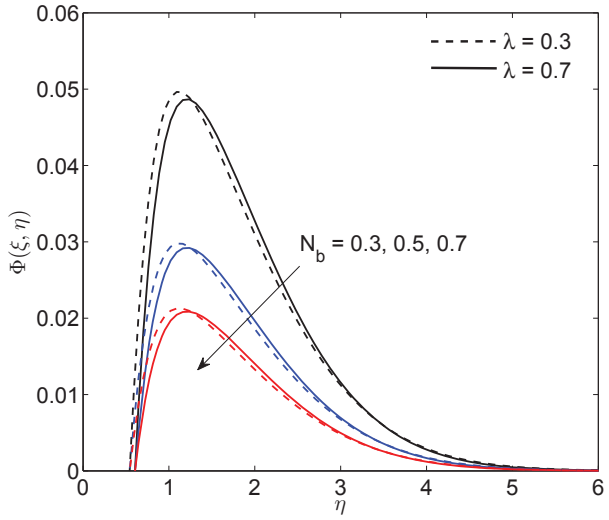

Figure 5: Influence of Brownian motion parameter N_b on the nanoparticle volume fraction profiles.

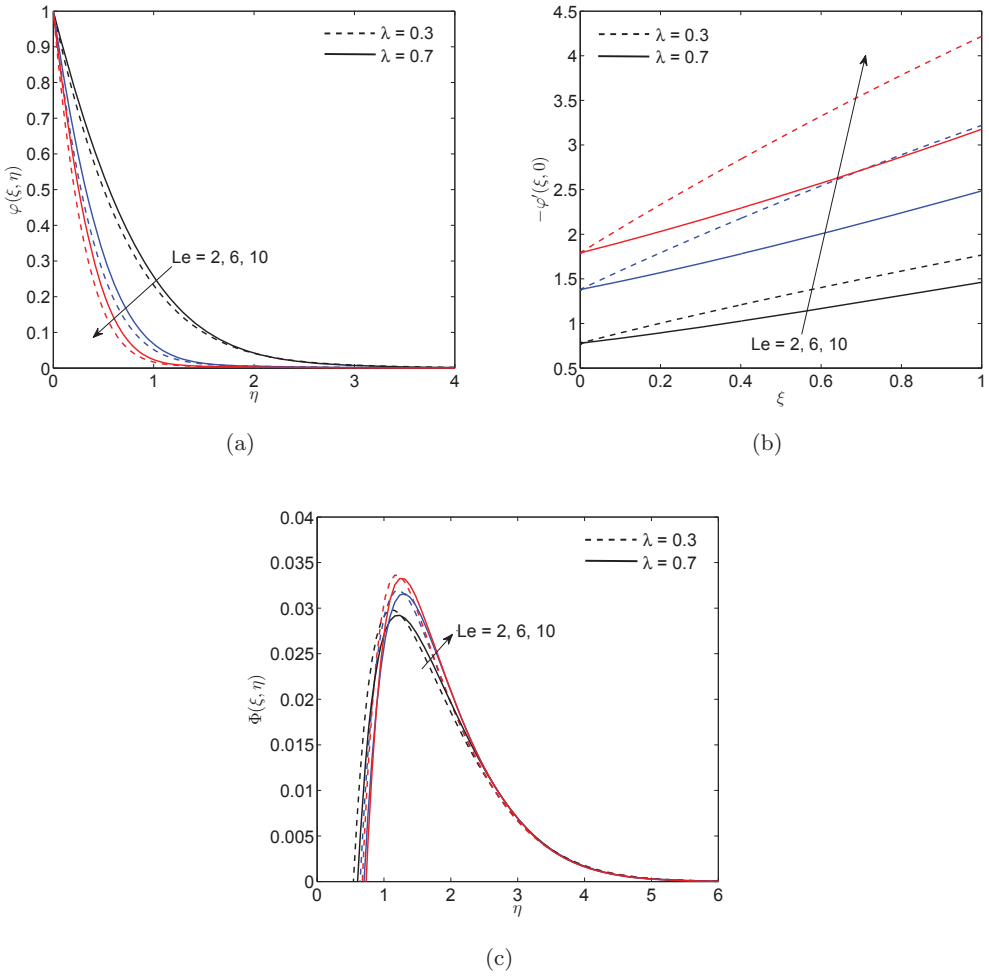

Figure 6: Influence of regular Lewis number Le on (a) solutal concentration profiles, (b) Sherwood number and (c) nanoparticle volume fraction profiles.

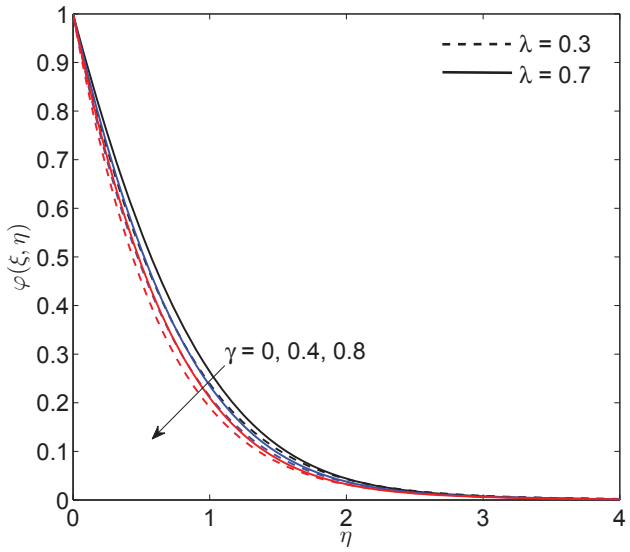

Figure 7: Influence of chemical reaction parameter γ on the solutal concentration profiles.

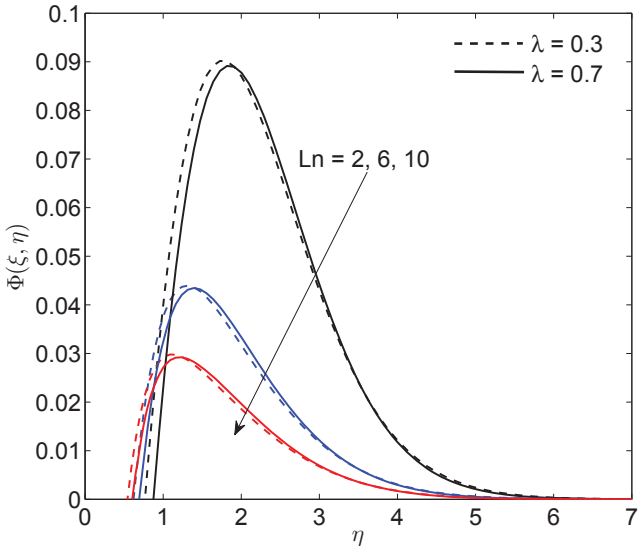

Figure 8: Influence of nanofluid Lewis number Ln on the nanoparticle volume fraction profiles.

Chapter 7

Conclusions

In this study, we have investigated mathematical models of unsteady nanofluid flow including heat and mass transfer in porous media and for different flow geometries. The study concerns the numerical solution of unsteady nanofluid flow models for different types of nanoparticles; namely, copper, silver and titanium oxide with water as the base fluid. We have studied the magneto-nanofluid flow due to a moving surface, the convective heat transport in polymer nanocomposites such as an Oldroyd-B nanofluid flow and nanofluid flow along a stretching cone subject to impulsive motion. The study sort, *inter alia*, to determine both qualitatively and quantitative how certain fluid and physical parameters impact the flow structure, the fluid properties as well as the heat and mass transfer from or to the fluid. The comparison between the copper-water, silver-water and titania-water nanofluids; and pure water in terms of heat and mass transfer coefficients is given. The results show that physical parameters such as the magnetic field, viscous dissipation, thermal radiation, Brownian motion and thermophoresis parameters have a significant influence on the fluid flow, and heat and mass coefficients.

Through these types of mathematical models that described the nanofluid flow, as the part of the main results, it was found that the nanofluid flows gave higher thermal conductivity than base fluid water. That is because the particle material is an important parameter that affects the thermal conductivity and concentration distribution of nanofluids. In this study, some of the nanoparticles such as copper, silver, and titanium oxide have been used to

prepare the nanofluids. The comparison showed that the copper-water nanofluid is better for heat transfer characteristics. The study showed that the thermal conductivity enhanced by the Brownian diffusion and movement of nanoparticle suspended in water base fluid. The magnetic field acts as the Lorentz force which it has the tendency to slow down the flows and nanoparticles movement. It clearly that the magnetic field opposes the transport of the nanofluid flows. So, the large resistances on the nanofluid particles lead to raising the nanoparticles concentration, which causes the heat to be generated in the nanofluid flows. It observed that the shear stress rose due to the irreversible processes such as viscous and electrical resistance. As result, a significant generation of heat inflows cannot be neglected. Also, The highest surface shear stress occurs with the no-slip velocity condition.

The mathematical models have been constructed in terms of systems of partial differential equations that describe transport processes in different flow geometries. The nonlinear conservation equations were transformed by introducing suitable dimensionless variables; and then solved using recent linearization and spectral techniques. In order to assess the accuracy, reliability and convergence of the methods, the results for the flow, heat and mass transfer coefficients have been compared with related work in the literature for certain limiting cases. The results obtained using the spectral local linearization method, the spectral relaxation method, and the spectral quasilinearization method showed that these methods used less number of iterations to get the convergence rate. In this study, the computations were done with 10^{-6} as the tolerance level. It was noted that increasing the number of iterations led to improved accuracy. The methods gave good accuracy with acceptable rates of convergence. We conclude that those methods are suitable for solving complex systems of differential equations and may be used in place of finite difference, finite elements and finite volume based approaches.

In Chapter 2, we investigated the flow of an unsteady magneto-nanofluid flow along an inclined cylinder with a chemical reaction, viscous and Ohmic dissipations. Some notable findings are that the buoyancy force, viscous and Ohmic dissipation all enhanced

the nanofluid temperature within the boundary layer. The nanofluid concentration reduced while the wall mass gradient increased with increases in the chemical reaction parameter, buoyancy force, viscous and Ohmic dissipations. Increasing the thermo-diffusion parameter tended to increase the nanofluid concentration. The buoyancy force and the Ohmic dissipation enhance the fluid velocity within the boundary layer region. The fluid velocity is reduced by an increase in the electromagnetic field leading to an increase in the temperature and concentration levels. An important observation is that copper nanoparticles give better performance than silver nanoparticles in terms of heat and mass transfer.

In Chapter 3, we investigated an unsteady nanofluid flow along a vertical stretching cone due to impulsive motion. The impact of viscous dissipation, internal heat generation and chemical reaction are taken into account. The study considered two different types of nanoparticles, namely, copper and titanium dioxide. The results showed that the viscous dissipation increases the nanofluid temperature, while the heat transfer rate decreases with viscous dissipation. The internal heat generation increases the nanofluid temperature, while reducing the heat transfer rate at the cone surface.

In Chapter 4, we studied the flow of an unsteady Oldroyd-B nanofluid over a stretching surface. The commonly used boundary conditions were substituted by the more realistic condition where the nanoparticle volume fraction is not controlled at the boundary. It was found that increasing the unsteadiness parameter tended to reduce the fluid motion, temperature and concentration levels within the boundary layer. The Deborah number is a measure of the viscoelastic properties of the nanofluid. Increasing the Deborah number leads to a reduction in the fluid motion. The nanofluid temperature and concentration increase with the relaxation time which is in terms of the Deborah number β_1, while the reverse is valid for the retardation time in terms of the Deborah number β_2. Increasing the thermophoresis parameter increases both the nanofluid temperature and the nanoparticle concentration.

In Chapter 5, the influence of an interior heat source or sink on the stagnation boundary layer flow of a magneto-hydrodynamic nanofluid over a stretching flat plate with an unsteady free stream and velocity slip condition was investigated. It was found that the internal heat source or sink enhances the nanofluid motion and the temperature while reducing the skin friction coefficient and rate of heat transfer at the surface of the stretching plate. The skin friction coefficient decreases, while the heat and mass transfer rates increase with increasing fluid buoyancy. Increasing the Brownian motion parameter and the Lewis number leads to a reduction in the nanoparticle volume fraction concentration. As a result, the mass transfer rate increases, but the reverse is true for the nanofluid velocity and the temperature. Increasing the thermophoresis increases the nanofluid velocity, temperature and nanoparticle volume fraction concentration. The skin friction coefficient was reduced by increasing the stretching parameter, while the heat and mass transfer rates increase. The nanofluid flow velocity, temperature, concentration, surface shear stress, heat and mass transfer rate on the stretching plate are strongly influenced by the slip parameter. Surface shear stress and heat transfer rates decrease with an increase in the velocity slip parameter while the mass transfer rate increases.

In Chapter 6, we investigated the flow of a magneto-nanofluid over a permeable moving surface, with thermal radiation and a chemical reaction. In general, the nanofluid velocity increases as the velocity ratio increases. Furthermore, the nanofluid velocity increases with an increase in the Prandtl number when the plate motion is faster compared to the velocity of the nanofluid. The velocity however decreased with the porous media inertia, permeability and the Hartmann number. When the nanofluid movement is more rapid than the surface, an increase in the Prandtl number and the porous media inertia increases the nanofluid temperature.

In summary, in this study we applied recent linearization and spectral methods to solve highly nonlinear coupled equations that describe the flow, heat and mass transfer in certain nanofluids. The findings in this study have not been tested experimentally and in future,

it would be useful to work towards an experimental validation of these results. There is a need for more research on unsteady flow of non-Newtonian fluids including triple-diffusion problems which have wide usage in industry. The solution of the highly couple nonlinear flow equations still presents challenges and there is a need to continuously improve the range of computational techniques for accurate solutions.

References

[1] H. Rouse and S. Ince. *History of hydraulics*. Dover Publications, New York, 1963.

[2] H. Rouse. *Hydraulics in the United States 1776 - 1976*. Institute of Hydraulic Research, University of Iowa, 1976.

[3] T. Cebeci and J. Cousteix. *Modeling and computation of boundary-layer flows: laminar, turbulent and transitional boundary layers in incompressible and compressible flows*. Springer, 2005.

[4] L. Prandtl. Über flüssigkeitsbewegungen bei sehr kleiner reibung. *Internationalen Mathematiker-Kongresses Heidelberg*, 2:484–491, 1904.

[5] H. Schlichting. *Boundary-Layer Theory*. McGraw-Hill Company, New York, 1960.

[6] K. Gersten, E. Krause, H. Oertel, and H. Schlichting. *Boundary-Layer Theory*. Springer, 2017.

[7] A. Kluwick. *Recent Advances in Boundary Layer Theory*. Springer-Verlag Wien, 1998.

[8] F. M. White. *Fluid Mechanics*. McGraw-Hill College, 1998.

[9] H. Schlichting. *Boundary-layer theory*. McGraw-Hill, New York, 1979.

[10] B. R. Munson, D. F. Young, T. H. Okiishi, and W. W. Huebsch. *Fundamentals of Fluid Mechanics*. John Wiley and Sons, Inc., 2009.

[11] J. Ran, R. Wang, L. Zhang, W. Li, and D. Yang. Influencing factors of methane/moist-air laminar boundary layer in micro-channel. *Procedia Computer Science*, 19:786–793, 2013.

[12] K. Suzuki, I. Okada, and M. Yoshino. Accuracy of the laminar boundary layer on a flat plate in an immersed boundary-lattice Boltzmann simulation. *Journal of Fluid Science and Technology*, 11(3):JFST0017, 2016.

[13] A. Mager. Three-dimensional laminar boundary layer with small cross-flow. *Journal of the Aeronautical Sciences*, 21(12):835–845, 1954.

[14] S. Shateyi and G. T. Marewo. A new numerical approach for the laminar boundary layer flow and heat transfer along a stretching cylinder embedded in a porous medium with variable thermal conductivity. *Journal of Applied Mathematics*, 2013: Article ID 576453:7, 2013.

[15] M. K. A. Mohamed, M. Z. Salleh, N. A. Z. M. Noar, and A. Ishak. Effect of thermal radiation on laminar boundary layer flow over a permeable flat plate with Newtonian heating. *Journal of Physics: Conference Series*, 890(1):012007, 2017.

[16] N. Beratlis, E. Balaras, and K. Squires. Effects of dimples on laminar boundary layers. *Journal of Physics: Conference Series*, 15(9):611–627, 2014.

[17] M.J. Uddin, W. A. Khan, and A. I. M. Ismail. MHD forced convective laminar boundary layer flow from a convectively heated moving vertical plate with radiation and transpiration effect. *PLoS ONE*, 8(5):e62664, 2013.

[18] A. A. Avramenko, D. G. Blinov, I. V. Shevchuk, and A. V. Kuznetsov. Symmetry analysis and self-similar forms of fluid flow and heat-mass transfer in turbulent boundary layer flow of a nanofluid. *Physics of Fluids*, 24(9):092003, 2012.

[19] A. Elsayed, R. K. Al-dadah, S. Mahmoud, and A. Rezk. Numerical investigation of turbulent flow heat transfer and pressure drop of AL_2O_3/water nanofluid in helically coiled tubes. *International Journal of Low-Carbon Technologies*, 10:275–282, 2015.

[20] X. Wang and N. Zhang. Numerical analysis of heat transfer in pulsating turbulent

flow in a pipe. *International Journal of Heat and Mass Transfer*, 48:3957–3970, 2005.

[21] R. B. Stull. *An Introduction to Boundary Layer Meteorology*. Springer Netherlands, 1988.

[22] J. C. Kaimal and J. J. Finnigan. *Atmospheric Boundary Layer Flows: Their Structure and Measurement*. Oxford University Press, 1994.

[23] T. R. Oke. *Boundary Layer Climates*. Routledge, 1988.

[24] M. Dörenkämper, B. Witha, G. Steinfeld, D. Heinemann, and M. Kühn. The impact of stable atmospheric boundary layers on wind-turbine wakes within offshore wind farms. *Journal of Wind Engineering and Industrial Aerodynamics*, 144:146–153, 2015.

[25] L. B. M. Pires, I. B. de Paula, G. Fisch, R. Gielow, and R. da M. Girardi. Simulations of the atmospheric boundary layer in a wind tunnel with short test section. *Journal of Aerospace Technology and Management*, 5(3):305–314, 2013.

[26] M. Wächter, H. Heißelmann, M. Hölling, A. Morales, P. Milan, T. Mücke, J. Peinke, N. Reinke, and P. Rinn. The turbulent nature of the atmospheric boundary layer and its impact on the wind energy conversion process. *Journal of Turbulence*, 13(26): 1–21, 2012.

[27] J. Bear and Y. Bachmat. *Introduction to modeling of transport phenomena in porous media*. Kluwer Academic Publisher, Netherlands, 1991.

[28] J. Bear and M. Y. Corapcioglu. *Fundamentals of transport phenomena in porous media*. Martinus Nijhoff Publishers, Dordrecht, 1984.

[29] F. A. L. Dullien. *Porous Media Fluid Transport and Pore Structure*. Academic Press, 1991.

[30] D. A. Nield and A. Bejan. *Convection in porous media*. Springer, New York, 2013.

[31] A. Mitzithras, F. M. Coveney, and J. H. Strange. Nuclear magnetic resonance studies (NMR-studies) of the diffusion of cyclohexane in porous silica. *Journal of Molecular Liquids*, 54(4):273–281, 1992.

[32] R. R. Valiullin, V. D. Skirda, S. Stapf, and R. Kimmich. Molecular exchange processes in partially filled porous glass as seen with nuclear magnetic resonance (NMR) diffusometry. *Physical Review E*, 55(3):2664–2671, 1997.

[33] A. E. Scheidegger. Statistical hydrodynamics in porous media. *Journal of Applied Physics*, 25(8):994–1001, 1954.

[34] H. Darcy. *Les Fontaines publiques de la ville de Dijon: exposition et application*. Victor Dalmont, 1856.

[35] P. Forchheimer. Wasserbewegung durch boden. *Zeitschrift des Vereines Deutscher Ingenieure*, 45:1736–1741 and 1781–1788, 1901.

[36] H. C. Brinkman. A calculation of the viscous force exerted by a flowing fluid on a dense swarm of particles. *Journal of Applied Sciences Research*, Al:27–34, 1947.

[37] G. Lauriat and V. Prasad. Non-Darcian effects on natural convection in a vertical porous enclosure. *International Journal of Heat and Mass Transfer*, 32(11):2135–2148, 1989.

[38] P. H. Holst and K. Aziz. Transient three-dimensional natural convection in confined porous media. *International Journal of Heat and Mass Transfer*, 15(1):73–90, 1972.

[39] J. Bear. *Dynamics of Fluids in Porous Media*. Dover Publications, New York, 1972.

[40] D. A. Nield and A. Bejan. *Convection in porous media*. Springer-Verlag, New York, 1999.

[41] D. K. Todd and L. W. Mays. *Groundwater Hydrology*. John Wiley and Sons, Hoboken, 2005.

[42] C. T. Hsu and P. Cheng. Thermal dispersion in porous medium. *International Journal of Heat and Mass Transfer*, 33(8):1587–1597, 1990.

[43] S. P. Neuman. Theoretical derivation of Darcy's law. *Acta Mechanica*, 25:153–170, 1977.

[44] P. W. Bridgman. *The Physics of High Pressure*. Dover Publications, University of California, 1931.

[45] K. B. Nakshatrala and K. R. Rajagopal. A numerical study of fluids with pressure dependent viscosity owing through a rigid porous medium. *International Journal for Numerical Methods in Fluids*, 67:342–368, 2011.

[46] X. Wang, F. Thauvin, and K. K. Mohanty. Non-Darcy flow through anisotropic porous media. *Chemical Engineering Science*, 54:1859–1869, 1999.

[47] F. Thauvin and K. K. Mohanty. Network modeling of non-Darcy flow through porous media. *Transport in Porous Media*, 19:19–37, 1998.

[48] H. A. Belhaj, K. R. Agha, A. M. Nouri, S. D. Butt, and M. R. Islam. Numerical and experimental modeling of non-Darcy flow in porous media. *Society of Petroleum Engineers*, (SPE-81037-MS):9, 2003.

[49] E. R. Sullivan. *Heat and moisture transport in unsaturated porous media: a couple model in terms of chemical potential*. PhD thesis, University of Colorado, 2013.

[50] H. Beji and D. Gobin. Influence of thermal dispersion on natural convection heat transfer in porous media. *Numerical Heat Transfer, Part A*, 22:487–500, 1992.

[51] Y. Wu, B. Lai, J. L. Miskimins, P. Fakcharoenphol, and Y. Di. Analysis of multiphase non-Darcy flow in porous media. *Transport in Porous Media*, 88:205–223, 2011.

[52] E. Aulisa, L. Bloshanskaya, L. Hoang, and A. Ibragimov. Analysis of generalized Forchheimer flows of compressible fluids in porous media. *Journal of Mathematical Physics*, 50(10):103102, 2009.

[53] M. I. Khan, T. Hayat, and A. Alsaedi. Numerical analysis for Darcy-Forchheimer flow in presence of homogeneous-heterogeneous reactions. *Results in Physics*, 7: 2644–2650, 2017.

[54] T. Muhammad, A. Alsaedi, T. Hayat, and S. A. Shehzad. A revised model for Darcy-Forchheimer three-dimensional flow of nanofluid subject to convective boundary condition. *Results in Physics*, 7:2791–2797, 2017.

[55] T. Hayat, F. Haider, T. Muhammad, and A. Alsaedi. Darcy-Forchheimer flow with Cattaneo-Christov heat flux and homogeneous-heterogeneous reactions. *PLoS ONE*, 12(4):e0174938, 2017.

[56] N. Kishan and S. Maripala. Thermophoresis and viscous dissipation effects on Darcy-Forchheimer MHD mixed convection in a fluid saturated porous media. *Advances in Applied Science Research*, 3(1):60–74, 2012.

[57] H. C. Brinkman. On the permeability of media consisting of closely packed porous particles. *Applied Scientific Research*, A1:81–86, 1947.

[58] K. Vafai. *Handbook of porous media*. Taylor and Francis Group, New York, 2005.

[59] B. K. Jha and M. L. Kaurangini. Approximate analytical solutions for the nonlinear Brinkman-Forchheimer-Extended Darcy flow model. *Applied Mathematics*, 2:1432–1436, 2011.

[60] D. R. Marpu. Forchheimer and Brinkman extended Darcy flow model on natural convection in a vertical cylindrical porous annulus. *Acta Mechanica*, 109:41–48, 1995.

[61] D. S. Kumar, A. K. Dass, and A. Dewan. Analysis of non-Darcy models for mixed convection in a porous cavity using a multigrid approach. *Numerical Heat Transfer, Part A*, 56:685–708, 2009.

[62] X. B. Chen, P. Yu, H. T. Low, and S. H. Winoto. Free convection in a porous wavy cavity based on the Darcy-Brinkman-Forchheimer extended model. *Numerical Heat Transfer, Part A*, 52:377–397, 2007.

[63] G. Juncu. Brinkman-Forchheimer-Darcy flow past an impermeable sphere embedded in a porous medium. 23(3):97–112, 2015.

[64] Y. Cengel and A. Ghajar. *Heat and Mass Transfer: Fundamentals and Applications*. McGraw-Hill, 2014.

[65] M. Mahmood. *Heat and mass transfer analysis of unsteady flow over a horizontal surface inside a squeezing channel*. PhD thesis, COMSATS Institute of Information Technology, Islamabad, 2009.

[66] A. L. Hines and R. N. Maddox. *Mass Transfer-Fundamentals and Applications*. Prentice Hall, 1984.

[67] V. S. Arpaci. *Conduction Heat Transfer*. Addison-wesley Company, 1966.

[68] A. Ahsan. *Convection and conduction heat transfer*. Intech, 2011.

[69] Y. A. Cengel. *Heat and mass transfer: A practical approach*. McGraw-Hill, New York, 2006.

[70] Y. Cengel and A. Ghajar. *Heat and Mass Transfer: Fundamentals and Applications*. McGraw-Hill Education, 2015.

[71] J. R. Welty, C. E. Wicks, R. E. Wilson, and G. L. Rorrer. *Fundamentals of Momentum, Heat, and Mass Transfer*. John Wiley and Sons Corporation, 2008.

[72] M. Modest. *Radiative Heat Transfer*. Academic Press, 2003.

[73] J. Bear and Y. Bachmat. *Introduction to Modeling of Transport Phenomena in Porous Media*. Kluwer Academic Publisher, Dordrecht, 1990.

[74] B. N. Hewakandamby. *A first course in fluid mechanics for engineers*. Ventus, 2012.

[75] P. C. Huang and K. Vafait. Analysis of forced convection enhancement in a channel using porous blocks. *Journal of Thermophysics and Heat Transfer*, 8(3):563–573, 1994.

[76] Y. Su and J. H. Davidson. *Modeling Approaches to Natural Convection in Porous Media*. Springer Briefs in Applied Sciences and Technology. Springer, 2015.

[77] K. Vafai. *Handbook of porous media*. Taylor and Francis Group, New York, 2015.

[78] P. Vadasz. *Emerging Topics in Heat and Mass Transfer in Porous Media*. Springer, 2008.

[79] R. Bennacer, A. A. Mohamad, and M. El Ganaoui. Thermodiffusion in porous media: Multi-domain constitutant separation. *International Journal of Heat and Mass Transfer*, 52(7–8):1725–1733, 2009.

[80] H. Davarzani, M. Marcoux, and M. Quintard. Theoretical predictions of the effective thermodiffusion coefficients in porous media. *International Journal of Heat and Mass Transfer*, 53(7–8):1514–1528, 2010.

[81] G. Makanda, O. D. Makinde, and P. Sibanda. Natural convection of viscoelastic fluid from a cone embedded in a porous medium with viscous dissipation. *Mathematical Problems in Engineering*, 2013: Article ID 934712:11, 2013.

[82] T. Hayat, S. A. Shehzad, M. Qasim, and S. Obaidat. Radiative flow of Jeffery fluid in a porous medium with power law heat flux and heat source. *Nuclear Engineering and Design*, 243:15–19, 2012.

[83] P. S. Gupta and A. S. Gupta. Heat and mass transfer on a stretching sheet with suction or blowing. *The Canadian Journal of Chemical Engineering*, 55(6):744–746, 1977.

[84] D. Pal and S. Chatterjee. Soret and Dufour effects on MHD convective heat and mass transfer of a power-law fluid over an inclined plate with variable thermal conductivity in a porous medium. *Applied Mathematics and Computation*, 219(14): 7556–7574, 2013.

[85] T. Hayat and M. Qasim. Influence of thermal radiation and Joule heating on MHD flow of a Maxwell fluid in the presence of thermophoresis. *International Journal of Heat and Mass Transfer*, 53(21–22):4780–4788, 2010.

[86] O. A. Bég, V. R. Prasad, B. Vasu, N. B. Reddy, Q. Li, and R. Bhargava. Free convection heat and mass transfer from an isothermal sphere to a micropolar regime with Soret/Dufour effects. *International Journal of Heat and Mass Transfer*, 54 (1–3):9–18, 2011.

[87] S. Hina, T. Hayat, S. Asghar, and A. A. Hendi. Influence of compliant walls on peristaltic motion with heat/mass transfer and chemical reaction. *International Journal of Heat and Mass Transfer*, 55(13–14):3386–3394, 2012.

[88] S. Hina, T. Hayat, and A. Alsaedi. Heat and mass transfer effects on the peristaltic flow of Johnson-Segalman fluid in a curved channel with compliant walls. *International Journal of Heat and Mass Transfer*, 55(13–14):3511–3521, 2012.

[89] M. M. Rahman, H. F. Oztop, A. Ahsan, and J. Orfi. Natural convection effects on heat and mass transfer in a curvilinear triangular cavity. *International Journal of Heat and Mass Transfer*, 55(21–22):6250–6259, 2012.

[90] F. Mabood, W. A. Khan, and A. I. M. Ismail. Approximate analytical modeling of heat and mass transfer in hydromagnetic flow over a non-isothermal stretched surface with heat generation/absorption and transpiration. *Journal of the Taiwan Institute of Chemical Engineers*, 54:11–19, 2015.

[91] P. M. Patil and A. J. Chamkha. Heat and mass transfer from mixed convection flow

of polar fluid along a plate in porous media with chemical reaction. *International Journal of Numerical Methods for Heat and Fluid Flow*, 23(5):899–926, 2013.

[92] P. V. S. Narayana and D. H. Babu. Numerical study of MHD heat and mass transfer of a Jeffrey fluid over a stretching sheet with chemical reaction and thermal radiation. *Journal of the Taiwan Institute of Chemical Engineers*, 59:18–25, 2016.

[93] K. S. Mekheimer, N. Saleem, T. Hayat, and A. A. Hendi. Simultaneous effects of induced magnetic field and heat and mass transfer on the peristaltic motion of second-order fluid in a channel. *International Journal for Numerical Methods in Fluids*, 70:342–358, 2012.

[94] H. Yasmin, T. Hayat, N. Alotaibi, and H. Gao. Convective heat and mass transfer analysis on peristaltic flow of Williamson fluid with hall effects and Joule heating. *International Journal of Biomathematics*, 7(5):1–27, 2014.

[95] A. Postelnicu. Thermophoresis particle deposition in natural convection over inclined surfaces in porous media. *International Journal of Heat and Mass Transfer*, 55(7–8):2087–2094, 2012.

[96] N. F. M. Noor, S. Abbasbandy, and I. Hashim. Heat and mass transfer of thermophoretic MHD flow over an inclined radiate isothermal permeable surface in the presence of heat source/sink. *International Journal of Heat and Mass Transfer*, 55 (7–8):2122–2128, 2012.

[97] T. Hayat, A. Safdar, M. Awais, and S. Mesloub. Soret and Dufour effects for three-dimensional flow in a viscoelastic fluid over a stretching surface. *International Journal of Heat and Mass Transfer*, 55:2129–2136, 2012.

[98] C. G. Bell, H. M. Byrne, J. P. Whiteley, and S. L. Waters. Heat or mass transfer at low Péclet number for Brinkman and Darcy flow round a sphere. *International Journal of Heat and Mass Transfer*, 68:247–258, 2014.

[99] D. Pala and H. Mondal. Influence of Soret and Dufour on MHD buoyancy-driven heat and mass transfer over a stretching sheet in porous media with temperature-dependent viscosity. *Nuclear Engineering and Design*, 256:350–357, 2013.

[100] K. Ramesh. Influence of heat and mass transfer on peristaltic flow of a couple stress fluid through porous medium in the presence of inclined magnetic field in an inclined asymmetric channel. *Journal of Molecular Liquids*, 219:256–271, 2016.

[101] V. R. Prasad, B. Vasu, O. A. Bég, and R. D. Parshad. Thermal radiation effects on magnetohydrodynamic free convection heat and mass transfer from a sphere in a variable porosity regime. *Communications in Nonlinear Science and Numerical Simulation*, 17(2):654–671, 2012.

[102] V. R. Prasad, B. Vasu, and O. A. Bég. Thermo-diffusion and diffusion-thermo effects on MHD free convection flow past a vertical porous plate embedded in a non-Darcian porous medium. *Chemical Engineering Journal*, 173(2):598–606, 2011.

[103] M. M. Rashidi, B. Rostami, N. Freidoonimehr, and S. Abbasbandy. Free convective heat and mass transfer for MHD fluid flow over a permeable vertical stretching sheet in the presence of the radiation and buoyancy effects. *Ain Shams Engineering Journal*, 5(3):901–912, 2014.

[104] K. Javaherdeh, M. M. Nejad, and M. Moslemi. Natural convection heat and mass transfer in MHD fluid flow past a moving vertical plate with variable surface temperature and concentration in a porous medium. *Engineering Science and Technology, an International Journal*, 18(3):423–431, 2015.

[105] C. S. K. Raju, N. Sandeep, V. Sugunamma, M. J. Babu, and J. V. R. Reddy. Heat and mass transfer in magnetohydrodynamic Casson fluid over an exponentially permeable stretching surface. *Engineering Science and Technology, an International Journal*, 19(1):45–52, 2016.

[106] F. Ibrahim, S. M. Abdel-Gaid, and R. Gorla. Non-Darcy mixed convection flow along a vertical plate embedded in a non-Newtonian fluid saturated porous medium with surface mass transfer. *International Journal of Numerical Methods for Heat and Fluid Flow*, 10:397–408, 2000.

[107] A. Mahdy and A. J. Chamkha. Chemical reaction and viscous dissipation effects on Darcy-Forchheimer mixed convection in a fluid saturated porous media. *International Journal of Numerical Methods for Heat and Fluid Flow*, 20(8):924–940, 2010.

[108] A. M. Rashad, A. J. Chamkha, and S. M. M. El-Kabeir. Effect of chemical reaction on heat and mass transfer by mixed convection flow about a sphere in a saturated porous media. *International Journal of Numerical Methods for Heat and Fluid Flow*, 21(4):418–433, 2011.

[109] A. Rashad and A. Chamkha. Heat and mass transfer by natural convection flow about a truncated cone in porous media with Soret and Dufour effects. *International Journal of Numerical Methods for Heat and Fluid Flow*, 24(3):595–612, 2014.

[110] N. T. M. Eldabe, B. M. Agoor, and H. Alame. Peristaltic motion of non-Newtonian fluid with heat and mass transfer through a porous medium in channel under uniform magnetic field. *Journal of Fluids*, 2014: Article ID 525769:12, 2014.

[111] D. Bhukta, G. C. Dash, and S. R. Mishra. Heat and mass transfer on MHD flow of a viscoelastic fluid through porous media over a shrinking sheet. *International Scholarly Research Notices*, 2014: Article ID 572162:11, 2014.

[112] R. Kandasamy and I. Muhaimin. Scaling transformation for the effect of temperature-dependent fluid viscosity with thermophoresis particle deposition on MHD-free convective heat and mass transfer over a porous stretching surface. *Transport in Porous Media*, 84(2):549–568, 2010.

[113] M. Sheikholeslami, H. R. Ashorynejad, D. D. Ganji, and M. M. Rashidi. Heat and mass transfer of a micropolar fluid in a porous channel. *Communications in Numerical Analysis*, 2014:1–20, 2014.

[114] A. J. Chamkha and J. M. Al-Humoud. Mixed convection heat and mass transfer of non-Newtonian fluids from a permeable surface embedded in a porous medium. *International Journal of Numerical Methods for Heat and Fluid Flow*, 17(2):195–212, 2007.

[115] A. J. Chamkha, S. M. M. EL-Kabeir, and A. M. Rashad. Heat and mass transfer by non-Darcy free convection from a vertical cylinder embedded in porous media with a temperature-dependent viscosity. *International Journal of Numerical Methods for Heat and Fluid Flow*, 21(7):847–863, 2011.

[116] M. M. Rashidi, N. Rahimzadeh, M. Ferdows, M. D. Jashim Uddin, and O. A. Bég. Group theory and differential transform analysis of mixed convective heat and mass transfer from a horizontal surface with chemical reaction effects. *Chemical Engineering Communications*, 199(8):1012–1043, 2012.

[117] T. Hayat, M. S. Anwar, M. Farooq, and A. Alsaedi. MHD stagnation point flow of second grade fluid over a stretching cylinder with heat and mass transfer. *International Journal of Nonlinear Sciences and Numerical Simulation*, 15(6):365–376, 2014.

[118] A. J. Chamkha and A. M. Aly. Heat and mass transfer in stagnation-point flow of a polar fluid towards a stretching surface in porous media in the presence of Soret, Dufour and chemical reaction effects. *Chemical Engineering Communications*, 198 (2):214–234, 2010.

[119] R. Y. Jumah, F. A. Banat, and F. Abu-Al-Rub. Darcy-Forchheimer mixed convection heat and mass transfer in fluid saturated porous media. *International Journal of Numerical Methods for Heat and Fluid Flow*, 11(6):600–618, 2001.

[120] B. Mallikarjuna, A. M. Rashad, A. J. Chamkha, and S. H. Raju. Chemical reaction effects on MHD convective heat and mass transfer flow past a rotating vertical cone embedded in a variable porosity regime. *Afrika Matematika*, 27(3–4):645–665, 2016.

[121] O. D. Makinde and A. Ogulu. The effect of thermal radiation on the heat and mass transfer flow of a variable viscosity fluid past a vertical porous plate permeated by a transverse magnetic field. *Chemical Engineering Communications*, 195(12):1575–1584, 2008.

[122] Md. Jashim Uddin, W. A. Khan, and A. I. Ismail. Lie group analysis and numerical solutions for magnetoconvective slip flow along a moving chemically reacting radiating plate in porous media with variable mass diffusivity. *Heat Transfer-Asian Research*, 45(3):239–263, 2016.

[123] J. C. Williams III and T. B. Rhyne. Boundary layer development on a wedge impulsively set into motion. *SIAM Journal on Applied Mathematics*, 38(2):215–224, 1980.

[124] H. S. Takhar, A. J. Chamkha, and G. Nath. Unsteady three-dimensional MHD-boundary-layer flow due to the impulsive motion of a stretching surface. *Acta Mechanica*, 146(1–2):59–71, 2001.

[125] H. Xu and S. J. Liao. Series solutions of unsteady magnetohydrodynamic flows of non-Newtonian fluids caused by an impulsively stretching plate. *Journal of Non-Newtonian Fluid Mechanics*, 129(1):46–55, 2005.

[126] S. Liao. An analytic solution of unsteady boundary-layer flows caused by an impulsively stretching plate. *Communications in Nonlinear Science and Numerical Simulation*, 11(3):326–339, 2006.

[127] S. A. Kechil and I. Hashim. Series solution for unsteady boundary-layer flows due to impulsively stretching plate. *Chinese Physics Letters*, 24(1):139–142, 2007.

[128] F. Md Ali, R. Nazar, and N. M. Arifin. Numerical solutions of unsteady boundary layer flow due to an impulsively stretching surface. *Journal of Applied Computer Science and Mathematics*, 4(8):25–30, 2010.

[129] Y. Khan, A. Hussain, and N. Faraz. Unsteady linear viscoelastic fluid model over a stretching/shrinking sheet in the region of stagnation point flows. *Scientia Iranica*, 19(6):1541–1549, 2012.

[130] Y. Y. Lok and I. Pop. Stretching or shrinking sheet problem for unsteady separated stagnation-point flow. *Meccanica*, 49(6):1479–1492, 2014.

[131] R. Kumar, I. A. Abbas, and V. Sharma. A numerical study of free convection heat and mass transfer in a Rivlin-Ericksen viscoelastic flow past an impulsively started vertical plate with variable temperature and concentration. *International Journal of Heat and Fluid Flow*, 44:258–264, 2013.

[132] M. Turkyilmazoglu and I. Pop. Soret and heat source effects on the unsteady radiative MHD free convection flow from an impulsively started infinite vertical plate. *International Journal of Heat and Mass Transfer*, 55(25–26):7635–7644, 2012.

[133] M. Das, R. Mahato, and R. Nandkeolyar. Newtonian heating effect on unsteady hydromagnetic Casson fluid flow past a flat plate with heat and mass transfer. *Alexandria Engineering Journal*, 54(4):871–879, 2015.

[134] S. Shateyi and S. S. Motsa. Boundary layer flow and double diffusion over an unsteady stretching surface with hall effect. *Chemical Engineering Communications*, 198(12):1545–1565, 2011.

[135] A. J. Chamkha, S. M. M. EL-Kabeir, and A. M. Rashad. Unsteady coupled heat and mass transfer by mixed convection flow of a micropolar fluid near the stagnation point on a vertical surface in the presence of radiation and chemical reaction. *Progress in Computational Fluid Dynamics*, 15(3):186–196, 2015.

[136] A. J. Chamkha and S. M. M. EL-Kabeir. Unsteady heat and mass transfer by MHD mixed convection flow over an impulsively stretched vertical surface with chemical reaction and Soret and Dufour effects. *Chemical Engineering Communications*, 200 (9):1220–1236, 2013.

[137] B. Mohanty, S. R. Mishra, and H. B. Pattanayak. Numerical investigation on heat and mass transfer effect of micropolar fluid over a stretching sheet through porous media. *Alexandria Engineering Journal*, 54(2):223–232, 2015.

[138] I. L. Animasaun. Double diffusive unsteady convective micropolar flow past a vertical porous plate moving through binary mixture using modified boussinesq approximation. *Ain Shams Engineering Journal*, 7(2):755–765, 2016.

[139] A. J. Chamkha, A. M. Aly, and M. A. Mansour. Similarity solation for unsteady heat and mass transfer from a stretching surface embedded in a porous medium with suction/injection and chemical reaction effects. *Chemical Engineering Communications*, 197(6):846–858, 2010.

[140] M. A. Mansour, M. M. Abd-Elaziz, R. Abdalla, and S. Elsayed. Effect of sinusoidal variations of boundary conditions on unsteady double diffusive convection in a square enclosure filled with a porous medium. *International Journal of Numerical Methods for Heat and Fluid Flow*, 22(1):129–146, 2012.

[141] V. Rajesh and A. J. Chamkha. Unsteady convective flow past an exponentially accelerated infinite vertical porous plate with Newtonian heating and viscous dissipation. *International Journal of Numerical Methods for Heat and Fluid Flow*, 24(5):1109–1123, 2014.

[142] A. J. Benazir, R. Sivaraj, and O. D. Makinde. Unsteady magnetohydrodynamic Casson fluid flow over a vertical cone and flat plate with non-uniform heat source/sink. *International Journal of Engineering Research in Africa*, 21:69–83, 2016.

[143] M. S. Alam and M. M. Rahman. Thermophoretic particle deposition on unsteady hydromagnetic radiative heat and mass transfer flow along an infinite inclined permeable surface with viscous dissipation and Joule heating. *Engineering e-Transaction*, 7(2):116–126, 2012.

[144] G. S. Seth, S. M. Hussain, and S. Sarkar. Effects of hall current and rotation on unsteady MHD natural convection flow with heat and mass transfer past an impulsively moving vertical plate in the presence of radiation and chemical reaction. *Bulgarian Chemical Communications*, 46(4):704–718, 2014.

[145] A. J. Chamkha and A. M. Rashad. Unsteady heat and mass transfer by MHD mixed convection flow from a rotating vertical cone with chemical reaction and Soret and Dufour effects. *The Canadian Journal of Chemical Engineering*, 92(4):758–767, 2014.

[146] P. O. Olanrewaju, O. J. Fenuga, J. A. Gbadeyan, and T. G. Okedayo. Dufour-Soret effects on convection heat and mass transfer in an electrical conducting power law flow over a heated porous plate. *International Journal for Computational Methods in Engineering Science and Mechanics*, 14(1):32–39, 2013.

[147] F. Ali, I. Khan, Samiulhaq, and S. Shafie. Conjugate effects of heat and mass transfer on MHD free convection flow over an inclined plate embedded in a porous medium. *PLoS ONE*, 8(6):e65223, 2013.

[148] B. V. Sagar, M. C. Raju, S. V. K. Varma, and S. Venkataramana. Unsteady MHD convection boundary layer flow of radiation absorbing Kuvshinski fluid through porous medium. *Review of Advances in Physics Theories and Applications*, 1:48–62, 2014.

[149] O. D. Makinde and P. O. Olanrewaju. Unsteady mixed convection with Soret and Dufour effects past a porous plate moving through a binary mixture of chemically reacting fluid. *Chemical Engineering Communications*, 198(7):920–938, 2011.

[150] S. U. S. Choi, Z. G. Zhang, and P. Keblinski. "Nanofluids", in Encyclopedia of Nanoscience and Nanotechnology. *American Scientific Publishers*, 6:757–773, 2004.

[151] S. K. Das. Nanofluids - The cooling medium of the future. *Heat Transfer Engineering*, 27(10):1–2, 2006.

[152] S. K. Das, S. U. S. Choi, and H. E. Patel. Heat transfer in nanofluids - A review. *Heat Transfer Engineering*, 27(10):3–19, 2006.

[153] J. A. Eastman, S. R. Phillpot, S. U. S. Choi, and P. Keblinski. Thermal transport in nanofluids. *Annual Review of Material Research*, 34:219–246, 2004.

[154] P. Keblinski, J. A. Eastman, and D. G. Cahill. Nanofluids for thermal transport. *Materials Today*, 8(6):36–44, 2005.

[155] S. U. S. Choi. "Enhancing thermal conductivity of fluids with nanoparticles," in Developments and applications of non-Newtonian flows. *The American Society of Mechanical Engineers, New York*, 66:99–105, 1995.

[156] L. C. Thomas. *Heat Transfer Professional Version*. Capstone Publishing Corporation, 1999.

[157] S. U. S. Choi. Nanofluids: from vision to reality through research. *Journal of Heat Transfer*, 131(3):1–9, 2009.

[158] T. Tyler, O. Shenderova, G. Cunningham, J. Walsh, J. Drobnik, and G. McGuire. Thermal transport properties of diamond-based nanofluids and nanocomposites. *Diamond and Related Materials*, 15(11–12):2078–2081, 2006.

[159] M. Liu, M. C. Lin, I. Huang, and C. Wang. Enhancement of thermal conductivity with carbon nanotube for nanofluids. *International Communications in Heat and Mass Transfer*, 32(9):1202–1210, 2005.

[160] W. Yu, D. M. France, J. L. Routbort, and S. U. S. Choi. Review and comparison of nanofluid thermal conductivity and heat transfer enhancements. *Heat Transfer Engineering*, 29(5):432–460, 2008.

[161] F. M. Abbasi, S. A. Shehzad, T. Hayat, A. Alsaedi, and M. A. Obid. Influence of heat and mass flux conditions in hydromagnetic flow of Jeffrey nanofluid. *American Institute of Physics Advances*, 5(3):037111–1/12, 2015.

[162] F. G. Awad, P. Sibanda, and A. A. Khidir. Thermodiffusion effects on magneto-nanofluid flow over a stretching sheet. *Boundary Value Problems*, 2013(1):136, 2013.

[163] D. Pal and G. Mandal. Influence of thermal radiation on mixed convection heat and mass transfer stagnation-point flow in nanofluids over stretching/shrinking sheet in a porous medium with chemical reaction. *Nuclear Engineering and Design*, 273: 644–652, 2014.

[164] K. Y. Yohannes and B. Shankar. Heat and mass transfer in MHD flow of nanofluids through a porous media due to a stretching sheet with viscous dissipation and chemical reaction effects. *Caribbean Journal of Science and Technology*, 1:001–017, 2013.

[165] S. A. Moshizi. Forced convection heat and mass transfer of MHD nanofluid flow inside a porous microchannel with chemical reaction on the walls. *Engineering Computations*, 32(8):2419–2442, 2015.

[166] E. Haile and B. Shankar. Heat and mass transfer through a porous media of MHD flow of nanofluids with thermal radiation, viscous dissipation and chemical reaction effects. *American Chemical Science Journal*, 4(6):828–846, 2014.

[167] M. Qasim, I. Khan, and S. Shafie. Heat transfer and mass diffusion in nanofluids over a moving permeable convective surface. *Mathematical Problems in Engineering*, 2013: Article ID 254973:7, 2013.

[168] S. Agarwal and B. S. Bhadauria. Unsteady heat and mass transfer in a rotating nanofluid layer. *Continuum Mechanics and Thermodynamics*, 26(4):437–445, 2014.

[169] J. V. R. Reddy, V. Sugunamma, and N. Sandeep. Thermo diffusion and hall current effects on an unsteady flow of a nanofluid under the influence of inclined magnetic field. *International Journal of Engineering Research in Africa*, 20:61–79, 2016.

[170] M. F. Iqbal, K. Ali, and M. Ashraf. Heat and mass transfer analysis in unsteady titanium dioxide nanofluid between two orthogonally moving porous coaxial disks: a numerical study. *Canadian Journal of Physics*, 93(3):290–299, 2015.

[171] K. Bhattacharyya. Effects of heat source/sink on MHD flow and heat transfer over a shrinking sheet with mass suction. *Chemical Engineering Research Bulletin*, 15(1): 12–17, 2011.

[172] P. M. Patil, S. Roy, and A. J. Chamkha. Double diffusive mixed convection flow over a moving vertical plate in the presence of internal heat generation and a chemical reaction. *Turkish Journal of Engineering and Environmental Sciences*, 33:193–205, 2009.

[173] S. Roy. Non-uniform mass transfer or wall enthalpy into a compressible flow over yawed cylinder. *International Journal of Heat and Mass Transfer*, 44(16):3017–3024, 2001.

[174] P. Saikrishnan and S. Roy. Non-uniform slot injection (suction) into water boundary layers over (i) a cylinder and (ii) a sphere. *International Journal of Engineering Science*, 41(12):1351–1365, 2003.

[175] S. Ponnaiah. Boundary layer flow over a yawed cylinder with variable viscosity role of non-uniform double slot suction (injection). *International Journal of Numerical Methods for Heat and Fluid Flow*, 22(3):342–356, 2012.

[176] J. Strikwerda. *Finite Difference Schemes and Partial Differential Equations*. Society for Industrial and Applied Mathematics, 2004.

[177] C. Johnson. *Numerical Solutions of PDEs by the Finite Element Method*. Cambridge, 1987.

[178] J. H. Argyris. Energy theorems and structural analysis, part I-General theory. *Aircraft Engineering*, 26(10):347–356, 1954.

[179] M. J. Turner, R. W. Clough, H. C. Martin, and L. J. Topp. Stiffness and deflection analysis of complex structures. *Journal of Aeronautical Science*, 23(9):805–824, 1956.

[180] A. Hrennikov. Solution of problems in elasticity by the frame work method. *Journal of Applied Mechanics*, 8:169–175, 1941.

[181] B. S. Jovanovic and E. Süli. *Analysis of finite difference schemes-For linear PDEs with generalized solutions*. Springer Series in Computational Mathematics. Springer, 2014.

[182] A. Quarteroni T. A. Zang C. Canuto, M. Y. Hussaini. *Spectral Methods in Fluid Dynamics*. Springer Science and Business Media, 2012.

[183] B. Fornberg. *A Practical Guide to Pseudo spectral Methods*. Cambridge University Press, New York, 1998.

[184] L. N. Trefethen. *Spectral Methods in MATLAB*. Software, Environments, Tools. Society for Industrial and Applied Mathematics, Philadelphia, 2000.

[185] S. S. Motsa. A new spectral local linearization method for nonlinear boundary layer flow problems. *Journal of Applied Mathematics*, 2013: Article ID 423628:15, 2013.

[186] S. S. Motsa. On the practical use of the spectral homotopy analysis method and local linearisation method for unsteady boundary-layer flows caused by an impulsively stretching plate. *Numerical Algorithms*, 66(4):865–883, 2014.

[187] S. S. Motsa. A new spectral relaxation method for similarity variable nonlinear boundary layer flow systems. *Chemical Engineering Communications*, 201(2):241–256, 2014.

[188] S. S. Motsa, P. G. Dlamini, and M. Khumalo. Spectral relaxation method and spectral quasi-linearization method for solving unsteady boundary layer flow problems. *Advances in Mathematical Physics*, 2014: Article ID 341964:12, 2014.

[189] R. E. Bellman and R. E. Kalaba. *Quasi-linearization and Nonlinear Boundary-Value Problems*. Elsevier, 1965.

[190] S. S. Motsa, Z. G. Makukula, and S. Shateyi. Spectral local linearisation approach for natural convection boundary layer flow. *Mathematical Problems in Engineering*, 2013: Article ID 765013:7, 2013.

[191] H. M. Sithole, S. Mondal, P. Sibanda, and S. S. Motsa. An unsteady MHD Maxwell nanofluid flow with convective boundary conditions using spectral local linearization method. *Open Physics*, 15:637–646, 2017.

[192] S. Shateyi and G. T. Marewo. Numerical analysis of MHD stagnation-point flow of Casson fluid, heat and mass transfer over a stretching sheet. *Advances in Applied and Pure Mathematics*, 127:1018–1025, 2015.

[193] S. Shateyi and G. T. Marewo. Numerical analysis of unsteady MHD flow near a stagnation point of a two-dimensional porous body with heat and mass transfer, thermal radiation, and chemical reaction. *Boundary Value Problems*, 2014(1):218, 2014.

[194] S. S. Motsa and Z. G. Makukula. On spectral relaxation method approach for steady Von kármán flow of a Reiner-Rivlin fluid with Joule heating, viscous dissipation and suction/injection. *Central European Journal of Physics*, 11(3):363–374, 2013.

[195] S. S. Motsa, P. G. Dlamini, and M. Khumalo. Solving hyperchaotic systems using

the spectral relaxation method. *Abstract and Applied Analysis*, 2012: Article ID 203461:18, 2012.

[196] S. S. Motsa, P. Dlamini, and M. Khumalo. A new multistage spectral relaxation method for solving chaotic initial value systems. *Nonlinear Dynamics*, 72(1–2): 265–283, 2013.

[197] I. S. Oyelakin, S. Mondal, and P. Sibanda. Unsteady Casson nanofluid flow over a stretching sheet with thermal radiation, convective and slip boundary conditions. *Alexandria Engineering Journal*, 55:1025–1035, 2016.

[198] P. K. Kameswaran, P. Sibanda, and S. S Motsa. A spectral relaxation method for thermal dispersion and radiation effects in a nanofluid flow. *Boundary Value Problems*, 2013(1):242, 2013.

[199] S. Shateyi, S. S. Motsa, and Z. Makukula. On spectral relaxation method for entropy generation a MHD flow and heat transfer of a Maxwell fluid. *Journal of Applied Fluid Mechanics*, 8(1):21–31, 2015.

[200] S. S. Motsa, P. Sibanda, J. M. Ngnotchouye, and G. T. Marewo. A spectral relaxation approach for unsteady boundary-layer flow and heat transfer of a nanofluid over a permeable stretching/shrinking sheet. *Advances in Mathematical Physics*, 2014: Article ID 564942:10, 2014.

[201] U. Rao and G. K. Rao. Boundary layer flow of MHD tangent hyperbolic fluid past a vertical plate in the presence of thermal dispersion using spectral relaxation method. *International Journal of Computational Engineering Research*, 7(6):2250–3005, 2017.

[202] G. Makanda and P. Sibanda. Numerical analysis of free convection Casson fluid flow from a spinning cone in non-Darcy porous medium with partial slip and viscous dissipation effects. *International Journal of Mathematical and Computational Methods*, 1:221–230, 2016.

[203] U. Rao and G. K. Rao. Spectral relaxation method for laminar flow of electrically conducting non-Newtonian power law fluid in the presence of thermal dispersion. *Global Journal of Pure and Applied Mathematics*, 13(10):7131–7152, 2017.

[204] C. RamReddy. A novel spectral relaxation method for mixed convection in the boundary layers on an exponentially stretching surface with MHD and cross-diffusion effects. *International Journal of Computer Science and Electronics Engineering*, 3(1):2320–4028, 2015.

[205] S. S. Motsa, T. Hayat, and O. M. Aldossary. MHD flow of upper-convected Maxwell fluid over porous stretching sheet using successive Taylor series linearization method. *Applied Mathematics and Mechanics*, 33(8):975–990, 2012.

[206] S. S. Motsa and S. Shateyi. Successive linearization analysis of the effects of partial slip, thermal diffusion, and diffusion thermo on steady MHD convective flow due to a rotating disk. *Mathematical Problems in Engineering*, 2012: Article ID 397637: 15, 2012.

[207] F. G. Awad, P. Sibanda, S. S. Motsa, and O. D. Makinde. Convection from an inverted cone in a porous medium with cross-diffusion effects. *Computers and Mathematics with Applications*, 61(5):1431–1441, 2011.

[208] C. RamReddy and T. Pradeepa. The effect of suction/injection on free convection in a micropolar fluid saturated porous medium under convective boundary condition. *Procedia Engineering*, 127:235–243, 2015.

[209] C. RamReddy and T. Pradeepa. Spectral quasi-linearization method for homogeneous-heterogeneous reactions on nonlinear convection flow of micropolar fluid saturated porous medium with convective boundary condition. *Open Engineering*, 6(1):106–119, 2016.

[210] I.S. Oyelakin, S. Mondal, and P. Sibanda. Unsteady MHD three-dimensional Casson

nanofluid flow over a porous linear stretching sheet with slip condition. *Frontiers in Heat and Mass Transfer*, 8(37), 2017. doi: http://dx.doi.org/10.5098/hmt.8.37.

[211] A. V. Kuznetsov and D. A. Nield. The Cheng-Minkowycz problem for natural convective boundary layer flow in a porous medium saturated by a nanofluid: A revised model. *International Journal of Heat and Mass Transfer*, 65:682–685, 2013.

[212] S. K. Nandy and T. R. Mahapatra. Effects of slip and heat generation/absorption on MHD stagnation flow of nanofluid past a stretching/shrinking surface with convective boundary conditions. *International Journal of Heat and Mass Transfer*, 64: 1091–1100, 2013.

[213] A. V. Kuznetsov and D. A. Nield. Double-diffusive natural convective boundary-layer flow of a nanofluid past a vertical plate. *International Journal of Thermal Sciences*, 50(5):712–717, 2011.